J. Hydrol. Hydromech., 68, 2020, 2, 99–110
DOI: 10.2478/johh-2020-0006
ISSN 1338-4333

sciendo Journal of Hydrology and Hydromechanics

Response of the parameters of excess infiltration and excess storage model to land use cover change

Yuexiu Wen[1], Caihong Hu[1], Guodong Zhang[2], Shengqi Jian[1*]

[1] College of Water Conservancy & Environment, Zhengzhou University, Science road 100, Zhengzhou, China.
[2] Henan Yellow River Hydrological Survey and Design Institute, Chengdong road 100, Zhengzhou, China.
[*] Corresponding author. Tel.: +86 18603814081. E-mail: jiansq@zzu.edu.cn

Abstract: The Loess Plateau is the main source of water in Yellow River, China. After 1980s, the Yellow river water presented a significant reduction, what caused the decrease of the Yellow river discharge had been debated in academic circles. We proceeded with runoff generation mechanisms to explain this phenomenon. We built saturation excess runoff and infiltration excess runoff generation mechanisms for rainfall–runoff simulation in Jingle sub-basin of Fen River basin on the Loess Plateau, to reveal the influence of land use change on flood processes and studied the changes of model parameters under different underlying conditions. The results showed that the runoff generation mechanism was mainly infiltration-excess overland flow, but the flood events of saturation-excess overland flow had an increasing trend because of land use cover change (the increase of forestland and grassland areas and the reduction of cultivated land). Some of the model parameters had physical significances，such as water storage capacity (*WM*), infiltration capacity (*f*), evapotranspiration (*CKE*), soil permeability coefficient (*k*) and index of storage capacity distribution curve (*n*) showed increasing trends, and index of infiltration capacity distribution curve (*m*) showed a decreasing trend. The above results proved the changes of runoff generation mechanism from the perspective of model parameters in Jingle sub-basin, which can provide a new perspective for understanding the discharge reduction in the Yellow River basin.

Keywords: Land use; Saturation excess and infiltration excess model; Model parameters; Fen River.

INTRODUCTION

Intensive soil erosion, soil desertification, and vegetation degradation are features of the soil and water transition zone in the Loess Plateau region in China (Gao et al., 2018). Numerous vegetation restoration measures have been implemented by the Chinese government, including the planting of perennial shrubs and grasses, in an attempt to restore the environment and reduce soil and water loss in the region. Improving the hydrological aspects of the environment via ecological restoration is two-tiered and involves (1) the prevention of water and soil loss by altering water cycle paths. Indigenous perennial plants can achieve this by increasing the effective vegetation coverage and thus minimizing surface runoff. The second aspect is related to (2) increasing the soil moisture content in order to effectively enhance productivity (Desilets et al., 2007).

Climate change may be a significant driver of changes in the flood frequency which has been widely investigated (Viglione et al., 2016). And many studies have reported that land cover change had an effect on the water cycle and resulted in variations in water resources supply and demand (Finch et al., 2004; Molina et al., 2012). However, there are only a few studies on the role of land use change in modifying river floods. Land use change has, potentially, a very strong effect on floods as humans have heavily modified natural landscapes. Large areas have been deforested or drained, thus either increasing or decreasing antecedent soil moisture and triggering erosion (Rogger et al., 2017). The Loess Plateau is the main source of water in Yellow River, China. After 1980s, the Yellow river discharge presented a significant reduction, what caused the decrease of the Yellow river discharge had been debated in academic circles. Liu et al. (2018) reported that vegetation restoration in Loess Plateau would result in water reduction in the Yellow River, however, Mu et al. (2013) found that climate change played a decreasing role in runoff reduction comparing with vegetation restoration. Also, Rozalis et al. (2010) pointed out that it was necessary to study the hydrological impacts of land use changes because that it was still controversial. But most studies focused on quantitative analyses of the effect of land use on water circle. There is a great need to study the effect of this change on future environmental flows.

Hydrological model is a generalization of hydrological phenomena in nature and often used to simulate hydrological processes (Park and Markus, 2014). From the scientific and complex degree of reflecting the rules of physical motion of water flow, there are mainly three types of models (Meng et al., 2017): conceptual models, systematic models (black box models) and physical-based models (Calver, 1988; Lee et al., 2005; Kan et al., 2017). Through accurate modeling of rainfall-runoff dynamics, it not only provides flood warnings to reduce disasters, but also enhances proper reservoir management during drought periods. However, the process of rainfall runoff conformation is affected and restricted by many factors (such as temporal, spatial variability of basin characteristics, rainfall, and coverage of vegetation). According to Grayson et al. (1992), conceptual models are better than physically based models since they are faster computationally and have less number of parameters when the suitable scale is adopted. Sorooshian et al. (1993) indicated that conceptual rainfall-runoff models are difficult to calibrate using automatic methodologies. The successful application of a conceptual rainfall-runoff model depends on how well the model is calibrated. Beven (1989) had presented the limitations of current rainfall-runoff models and argued that the possible way forward must be based on a realistic assessment of predictive uncertainty. With the increasing enrichment of distributed hydro meteorological information

and underlying surface information (such as rainfall, temperature, land use and soil properties) and the rapid improvement of computer, the development of physical-based distributed hydrological models have been a research hot spot (Apostolopoulos et al., 1997; Blyth, 1993).

Flood simulation and prediction is one of the most active researching areas in surface water hydrology. Flood takes place whenever there is a heavy or a long period of precipitation. An accurate prediction of flood under changeable meteorological and layer conditions can not only help in the water resources management especially in hydropower, but also reduce the loss of lives and property to the minimum in floodplain areas. A special problem in hydrological model simulation analysis is model parameters. The general idea of parameters in dynamic models is that they represent the stable catchment conditions while the rainfall and other inputs are the time-varying boundary conditions. In most cases, some level of model calibration will be useful to reduce bias (Beven, 2000a,b). Du et al. (2016) used Xinanjiang model to simulate runoff of the reservoirs and flood hydrology graphs of all sub-catchments of the basin, and simple reservoir operation rules were established for calculating effluent of the reservoirs. But, the runoff model of basin is not single, with the change of rainfall conditions, including both saturation excess runoff and infiltration excess runoff. At this time, it is often difficult to obtain satisfactory results if only one runoff model is adopted for calculation (Luo et al., 1992). However, under the influence of climate change and human activities, the consistency hypothesis in the traditional hydrological simulation process has been questioned (Ren et al., 2016), and the assumption that the basin hydrological model parameters are constant over time is no longer applicable. On the one hand, the structural and data problems of the model and on the other hand, the changes of the boundary conditions of the basin, such as changes in the land use may result in changes in the model parameters (Andreássian et al., 2003; Brown et al., 2005; Wagener et al., 2003). There are similar parameters in continuous runoff models related to runoff generation that may also vary in response to climate fluctuations. However, just how calibrated model parameters change with time is currently not very well understood (Wagener et al., 2010). In order to account for any changes in the parameters caused by changes in the catchment characteristics, a unique relationship between the two would be needed, but often, there are complex correlations among the parameters and with various catchment characteristics (Wagener, 2007). Therefore, it is necessary to study the variation of hydrological model parameters in a changing environment to improve the simulation accuracy and study the rules of model parameters.

The objective of this study is to (1) to build a new conceptual model for simulating effect of land use change on floods, to reveal the influence of land use change on flood processes; (2) study the changes of model parameters under different underlying conditions.

METHODOLOGIES

M-EIES model

The *M-EIES* model was improved on the basis of the Xinanjiang model. The original Xinanjiang model just considers excess storage runoff, which is based on the water storage capacity distribution curve of the basin, with poor practicality in semi-arid and semi-humid areas (Zhao, 1992). In the *M-EIES* model, the excess infiltration runoff part is added on the basis of excess storage, which is based on the basin infiltration curve and the infiltration capacity distribution curve of the basin. Compared with the Xinanjiang model, in *M-EIES* model, the excess infiltration runoff mode is based on the basin infiltration curve and the infiltration capacity distribution curve of the basin, and the storage runoff mode is based on the water storage capacity distribution curve of the basin. According to the characteristics of runoff in the Loess Plateau, the two types of runoff modes are organically combined. Moreover, according to the characteristics of different land use types, different infiltration and evaporation are adopted in the *M-EIES* model.

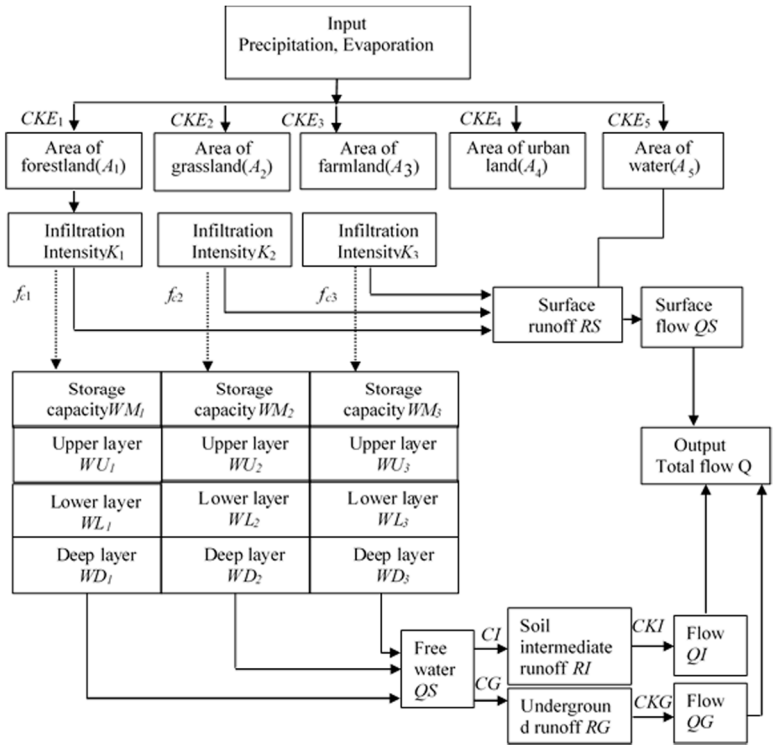

Fig. 1. Structure of *M-EIES* model.

According to the use of the free water storage capacity curve to divide the water source into surface runoff (*RS*), soil intermediate runoff (*RI*) and underground runoff (*RG*), the complex runoff formation process is transformed into the relationship between the water storage capacity and the runoff of the basin. It satisfies the different conditions that the movement process of different water sources in the outlet section of the basin is affected by the regulation and storage of the basin. A schematic diagram for *M-EIES* model is shown in Fig. 1.

Under the condition of sufficient water supply, the average infiltration rate curve of each point in the basin is called the infiltration capacity curve of the basin, which is also called the infiltration capacity curve of the basin. Many data indicate that the Horton infiltration formula and the measured points are well fitted and have a certain theoretical basis as follow:

$$f = f_c + (f_0 - f_c)e^{-kt} \tag{1}$$

where f is the infiltration capacity at time t; f_c is the steady infiltration rate (mm/h); f_0 is the initial infiltration capacity (mm/h); and k is the index related to soil permeability characteristics (h^{-1}). In this study, different infiltration rates were used to simulate forestland, grassland and cultivated land.

The infiltration capacity of the basin during the period is expressed as the mean value of the infiltration water volume in the basin during the period when the water supply is sufficient. For the integral of the infiltration capacity curve of the basin in the time period, the calculation formula is as follows:

$$F_{m\Delta t} = \int_t^{t+\Delta t} f dt = f_c \Delta t + \frac{1}{k}(f_0 - f_c)e^{-kt}(1 - e^{-k\Delta t}) \tag{2}$$

where, $F_{m\Delta t}$ is infiltration capacity during the basin; others are the same as Eq. (l).

According to experience (Luo et al., 1992), the parabolic equation of m times is used to represent the distribution curve on the watershed, and the formula is:

$$\beta = 1 - (1 - \frac{F'_{\Delta t}}{F'_{m\Delta t}})m \tag{3}$$

$$F_{m\Delta t} = \int_0^t F'_{\Delta t} d\beta = \int_0^{F'_{m\Delta t}} (1-\beta) dF'_{\Delta t} = \frac{F'_{m\Delta t}}{m+1} \tag{4}$$

$$F'_{m\Delta t} = (m+1)F_{m\Delta t} \tag{5}$$

where, $F'_{\Delta t}$ is the infiltration capacity of certain point; $F'_{m\Delta t}$ is the maximum infiltration time of the basin; m is an empirical index; β is the relative area.

Where *SM* is the free water storage capacity of the basin; *S* is the average water storage depth on the flow area, *R* is runoff. If $R+S > SM$, then:

$$RS = R + S - SM \tag{6}$$

$$RI = CI \times SM \tag{7}$$

$$RG = CG \times SM \tag{8}$$

when $R+S \le SM$, then: $RS = 0$ (9)

$$RI = CI \times (R + S) \tag{10}$$

$$RG = CG \times (R + S) \tag{11}$$

where *RS* is surface runoff; *RI* is soil intermediate runoff; *RG* is underground runoff; *CI* is outflow coefficient of soil; *CG* is underground runoff coefficient.

The model considers the water storage capacity at each point of the basin differently. According to experience, the parabolic type is introduced into the water storage capacity distribution curve.

$$\partial = 1 - (1 - \frac{W'}{W'_m})^n \tag{12}$$

where W' is the storage capacity value of a certain point; W_m' is the maximum water storage capacity of the basin; n is the empirical index; ∂ is the relative area, indicating the ratio of the area under W' to the total drainage area.

$$W_m = \int_0^{W'_m} (1 - \partial) dW' = \frac{W'_m}{n+1} \tag{13}$$

where W_m is average water storage capacity of the basin.

The surface runoff calculation uses the instantaneous unit line method to simulate the ground confluence process of the basin. The confluence calculation of the soil middle stream and the underground runoff is calculated by the linear reservoir storage model.

Compared with the original model (16 model parameters), the *M-EIES* model have 24 parameters, some of them have physical significances, including *WM*, f_c, *C*, *m*, *n*, *k* and *CKE*, which would be obtained by the basin feature statistics. Others are the process parameters, which would be obtained by the parameter optimization. The model parameters can be grouped into four categories based on the model module, (1) evapotranspiration parameters, including *WUM*, *WLM*, *C*, CKE_1, CKE_2, CKE_3 and CKE_4; (2) flow parameters, including *WM*, *m*, *n*, f_{c1}, f_{c2}, f_{c3}, k_1, k_2 and k_3; (3) water source parameters, including *SM*, *EX*, *CI* and *CG*; (4) confluence parameters, including *CKI*, *CKG*, *N* and *NK*. The concepts of these parameters are presented in Table 1.

Model calibration and validation parameter optimization

To analyze the impact of land use change on flood process, we established *M-EIES* model based on land use. Combined with the land use data, we divided the flood event into three stages and calibrated and validation each stage. The calibration makes use of an objective functionthat involves theNash-Sutcliffe efficiency coefficient (*NSE*) and the coefficient of determination (R^2) and the relative error (R_e).

The *NSE* was proposed by Nash and Sutcliffe (1970) is as follow:

$$NSE = (1 - \frac{\sum (Q_i - Q_{si})^2}{\sum (Q_i - Q_m)^2}) \tag{14}$$

where Q_i, the measured discharge (m^3/s); Q_{si}, the simulated discharge (m^3/s); Q_m, the averaged measured discharge (m^3/s).

The coefficient of determination (R^2) is expressed as

$$R^2 = (\frac{\sum (Q_{si} - Q_{sm})(Q_i - Q_m)}{\sqrt{(Q_{si} - Q_{sm})^2}\sqrt{(Q_i - Q_m)^2}})^2 \tag{15}$$

where Q_{sm} the averaged simulated discharge (m^3/s). Other symbols have the same meanings.

The relative error (R_e) is used to evaluate the difference between observed discharge and model simulated discharge.

$$R_e = \left| \frac{\sum (Q_i - Q_{sm})}{\sum Q_i} \right| \times 100\% \quad (16)$$

In calibration procedures, the parameter values are usually bounded between two limits (Duan et al., 1992). The bounds are given (Table 1). However, some parameters are not the result of a single process or a single influencing factor, so it is unlikely to be determined by actual measurement. It can only rely on the system method and solve with the optimization technique. In this study, we mainly use *SCE-UA*. The *SCE-UA* combines the strengths of the simplex procedure with: (1) the concept of controlled random search; (2) competitive evolution; (3) the concept of complex shuffling. The synthesis of these three concepts makes the *SCE-UA* robust, flexible and efficient (Duan et al., 1992). First, according to the physical meaning of the model parameters, we gave the initial value of the model parameter (Table 6), and then the *SCE-UA* was further preferred to obtain the approximate optimal values of the various parameters of the model.

STUDY AREA AND DATA

Study area

The Fen River, being located in the Shanxi province in northern China, is one of the largest tributaries of the Yellow River. The drainage area of the Fen River basin is 39471 km^2. The river basin has a temperature continental monsoon climate with monthly average air temperature varies from 4 to 13˚C and the maximum evaporation capacity of the water surface is 1120mm. The area has an average annual precipitation of 503 mm, 60% of which occurs between July and September. The average annual runoff of the basin was 57.9mm. The major land use type of this area is forest and farmland, although the construction land of towns has extended year by year with the fast pace of urbanization since the 1980s, in Jingle sub-basin. Which located in the north and upper reaches of Fen River basin, was selected as case studies (Fig. 2).

The drainage area of sub-basin (Jingle) is 2799 km^2 with a large number of floods. The main channel length is 83.9 km, the average slope of the main stream is 6.7%, the shape coefficient of the basin is 0.398. The underlying surface conditions changed greatly since 1980s, the “Grain for Green” project was conducted, which has a great impact on water resource and flood (Uchida et al., 2005). In addition, there is no coal mining activity, the amount of water diversion is small and no water conservancy projects in the Jingle sub-basin.

Table 1. The meanings of the *M-EIES* model parameters.

Parameter	Parameter meaning	Range	Parameter	Parameter meaning	Range
WM	Average catchment storage capacity	100–200	fc_3	Farmland steady infiltration rate	4–6
n	Index of storage capacity distribution curve	0.01–0.7	k_3	Farmland soil permeability coefficient	0.1–0.8
m	Index of infiltration capacity distribution curve	0.01–0.7	CKE_4	water area evaporation conversion	0.5–2
C	Deep evaporation coefficient	0.01–0.4	*SM*	Free water storage capacity	10–20
CKE_1	Forest land evaporation conversion	0.5–2	*EX*	Index of free water storage capacity curve	1–5
fc_1	Forest land steady infiltration rate	4–6	*CI*	Outflow coefficient of soil	0.01–0.7
k_1	Forest land soil permeability coefficient	0.1–0.8	*CG*	Underground runoff coefficient	0.01–0.7
CKE_2	Grass land evaporation conversion	0.5–2	*CKI*	Extinction coefficient of flow in soil	0.9–1
fc_2	Grass land steady infiltration rate	4–6	*CKG*	Extinction coefficient of underground runoff	0.9–1
k_2	Grass land soil permeability coefficient	0.1–0.8	*N*	River convergence parameter	\
CKE_3	Farmland evaporation conversion	0.5–2	*NK*	River convergence parameter	\

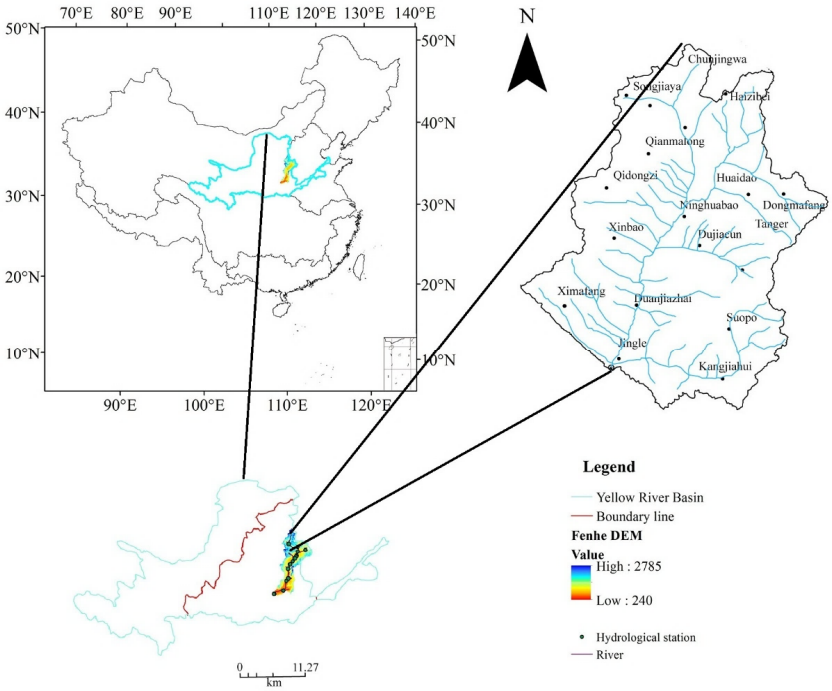

Fig. 2. Locations of the Fen River basin and Jingle sub-basin.

Dataset

We got the Landsat Thematic Mapper (TM) imagery of the years 1978, 1998 and 2010 from Global Land Cover Facility which were used to show the variation of land use in the experimental period (Fig. 3). The digital elevation model (DEM) with a spatial resolution of 30 m was downloaded from China Soil Scientific Database (CSSD). Soil type data of the sub-basin was gotten from Consultative Group on International Agricultural Research-Consortium for Spatial Information (CGIAR-CSI). The hydrological data included precipitation, evaporation and runoff from 1965 to 2014. There are 16 hydrological stations in the Jingle sub-basin of the Fen River basin, about 1 per 175 km^2. Area-averaged rainfall and evaporation are obtained from Thiessen polygon method. The basin-averaged minimum required hourly input data for basin are: rainfall and evaporation. And hydrological stations were extracted from <<Data of the Yellow River basin>> (http://www.yrcc.gov.cn/). During the study period (from 1965 to 2014), 63 flood events were observed, we selected 29 flood events to build the *M-EIES* model.

Table 2 and Table 3 showed the detailed information of the land use change. From 1978 to 1998, the areas of farmland and grassland changed greatly. The farmland decreased by 74.14 km^2, the grassland decreased by 22.02 km^2, and the woodland area increased by 96.7 km^2, which was mainly caused by the conversion from grassland and cultivated land to woodland. From 1998 to 2010, the areas occupied by farmland, grassland and forest changed greatly. Among them, the farmland decreased by 109.11 km^2, the grassland increased by 42.8 km^2, and the woodland increased by 65.9 km^2, showing the conversion from farmland to grassland, from grassland and farmland to woodland. Water areas and urban construction land have changed not much.

Table 2. Land use transfer matrix from 1978 and 1998.

1978 \ 1998	Farmland/km^2	Forest/km^2	Grass/km^2	Water/km^2	Urban/km^2	Total/km^2
Farmland/km^2	679.41	13.52	64.95	0.02	0.22	758.12
Forest/km^2	0.64	894.24	4.65	0.00	0.00	899.53
Grass/km^2	3.90	88.30	996.14	0.12	0.09	1088.55
Water/km^2	0.00	0.00	0.45	35.76	0.00	36.21
Urban/km^2	0.03	0.16	0.34	0.00	16.05	16.58
Total/km^2	683.98	996.23	1066.53	35.90	16.35	2799.00

Table 3. Land use transfer matrix from 1998 and 2010.

1998 \ 2010	Farmland/km^2	Forest/km^2	Grass/km^2	Water/km^2	Urban/km^2	Total/km^2
Farmland/km^2	568.99	13.55	100.95	0.23	0.04	683.77
Forest/km^2	0.91	987.02	8.38	0.00	0.14	996.45
Grass/km^2	4.71	61.57	999.69	0.37	0.18	1066.52
Water/km^2	0.05	0.10	0.12	35.64	0.00	35.91
Urban/km^2	0.00	0.11	0.25	0.00	16.01	16.36
Total/km^2	574.66	1062.35	1109.38	36.24	16.37	2799.00

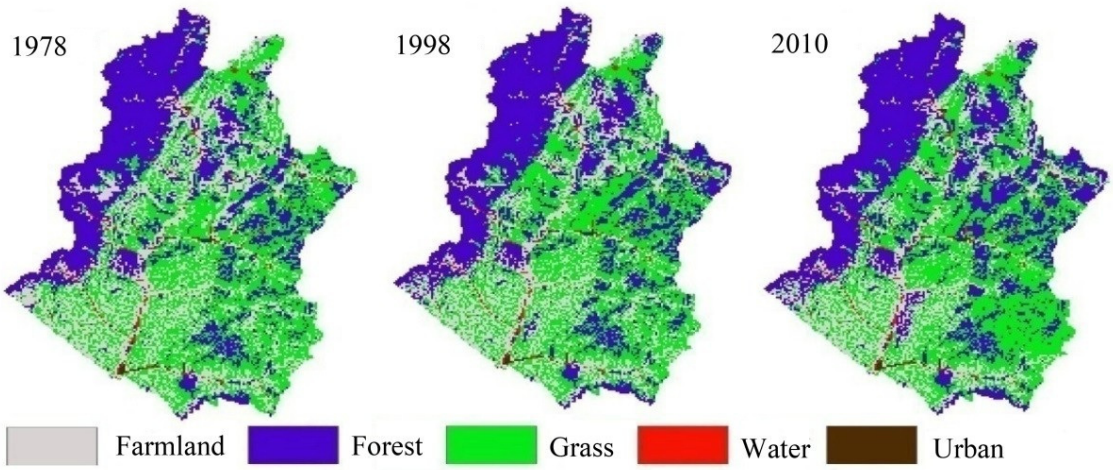

Fig. 3. Land uses of the Jingle sub-basin.

RESULT AND DISCUSSION

Runoff characteristics

The time periods from 1965 to 2014 were divided into three periods (1965–1978, 1979–1998 and 1999–2014) (12 flood events from 1965 to 1978, 12 flood events from 1979 to 1998, and 6 flood events from 1999 to 2014). Due to the influence of rainfall and underlying surface changes, runoff coefficient has an obvious decreasing trend from 1965 to 2014 (Fig. 4), which indicated that with the change of land use, the runoff yield and confluence conditions of the basin changed greatly, resulting in the change of flood process of the basin outlet section. The rainfall-runoff relationship at each stage is different. The rainfall-runoff correlation coefficients of each stage were 0.80, 0.64

and 0.57, respectively. In comparison, the third-stage runoff has the strongest dependence on rainfall, and the runoff in the third stage has decreased significantly (Fig. 5A). The R^2 were 0.58, 0.55 and 0.51 between rainfall intensity and runoff in each stage, respectively. For the rainfall events of the same magnitude of rainfall intensity, in the three stages, the first stage has the largest runoff and the third stage has the smallest runoff (Fig. 5B), which indicated that the effect of underlying surface conditions change on runoff was increasingly intensified.

Flood simulation

During the period of 1965–1978, we selected 12 flood events (8 flood events for model calibration and 4 flood events for model validation) with the flood peaks from 216 to 2165 m^3/s. 11 and 6 flood events were selected from 1979 to 1998 (7 flood events for model calibration and 4 flood events for model validation), from 1999 to 2014 (4 flood events for model calibration and 2 flood events for model validation). The Xinanjiang model and the *M-EIES* model were used to calculate the runoff (Table 4).

From 1965 to 1978, Nash–Sutcliffe efficiency coefficient (*NSE*) of all floods were greater than 0.7; the coefficient of determination (R^2) were greater than 0.8, and the relatively error (R_e) was smaller than 6% at the hourly scale. From 1979 to 1998 and 1999 to 2014, The *NSE* of floods were greater than 0.7; the R^2 were greater than 0.8, and the R_e were smaller than 15%. The simulated and observed values for Jingle sub-basin was shown in Fig. 6, Fig. 7, Fig. 8 and Fig. 9. These three indices (*NSE*, R^2 and *Re*) of the Xinanjiang model were compared with that of the *M-EIES* model (Table 5). The *NSE* of *M-EIES* model was greater than 0.7 for both calibration and validation period no matter what period. However, the *NSE* of Xinanjiang model was just about 0.5 in calibration and validation period.

Table 4. Simulation results of Jingle sub-basin in the calibration and validation periods in the three stages.

Stages		Flood time	*NSE*	R^2	*Re* (%)	Number of hours(h)
1965–1978	Calibration	19660815	0.96	0.81	9.2	67
		19670810	0.90	0.79	14.4	176
		19690726	0.80	0.82	14.4	57
		19690806	0.88	0.87	1.9	178
		19710701	0.71	0.75	14.7	40
		19710807	0.74	0.81	13.4	34
		19730819	0.86	0.86	15.5	107
		19740706	0.81	0.81	13.5	54
	Validation	19750805	0.92	0.80	1.5	48
		19770706	0.91	0.75	0.4	110
		19770802	0.91	0.66	2.3	56
		19780808	0.88	0.74	12.0	75
1979–1998	Calibration	19810722	0.78	0.88	9.1	48
		19810805	0.77	0.87	11.5	72
		19830821	0.75	0.83	10.6	48
		19850511	0.79	0.84	12.4	46
		19880720	0.81	0.84	15.2	60
		19890721	0.76	0.79	11.3	87
		19920831	0.72	0.84	6.5	165
	Validation	19940706	0.87	0.81	9.4	102
		19960614	0.79	0.76	9.9	79
		19960719	0.88	0.72	11.5	95
		19980630	0.75	0.79	14.5	76
1999–2014	Calibration	20010711	0.75	0.84	13.4	36
		20010720	0.78	0.86	9.5	84
		20020811	0.85	0.87	8.7	103
		20080923	0.90	0.82	10.1	181
	Validation	20110729	0.88	0.87	9.3	117
		20130715	0.78	0.77	14.6	180

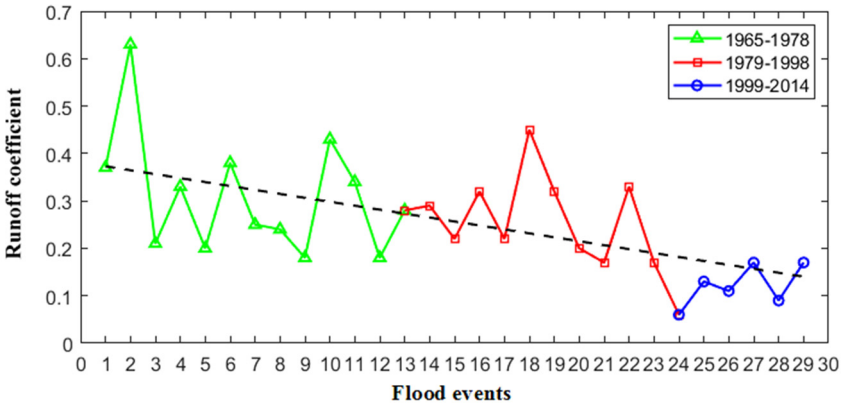

Fig. 4. Variation trend of flood runoff coefficient in the Jingle sub-basin from 1965 to 2014.

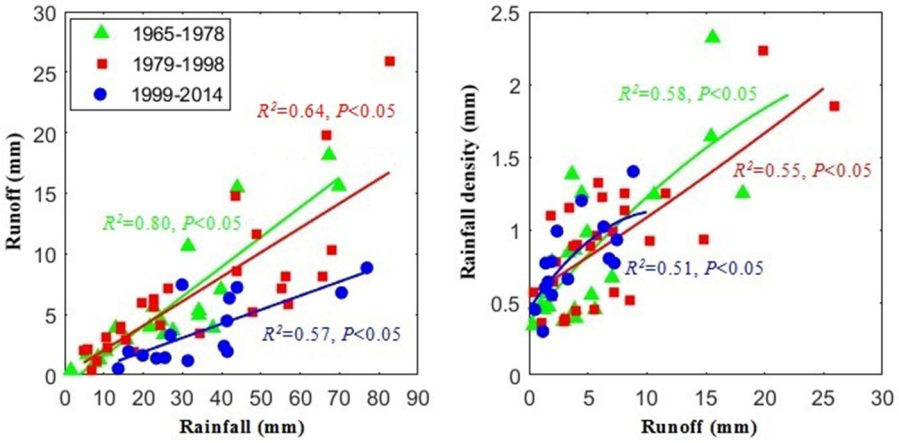

Fig. 5. The relationships between rainfall and runoff for per flood (The left is Fig. 5A, the right is Fig. 5B. The green line is the trend line from 1965 to 1978; red line: 1979–1998; blue line: 1999–2014).

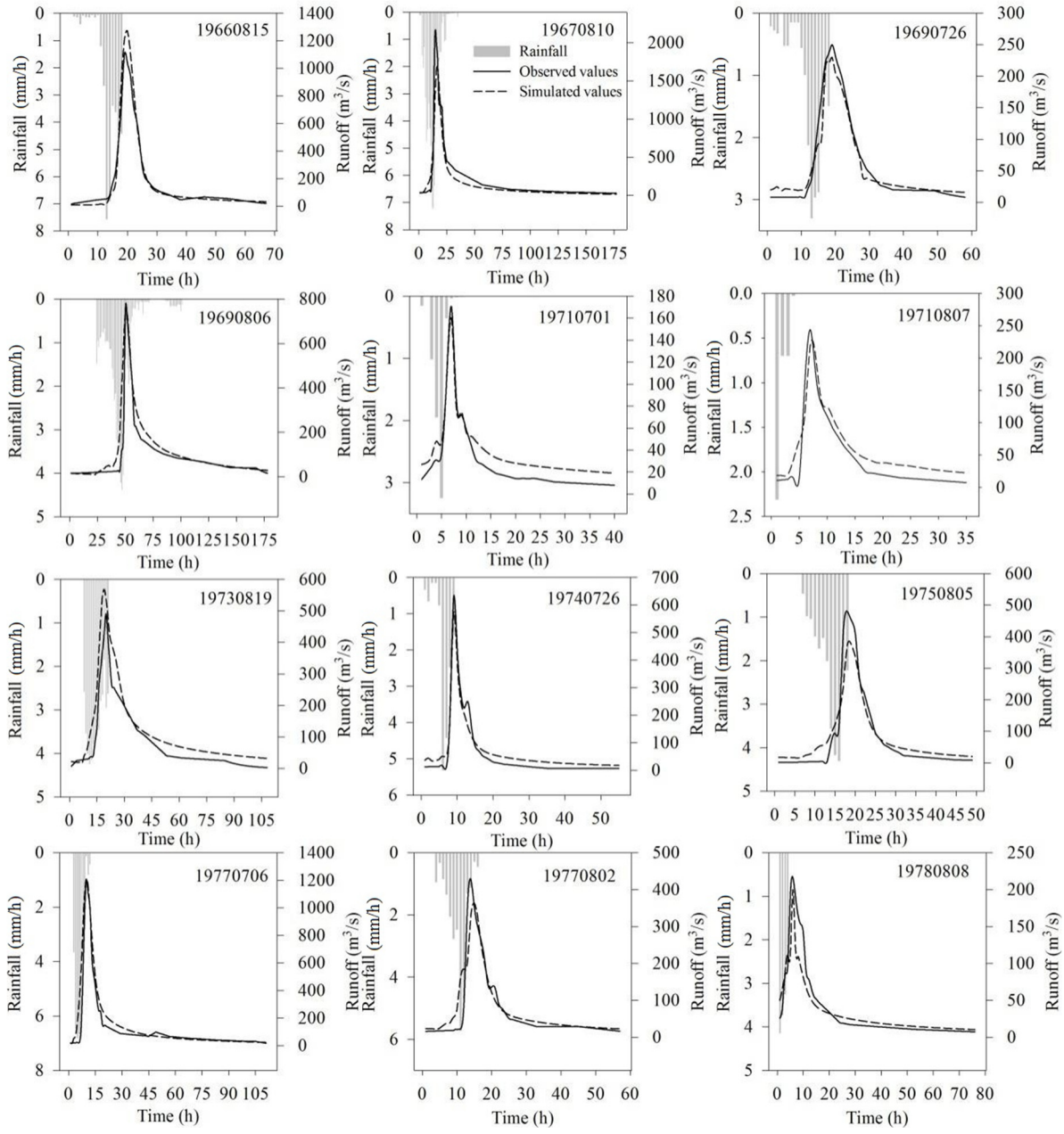

Fig. 6. Simulation results of Jingle sub-basin in the calibration and validation periods from 1965 to 1978.

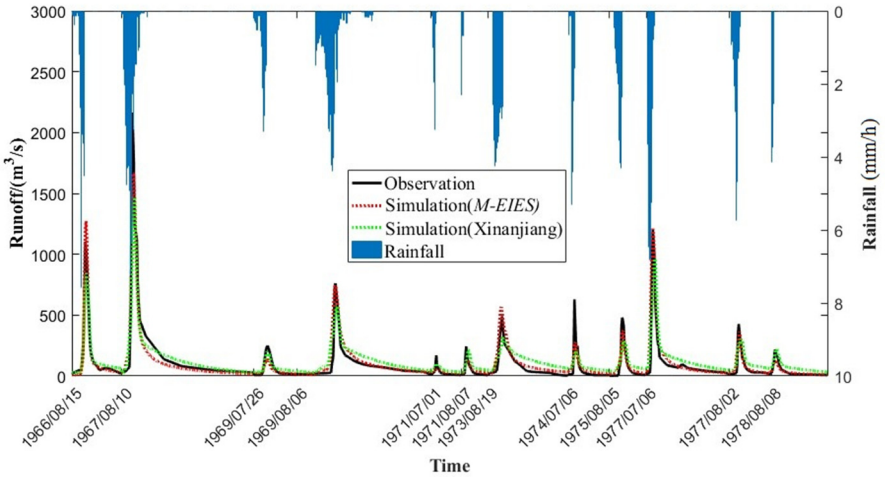

Fig. 7. Simulation results of Jingle sub-basin from 1965 to 1978 (The time step is 1 hour).

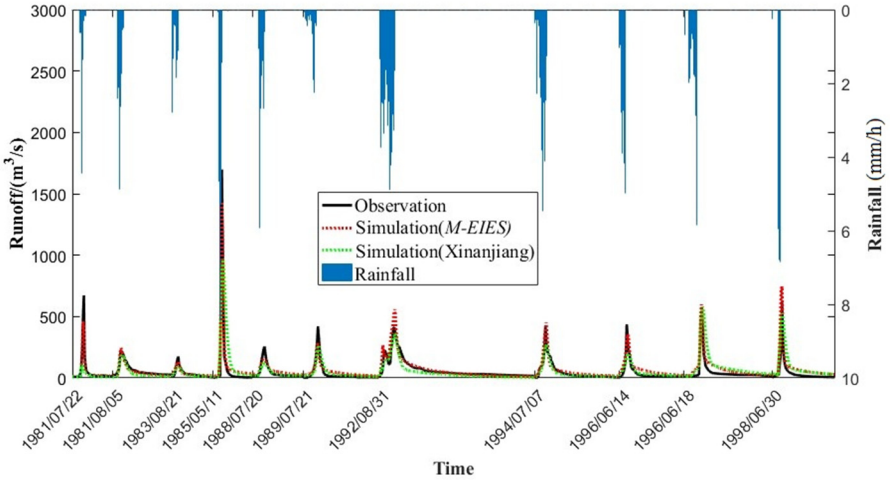

Fig. 8. Simulation results of Jingle sub-basin from 1979 to 1998 (The time step is 1 hour).

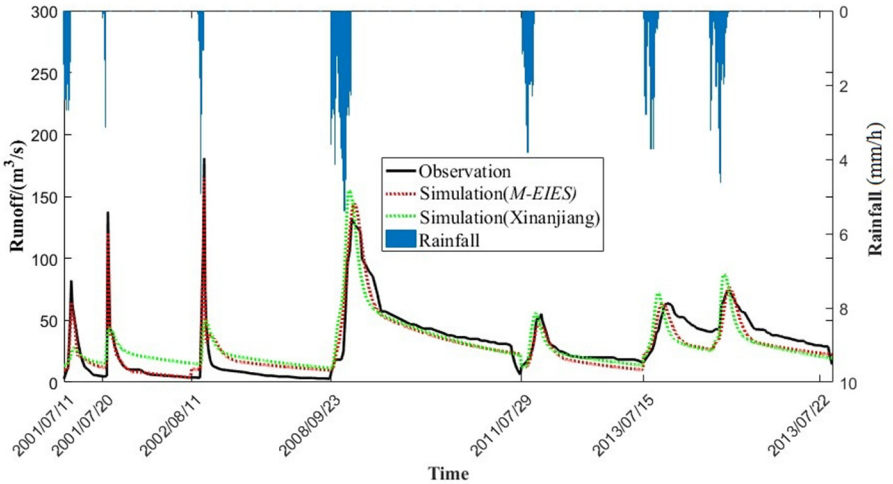

Fig. 9. Simulation results of Jingle sub-basin from1999 to 2014 (The time step is 1 hour).

Similarly, the R^2 of *M-EIES* model varying from 0.72 to 0.85 in calibration and validation period were greater than that of Xinanjiang model. In addition, the *Re* of *M-EIES* model was obviously smaller than that of Xinanjiang model. The results indicated that *M-EIES* model performed well in Jingle sub-basin and can be used to simulate runoff with different land use stages.

The climate change and human activities have influences on model parameters. In each stage, we selected several floods events to calibrate model parameters, respectively. The simulation accuracy can be improved, due to considering the effects of land use changes on the flood process. The same method can be found in some studies (Pathiraja et al., 2016; Wallner and Haberlandt, 2015).

Table 5. The results of *NSE*, R^2, and *Re* in calibration and validation periods.

Stages		*M-EIES*			Xinanjiang model		
		NSE	R^2	*Re* (%)	*NSE*	R^2	*Re* (%)
1965–1978	Calibration	0.83	0.72	12.12	0.54	0.56	18.45
	Validation	0.91	0.74	4.05	0.57	0.64	16.54
1979–1998	Calibration	0.77	0.84	10.94	0.48	0.57	19.78
	Validation	0.83	0.77	11.32	0.52	0.62	22.54
1999–2014	Calibration	0.82	0.85	10.42	0.56	0.54	15.43
	Validation	0.83	0.82	11.95	0.58	0.62	13.25

M-EIES model parameters and land use cover changes

Parameters for physical significances

The model parameters in the three stages were presented in Table 6. It can be seen that different land use types reflect different values of runoff parameters. To analyze this, we discuss different types of parameters and study the effects of land use change on them. (Merz et al., 2008) argued that long-term interactions, climate change and changes in land characteristics can affect model parameters, but they are considered small for the 30 years considered. But in this study, land use change is booming, for most models, the parameters also vary significantly. For example, the *f* and *CKE* of different land use types are different. (Xie et al., 2007) got the same conclusion. The parameters, *WM*, *f*, *CKE* and *k* showed increasing trends during the experimental period. Vegetation is closely related to the soil water permeability, water holding capacity and water storage capacity. The soil compactness would increase with degraded vegetation, resulted in the reduction of soil saturated hydraulic conductivity, infiltration rate and water storage capacity. The surface runoff would increase with the decreased underground runoff (Wang et al., 2015). Vegetation could increase rainfall infiltration by improving the soil organic matter and soil porosity. Therefore, land use cover changes are the important reason for rainfall-runoff characteristics (Gonzalez-Sosa et al., 2010), which has an influence on the processes of runoff generation and confluence by affecting groundwater outflow capacity, infiltration capacity and watershed water storage capacity (Pirastru et al., 2013).

(1) Groundwater outflow capacity

In the Jingle sub-basin, the forest area increased rapidly. Previous studies found groundwater outflow capacity had an influence on underground water, and the minimum daily discharge and the minimum daily discharge in flood season could reflect the discharge capacity of groundwater (Table 7). The annual mean minimum daily flow and the minimum daily flow in the flood season showed the obvious trends in the three stages. In the flood season, more rainfall, the groundwater recharge increased. Under the similar rainfall conditions, groundwater outflow capacity is stronger from 1999 to 2014, which is easier to generate underground flow and interflow, resulted in the decrease of flow. The confluence time expanded and changed the process of flood. The 12.08% increase in forest areas resulted in the 45.37% increase in groundwater outflow capacity.

(2) Infiltration capacity

The forest areas increased by 12.08%, averaged rainfall depth before generate flow increased by 157.67% and the duration of flood subsidence increased by 14.51% (Table 7). In the early stage of storm, the rainfall is mainly consumed by the infiltration. Flood subsidence is an important part of runoff generation and confluence. There is a certain amount of infiltration during the process of flood subsidence. Generally speaking, with the increase of rainfall and rainfall intensity, runoff coefficient will increase. As the years processed, more rainfall was needed in the Jingle sub-basin to produce runoff, indicating the infiltration increased gradually. Also, the duration of flood subsidence increased gradually (Table 7). The increase of infiltration is an important reason for changes of runoff generation and confluence mechanism in the basin. The increase of soil moisture enhancement, resulted in the decrease of surface runoff, runoff coefficient and flood peak flow, increase of underground runoff and confluence duration (Ogden et al., 2011). Also, our previous study found that the flood events of saturation excess over land flow increased with the decrease of flood events of infiltration-excess over land flow, due to the increase of forest areas (Li, 2018).

Forests and grass had greater steady infiltration rates than farmland (Table 6). Vegetation influences the chemistry, structure, organic content, and strength of soils. Roots and burrowing organisms' bioturbated soils, changing the pathways and generally increasing porosity and infiltration capacity (Moussa et al., 2002). As a consequence, alterations in vegetation may create broad-scale changes in the way rainfall is partitioned into runoff and recharge. Infiltration capacity is a commonly used term which is the maximum rate at which soils can absorb water, generally occurring under dry conditions when sportive influences are greatest. The infiltration capacity tends to decrease as the soil moisture content of the surface layers increases (Jian et al., 2014). In general, deeper rooted species can change

Table 6. The *M-EIES* model parameters in the three stages.

Model parameters	Initialization parameter	1965–1978	1979–1998	1999–2014
WM	150	101.369	124.731	156.36
X	0.2	0.15	0.143	0.283
Y	0.3	0.201	0.252	0.296
n	0.1	0.586	0.418	0.365
m	0.1	0.065	0.175	0.169
C	0.1	0.133	0.126	0.318
CKE_1	1	0.901	0.989	1.104
f_{c1}	4.5	4.986	4.991	5.231
K_1	0.5	0.381	0.231	0.348
CKE_2	1	0.531	0.893	0.985
f_{c2}	4	4.868	4.957	5.024
K_2	0.5	0.15	0.306	0.415
CKE_3	1	1.04	1.113	1.423
f_{c3}	3.8	4.02	4.458	4.89
K_3	0.5	0.385	0.426	0.441
EX	3	3.761	2.97	2.67
SM	12	12.815	14.474	16.088
CKG	0.8	0.918	0.983	0.99
CKI	0.8	0.986	0.948	0.999
CI	0.5	0.458	0.126	0.37
CG	0.3	0.139	0.121	0.203
N	3	3.189	3.189	3.505
NK	2.5	3.315	1.404	1.892

Table 7. Daily flow, averaged rainfall depth before generate flow and Duration of flood subsidence in the three stages.

Items	1965–1978	1979–1998	1999–2014
Forest areas (km²)	899.53	996.23	1062.35
Annual mean minimum daily flow (m³/s)	0.68	1.26	1.40
Minimum daily flow in the flood season (m³/s)	1.93	2.61	3.30
Averaged rainfall depth before generate flow(mm)	6.9	9.4	21.0
Duration of flood subsidence (h)	14.22	14.39	16.38
Catchment water storage capacity (mm)	101.37	124.73	156.36

soil properties to suit their needs of water use (Yüksek et al., 2009). There are spatial variations in hydrology and soil characteristics which are not represented in this analysis, and those differences are likely the reason for the large differences of site-to-site. For example, bare soil in one location may have higher infiltration than grasses at another location, likely attributable to other soil forming factors such as parent material, topography, aspect, climate, and soil age. However, this study does show promise for generalization of local or perhaps even island-wide trends, which would allow for mappable units of infiltration properties that can be related to processes of interest including areas of potentially high aquifer recharge or erosion susceptibility.

(3) Water storage capacity

The water storage capacity of the Jingle sub-basin increased year by year. Previous studies have shown that the water storage capacity of woodland is higher than other land use covers, and the increase of forest areas would result in the increase of catchment water storage capacity, and reducing runoff (Jian et al., 2016). The forest areas increased by 12.08% with the water storage capacity increased by 27.84% (Table 6), other studies had found the similar results (Zhang et al., 2014). The water storage capacity distribution curve index (n) and the infiltration capacity distribution curve index (m) are the main indicators to determine the runoff generation mechanism. When $m = 0$, it is a typical flood event of saturation-excess overland flow; when $n = 0$, it is a typical flood event of infiltration-excess overland flow. In Jingle sub-basin, both saturation-excess overland flow and infiltration-excess overland flow existed (Table 5). Our previous study found that the flood events were mainly infiltration-excess overland flow, the flood events of saturation-excess overland flow showed an increasing trend in Jingle sub-basin (Li, 2018). The current study demonstrated the results from the perspective of model parameters.

Evapotranspiration parameters

Evapotranspiration is highly affected by land cover types such as leaf area index (Zhang et al., 2014). Some researchers found that land use cover changes had greater impact on the hydrological cycle than climate change (Georgescu, 2013) and may cancel or mask the effects of climate change (Voss et al., 2002). Land use cover changes affects evapotranspiration on the regional scale mainly through vegetation changes (e.g., deforestation and afforestation, or grassland reclamation), agricultural development activities (e.g., farmland reclamation, crop cultivation, and agricultural management), and urbanization (Yang et al., 2008). Evapotranspiration change rates differ among land cover types that have different underlying surfaces (Mwangi et al., 2016). In the current study the evapotranspiration of different land use types is ranked as cultivated land > forest land > grassland > unused land, and the evapotranspiration increased year by year. Changes from forests and natural vegetation to other land use types can increase water yield and decrease evapotranspiration (Olang and Fürst, 2011). Deforestation and afforestation are the most influential types of land use cover changes that affect evapotranspiration (Wan et al., 2008). Olchev et al. (2008) found that transpiration and the evaporation of intercepted rainfall were reduced after tropical rainforests were converted to croplands in Indonesia. Although the land use conversion also increased soil evaporation there was overall a decrease in mean evapotranspiration. Oliveira et al. (2014) reported that deforestation reduced evapotranspiration by 36% in Brazil because the leaf area index and vegetation coverage of croplands are relatively smaller than those of forests.

Water source parameters

There are four water source parameters in the model, namely free water storage capacity (*SM*), free water storage capacity curve index (*EX*), soil effluent coefficient (*CI*) and underground diameter effluent coefficient (*CG*). *SM* is a quantitative representation of soil water storage capacity in the basin, and plays an important role in the proportion of surface runoff, interflow and underground flow. According to the previous studies (Karahan et al., 2013), *SM* has an influence on the flood peak flow, and the *SM* in the study basin showed an increasing trend. The *SM* increased and improved the free water storage reservoir in the basin. The land use change in the control basin of Jingle station increases the storage capacity of the basin. *CI* and *CG* can reflect the speed of flood submergence, and the increase of *CI* and *CG* could change the flood withdrawal curve, indicating that the soil flow and underground runoff have changed in the study area with the change of land use.

CONCLUSIONS

Based on the results from this study, the main conclusions are summarized as follows:

(1) A new model, the modified saturation excess and infiltration excess model, had been developed based on the original saturation excess and infiltration excess model. The land uses, soil properties, rainfall and streamflow were taken as input data for the modified model. The developed *M-EIES* model is therefore used to simulate surface flow, interflow and groundwater flow. Based on the modified model, the effects of land use change on flow were investigated.

(2) The *M-EIES* model simulated runoff within the range of acceptable accuracy, which is reflected by the goodness-of-fit measure. For model results, the efficiency of Nash and Sutcliffe for 29 flood events of the Jingle sub-basin are greater than 0.7, in both the calibration and validation periods. This indicates that the *M-EIES* model based on the original saturation excess and infiltration excess model is suitable for rainfall-runoff simulation.

(3) Most of the model parameters showed increasing trends, but index of infiltration capacity distribution curve (m) showed a decreasing trend, which proved the changes of runoff generation mechanism from the perspective of model parameters in Jingle sub-basin, it can provide a new perspective for

understanding the discharge reduction in the Yellow River basin.

As a key fact causing the change in runoff, the land-use change should not be neglected, especially for its impact in the flood season. The role played by land-use change should be appropriately considered due to its impact on water resources and ecosystem health in the Fen River basin. In fact, climate change should be taken into account when assessing the impacts of land use cover change in the future. However, the compound effect of climate and land use cover change is complicated and beyond the scope of this paper. In the future research, a land use projection model based on cellular automata and Markov chain, and the regional future climate scenarios would be considered together to quantitatively predict streamflow in response to possible future land use and climate changes.

Acknowledgements. This project was supported by the National Natural Science Foundation of China (51979250); National Key Research Priorities Program of China (2016YFC0402402); National Natural Science Foundation of China (31700370); National Natural Science Foundation of China (51409116); Startup Research Fund of Zhengzhou University (1512323001); Institution of higher learning key scientific research project, Henan Province (16A570010); Foundation of drought climate science (IAM201705); China postdoctoral science foundation (2016M602255); Henan province postdoctoral science foundation; National Natural Science Foundation of China (91025015). We would like to thank LetPub (www.letpub.com) for providing linguistic assistance during the preparation of this manuscript.

REFERENCES

Andreássian, V., Parent, E., Michel, C., 2003. A distribution-free test to detect gradual changes in watershed behavior. Water Resour. Res., 39, 9, 1252.

Apostolopoulos, T.K., Georgakakos, K.P., 1997. Parallel computation for streamflow prediction with distributed hydrologic models. Journal of Hydrology, 197, 1–24.

Blyth, K., 1993. The use of microwave remote sensing to improve spatial parameterization of hydrological models. Journal of Hydrology, 152, 103–129.

Beven, K., 1989. Changing ideas in hydrology – The case of physically-based models. Journal of Hydrology, 105, 157–172.

Beven, K., 2000a. Rainfall-Runoff Modelling: The Primer. John Wiley and Sons Ltd. Chichester, UK, 360 p.

Beven, K.J., 2000b. Uniqueness of place and process representations in hydrological modelling. Hydrol. Earth Syst. Sci., 4, 203–213.

Brown, A.E., Zhang, L., McMahon, T.A., Western, A.W., Vertessy, R.A., 2005. A review of paired catchment studies for determining changes in water yield resulting from alterations in vegetation. J. Hydrol., 310, 28–61.

Calver, A., 1988. Calibration, sensitivity and validation of a physicality based rainfall-runoff model. Journal of Hydrology, 103, 103–115.

Du, J.K., Zheng, D.P., Xu, Y.P., Hu, S.F., Xu, C.Y., 2016. Evaluating functions of reservoirs storage capacities and locations on daily peak attenuation for Ganjiang River Basin using Xinanjiang model. Chinese Geographical Science, 26, 789–802. (In Chinese with English abstract.)

Desilets, S.L.E., Nijssen, B., Ekwurzel, B., Ferré, T.P.A., 2007. Post-wildfire changes in suspended sediment rating curves: Sabino Canyon, Arizona. Hydrological Processes, 14, 1413–1423.

Duan, Q.Y., Sorooshian, S., Gupta, V.K., 1992. Effective and efficient global optimization for conceptual rainfall-runoff models. Water Resources Research, 28, 1015–1031.

Finch, J.W., Bradford, R.B., Hudson, J.A., 2004. The spatial distribution of groundwater flooding in a chalk catchment in southern England. Hydrological Processes, 18, 959–971.

Gao, G., Fu, B., Zhang, J., 2018. Multiscale temporal variability of flow-sediment relationships during the 1950s–2014 in the Loess Plateau, China. Journal of Hydrology, 563, 609–619.

Georgescu, M., 2013. Impact of anthropogenic land-use/land-cover change on climate and hydrologic cycle over the Greater Phoenix Area. Journal of Urology, 189, e872-e873.

Grayson, R.B., Moore, I.D., Mcmahon, T.A., 1992. Physically based hydrologic modeling: 2. Is the concept realistic? Water Resources Research, 28, 2659–2666.

Gonzalez-Sosa, E., Braud, I., Dehotin, J., 2010. Impact of land use on the hydraulic properties of the topsoil in a small french catchment. Hydrological Processes, 24, 2382–2399.

Jian, S., Zhao, C., Fang, S., Yu, K., 2014. Soil water content and water balance simulation of *Caragana korshinskii* Kom. in the semiarid Chinese Loess Plateau. Journal of Hydrology and Hydromechanics, 62, 89–96.

Jian, S., Wu, Z., Hu, C., Zhang, X., 2016. Sap flow in response to rainfall pulses for two shrub species in the semiarid Chinese Loess Plateau. Journal of Hydrology and Hydromechanics, 64, 121–132.

Kan, G., Li, J., Zhang, X., Ding, L., He, X., Liang, K., Jiang, X., Ren, M., Li, H., Wang, F., Zhang, Z., Hu, Y., 2017. A new hybrid data-driven model for event-based rainfall-runoff simulation. Neural Computing and Applications, 28, 2519–2534.

Karahan, H., Gurarslan, G., Zong, W.G., 2013. Parameter estimation of the nonlinear muskingum flood routing model using a hybrid harmony search algorithm. Journal of Hydraulic Engineering - ASCE, 18, 352–360.

Lee, H., Mclntyre, N., Wheater, H., 2005. Selection of conceptual models for regionalization of the rainfall-runoff relationship. Journal of Hydrology, 312, 140–147.

Liu, X., Gao, Y., Ma, S., Dong, G., 2018. Sediment reduction of warping dams and its timeliness in the Loess Plateau. Journal of Hydraulic Engineering, 49, 145–155.

Li, N., 2018. Study on the mechanism of runoff production and confluence in the Loess Plateau under the change of underlying surface. Master's Thesis. Zhengzhou University, Zhengzhou.

Luo, W.S., Hu, C.Q., Han, J.T., 1992. Research on a model of runoff yield reflecting excess infiltration and excess storage simultaneously. Chinese Journal of Water and Soil Conservation, 4, 6–13. (In Chinese with English abstract.)

Meng, C., Zhou, J., Dai, M., 2017. Variable infiltration capacity model with bgsa-based wavelet neural network. Stochastic Environmental Research and Risk Assessment, 31, 1871–1885.

Merz, B., Aerts, J., Arnbjerg-Nielsen, K., Baldi, M., Becker, A., Bichet, A., Blöschl, G., Bouwer, L.M., Brauer, A., Cioffi, F., Delgado, J.M., Gocht, M., Guzzetti, F., Harrigan, S., Hirschboeck, K., Kilsby, C., Kron, W., Kwon, H.-H., Lall, U., Merz, R., Nissen, K., Salvatti, P., Swierczynski, T., Ulbrich, U., Viglione, A., Ward, P.J., Weiler, M., Wilhelm, B., Nied, M., 2014. Floods and climate: Emerging perspectives for flood risk assessment and management. Nat. Hazards Earth Syst. Sci., 14, 1921–1942.

Molina, A., Vanacker, V., Balthazar, V., 2012. Complex land cover change, water and sediment yield in a degraded and environment. Journal of Hydrology, 472, 25–35.

Moussa, R., Voltz, M., Andrieux, P., 2002. Effects of the spatial organization of agricultural management on the hydrological behaviour of a farmed catchment during flood events. Hydrological Processes, 16, 393–412.

Mu, S., Zhou, S., Chen, Y., 2013. Assessing the impact of restoration-induced land conversion and management alternatives on net primary productivity in inner Mongolian grassland, China. Global & Planetary Change, 108, 29–41.

Mwangi, H.M., Julich, S., Patil, S.D., 2016. Relative contribution of land use change and climate variability on discharge of upper Mara River, Kenya. Journal of Hydrology Regional Studies, 5, 244–260.

Nash, J.E., Sutcliffe, J.V., 1970. River flow forecasting through the conceptual models. 1: A discussion of principles. Journal of Hydrology, 10, 282–290.

Ogden, F.L., Pradhan, N.R., Charles, W.D., 2011. Relative importance of impervious area, drainage density, width function, and subsurface storm drainage on flood runoff from an urbanized catchment. Water Resources Research, 47, 1–12.

Olang, L.O., Fürst, J., 2011. Effects of land cover change on flood peak discharges and runoff volumes: model estimates for the Nyando River basin, Kenya. Hydrological Processes, 25, 80–89.

Olchev, A., Ibrom, A., Ross, T., Falk, U., Rakkibu, G., Radler, K., Grote, S., Kreilein, H., Gravenhorst, G., 2008. A modelling approach for simulation of water and carbon dioxide exchange between multi-species tropical rain forest and the atmosphere. Ecological Modelling, 212, 122–130.

Oliveira, P.T.S, Nearing, M.A., Moran, M.S., 2014. Trends in water balance components across the Brazilian Cerrado. Water Resources Research, 50, 7100–7114.

Park, D., Markus, M., 2014. Analysis of a changing hydrologic flood regime using the variable infiltration capacity model. Journal of Hydrology, 515, 267–280.

Pathiraja, S., Marshall, L., Sharma, A., 2016. Hydrologic modeling in dynamic catchments: A data assimilation approach. Water Resources Research, 52, 3350–3372.

Pirastru, M., Castellini, M., Giadrossich, F., Niedda, M., 2013. Comparing the hydraulic properties of forested and grassed soils on an experimental hillslope in a Mediterranean environment. Procedia Environmental Sciences, 19, 341–350.

Ren, L, Shen, H., Yuan, F., Zhao, C., Yang, X., Zheng, P., 2016. Hydrological drought characteristics in the Weihe catchment in a changing environment. Advances in Water Science, 27, 492–500. (In Chinese with English abstract.)

Rogger, M., Agnoletti, M., Alaoui, A., Bathurst, J.C., Bodner, G., Borga, M., Chaplot, V., Gallart, F., Glatzel, G., Holko, L., Horn, R., Kiss, A., Kohnová, S., Leitinger, G., Lennartz, B., Parajka, J., Perdigão, R., Peth, S., Plavcová, L., Quinton, J.N., Salinas, J.L., Santoro, A., Szolgay, J., Tron, S., van den Akker, J.J.H., Viglione, A., Blöschl, G., 2017. Land use change impacts on floods at the catchment scale: Challenges and opportunities for future research. Water Resour. Res., 53, 7, 5209–5219. DOI: 10.1002/2017WR020723.

Rozalis, S., Morin, E., Yair, Y., Price, C., 2010. Flash flood prediction using an uncelebrated hydrological model and radar rainfall data in a Mediterranean watershed under changing hydrological conditions. Journal of Hydrology, 394, 245–255.

Sorooshian, S., Duan, Q., Gupta, V.K., 1993. Sthocastic parameter estimation procedures for hydrologic rainfall-runoff models: Correlated and heteroscedastic error cases. Water Resource, 29, 1185–1194.

Uchida, E., Xu, J.T., Rozelle, S., 2005. Grain for green: Cost-effectiveness and sustainability of China's Conservation Set-Aside Program. Land Economics, 81, 247–264.

Viglione, A., Merz, B., Dung, N.V., Parajka, J., Nester, T., Blöschl, G., 2016. Attribution of regional flood changes based on scaling fingerprints. Water Resour. Res., 52, 5322–5340.

Voss, R., May, W., Roeckner, E., 2002. Enhanced resolution modelling study on anthropogenic climate change: changes in extremes of the hydrological cycle. International Journal of Climatology, 22, 755–777.

Wagener, T., McIntyre, N., Lees, M.J., Wheater, H.S., Gupta, H.V., 2003. Towards reduced uncertainty in conceptual rainfall-runoff modeling: Dynamic identifiability analysis. Hydrol. Processes, 17, 455–476.

Wagener, T., 2007. Can we model the hydrological impacts of environmental change? Hydrol. Processes, 21, 3233– 3236.

Wagener, T., Sivapalan, M., Troch, P.A., McGlynn, B.L., Harman, C.J., Gupta, H.V., Kumar, P., Rao, P.S.C., Basu, N.B., Wilson, J.S., 2010. The future of hydrology: An evolving science for a changing world. Water Resour. Res., 46, W05301.

Wallner, M., Haberlandt, U., 2015. Non-stationary hydrological model parameters: a framework based on SOM-B. Hydrological Processes, 29, 3145–3161.

Wan, R., Shan, G., 2004. Progress in the hydrological impact and flood response of watershed land use and land cover change. Journal of Lake Science, 16, 3, 258–264.

Wang, T., Istanbulluoglu, E., Wedin, D., Hanson, P., 2015. Impacts of devegetation on the temporal evolution of soil saturated hydraulic conductivity in a vegetated sand dune area. Environmental Earth Sciences, 73, 1–10.

Yang, X., Ren, L., Yong, B., Wei, Z., 2008. The impact of land use change on hydrological cycle at a semiarid headwater catchment in north china. In: Education Technology & Training & International Workshop on Geoscience & Remote, 2, pp. 508–512.

Yüksek, T., Göl, C., Yüksek, F., Yüksel, E.E., 2009. The effects of land-use changes on soil properties: the conversion of alder coppice to tea plantations in the humid northern Black Sea region. African Journal of Agricultural Research, 4, 665–674.

Zhang, Y., Guan, D., Jin, C., Wang, A., Wu, J., Yuan, F., 2014. Impacts of climate change and land use change on runoff of forest catchment in northeast China. Hydrological Processes, 28, 186–196.

Zhao, R.J., 1992. The Xinanjiang model applied in China. Journal of Hydrology, 135, 371–381. (In Chinese with English abstract.)

Received 3 June 2019
Accepted 8 February 2020

J. Hydrol. Hydromech., 68, 2020, 2, 111–118
DOI: 10.2478/johh-2020-0007
ISSN 1338-4333

sciendo Journal of Hydrology and Hydromechanics

Simultaneous determination of wettability and shrinkage in an organic residue amended loamy topsoil

Steffen Beck-Broichsitter[1*], Saskia Ruth[2], Richard Schröder[2], Heiner Fleige[2], Horst H. Gerke[1], Rainer Horn[2]

[1] Research Area 1 "Landscape Functioning", Leibniz Centre for Agricultural Landscape Research (ZALF), Eberswalder Str. 84, 15374 Müncheberg, Germany.
[2] Institute of Plant Nutrition and Soil Science, Christian-Albrechts-University Kiel, Hermann-Rodewaldstr. 2, 24118 Kiel, Germany.
[*] Corresponding author. Tel.: +49 33432 82412. E-mail: steffen.beck-broichsitter@zalf.de

Abstract: In agricultural land use, organic residues such as compost, digestate, and sewage sludge are discussed as cost-effective soil conditioner that may improve the water holding capacity and crop available soil moisture. The objective of this study is to determine the effect of application of digestates with different compositions in maize, sugar beet and winter wheat, compost of shrub debris and sewage sludge on shrinkage behaviour and contact angle of till-derived loamy topsoil of a Haplic Luvisol under agricultural use. Novelty is the simultaneous determination of contact angle and shrinkage of soils amended with digestates composed of different composition in maize, sugar beet and winter wheat, compost of shrub debris and sewage sludge. The results suggest that the application of organic residues impacts the air capacity, while the contact angles remained in the subcritical range between > 0° and < 90°. The relationship between CA values and moisture ratios, ϑ, during proportional shrinkage was positive and linear (r^2 of 0.98) and negative during residual- and zero-shrinkage (r^2 of 0.93).

Keywords: Luvisol; Organic residues; Contact angle; Wettability; Shrinkage.

INTRODUCTION

Organic residues like aerobically composted or anaerobically digested organic materials and sewage sludge are used as organic fertilizers in agriculture (Risberg et al., 2017; Voelkner et al., 2015) and soil structure conditioner in post-mining landscapes (Beck-Broichsitter et al., 2018b).

Apart from the positive effects of the organic residues on soil properties and functions, the critical impact of organic residues, consisting of hydrophobic substances (humic fulvic or long-chained fatty acids) and hydrophobic functional groups (i.e., Ruggieri et al., 2008), on the soil wettability should also be considered. Interactions between organic matter-containing soil matrix and organic residues can modify soil wettability (i.e., Goebel et al., 2007), especially through volatile fatty acids containing anaerobically attended residues (Risberg et al., 2017) which cause hydrophobic soil conditions (Goebel et al., 2007). In particular, the adsorption of humic acids to mineral particles of sand-dominated soils with low specific surfaces results in higher contact angles and therefore an increase in hydrophobic behaviour (i.e., Wang et al., 2010).

Under dry conditions, the application of organic residues may decrease the wettability of topsoil surface due to an increased hydrophobicity of the soil organic matter (i.e., Vogelmann et al., 2013) that in combination with shrinkage-induced soil crack formation can enhance preferential flow (Gerke, 2006). When bypassing the lower permeable soil matrix through cracks (Bebej et al., 2017), the soil's filtering function is strongly reduced and preferentially transported organic residue solutes containing plant nutrients can negatively impact the ground water quality (Kodešová et al., 2012; Köhne et al., 2009), while at the same time the plant nutrient supply can be deficient.

The soil shrinkage curve is the relation between the void ratio, e, and the moisture ratio, ϑ, and can be divided into four characteristic stages: structural-, proportional-, residual-, and zero shrinkage (Braudeau, et al., 2004; Peng and Horn, 2005; Peng and Horn, 2013) and into a capillary-affected and an adsorption-affected region (i.e., Lu and Dong, 2016). The definition of residual- and zero-shrinkage is that the soil volume loss is negligibly smaller than the water volume loss (Beck-Broichsitter et al., 2018b; Braudeau et al., 2004). The residual- and zero-shrinkage phase in the range of low moisture ratios, ϑ, is of major interest for the contact angles, CA, and therefore the wettability of intact soil surfaces (Chen and Ning, 2018), because a reduced water adsorption capability of intact crack surfaces may intensify the preferential flow through shrinkage cracks (i.e., Kodešová et al., 2011; Leue et al., 2015).

The impact of organic residues and its organic matter composition on soil chemical properties has already been evaluated (i.e., Fér et al., 2016; Kodešová et al., 2011, 2012; Voelkner et al., 2015), and the application of for example compost can have a positive effect on air capacity and water holding capacity of soils (Beck-Broichsitter et al., 2018b), but a lack of information in case of the impact on physical properties and especially the shrinkage behaviour is still existing.

The objective of this study is to determine the effect of application of digestates with different compositions in maize, sugar beet and winter wheat, compost of shrub debris and sewage sludge on shrinkage behaviour and contact angle of till-derived loamy topsoil (Ap-horizon, 0–0.2 m depth) of a Haplic Luvisol under agricultural use.

The authors hypothesized that the application of organic residues on loamy topsoil can increase the air capacity and plant available water capacity, and can lower the shrinkage crack formation tendency and the contact angles especially in the low moisture ratio range.

MATERIALS AND METHODS

Sample preparation and laboratory analysis

Soil material was sampled from the topsoil (Ap-horizon, 0–0.2 m depth) of a Haplic Luvisol (Ap/E/Bt/Bw/C) (IUSS Working Group WRB, 2014), derived from glacial till, located at the research farm in Hohenschulen (54°31'28"N, 9°98'35"E), near Kiel (Schleswig Holstein) in Northern Germany. Organic residues in form of shrub-derived compost (C), sewage sludge (S), and three digestates consisting of (i) 80% maize and 20% sugar beet (80M20B), (ii) 20% maize and 80% sugar beet (20M80B), (iii) 20% winter wheat and 80% sugar beet (20W80B) were used for application to the till-derived loam (L).

At first, organic residues were air-dried, sieved (≤ 2 mm) and then mechanically mixed with the loam (θ of approx. 0.1 cm^3 cm^{-3}) to simulate the common annual application rates per hectare for fertilizer in 0.2 m topsoil with 30 Mg dry mass ha^{-1} for compost and 30 m^3 moist mass ha^{-1} for digestates and sewage sludge. After application of the organic residues, the organic carbon content, OC (g kg^{-1}), (by coulometric carbon dioxide measurement), soil texture (by combined sieve and pipette method), and soil pH values (in 0.01M $CaCl_2$ solution) were analysed for more details see Hartge and Horn (2016).

In a second step, the loam and loam-residue-mixtures were compacted to a dry bulk density, ρ_b, of 1.45 g cm^{-3} with a load frame (Instron 8871, Norwood, USA) with pressing force of 5 kN, resulting in 8–10 density-defined soil cores (diameter: 5.5 cm, height: 5 cm), each.

Contact angle measurements

The contact angle, CA, was determined by the sessile drop method through application of a water droplet on surfaces of soil cores with 8–10 repetitions for loam and loam-residue mixtures each for pressure heads, h, of –60 hPa, –300 hPa, –15000 hPa, and oven-dried at 105°C, respectively (Figure 1).

The CA was determined with CCD-equipped contact angle microscope (OCA 15, DataPhysics, Filderstadt, Germany) and the placement of 2 µg of water (5 repetitions on identic points per drying stage) was recorded by a highspeed camera allowing the evaluation of the CA (resolution: 0.1°) with SCA20 program (DataPhysics, Filderstadt, Germany). The contact angle, CA (°), was calculated following Bachmann et al. (2013) in the first five seconds after drop placement on the soil surface:

$$CA = \arccos\left(\frac{\sigma_S - \sigma_{SL}}{\sigma_L}\right) \quad (1)$$

where σ_S is the surface energy of the solid (J m^{-2}), σ_{SL} is the solid-liquid interfacial energy (J m^{-2}), and σ_L is the surface tension of the liquid (J m^{-2}). The CA can be classified as follows: CA = 0° indicates complete wettability of the surface, 0° > CA < 90° = subcritical, subhydrophilic material, CA > 90° = hydrophobic material and CA = 160° indicates super hydrophobic material (i.e., Lamparter et al., 2006).

Soil water retention and shrinkage measurements

The volumetric water content, θ, for the prepared soil cores with 8–10 repetitions for loam and loam-residue mixtures with ρ_b values of 1.45 g cm^{-3} each were determined by a combined pressure plate (saturated, –60, –300 hPa) and ceramic vacuum outflow method (–15000 hPa) as well as oven-dried for 24 hours at 105°C, respectively. Simultaneously, the soil volume change was determined with the 3D laser triangulation method (Beck-Broichsitter et al., 2018a, 2020; Seyfarth et al., 2012). In brief, the line laser CMS 106 with λ = 660 nm (Control Micro Systems, Orlando, FL, USA) illuminates a soil core along the cylindrical surface (rotation centre at the z-axis), depending on the scan area. During the rotation process, a CCD camera captures a predefined number of profiles, while the camera

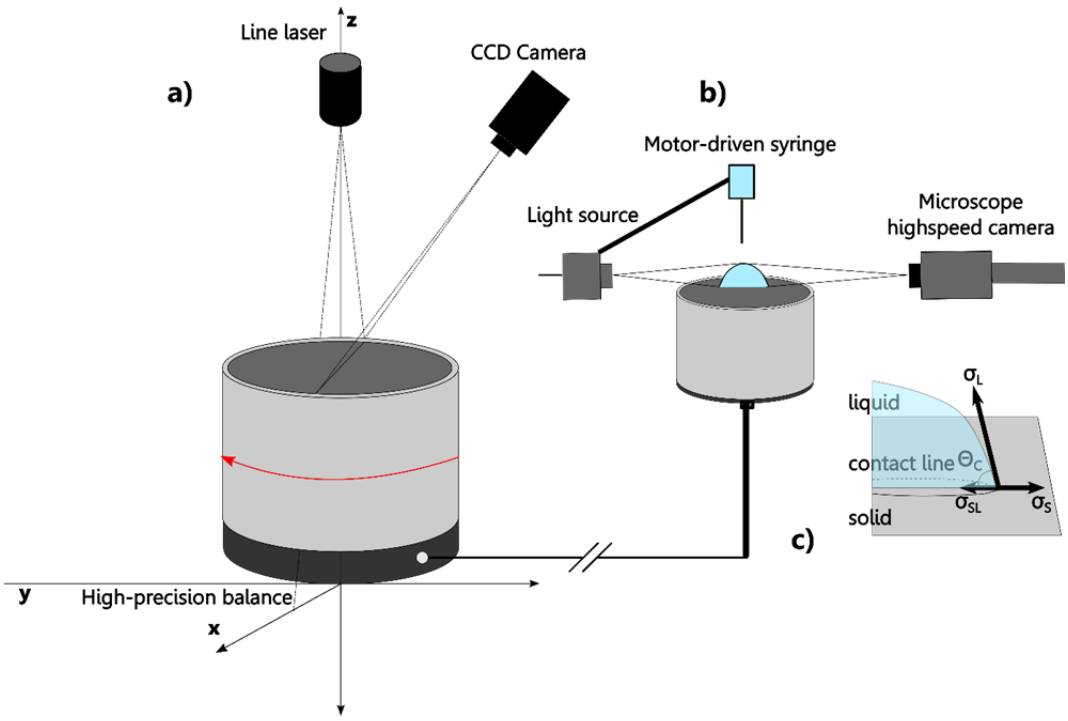

Fig. 1. Experimental setup for a) automatic determination of contact angle, CA, of intact soil surfaces through sessile liquid drop method, and b) concept of equlilibrium contact angle, Θ_C, and three-phase contact line between solid, liquid and gas phase.

is provided with a band-pass filter to segregate the laser signal (highlighted profile) in the captured image from the background (Figure 1).

The soil porosity, ε, was calculated as:

$$\varepsilon = 1 - \frac{\rho_b}{\rho_s} \quad (2)$$

where ρ_s is solid particle density and ρ_b the bulk density of the soil. For ρ_s, a value of 2.65 g cm^{-3} was assumed for the sand-dominated loamy soil. From the observed water retention data, the air capacity, AC (cm^3 cm^{-3}), and the plant available water capacity, AWC (cm^3 cm^{-3}), were calculated as follows:

$$AC = \varepsilon - \theta_{-60hPa} \quad (3)$$

$$AWC = \theta_{-60hPa} - \theta_{-15000hPa} \quad (4)$$

where $\theta_{-60\ hPa}$ and $\theta_{-15000\ hPa}$ correspond to the water content at pressure heads of –60 hPa and –15000 hPa.

The soil shrinkage curve is generally divided into four phases (Figure 2): structural-, proportional-, residual-, and zero shrinkage (i.e., Braudeau et al., 2004). The shrinkage limit points e_{ae} and ϑ_{ae} of Eq. (9) indicate the air entry point or rather the beginning of residual shrinkage. This means that the soil volume loss and decrease in void ratio, e, during dehydration is lower than the water volume loss and decrease in moisture ratio, ϑ, while zero-shrinkage describes a more or less remaining soil volume or void ratio in spite of decreasing moisture ratio (Peng and Horn, 2005, 2013).

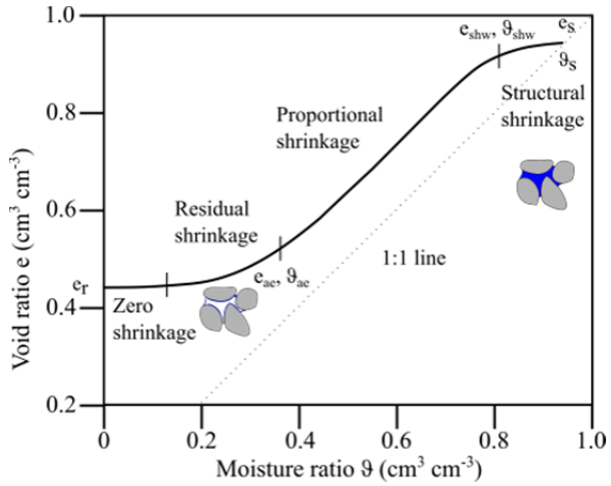

Fig. 2. Conceptual model of soil shrinkage curve with four characteristic shrinkage regions: structural-, proportional-, residual-, and zero shrinkage, while e_s and ϑ_s are the saturated void and moisture ratio, respectively, and e_r is the residual void ratio.

These soil shrinkage curves are defined by the relation between the void ratio, e (cm^3 cm^{-3}), and the moisture ratio, ϑ (cm^3 cm^{-3}), following Hartge and Horn (2016):

$$e = \frac{\rho_s}{\rho_b} - 1 \quad (7)$$

$$\vartheta = \rho_s \theta_m \quad (8)$$

where ρ_s, ρ_b, and θ_m are the particle and bulk density (g cm^{-3}), and gravimetric water content (g g^{-1}), respectively.

The model of Peng and Horn (2005) was selected in this study to describe the shrinkage curve as:

$$e(\vartheta) = \begin{cases} e_r & \vartheta = 0 \\ e_r + \dfrac{e_s - e_r}{\left[1 + (\chi\vartheta)^{-p}\right]^q} & 0 \le \vartheta \le \vartheta_s;\ n > 0 \\ e_s & \vartheta = \vartheta_s \end{cases} \quad (9)$$

where χ, p, and q are dimensionless fitting parameters, e_s and e_r are the saturated and residual void ratios, respectively, fulfilling the following boundary conditions:

$$\vartheta \to 0;\ \frac{\vartheta}{e_s - \theta} \to 0;\ e \to e_s \quad (10)$$

$$\vartheta \to \vartheta_s;\ \frac{\vartheta}{e_s - \vartheta} \to \infty;\ e \to e_s \quad (11)$$

The volume shrinkage index, ΔV, describes the shrinkage tendency of differently-textured soils as follows (Alaoui et al., 2011):

$$\Delta V = \frac{V_{0hPa}}{V_{105°C}} - 1 \quad (12)$$

where ΔV is the change in soil volume as relation between the quasi-saturated (0 hPa) and the dry stage (105°C), while ΔV < 5% corresponds to good, ΔV = 5–10% to medium, and ΔV > 10% to poor shrinkage tendency.

Statistical analysis

The statistical software R (R Development Core Team, 2014) was used to evaluate the data. The data were tested for normal distribution and heteroscedastic on the Shapiro-Wilk-Test and graphical residue analysis. An analysis of variance (ANOVA) was conducted with $p < 0.05$ followed by Tukey`s HSD (honesty significant difference) test (*$p \le 0.05$, **$p \le 0.01$, ***$p \le 0.001$, ****$p \le 0.0001$) following Hasler and Horton (2008) to evaluate the differences between loam and the loam-residue-mixture in air capacity, AC, plant available water capacity, AWC, contact angle, CA, volume shrinkage index, ΔV and their interaction terms (two- fold and three-fold), respectively. The coefficient of determination (r^2) was used as an index for the goodness of fit.

RESULTS

Soil water retention characteristics after application of organic residues

The soil material before application of organic residues was classified as loam following FAO (2006) with 550 g kg^{-1} sand, 300 g kg^{-1} silt, and 150 g kg^{-1} clay and an organic carbon content of 12 g kg^{-1}, and weak acidic pH value of 6.8. The applicated organic residues are characterised by alkaline pH values between 7.5 and 8.1 (Table 1) and nitrogen contents between 1.2 and 4.0 kg m^{-3}.

The OC content of the loam was improved through organic residue application (12.4 g kg^{-1} up to 14.3 g kg^{-1}); there are small differences in pH values between 6.6 and 6.9, while compost application increases and digestate application decreases the pH value (Table 2).

Table 1. Basic properties considering pH values, dry matter, dm, and nitrogen, N_{total}, of shrub-derived compost (C), sewage sludge (S), and three digestates: (i) 80% maize and 20% sugar beet (80M20B), (ii) 20% maize and 80% sugar beet (20M80B), (iii) 20% winter wheat and 80% sugar beet (20W80B) with two repeated measurements each and symbol ± corresponds to the standard deviation.

Parameters	C	S	80M20B	20M80B	20W80B
pH_{CaCl2} (–)	8.1 ± 0.6	7.5 ± 0.3	7.7 ± 0.3	7.7 ± 0.3	7.8 ± 0.4
dm (%)	52 ± 4	n.a.	5.5 ± 0.2	5.4 ± 0.3	5.4 ± 0.1
N_{total} (kg m^{-3} om^{-1})	1.2 ± 0.2	4.0 ± 0.3	2.8 ± 0.1	2.9 ± 0.2	2.3 ± 0.1

dm: dry matter, om: organic matter, n.a.: not analysed

Table 2. Soil characteristics considering pH values and organic carbon, OC, after the application of shrub-derived compost (C), sewage sludge (S), and three digestates: (i) 80% maize and 20% sugar beet (80M20B), (ii) 20% maize and 80% sugar beet (20M80B), (iii) 20% winter wheat and 80% sugar beet (20W80B) to the loam (L), mean values with two repeated measurements each and symbol ± corresponds to the standard deviation. AC = air capacity, AWC = available water capacity. Differences in mean values compared to loam were significant at $p < 0.05$ (*), < 0.01 (**), < 0.001 (***), < 0.0001 (****) for ANOVA.

Parameters	L	C	S	80M20B	20M80B	20W80B
pH_{CaCl2} (–)	6.79 ± 0.3	6.87 ± 0.3	6.75 ± 0.3	6.62 ± 0.4	6.59 ± 0.6	6.65 ± 0.3
OC (g kg^{-1})	12.4 ± 1.4	13.5 ± 1.9	12.2 ± 1.1	14.1 ± 1.7	14.3 ± 1.5	13.2 ± 1.2
AC (cm^3 cm^{-3})	0.149	0.166	0.168	0.152	0.203***	0.122
AWC (cm^3 cm^{-3})	0.145	0.115**	0.124	0.133	0.114****	0.149

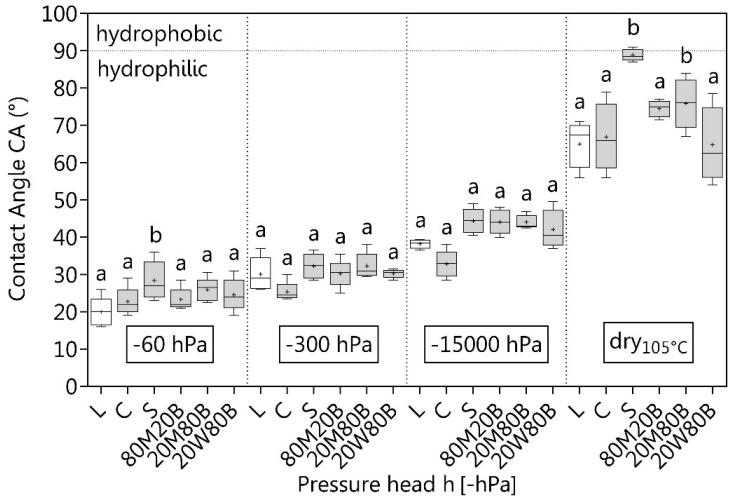

Fig. 3. Contact angles, CA, with 8–10 repeated measurements each at –60 hPa, –300 hPa, –15000 hPa and in dry stage (105°C). Different small letters indicate statistically differences in mean values at $p < 0.05$ for shrub-derived compost (C), sewage sludge (S), and three digestates: (i) 80% maize and 20% sugar beet (80M20B), (ii) 20% maize and 80% sugar beet (20M80B), (iii) 20% winter wheat and 80% sugar beet (20W80B) compared to the loam (L) for each stage, respectively.

The application of organic residues increased the air capacity of up to 0.203 cm^3 cm^{-3} for 20M80B while the plant available ater capacities decreased after application of organic residues, except for 20W80B (Table 2).

Soil wettability after application of organic residues

The loam and the added organic residues show contact angles, CA, > 0° and ≤ 90°, thus, the intact soil sample surfaces are characterised by subcritical hydrophilic conditions (Figure 3). The four dehydration stages show a relatively unique increase in CA through digestate application with no clear tendency between the differently composed digestates, while the sewage sludge is close to hydrophobic contact angles > 90° in the dry stage (105°C).

Shrinkage behaviour after application of organic residues

The loam-residue mixtures show comparatively higher void ratios than the untreated loam soil (Figure 4) and considering the maximum of the curve at the wet-side (ϑ_{shw}, e_{shw}) obtained with Eq. (9) (Table 3), the soil material shows a proportional volume and water loss with beginning of dehydration without structural shrinkage. The air entry point (ϑ_{ae}, e_{ae}), which separates the proportional shrinkage from the residual shrinkage indicates a more distinct residual than proportional shrinkage phase, except for loam and digestate (80M20B), respectively. The volume shrinkage indices indicated a low shrinkage tendency between 1.8% and 3.7%, while the loam-compost-mixture significantly increased the shrinkage tendency compared to the untreated loam.

The shrinkage model in Eq. (9) fitted the observed shrinkage data with r^2 between 0.97 and 0.99 (Table 3). The fitting pa-

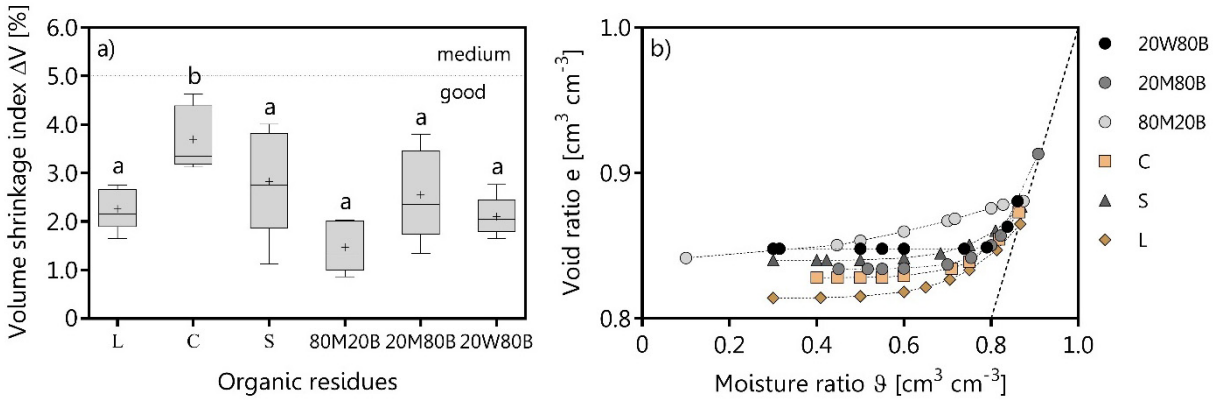

Fig. 4. a) volume shrinkage indices with boundary (ΔV = 5%) between good and medium shrinkage tendency and b) fitted shrinkage curves obtained by Eq. (9) after application of organic residues with 8–10 repeated measurements each (symbols). Different small letters indicate statistically differences in mean values at $p < 0.05$ for shrub-derived compost (C), sewage sludge (S), and three digestates: (i) 80% maize and 20% sugar beet (80M20B), (ii) 20% maize and 80% sugar beet (20M80B), (iii) 20% winter wheat and 80% sugar beet (20W80B) compared to the loam (L) for each stage, respectively.

Table 3. Parameter fits from the mean of 8–10 data points of the loam (L) and loam-residue-mixtures considering shrub-derived compost (C), sewage sludge (S), and three digestates: (i) 80% maize and 20 % sugar beet (80M20B), (ii) 20% maize and 80% sugar beet (20M80B), (iii) 20% winter wheat and 80% sugar beet (20W80B) obtained with Eq. (9); χ, p, q are dimensionless fitting parameters, e_{shw} and ϑ_{shw} indicate void and moisture ratio at the transition between the structural and proportional shrinkage, e_{ae} and ϑ_{ae} indicate void and moisture ratio at the transition between the proportional and residual shrinkage. The coefficient of determination (r^2) was used as an index for the goodness of fit.

Parameter	χ (–)	p (–)	q (–)	r^2 (–)		e_{shw}, ϑ_{shw} ($cm^3\ cm^{-3}$)	e_{ae}, ϑ_{ae} ($cm^3\ cm^{-3}$)
L	1.137	479.6	0.014	0.99	ϑ	0.880	0.498
					e	0.870	0.843
C	1.153	714.8	0.014	0.98	ϑ	0.868	0.859
					e	0.875	0.869
S	1.137	609.7	0.014	0.97	ϑ	0.879	0.869
					e	0.881	0.877
80M20B	1.116	284.4	0.007	0.97	ϑ	0.896	0.579
					e	0.885	0.859
20M80B	1.097	889.5	0.014	0.99	ϑ	0.907	0.889
					e	0.913	0.895
20W80B	1.196	279.4	1.615	0.99	ϑ	0.846	0.833
					e	0.879	0.853

rameter χ was on a relatively low level and also nearly identical for loam and the loam-residue-mixtures, thus, the volume and water loss in the structural shrinkage phase and therefore the structural shrinkage phase itself was of minor importance in case of initially homogenized soil samples.

Relationship between wettability and shrinkage behaviour

In terms of the wettability, the results indicate a strong negative relationship between the contact angles, CA, and the shrinkage-derived moisture ratio, ϑ, of the loam and loam-residue-mixtures ($r^2 \geq 0.95$). The lower the moisture ratio the higher is the contact angle (Figure 5).

The linear functions in Figure 5 were used for predicting the contact angles, CA*, on the basis of the fitted moisture ratios, ϑ, and the results indicate a strong positive relationship between ΔCA* and Δϑ* values during proportional shrinkage phase (e_s–e_{ae}, ϑ_s–ϑ_{ae}) with r^2 of 0.98 and strong negative relationship between CA and ϑ values at transition point between proportional and residual shrinkage (e_{ae}, ϑ_{ae}) with r^2 of 0.93 (Figure 6). Thus, the more pronounced the proportional shrinkage phase and the lower the moisture ratio at beginning of the residual shrinkage phase, the higher is the contact angle.

DISCUSSION

Air capacity and plant available water capacity after application of organic residues

The results indicate higher organic carbon contents after application of organic residues of up to 14.3 g kg^{-1} compared to the untreated loam with 12.4 g kg^{-1} as proposed by Ojeda et al. (2015), while the lower OC content of sewage sludge is related to the thermal treatment of wastewater, whereby ammonia can be volatilized.

The results also indicate higher air capacities, AC, of up to 0.203 $cm^3\ cm^{-3}$ for digestate 20M80B compared to 0.149 $cm^3\ cm^{-3}$ of the untreated loam in Table 2 as hypothesised before. The increase in AC values is in agreement with findings of

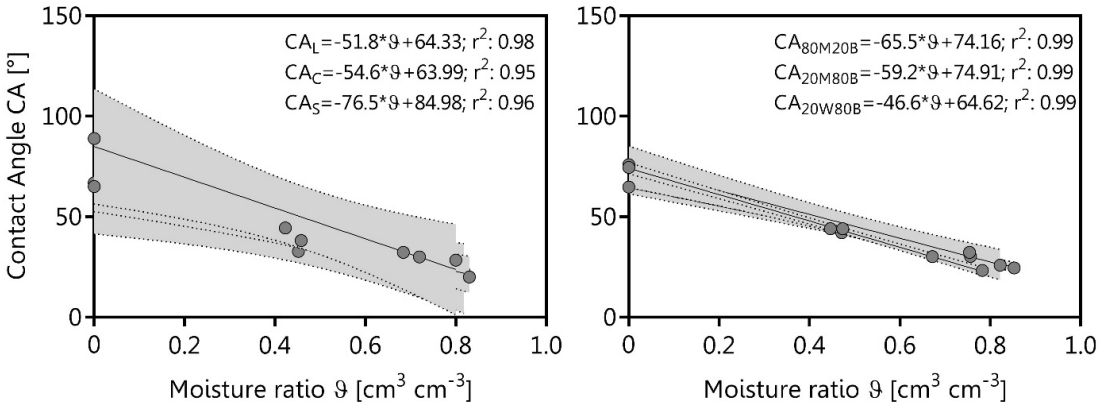

Fig. 5. Linear regression of mean values of observed contact angle, CA, and moisture ratios, ϑ, after application of shrub-derived compost (C), sewage sludge (S), and three digestates: (i) 80% maize and 20% sugar beet (80M20B), (ii) 20% maize and 80% sugar beet (20M80B), (iii) 20% winter wheat and 80% sugar beet (20W80B) compared to the loam (L). The r^2 indicates the coefficient of determination and the dashed lines indicate the confidence limits for a level of 95%.

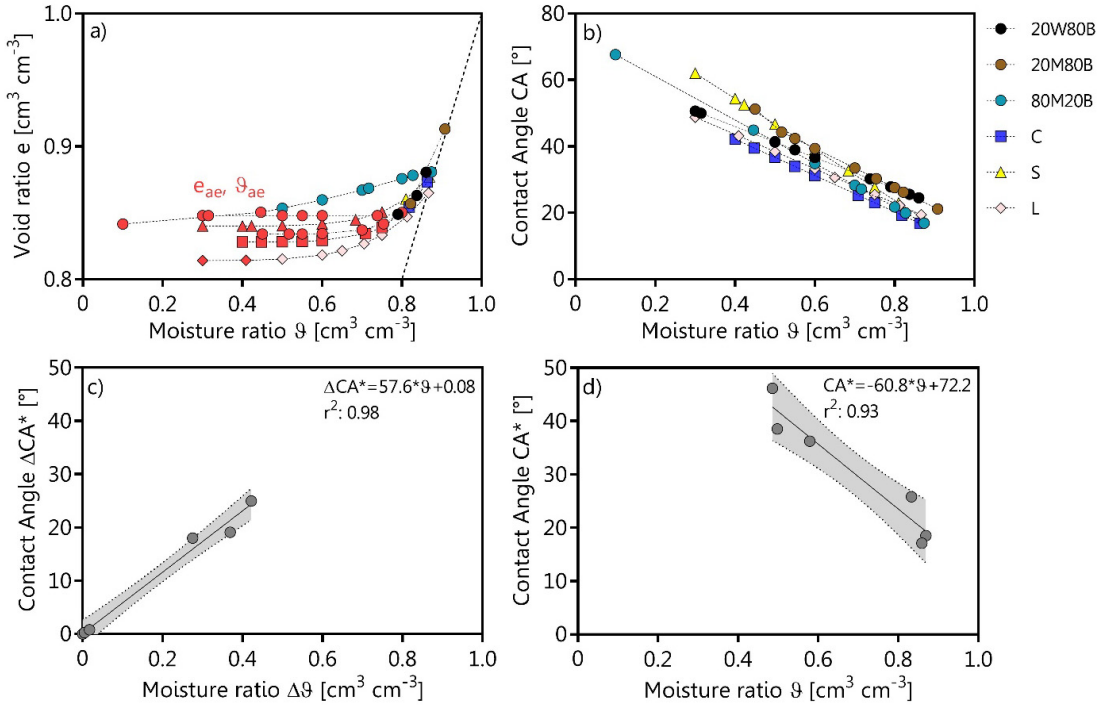

Fig. 6. a) fitted shrinkage curves on the basis of Eq. (9) with e_{ae} and ϑ_{ae} (red symbols) as transition points between proportional and residual shrinkage; b) contact angles, CA*, as function of fitted moisture ratios, ϑ, of shrub-derived compost (C), sewage sludge (S), and three digestates: (i) 80% maize and 20% sugar beet (80M20B), (ii) 20% maize and 80% sugar beet (20M80B), (iii) 20% winter wheat and 80% sugar beet (20W80B) and loam (L); c) change, Δ, of CA* and ϑ during proportional shrinkage phase (e_s–e_{ae}, ϑ_s–ϑ_{ae}); d) CA* values at transition point between proportional and residual shrinkage phase (e_{ae}, ϑ_{ae}) see Table 3. The r^2 indicates the coefficient of determination and the dashed lines indicate the confidence limits for a level of 95%.

Ojeda et al. (2015) and a positive effect on AC values was also shown for highly compacted soils ($\rho_b \geq 1.8$ g cm^{-3}), where the application of compost compensated low AC values (Jasinska et al., 2006; Beck-Broichsitter et al., 2018b). The plant available water capacities, AWC, in Table 2 were equal (20W80B) or lower than the AWC value of the untreated loam of 0.145 cm^3 cm^{-3} which is in contrast to findings of Beck-Broichsitter et al. (2018b).

Impact of organic residues on soil wettability

The results indicate that the contact angle of the untreated loam was not seriously affected by the organic-residue mixtures as hypothesized before, but with decreasing moisture ratios, ϑ, during dehydration of the soil samples from –60 hPa to oven-dried state, the CA values ranged between > 0° and < 90° and can be characterised as subcritical hydrophilic, resulting in a reduced wettability (Lamparter et al., 2006; Goebel et al., 2007).

It should be taken into account that the impact of the soil organic matter on the contact angles is less examined, while especially aliphatic and nonpolar C–H groups can make up a significant portion of the soil organic matter (Kodešová et al., 2012). Considering the potential wettability index analysis (PWI: C–H/C=O ratio) of Fér et al. (2016), these groups may lower the wettability on aggregate surfaces. However, the results of

Leue et al. (2015) indicate that the wetter the soil core surface, the less pronounced is the effect of SOM on surface contact angles and therefore the mm-scale variability of soil wettability (Hallett et al., 2004). In this case, the field situation with annual average pressure heads between –60 hPa and –300 hPa are realistic for agricultural-used topsoils, thus, there is only a less pronounced tendency pointing out the negative impact of applied organic residues on the soil surface wettability.

Interaction between shrinkage and wettability

The soil shrinkage curves are displayed only with proportional-, residual-, and zero-shrinkage phases that is typical for initially homogenized soil material (Beck-Broichsitter et al., 2018a; Peng and Horn, 2013). The results in Figure 4 indicate a low shrinkage tendency with ΔV values between 1.8% and 3.7% compared to ΔV values of 2.3% of landfill topsoil layer (0.05 m; 12 g kg^{-1} OC) after application of compost (Beck-Broichsitter et al., 2018a). Thus, the application of the presented organic residues not necessarily reduced the shrinkage crack formation tendency of untreated loam (ΔV = 2.2%) as hypothesized before (iii). The overall ΔV values < 5% in Figure 4 indicate a reduced shrinkage crack tendency of organic residues that can prevent deeper shrinkage cracks in drier periods (Horn et al., 2014) thus limiting the potential of preferential leaching of plant nutrients through soil macropores.

The shrinkage model of Peng and Horn (2005) fitted the observed void ratios, e, and moisture ratios, ϑ, well with $r^2 \geq 0.96$ in Table 3 and the contact angles were also well predicted through fitted ϑ values with $r^2 \geq 0.95$ (Figure 5). Therefore, it seems as if we can regression-based predict contact angles especially in the low moisture ratio range. The evaluation of the contact angles in the proportional shrinkage phase where a proportional loss in soil and water volume is assumed (i.e., Bradeau et al., 2004) is essential for ϑ values in the residual- and zero-shrinkage phase that is of major interest for the wettability of intact soil core surfaces (e.g, Goebel et al., 2007).

Thus, untreated loam and digestates consisting of maize and sugar beet are of special interest because of its more pronounced proportional shrinkage behaviour and reduced ϑ values in the dry range that may intensify the infiltration through shrinkage cracks in deeper soil layers (Gerke, 2012; Kodešová et al., 2011, 2012) compared to compost, sewage sludge and wheat-derided digestate (20W80B). In a positive way, intense shrinkage cracks can also reduce potential surface runoff and soil erosion by increasing infiltration (Horn et al., 2014).

CONCLUSION

The objective of the study was to determine the effect of application of digestates with different composition in maize, sugar beet and winter wheat, compost of shrub debris and sewage sludge on shrinkage behaviour and contact angle of till-derived loamy topsoil of a Haplic Luvisol under agricultural use.

The contact angle of the loam was not affected by application of the organic-residues, and the contact angles remained in the range between >0° and <90° indicating subcritical hydrophobic conditions, while the shrinkage crack formation tendency of untreated loam was not necessarily lowered. The combined determination of shrinkage behaviour and contact angles enabled a regression-based predicting of contact angels especially in the low moisture ratio range.

For a more quantitative relation between soil cracking, drying, and wettability, studies on the impact of shrinkage regime on wettability should focus on the finer-textured soils and include field conditions.

Acknowledgements. This research was supported by the Innovation Foundation Schleswig-Holstein and the ZMD Rastorf GmbH, Germany. The authors thank the technicians Ines Schütt and Sabine Hamann (University of Kiel) for supporting the soil chemical and physical analysis.

REFERENCES

Alaoui, A., Lipiec, J., Gerke, H.H., 2011. A review of the changes in the soil pore system due to soil deformation: A hydrodynamic perspective. Soil Till Res., 115–116, 1–15.

Bachmann, J., Woche, S.K., Goebel, M.O., 2013. Small-scale contact angle mapping on undisturbed soil surfaces. J. Hydrol. Hydromech., 61, 3–8.

Bebej, J., Homolák, M., Orfánus, T., 2017. Interaction of Brilliant Blue dye solution with soil and its effect on mobility of compounds around zones of preferential flows at spruce stand. Dent. Eur. For. J., 63, 79–90. DOI: 10.1515/forj-2017-0020.

Beck-Broichsitter, S., Gerke, H.H., Horn, R., 2018a. Shrinkage characteristics of boulder marl as sustainable mineral liner material of landfill capping systems. Sustainability, 10, 4025.

Beck-Broichsitter, S., Fleige, H., Horn, R., 2018b. Compost quality and its function as a soil conditioner of recultivation layers – a critical review. Int. Agrophys., 32, 11–18.

Beck-Broichsitter, S., Fleige, H., Gerke, H.H., Horn, R., 2020. Effect of artificial soil compaction in landfill capping systems on anisotropy of air-permeability. J. Plant. Nutr. Soil Sci., 1–11. DOI: 10.1002/jpln.201900281.

Braudeau, E., Frangi, J.P., Mothar, R.H., 2004. Characterizing non-rigid dual porosity structured soil medium using its characteristic SC. Soil Sci. Soc. Am. J., 68, 359–370.

Chen, P., Ning, L., 2018. Generalized equation for soil shrinkage curve. J. Geotech. Geoenviron., 144, 8, 04018046.

FAO, 2006. Guidelines for soil profile description. 4th edition. Land and water development division. Rome, Italy.

Fér, M., Leue, M., Kodešová, R., Gerke, H.H., Ellerbrock, R.H., 2016. Droplet infiltration dynamics and soil wettability related to soil organic matter of soil aggregate coatings and interiors. J. Hydrol. Hydromech., 64, 111–120.

Gerke, H.H., 2006. Preferential flow descriptions for structured soils. J. Plant Nutr. Soil Sci. 169, 382–400. DOI: 10.1002/jpln.200521955.

Gerke, H.H., 2012. Macroscopic representation of the interface between flow domains in structured soil. Vadose Zone J., 11, 3. DOI: 10.2136/vzj2011.0125.

Goebel, M.-O., Woche, S.K., Bachmann, J., Lamparter, A., Fischer, W.R., 2007. Significance of wettability-induced changes in microscopic water distribution for soil organic matter decomposition. Soil Sci. Soc. Am. J., 71, 5, 1593–1599.

Hallett, P.D., Nuna, N., Douglas, J.T., Young, I.M., 2004. Millimeter-scale spatial variability in soil water sorptivity: scale, surface elevation, and subcritical repellency effects. Soil Sci. Soc. Am. J., 68, 352–358.

Hartge, K.H., Horn, R., 2016. Essential Soil Physics. In: Horton, R., Horn, R., Bachmann, J., Peth, S. (Eds.): An introduction to soil processes, structure, and mechanics. Schweizerbart Science Publishers, Stuttgart, Germany, 391 p.

Hasler, M., Horton, L.A., 2008. Multiple contrast tests in the presence of heteroscedasticity. Biometrical J., 50, 793–800. DOI: 10.13140/RG.2.2.29821.36320.

Horn, R., Peng, X., Fleige, H., Dörner, J., 2014. Pore rigidity in structured soils – only a theoretical boundary condition for hydraulic properties? J. Soil Sci. Plant Nutr., 60, 3–14.

IUSS Working Group WRB, 2014. World reference base for soil resources 2006. 2nd ed. World Soil Resources Reports No. 103. FAO, Rome.

Jasinska, E., Wetzel, H., Baumgartl, T., Horn, R., 2006. Heterogeneity of physico-chemical properties in structured soils and its consequences. Pedosphere, 16, 284–296.

Kodešová, R., Jirků, V., Kodeš, V., Mühlhanselová, M., Nikodem, A., Žigová, A., 2011. Soil structure and soil hydraulic properties of Haplic Luvisol used as arable land and grassland. Soil Till. Res., 1112, 154–161.

Kodešová, R., Němeček, K., Kodeš, V., Žigová, A., 2012. Using dye tracer for visulization of preferential flow at macro- and microscales. Vadose Zone J., 11, 1–10.

Köhne J.M., Köhne, S., Simunek, J., 2009. A review of model applications for structured soils: b) Pesticide transport. J. Cont. Hydrol., 104, 36–60. DOI: 10.1016/j.jconhyd.2008.10.003.

Lamparter, A., Deurer, M., Bachmann, J., Duijnisveld, W.H.M., 2006. Effect of subcritical hydrophobicity in a sandy soil on water infiltration and mobile water content. J. Plant Nutr. Soil Sci., 169, 1, 38–46.

Leue, M., Gerke, H., Godow, S.C., 2015. Droplet infiltration and organic matter composition of intact crack and biopore surfaces from clay-illuvial horizons. J. Plant Nutr. Soil Sci., 178, 250–260.

Lu, N., Dong, Y., 2016. Correlation between soil shrinkage curve and water retention characteristics. J. Geotech. Geoenviron., 144, 8, 04017054.

Ojeda, G., Mattana, S., Àvila, A., Alcañiz, J.M., Volkmann, M., Bachmann, J., 2015. Are soil-water functions affected by biochar application? Geoderma, 249–250, 1–11.

Peng, X., Horn, R., 2005. Modeling soil shrinkage curve across a wide range of soil types. Soil Sci. Soc. Am. J., 69, 3, 584–592.

Peng, X., Horn, R., 2013. Identifying six types of soil shrinkage curves from a large set of experimental data. Soil Sci. Soc. Am. J., 77, 372–381.

R Development Core Team, 2014. R: A language and environment for statistical computing. R Foundation for Statistical Computing, Vienna, Austria.

Risberg, K., Cederlund, H., Pell, M., Arthurson, V., Schnürer, A., 2017. Comparative characterization of digestate versus pig slurry and cow manure – chemical composition and effects on soil microbial activity. Waste Manage., 61, 529–538.

Ruggieri, L., Artola, A., Gea, T., Sanchez, A., 2008. Biodegradation of animal fats in a co-composting process with wastewater sludge. Int. Biodeter Biodegr., 62, 3, 297–303.

Seyfarth, M., Holldorf, J., Pagenkemper, S.K., 2012. Investigation of shrinkage induced changes in soil volume with laser scanning technique and automated soil volume determination - A new approach/method to analyze pore rigidity limits. Soil Till. Res., 125, 105–108.

Voelkner, A., Holthusen, D., Horn, R., 2015. Influence of homogenized residues of anaerobic physicochemical properties of differently textured soils. J. Plant Nutr. Soil Sci., 178, 261–269.

Vogelmann, E.S., Reichert, J.M., Prevedello, J., Consensa, C.O.B., Oliveira, A.É., 2013. Threshold water content beyond which hydrophobic soil become hydrophilic. The role of soil texture and organic matter content. Geoderma, 209–210, 177–187.

Wang, X.Y., Zhao, Y., Horn, R., 2010. Soil wettability as affected by soil characteristics and land use. Pedosphere, 20, 43–54.

Received 14 October 2019
Accepted 31 January 2020

J. Hydrol. Hydromech., 68, 2020, 2, 119–127
DOI: 10.2478/johh-2020-0005
ISSN 1338-4333

sciendo Journal of Hydrology and Hydromechanics

Validation of friction factor predictions in vertical slurry flows with coarse particles

Artur Bartosik

Faculty of Management and Computer Modelling, Kielce University of Technology, Al. Tusiaclecia P.P. 7, 25-314 Kielce, Poland.
E-mail: artur.bartosik@tu.kielce.pl

Abstract: The paper presents validation of a mathematical model describing the friction factor by comparing the predicted and measured results in a broad range of solid concentrations and mean particle diameters. Three different types of solids, surrounded by water as a carrier liquid, namely Canasphere, PVC, and Sand were used with solids density from 1045 to 2650 kg/m^3, and in the range of solid concentrations by volume from 0.10 to 0.45. All solid particles were narrowly sized with mean particle diameters between 1.5 and 3.4 mm. It is presented that the model predicts the friction factor fairly well. The paper demonstrates that solid particle diameter plays a crucial role for the friction factor in a vertical slurry flow with coarse solid particles. The mathematical model is discussed in reference to damping of turbulence in such flows. As the friction factor is below the friction for water it is concluded that it is possible that the effect of damping of turbulence is included in the K_B function, which depends on the Reynolds number.

Keywords: Flow with coarse particles; Particle-wall stress; Modelling of vertical flow.

INTRODUCTION

Solid-liquid flow in a pipeline exists widely in the chemical and mining industry and it is still an ecological alternative when compared to traditional forms of transportation. It is well known that the size of solid particles strongly affects frictional losses in a pipeline, therefore, the first step should be to identify the particles' size and their concentration (Shook and Roco, 1991; Sumner at al., 1990; Sumner, 1992).

The transport of coarse particles, using liquid as a carrier phase, requires careful consideration and the analysis of numerous factors, such as the constitutive relation between stress and deformation, the particles' diameter, solid concentration, deposition velocity, solid and liquid properties, as well as *particle – fluid*, *particle – particle*, and *particle – wall* interactions, and also adequately matched characteristics of the pipeline and the pump (Peker and Helvaci, 2008; Wennberg, 2010; Wilson et al., 2006).

Slurry flow mainly occurs in horizontal pipelines, however, vertical hydraulic transport over long distances is of special interest in the fields of dredging and ocean mining (Van Wijk, 2016; Van Wijk et al., 2014). One of the earlier researchers dealing with solid–liquid flow in vertical pipes was Wing (1972). The author considered hydraulic transport of marine minerals from the seabed to the sea surface. The test parameters that varied were solids with particle diameters of 0.325 mm and 0.749 mm, pipes with diameters of 0.023 m and 0.048 m, bulk velocities up to 0.305 m/s, and solid concentrations by volume up to 0.30. The researcher concluded that within the parameter limits of this experiment there is no evidence to indicate that the solids being transported contribute any extra friction loss to the normal plain water friction loss associated with pipe flow.

If turbulent flow with sufficiently small solid particles is considered, i.e. particles can move freely inside the viscous sublayer, the friction process proceeds similarly to a single-phase flow (Coulson et al., 1996). When solid particles are larger than the thickness of the viscous sublayer, like coarse–dispersion slurry, their contact with the pipe wall is limited due to the emerging *lift forces* that push solid particles from the wall. Therefore, assuming there is limited contact of the solid phase with the pipe wall, it can be presumed that the wall shear stress should be similar to the flow of the carrier liquid. We know examples in the literature that in some cases the frictional head loss, in turbulent slurry flow in a vertical pipe, is similar or below that for carrier liquid. This was proven by experiments in a vertical slurry flow of sand–water mixture, conducted by Charles and Charles (1971) for d_{50} = 0.216 mm, Ghosh and Shook (1990) for d_{50} = 0.6 mm, Sumner (1992) for d_{50} = 0.47, Matousek (2005) for d_{50} = 0.37 mm, Talmon (2013) for d_{50} = 0.1–2 mm. The problem of defining the boundary above which the influence of the *solid phase – solid phase* interaction is dominant in the flow was provided by Caulet et al. (1996). Their research shows that when the solid concentration is greater than 0.20 by volume, the dominant stresses in the flow are *solid phase – solid phase*.

Shook and Bartosik conducted experimental studies of turbulent flow of slurry in a vertical pipe, with solid particles of density similar to water (ρ_P = 1045 kg/m^3), with mean solid particles diameter of d_{50} = 1.5 mm, showing that in the range of solids concentration $0 < C_V \leq 0.30$, the frictional head loss is lower than for a single-phase flow of the carrier liquid (Shook and Bartosik, 1994). Thus, it follows that a damping effect of the contact of solid particles with the pipe wall could take place. Similar experimental studies carried out for particles of identical density, but with a diameter d_{50} = 2.8 mm, showed that the frictional head losses are lower than for water only for $C_V \leq 0.10$ (Shook and Bartosik, 1994). However, for $C_V > 0.10$, the frictional head losses increased linearly and then exponentially as the solid's concentration increases. They concluded that:

– the wall friction in a turbulent vertical flow is strongly influenced by the diameter of the particles,
– in the case of flow with a sufficiently large particles diameter and particles density ($d_{50} > 1.5$ mm; $S_\rho >> 1$) and sufficiently high solid concentrations ($C_V \geq 0.20$), the importance of the transport mechanism is played by the *solid particle – pipe wall* interaction, which causes an increase of

wall shear stress when compared to carrier liquid flow.

Of course, the flow mechanism is much more complex as we know that solid particles can increase or attenuate the turbulence. Schreck and Kleis (1993) studied the movement of solid particles with a diameter of 0.65 mm, which were polystyrene and glass with a density ratio of S_ρ = 1.045 and 2.40, respectively. They used a Doppler Laser Anemometer. Their analysis showed that the solid particles follow liquid only partially, therefore, the fluctuating velocity components are smaller in relation to the carrier liquid, even when the density of the solid particles is similar to the density of the liquid. Faraj and Wang (2012) conducted laboratory experiments carried out on an open flow loop using Electrical Resistance Tomography (ERT) to interrogate the internal structure of horizontal and vertical slurry flow. They used the Fast Impedance Camera System, with a temporal resolution up to 1000 dual–frames per second. A set of experiments was carried out on coarse and medium particles of *sand–water* slurry flows with 2% and 10% throughput volumetric concentration and the transport velocity in the range of 1.5 – 5 m/s. The authors found that the coarse sand slurry flows in a plug or core flow pattern, whereas the flow of medium sand slurry demonstrated an annular-like flow pattern. Van Dijke (2010) conducted similar studies and developed a one-dimensional steady state model of the transport of differently sized solid particles in a vertical riser, which showed that concentration peaks could develop during transport. Concluding, one can say that phenomenon of slurry flow with coarse particles is very complex and still difficult for mathematical modelling of the frictional head loss. One crucial barrier for building reliable mathematical models is limited access to experimental data, especially regarding viscous and buffer layers with solid concentrations above 0.2 by volume.

If coarse-dispersed slurry flow is considered, we know that it is impossible to measure slurry viscosity as the sedimentation process is substantial. For this reason, predictions of frictional head loss assume that slurry viscosity is equal to the viscosity of the carrier liquid and the density is equal to the slurry density. For such cases, it is usually assumed that the pressure drop of a slurry with coarse particles can be determined as:

$$\left(\frac{\mathrm{d}p}{\mathrm{d}x}\right)_m = \left(\frac{\mathrm{d}p}{\mathrm{d}x}\right)_L \frac{\rho_m}{\rho_L} \tag{1}$$

From Equation (1) it follows that the density of the slurry is the main factor determining pressure losses. The difference between the pressure drop for the slurry $(\mathrm{d}p/\mathrm{d}x)_m$ and the carrier liquid $(\mathrm{d}p/\mathrm{d}x)_L$ is called the *solid phase effect*. However, with the increase of the particle diameter and/or the solid concentrations, this approach shows discrepancy between measurements and predictions.

The availability of mathematical models, which predict a vertical flow of slurry with coarse particles is very limited. For example, Krampa–Morlu et al. (2004) used CFX 4.4 (ANSYS Inc.) software to predict the velocity profiles of a turbulent slurry flow with coarse particles in an upward vertical pipeline. Two sets of sand particle diameters were used in this test: d_{50} = 0.47 mm and d_{50} = 1.7 mm, with a density of 2650 kg/m^3. The simulations were carried out for solid concentrations $0 < C_V < 0.30$. The results of numerical calculations were compared with the results of the experimental data of Sumner et al. (1990). The authors admitted that the simulation results significantly differ from the results of measurements.

The mathematical modelling of solid–liquid flow with coarse particles is still a long way from the knowledge gathered for single–phase flows (Bartosik and Shook, 1995; Messa and Malavasi, 2013; Miedema, 2015). The mathematical models, which are available in the literature, are usually not validated for industrial applications, which include a broad range of solid concentrations. It has been the endeavour of researchers around the world to develop accurate models to predict pressure drop and velocity distribution in a solid–liquid flow in pipelines. The friction factor is one of the most important technical parameters to be evaluated by the designers for designing a pipeline transportation system in a deep ocean, and the parameter which dictates frictional head loss and selection of the pump capacity (Rabinovich et al., 2012; Talmon and Rhee, 2011; Wilson et al., 2006). Therefore, the paper presents a predicted friction factor in an upward vertical pipeline for slurry flow with coarse solid particles and compares the results of predictions with measurements. Predictions of the friction factor were made using the mathematical model developed by Shook and Bartosik (1994) and next improved by Bartosik (1996). The mathematical model uses the Bagnold concept (Bagnold, 1954) and was detailly described by Bartosik (2009).

The paper presents a validation of the mathematical model describing the friction factor by comparing the predicted and measured results in a broad range of solid concentrations and mean solid particle diameters. Three different types of solids, surrounded by water as a carrier liquid, namely Canasphere, PVC, and Sand were used with solids density from 1045 to 2650 kg/m^3, and in the range of solid concentrations by volume from 0.10 to 0.45. It is demonstrated that the predicted friction factor matching well measurements, however, some exceptions exist. The paper demonstrates that mean solid particle diameter plays a crucial role in a vertical slurry flow with coarse particles.

The aim of the paper is to validate the mathematical model, which predicts the friction factor, by comparing predictions with measurements in vertical pipeline for up-ward slurry flow with coarse particles if additional stresses due to *particle – wall* interactions are included. It must be noted that such a comparison is not available in the literature.

The mathematical model

If vertical pipe flow of medium and coarse solid particles is considered it should be noted that several models are available in literature, as for instance:

- Shook and Bartosik (1994) and Bartosik (1996) for d_{50} = 1.4 – 3.4 mm
- Ferre and Shook (1998) for d_{50} = 1.8 – 4.6 mm
- Gillies and Shook (2000) for d_{50} = 0.175 mm
- Matousek (2005) for d_{50} = 0.37 mm
- Talmon for d_{50} = 0.1 – 2 mm

For the purpose of this research, the friction factor for slurry with coarse particles will be calculated using the mathematical model developed by Shook and Bartosik (1994) and next improved by Bartosik (1996), which compact delivery is presented below.

Let's consider up-ward slurry flow in a vertical straight pipeline of constant diameter. Assuming that the slurry flow is axially symmetrical (V = 0) and without circumferential eddies (W = 0), the linear momentum equation for quantities averaged over a pipe cross section can be expressed for main flow direction (ox), as follows (Longwell, 1966):

$$\rho\left(\frac{\partial U_b}{\partial t} + U_b\frac{\partial U_b}{\partial x} + g\frac{\partial h}{\partial x}\right) + \frac{\partial p}{\partial x} + 4\frac{\tau_w}{D} = 0 \tag{2}$$

Bulk velocity U_b is computed by integrating the local velocity

U across a pipe, as follows:

$$U_b = \frac{1}{A}\int\int U\, dA \tag{3}$$

where A is cross section of a pipe and is constant (D = const).

Assuming that flow is stationary ($\partial/\partial t = 0$) and fully developed ($\partial U_b/\partial x = 0$), Equation (2) can be simplified, as follows:

$$\rho g \frac{\Delta h}{\Delta x} + \frac{\Delta p}{\Delta x} + \frac{4}{D}\tau_w = 0 \tag{4}$$

The first term in Equation (4) is called the gravitational term and is denoted as:

$$\rho g \frac{\Delta h}{\Delta x} = \frac{\Delta p^*}{\Delta x} \tag{5}$$

The gravitational term is equal to zero for horizontal flow and its importance increases with increase of pipe inclination. Taking into account Equation (5), the final form of Equation (4) is, as follows:

$$\frac{p_1 - p_2}{\Delta x} = \frac{\Delta p^*}{\Delta x} + \frac{4}{D}\tau_w \tag{6}$$

where $p_1 - p_2$ is the total static pressure drop in a vertical up-ward pipe flow – see Fig. 1.

Looking for possibility of comparing a vertical up-ward flow with a horizontal flow the gravitational term in Equation (6) will be subtracted. Equation (6) can be rewritten in the following form:

$$\frac{p_1 - p_2}{\Delta x} - \frac{\Delta p^*}{\Delta x} = \frac{4}{D}\tau_w \tag{7}$$

Left hand side of Equation (7) represents pressure drop for a horizontal pipe flow. Now we consider a horizontal flow, with data obtained from a vertical flow. Of course, we know that the vertical flow is axially symmetrical, even for the ratio of slurry to liquid density much higher than unity, while the horizontal flow is pseudo-homogenous or heterogeneous. Nevertheless, such treatment is valuable as we consider horizontal flow, which is fully axially symmetrical, so analysis of such flow is simpler. In a vertical flow we measured the total pressure drop ($p_1 - p_2$). Therefore, it is necessary to calculate the gravitational term in order to subtract him form the total pressure drop. To do that let's consider Fig. 1, which shows the method of calculation of the gravitational term in a vertical up-ward slurry flow. Let's choose cross sections 1–1 and 2–2 and a datum level, denoted as 0–0 (dashed line), as it is presented in Fig. 1. Assuming that we consider stationary state, it means that slurry velocity is zero, it is possible to develop the equilibrium equation, which is following:

$$p_2 + \rho_m g \Delta x + \rho_L g h = p_2 + \rho_L g(\Delta x + h) + \Delta p^* \tag{8}$$

where $\Delta x = H - h$ in accordance with Fig. 1.

From Equation (8) we can get final form of the gravitational term, which is, as follows:

$$\frac{\Delta p^*}{\Delta x} = g(\rho_m - \rho_L) \tag{9}$$

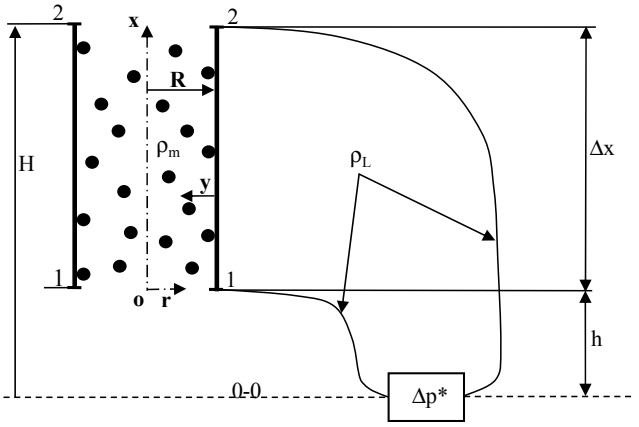

Fig. 1. Method of calculation of the gravitational term in a vertical up-ward slurry flow (Bartosik, 2010).

The gravitational term, calculated by Equation (9), was subtracted from the measured total pressure drop over the vertical test sections for each set of solid concentrations. Finally, we can convert experimental data for vertical flow into data for horizontal flow. The equation for axially-symmetrical horizontal slurry flow is following:

$$\frac{\Delta p}{\Delta x} = \frac{4\tau_w}{D} \tag{10}$$

or

$$i_m \rho_L g = \frac{4\tau_w}{D} \tag{11}$$

where $\Delta p/\Delta x$ in equation (10) represents pressure drop after subtraction of the gravitational term from the total pressure drop in a vertical up-ward slurry flow.

Taking into account the Bagnold concept, we can assume that the wall shear stress is a sum of the shear stresses at the pipe wall caused by two factors, namely: the *particle – wall* stress and the *liquid – wall* stress (Bagnold, 1954). So, Equation (11) can be written as:

$$i_m \rho_L g = \frac{4(\tau_L + \tau_P)}{D} \tag{12}$$

and considering carrier liquid flow only, i.e. the wall shear stress caused by solid particles is zero ($\tau_P = 0$), we can write Equation (12) for carrier liquid, as follows:

$$\tau_L = i_L \rho_L g \frac{D}{4} \tag{13}$$

Shook and Bartosik (1994) and next Bartosik (1996) took into account Bagnold's concept and they developed an equation describing *particle – wall* shear stress, as follows:

$$\tau_P = B_B \rho_P d_{50}^2 \lambda_B^{1.5} \left(\frac{dU}{dy}\right)^2 \tag{14}$$

Using Equations (12), (13) and (14), we can write:

$$i_m \rho_L g = \frac{4}{D}\left[\frac{D}{4} i_L \rho_L g + B_B \rho_P d_{50}^2 \lambda_B^{1.5} \left(\frac{dU}{dy}\right)^2\right] \tag{15}$$

Taking into account the Newtonian hypothesis, as:

$$\frac{dU}{dy}=\frac{\tau_L}{\mu_L} \tag{16}$$

it is possible to obtain the following equation describing frictional head losses i_m in a vertical up-ward pipe flow for slurry with coarse particles:

$$i_m\rho_L g=\frac{4}{D}\left[\frac{D}{4}i_L\rho_L g+B_B\,\rho_P\,d_{50}^2\,\lambda_B^{1.5}\left(\frac{\tau_L}{\mu_L}\right)^2\right] \tag{17}$$

It must be emphasized that Equation (17) fails in predictions of frictional head loss i_m in a vertical up-ward slurry flow with coarse particles. It is due to the fact that constant B_B is strongly depending on a pipe diameter, which Equation (14) does not include. Bartosik (1996) found that if B_B is divided by the square of pipe diameter D^2, the function B_B/D^2 smoothly depends on Reynolds number. Such a modification, called *linearization*, requires changes in Equations (14) and (17), which final form, can be written as follows:

$$\tau_P=K_B\,\rho_P\,d_{50}^2\,\lambda_B^{1.5}\,D^2\left(\frac{dU}{dy}\right)^2 \tag{18}$$

and finally:

$$i_m=i_L\left(1+K_B\,\rho_P\,d_{50}^2\,\lambda_B^{1.5}i_L\,\rho_L\,g\,D^3\frac{1}{4\mu_L^2}\right) \tag{19}$$

where the function K_B is as follows:

$$K_B=\frac{B_B}{D^2} \tag{20}$$

The function K_B was designated on the basis of measured frictional head loss in the range of mean solid particles from 1.4 mm to 3.4 mm and for the volumetric solid concentrations from 0 to 0.45 and for two different pipe diameters. It was found that the K_B function depends on the Reynolds number, as follows:

$$K_B=8.3018\cdot10^7\cdot Re_L^{-2.317} \tag{21}$$

while the Reynolds number is defined like for a carrier liquid flow, as follows:

$$Re_L=\frac{\rho_L U_b D}{\mu_L} \tag{22}$$

Linear concentration λ_B, which appears in Equations (14), (15) and (17) – (19), represents the ratio of the particle diameter to the mean distance between the particles and is expressed in terms of volumetric concentration C_V, and is as follows (Shook and Bartosik, 1994):

$$\lambda_B=\frac{1}{\left(\frac{C_{\max}}{C_V}\right)^{1/3}-1} \tag{23}$$

Finally, Equation (19), together with complementary relations (21) – (23), describes frictional head losses in a vertical up-ward slurry flow with coarse particles. The mathematical model is dedicated to predict frictional head loss in a smooth pipe in the range of mean particle diameters from 1.4 to 3.4 mm, and solid concentrations by volume from 0.1 to 0.45, and for narrowly sized solid particles with spherical, cylindrical and cubic shapes. It must be mentioned, however, that beyond the above parameters, the comparison of predictions with measurements were not made.

It is interesting to see how predicted friction factor for coarse slurries, converted from vertical to horizontal one, matches the measurements as we know that the friction factor is very sensitive to Reynolds number. Taking into account the general equation for the friction factor for slurry flow, described as:

$$\lambda_m=\frac{8\tau_w}{\rho_m U_b^2} \tag{24}$$

and using Equation (11) we can obtain a relation for the friction factor, as follows:

$$\lambda_m=\frac{2i_m\,\rho_L\,g\,D}{\rho_m U_b^2} \tag{25}$$

Equation (25) together with Equation (19) will be used to predict friction factor λ_m for the vertical up-ward flow of slurry with coarse particles.

The validation of friction factor predictions

Predictions of friction factor λ_m for a turbulent vertical up-ward flow of slurry with coarse particles were performed for two pipe diameters and for three different solid particle diameters and for broad range of solid concentrations. The predicted friction factor was calculated using Equation (25), however, frictional head loss i_m in this equation was calculated using Equation (19). The predicted friction factor was compared with the measurements. The measurements were made in vertical up-ward recirculating flow loop described by Shook and Bartosik (1994) and Bartosik (2009). Parameters used for the validation of the friction factor predictions are collected in Table.1.

Table 1. Summary of the parameters used for the validation of the friction factor.

D m	d_{50} mm	ρ_P kg/m^3	C_V –
0.026	1.5	1045	0.10 – 0.40
	1.5	2650	0.10 – 0.30
	2.8	1045	0.20 – 0.45
	3.4	1400	0.20 – 0.40
0.040	2.8	1045	0.20 – 0.45
	3.4	1400	0.20 – 0.40

Each figure listed below, representing predicted and measured friction factor, possesses a referenced solid line, which represents the friction factor for carrier liquid (water). The friction factor for carrier liquid (water) was calculated using the Churchill formula (Churchill, 1977), assuming that inner pipe wall is smooth, and is expressed by Equations (26) – (28).

$$\lambda=8\left[\left(\frac{8}{Re_L}\right)^{12}+(A+B)^{-1.5}\right]^{\frac{1}{12}} \tag{26}$$

$$A=\left\{2.457\ln\left[\left(\left(\frac{7}{Re_L}\right)^{0.9}+0.27\frac{\varepsilon}{D}\right)^{-1}\right]\right\}^{16} \tag{27}$$

$$B=\left(\frac{37530}{Re_L}\right)^{16} \tag{28}$$

Reynolds number in Equations (26) – (28) was calculated for water, in accordance with Equation (22), for temperature equal 25ºC, which is in accordance with performed experiments. The relative error, expressed by Equation (29), was calculated at the same Reynolds number for measurement and prediction.

$$Error=\frac{|(\lambda_m)_{\exp}-(\lambda_m)_{\mathrm{PRD}}|}{(\lambda_m)_{\mathrm{EXP}}}\cdot 100\% \tag{29}$$

The predicted versus the measured friction factor λ_m for polystyrene slurry in 0.026 m inner pipe diameter is presented in Fig. 1.

Fig. 2 shows that the experimental data for Cv = 0.30 are clearly below the friction factor for water. Analysing the data presented in Fig. 2, one can say that the highest relative error in predictions of friction factor λ_m is for C_V = 0.30 and Re_L = 185,000 and equals to 13.5%. This means that the model over-predict the friction factor. To analyse the data presented in Fig. 2, we have to consider Equation (25). Taking into account Equation (25) it is possible to set up condition when the frictional head loss for slurry should be lower than for water. Using Equation (25) for slurry and also for water, one can write:

$$\frac{i_m}{i_L}=\frac{\lambda_m}{\lambda_L}\frac{\rho_m}{\rho_L} \tag{30}$$

and finally, we can get the following condition:

$$i_m<i_L \;\Leftrightarrow\; \lambda_m S_m<\lambda_L \tag{31}$$

The ratio of slurry to liquid density, for data presented in Fig. 2, is equal S_m = 1.014. Let's consider the measured point of slurry friction factor for the highest Reynolds number and for C_V = 0.3, which is: λ_m = 0.01468 for Re = 185,000 – see Fig.2. For the same Reynolds number, the friction factor for water is λ_L = 0.0158. So, taking into account condition (31), we get: $\lambda_m S_m$ = 0.0149. It is seen that in this particular case the following condition exists $\lambda_m S_m < \lambda_L$. This means that frictional head loss for slurry should be lower than for water. To demonstrate that it is right, Fig. 3 shows experimental data of frictional head loss for the same slurry as presented in Fig. 2.

It is seen in Fig. 3 that the frictional head losses for slurry with C_V = 0.30 is lower than for water, which is in accordance with condition (31).

It is interesting to compare the predictions with the measurements for the same pipe and the same mean particle diameter, as presented in Fig. 2, but for sand slurry. In this case the particle density is about 2.6 times larger compared to polystyrene particles, presented in Fig. 2. Measurements and predictions presented in Fig. 4 explicitly proved that almost all points of friction factor are below data for water. In accordance with Equation (25) we can expect that if slurry density increases, the slurry friction factor should decrease. Nevertheless, it is surprising that friction factor λ_m is much below data for carrier liquid, which is pronounced for C_V = 0.20 and 0.30.

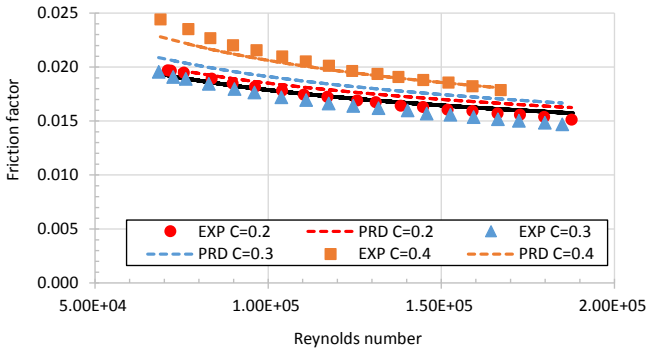

Fig. 2. Predicted versus measured friction factor λ_m in 0.026 m pipe for polystyrene slurry; d_{50} = 1.5 mm; ρ_P = 1045 kg/m^3.

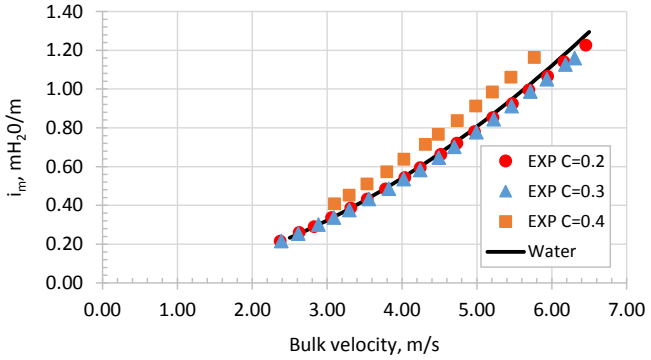

Fig. 3. Measured frictional head loss for slurry flow. Polystyrene particles: d_{50} = 1.5 mm, ρ_P = 1045 kg/m^3, pipe diameter D = 0.26 mm (Shook and Bartosik, 1994).

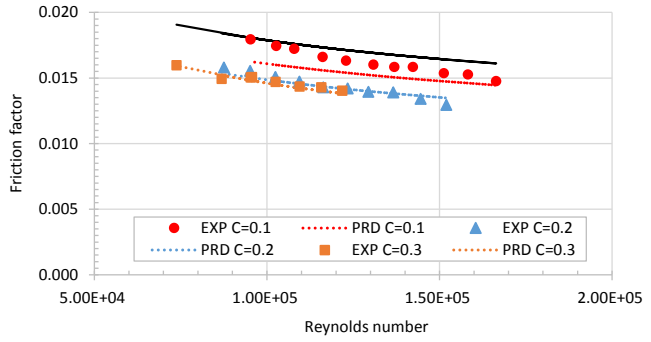

Fig. 4. Predicted versus measured friction factor λ_m in 0.026 m pipe for sand slurry; d_{50} = 1.5 mm; ρ_P = 2650 kg/m^3.

The results shown in Fig. 4 confirmed a fairly good agreement between the predicted and the measured friction factor λ_m if solid concentration was at least 0.20 by volume. The highest discrepancy appeared at C = 0.10 and Re_L = 95,200 and the relative error was about 9.4%. Considering condition, expressed by Equation (31), it can be found that in this case the frictional head loss should be slightly higher than for water.

With particle diameter increase we expected that the *particle – wall* interaction will increase too. The results shown in Fig. 5 confirmed high agreement between the predicted and the measured friction factor λ_m. Comparing the friction factor with the results presented in Fig. 2 and Fig. 5, it is obvious that increasing the mean solid particle diameter from 1.5 mm to 2.8 mm causes a substantial increase of friction factor λ_m. Results presented in Fig. 5 demonstrate that the highest relative error appears for C_V = 0.20 and Re_L = 180,000 and equals to 5%.

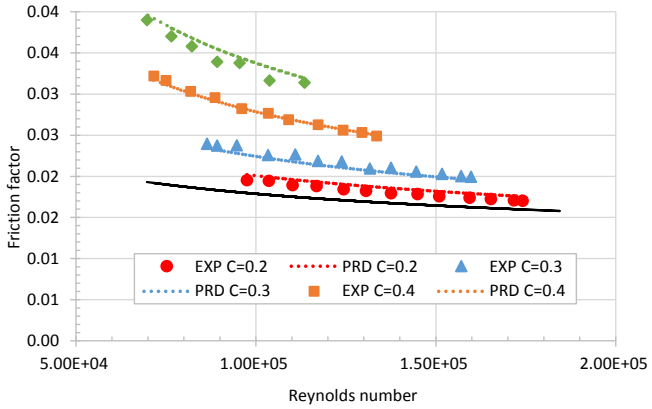

Fig. 5. Predicted versus measured friction factor in 0.026 m pipe for coarse polystyrene slurry; d_{50} = 2.8 mm; ρ_P = 1045 kg/m^3.

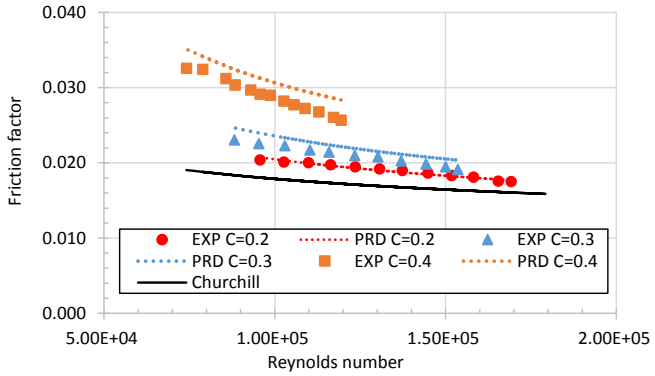

Fig. 6. Predicted versus measured friction factor in 0.026 m pipe for coarse PVC slurry; d_{50} = 3.4 mm; ρ_P = 1400 kg/m^3.

Predictions of λ_m for moderate solids density, like PVC, which is equal to 1400 kg/m^3, and for larger mean particle diameter, which is d_{50} = 3.4 mm, are presented in Fig. 6. In this case, it is seen that the model over predicts the friction factor mainly at C_V = 0.40, and the highest relative error is for Re_L = 119,000 and equals to 10.5%.

To ensure that the model is adequate for predictions of friction factor for coarse slurry flow, for different pipe diameters, comparisons of the predictions and measurements of the slurry friction factor were made for pipe with an inner diameter of 0.04 m. Results of friction factor for coarse polystyrene slurry with particles density 1045 kg/m^3 and mean particles diameter 2.8 mm are presented in Fig. 7. Predictions confirmed fairly good accuracy. The highest relative error exists for C_V = 0.20 and Re_L = 282,000 and equals to 8%.

The predicted and measured friction factor λ_m for coarse PVC slurry in pipe of D = 0.04 m was presented in Fig. 8. It is seen that the model over predicts the friction factor, especially for C_V = 0.30 and 0.40. In this particular case, the relative error is highest compared to all the presented figures thus far. The highest relative error is for C_V = 0.40 and Re_L = 111,000 and equals to 21.5%.

In conclusion, one can say that all the data presented in Fig. 2 and Fig. 4 – Fig. 8 showed that the predicted friction factor λ_m qualitatively follows the experimental data fairly well, although in some cases, like in Fig. 2 and Fig. 4, the friction factor was significantly below friction for water. Predicted friction factor confirmed that Equations (19) and (25) gave good qualitative and quantitative results for slurries presented in this study, except predictions for PVC, especially for pipe of inner diameter 0.04 m, where the highest discrepancy reaches 21.5%.

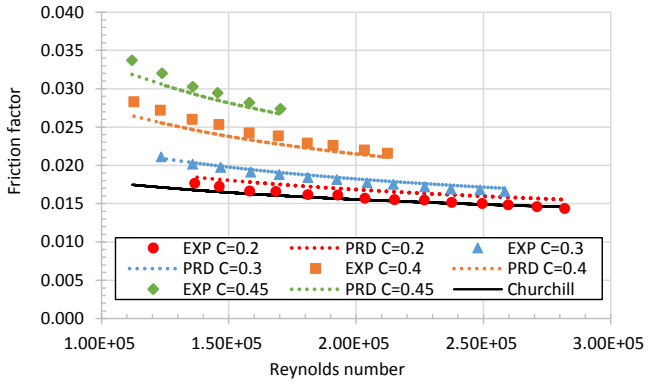

Fig. 7. Predicted versus measured friction factor in 0.04 m pipe for coarse polystyrene slurry; d_{50}=2.8 mm; ρ_P=1045 kg/m^3.

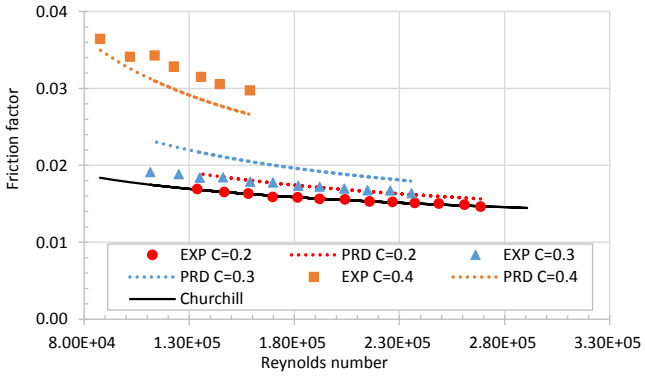

Fig. 8. Predicted versus measured friction factor in 0.04 m pipe for coarse polystyrene slurry; d_{50} = 3.4 mm; ρ_P = 1400 kg/m^3.

Comprehensive simulations of the dependence of particle diameter, solid concentration, solid particle density, and Reynolds number on *particle – wall* shear stresses were presented by Bartosik (2010).

DISCUSSION

A comparison of the predicted and measured friction factor λ_m for slurry flow with coarse particles demonstrate that the size of solid particles has a substantial influence on the friction. It is still not fully understood how slurry flow with coarse particles has a friction factor lower than for water flow, which was demonstrated in Fig. 2 and Fig. 4 for polystyrene and sand with d_{50} = 1.5 mm. Such results are in accordance with the measured frictional head loss for polystyrene and sand particles of d_{50} = 1.5 mm (Shook and Bartosik, 1994; Bartosik 2009). Shook and Bartosik (1994) subtracted the gravitational term from measured i_m values in vertical upward flow for polystyrene slurry with d_{50} = 1.5 mm and demonstrated that after the subtraction of the gravitational term, the frictional head loss for polystyrene slurry is lower than for water, which is presented in Fig.3. Such results suggest that damping of turbulence appears.

Bartosik (2009) subtracted the gravitational term from measured i_m values in vertical upward flow for sand slurry with d_{50} = 1.5 mm and demonstrated that after the subtraction of the gravitational term, the frictional head loss for sand slurry is slightly above that for water flow; even the slurry density was 50% higher than the water density (for C_V = 0.3). To illustrate this Fig. 9 presents measured frictional head loss for such slurry. Experiments were made for vertical up-ward flow, however, presented data were obtained in accordance with Equation (11),

after subtraction of gravitational term, expressed by Equation (9), from the total pressure drop, expressed by Equation (7). Coloured dashed line in Fig. 9, represents calculation of slurry frictional head loss for $C_V = 0.2$ using Equation (32). We expect that for solid concentration equal, for instance 0.2, which gives $S_m = 1.33$, the i_m should be much higher than it is. For instance, when bulk velocity equals to 4 m/s the i_m should be 23% higher than experiments proved. It is very probable again that in such a case damping of turbulence appears.

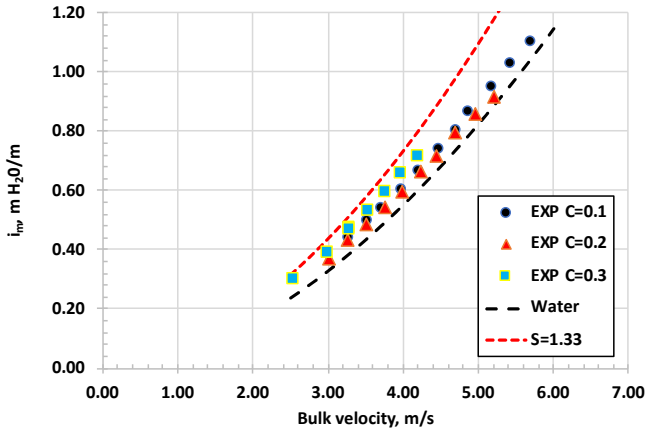

Fig. 9. Measured frictional head loss for slurry flow. Sand particles: $d_{50} = 1.5$ mm, $\rho_P = 2650$ kg/m^3, pipe diameter $D = 0.26$ mm (Bartosik, 2009).

$$i_m = S_m \, i_L \tag{32}$$

The measured and predicted friction factor for slurry flow with particle diameters equal to 2.8 and 3.4 mm demonstrated that the friction factor is significantly above friction for water, especially in the range of solid concentrations $0.2 < C_v \leq 0.3$ – see Fig. 5–Fig. 8. However, for pipe diameter $D = 0.04$ m and low solids concentration ($C_V = 0.20$) the friction factor was very close to friction for water – Fig. 7 and Fig. 8. In all the above cases, the friction factor decreases as Reynolds number increases.

Looking for an explanation of low friction factor, which is pronounced for mean particle diameter of polystyrene and sand, equal to 1.5 mm, we have to consider the region close to a pipe wall, as this region determines friction in a flow. If turbulent flow is considered, we know that the viscous sublayer and buffer layer play a crucial role in production of the friction. In those two regions the velocity gradient is highest and in buffer layer the intensity of turbulence achieves maximum values. It seems to be reasonable to assume that *lift forces* and damping of turbulence are additional important factors affecting shear stresses. Particle diameter, solid concentration, and particle density are important components influencing *lift forces* and turbulence damping, as was stated in Introduction.

Summer et al. (1990) are among others who have shown that the concentration distribution of the solids in a slurry flow in vertical pipe depends upon particle size and solids concentration. The results of their experiments showed that the tendency of particle concentrations to decrease near a pipe wall was independent of bulk velocity and pipe diameter but increased with bulk concentration. At high concentrations and larger particle diameters the particles tend to move towards the centre of the pipe with the result being a decreased concentration region near the wall of the pipe.

Several researchers emphasized the importance of *lift forces* acting on solid particles traveling near a pipe wall (Kaushal and Tomita, 2007; Matousek, 2009; Vlasak et al., 2013; Wilson, 2003). Some of researchers emphasized that the off wall forces are much more effective for medium than for coarse particles (Matousek, 2009; Sumner, 1992). If we assume that the existence of *lift forces* pushes particles away from a pipe wall, we could expect that the lowest possible frictional head loss would be that for the carrier liquid. However, we demonstrated it is not true, because the slurry frictional head loss is below water in some cases. Therefore, hypothetically one can say that despite the *lift forces*, there are other additional factors, which are responsible for damping of turbulence at a pipe wall. Of course, the damping of turbulence depends on several factors, among them there is size of solid particles, particles density, solid concentration, Reynolds number etc. Hypothetically, one can say that the damping of turbulence could be an important drive force, which causes that viscous sublayer becomes thicker. A similar observation was made by Wilson and Thomas (1985), however, for fine dispersive slurry flows, which exhibit non-Newtonian behaviour. To validate such hypothesis access to measurements of fluctuating components of velocity of carrier liquid and solid particles at a pipe wall is required.

CONCLUSIONS

The validation of predictions of friction factor in vertical pipes for slurry flow with coarse particles was made using the mathematical model, which contains Equations (19) and (25). Analysing Equation (19) it is seen that the frictional head loss strongly depends on solid particle diameter and next on solid concentration and solid density. The mathematical model assumes that two major factors affect the total wall shear stress. The first one is due to the *particle – wall* shear stress and the second is due to the wall shear stress caused by carrier liquid. As was mentioned, in such a case *lift forces* and damping of turbulence could exist. As the model predicts the friction factor fairly well, it is possible that the effect of *lift forces* and turbulence damping is included in the K_B function, which depends on Reynolds number. The K_B function was tuned on the basis of experimental data. Therefore, the function describes other phenomena, which the model in its nature does not assumes.

The mathematical model emphasised importance of mean particle diameter, solid concentration, particle density, carrier liquid viscosity and bulk velocity. It was found that mathematical model overpredicts friction factor for slurry flow with mean particles diameter 3.4 mm in pipe of inner diameter $D = 0.04$ m – see Fig. 8. In this particular case the highest relative error was 21.5%. Predictions of slurry friction factor for polystyrene and sand particles demonstrate fairly good agreement with measurements.

Results of predictions indicate that the assumption made in the mathematical model that the total shear stresses depend on two factors only, i.e. *particle – wall* shear stress and *liquid – wall* shear stress, is not sufficient.

The mathematical model of friction factor λ_m could be improved if more complex functions than (12) and (21) will be considered. Such functions could include turbulence damping, which is one of the most important factors of the transport phenomena.

REFERENCES

Bagnold, R.A., 1954. Experiments on a gravity-free dispersion of large solid spheres in a Newtonian fluid under shear. Proceedings of the Royal Society of London, Ser. A, Mathematical and Physical Sciences, 225, 1160, 49–63.

Bartosik, A.S., Shook, C.A., 1995. Prediction of vertical liquid-solid pipe flow using measured concentration distribution. J. Part. Sci. Technol., 13, 85–104.
Bartosik, A.S., 1996. Modelling the Bagnold stress effects in vertical slurry flow. J. Hydrol. Hydromech., 44, 1, 48–57.
Bartosik, A., 2009. Simulation and Experiments of Axially-Symmetrical Flow of Fine- and Coarse-Dispersive Slurry in Delivery Pipes. Monography M11, Kielce University of Technology, 257 p.
Bartosik, A., 2010. Influence of coarse–dispersive solid phase on the 'particles–wall' shear stress in turbulent slurry flow with high solid concentration. The Archive of Mechanical Engineering, 57, 1, 45–68.
Caulet, P.J.C., Van der Lans, R.G.J.M., Luyben, K.Ch.A.M., 1996. Hydrodynamical interactions between particles and liquid flows in biochemical applications. Chemical Engineering J., 62, 3, 193–206.
Charles, M.E., Charles, R.A., 1971. Advances in Solid-Liquid Flow and its Applications. Pergamon Press, New York.
Churchill, S.W., 1977. Friction factor equation spans all fluids regimes. Chem. Eng., 84, 24, 91–92.
Coulson, J.M, Richardson, J.F., Backhurst, J.R., Hraker, J.H., 1996. Chemical Engineering, vol. 1: Fluid Flow, Heat Transfer and Mass Transfer. Butterworth-Heinemann.
Faraj, Y., Wang, M., 2012. ERT investigation on horizontal and vertical counter-gravity slurry flow in pipelines. In: 20th Int. Congress of Chemical and Process Engineering, CHISA, Prague, pp. 588–606.
Ferre, A.L., Shook, C.A., 1998. Coarse particle wall friction in vertical slurry flows. Particulate Science and Technology, 16, 2, 125–133.
Gillies, R.G., Shook, C.A., 2000. Modelling high concentration settling slurry flows. Canadian Journal of Chemical Engineering, 78, 709–716.
Ghosh, T., Shook, C.A., 1990. Freight pipelines. In: Liu, H., Round, G.F. (Eds.): Freight Pipelines. Hemisphere, Washington, DC, pp. 281–288.
Kaushal, D.R., Tomita, Y., 2007. Experimental investigation for near-wall lift of coarser particles in slurry pipeline using γ-ray densitometer. Powder Tech., 172, 3, 177–187.
Krampa-Morlu, F.N., Bergstrom, D.J., Bugg, J.D., Sanders, R.S., Shaan, J., 2004. Numerical simulation of dens coarse particle slurry flows in a vertical pipe. In: Proc. 5th Int. Conf. on Multiphase Flow, ICMF'04, paper No. 460.
Longwell, P.A., 1966. Mechanics of Fluid Flow. Mc Graw-Hill, New York.
Matousek, V., 2005. Research developments in pipeline transport of settling slurries. Powder Technology, 156, 43–51.
Matoušek, V., 2009. Pipe wall friction in vertical sand-slurry flows. Particulate Science and Technology, 27, 5, 456–468.
Messa, G.V, Malavasi, S., 2013. Numerical investigation of solid-liquid slurry flow through an upward-facing step. J. Hydrol. Hydromech., 61, 2, 126–133.
Miedema, S.A., 2015. A head loss model for homogeneous slurry transport for medium sized particles. J. Hydrol. Hydromech., 63, 1, 1–12.
Peker, S.M., Helvaci, S.S., 2008. Solid-Liquid Two Phase Flow. Elsevier.
Rabinovich, E., Freund, N., Kalman, H., Klinzing, G., 2012. Friction forces on plugs of coarse particles moving upwards in a vertical column. Powder Technology, 219, 143–150.
Schreck, S., Kleis, S.J., 1993. Modification of grid-generated turbulence by solid particles. J. Fluid Mechanics, 249, 665–688.
Shook, C.A., Roco, M.C., 1991. Slurry Flow: Principles and Practice. Butterworth-Heinemann, Boston.
Shook, C.A., Bartosik, A.S., 1994. Particle-wall stresses in vertical slurry flows. J. Powder Technology, 81, 117–124.
Sumner, R.J., McKibben, M., Shook, C.A., 1990. Concentration and velocity distribution in turbulent slurry flow. Ecoulements Solide-Liquide, 2, 2, 33–42.
Sumner, R.J., 1992. Concentration variations and their effects in flowing slurries and emulsions. Ph.D. Thesis. University of Saskatchewan, Saskatoon, Canada.
Talmon, A.M., Rhee, C., 2011. Test setup for irregular vertical hydraulic transport in deep ocean mining. In: Proc. ASME 30th Int. Conf. on Ocean, Offshore and Arctic Engineering, pp. 319–328.
Talmon, A.M., 2013. Analytical model for pipe wall friction of pseudo-homogenous sand slurries. Particulate Science and Technology, 31, 3, 264–270.
Van Dijke, W., 2010. Vertical hydraulic transport of solids. Master's Thesis. Delft University of Technology, Delft.
Van Wijk, J.M., Van Rhee, C., Talmon, A.M., 2014. Wall friction of coarse-grained sediment plugs transported in a water flow through a vertical pipe. Ocean Engineering, 79, 50–57.
Van Wijk, J.M., 2016. Vertical hydraulic transport for deep sea mining a study into flow assurance. Ph.D. Thesis. Delft University of Technology, Delft.
Vlasak, P., Chara, Z., Kysela, B., Konfrst, J., 2013. Coarse grained particle flow in circular pipe. In: Proc. ASME 2013 Fluids Engineering Division Summer Meeting FEDSM2013, July 7–11, Incline Village, Nevada, USA.
Wennberg, T., 2010. Transporting highly concentrated slurries with centrifugal pumps. The thickened minerals tailings example. Universitetstryckeriet, Luleå.
Wilson, K.C., Addie, G.R., Sellgren, A., Clift, R., 2006. Slurry Transport Using Centrifugal Pumps. 3rd Ed., Springer-Verlag.
Wilson, K.C., Sellgren, A., 2003. Interaction of particles and near-wall lift in slurry pipelines. J. Hydraul. Eng., 129, 1, 73–76.
Wilson, K.C., Thomas, A.D., 1985. A new analysis of the turbulent flow of non-Newtonian fluids. Can. J. Chem. Eng., 63, 539–546.
Wing, R.H., 1972. Slurry flow in vertical pipes. NOAA Technical Report ERL 273-0D 8. U.S. Department of Commerce, Nat. Oceanic and Atmospheric Administration, Washington.

NOMENCLATURE

A	– cross section of a pipe, m^2 or variable in Churchill formula (–)
B	– variable in Churchill formula, –
B_B	– dimensionless function in Bagnold concept, –
C_V	– solids concentration by volume, –
$C_{\max}$	– maximum possible solids concentration in a pipe, –
d_{50}	– mean particle diameter, mm
D	– inner pipe diameter, m
EXP	– experimental data
g	– acceleration due to gravity, m/s^2
h	– elevation above datum, m
i_L	– frictional head loss for liquid, m/m
i_m	– frictional head loss for slurry, m/m
K_B	– empirical function, m^{-2}
p	– static pressure, Pa
PRD	– predicted data

r – distance from symmetry axis, m
Re_L – Reynolds number for carrier liquid phase, –
S_m – ratio of slurry to liquid density, –
S_ρ – ratio of solid to liquid density, –
U – axial component of velocity (bulk velocity), m/s
U_b – bulk velocity of flowing medium (slurry or water), m/s
V – radial component of velocity, m/s
W – circumferential component of velocity, m/s
x – main flow direction, m
y – radial coordinate, m
Δ – difference
λ_B – dimensionless linear concentration, –
λ_m – friction factor for slurry, –
μ_L – liquid viscosity, Pa s
ρ_L – liquid density, kg/m^3
ρ_m – slurry density, kg/m^3
ρ_P – particle density, kg/m^3
τ_L – liquid component of wall shear stress, Pa
τ_P – particle component of wall shear stress, Pa
τ_w – wall shear stress, Pa

Received 9 December 2019
Accepted 24 January 2020

J. Hydrol. Hydromech., 68, 2020, 2, 128–133
DOI: 10.2478/johh-2020-0017
ISSN 1338-4333

sciendo Journal of Hydrology and Hydromechanics

Hydrology of the Carpathian Basin: interactions of climatic drivers and hydrological processes on local and regional scales – HydroCarpath Research

Ján Szolgay[1*], Günter Blöschl[2], Zoltán Gribovszki[3], Juraj Parajka[2]

[1] Department of Land and Water Resources Management, Slovak University of Technology, Radlinského 11, 810 05, Bratislava, Slovakia.
[2] Institute of Hydraulic Engineering and Water Resources Management, TU Wien, Karlsplatz 13, A-1040 Vienna, Austria.
[3] Institute of Geomatics and Civil Engineering, University of Sopron, Bajcsy-Zsilinszky utca 4., Sopron, H-9400, Hungary.
[*] Corresponding author. E-mail: jan.szolgay@stuba.sk

Abstract: The paper introduces the Special Section on the Hydrology of the Carpathians in this issue. It is the result of an initiative of the Department of Land and Water Resources Management of the Slovak University of Technology in Bratislava, the Institute of Hydraulic Engineering and Water Resources Management of the TU Vienna and the Institute of Geomatics and Civil Engineering of the University of Sopron to allow young hydrologists in the Carpathian Basin (and from outside) to present their research and re-network on the emerging topics of the hydrology of the Carpathians at the HydroCarpath Conferences since 2012.

Keywords: Carpathian Basin; Evapotranspiration; Runoff coefficient; Hydrological regime; CN number; Climate change.

Challenges to the hydrology and water management in the Carpathian Basin

Signals of changing climate and recent extreme flood and drought events in the Carpathian Basin have stimulated scientific and public discussion on the issue of whether the frequency and severity of these events have been increasing, to what extent such changes could be attributed to anthropogenic influence and how to observe, monitor and model processes describing them. Despite the fact that a large amount of research has been undertaken to investigate the primary sources of natural drivers and societal pressures of hydrological phenomena globally, there is still an urgent need to achieve a comprehensive understanding of the impacts of current land use and management practices, and their changes, on runoff processes in general and those of extremes in particular. It is recognized in the Basin and globally that understanding the interactions of drivers and hydrological processes on local and regional scales is also an essential prerequisite for addressing practical water resources management problems (Blöschl et al., 2019).

The rich spatial and temporal heterogeneity of climatic drivers, regional and local control conditions in the Carpathian Basin, and the variety of active flow processes during particular seasons and events, makes it difficult to arrive at generalized descriptions of the genesis of particular types of regimes and events. The same applies to specific regional and local hazards and risk factors and to the design of generally applicable mitigation schemes. In this respect, the regional understanding and modelling of catchment hydrological processes are becoming increasingly important for addressing science as well as practical water resources management questions. Chances offered by new sources of data, based on latest developments in radar meteorology, experiments on hillslopes, and tracer studies in catchments have given hydrologists opportunities to compare different models of the same type (e.g., distributed) or different types of models (e.g., distributed vs lumped, process-based vs conceptual) on a regional basis (Bierkens, 2015). The confrontation of catchment experiments with results from catchment modelling has become more critical in recent years (Ceola et al., 2015).

On the other hand, the new data is also supporting the study and generalization of hydrological regimes. All these activities support better process representations in both deterministic and stochastic models in diverse hydrological environments and enable more reliable predictions in ungauged basins. International cooperation in science within hydrologically connected transnational basins is essential to meet these challenges. In the Carpathian Basin, established hydrologic scientific networks have suffered due to the significant societal and economic changes in the last decades. Previously, flourishing experimental research became underfinanced and international UNESCO supported education almost diminished (Brilly et al., 2010; Prohaska et al., 2020). Other negative aspects were the reorganization and vanishing of some hydrology related research organizations. For example, in Hungary, hydrological research was implemented or coordinated traditionally at the Water Resources Research Institute (acronym VITUKI). Which was Because of reorganization VITUKI has been dissolved in 2013. Some of its main research tasks had not continued (Gribovszki, 2015). Recently, it has been increasingly recognized that the cooperation in hydrology along the Danube needs to be revitalized. In the Common statement from the participants of the XXVII Danubian Conference on hydrological forecasting and hydrological base of water management (Ninov and Bojilova, 2017), the urgent needs of engineering hydrology and water resources management were summed up under 14 topics.

Against this background, the Department of Land and Water Resources Management of the Slovak University of Technology in Bratislava, the Institute of Hydraulic Engineering and Water Resources Management of the TU Vienna and the Institute of Geomatics and Civil Engineering of the University of Sopron launched an initiative to give an opportunity to young hydrologists in the Basin (and from outside) to present their research and re-network on the emerging topics of scientific hydrology connected to the hydrology of the Carpathians – the

HydroCarpath Conference series, starting in 2012 (HC, 2020). This conference series has continued to present results mainly from PhD research on problems of local and regional Carpathian hydrology (and that in the surroundings) around these topics:

- - Results from catchment experiments leading to better process understanding and representations.
- - The confrontation of hydrological catchment models with new types of data and process representation for distinct purposes: suitability of models for particular questions.
- - Regionalization and generalizations of hydrological regimes on various temporal and spatial scales using increased process knowledge.
- - Application of models and ensembles for improved characterization and predictions of changes in hydrological processes and climate change impacts on the water cycle.

This Special Section is organized along with these topics and presents contributions presented at recent conferences of this series.

Recent advances in the hydrology of the Carpathian Basin

Experimental research, after years of starvation and stagnation, has been revived recently in the Basin. Results from ongoing research from three research stations, the Hydrological Open Air Laboratory (HOAL) in Petzenkirchen in Austria (Blöschl et al., 2016), the Jalovecky creek catchment in Slovakia (e.g., Holko et al., 2020a; Krajčí et al., 2016) and the Hidegvíz Valley experimental watershed in Hungary (Csáfordi et al., 2012) are presented in this Special Section.

Evapotranspiration plays an important role in the estimation of the water balance on many hydrologically relevant spatial and temporal scales (Casper et al., 2019). Without measuring evaporation and transpiration on the field scale, which is complicated due to the extreme heterogeneity of the whole relevant factors in the environment, the upscaling of point measurements to hillslope, catchment and regional scales cannot be completed (Burt et al., 2005). Without the parameterization of the evapotranspiration process in hydrological modelling (Széles et al., 2018), including its partitioning into the two basic components, we cannot succeed in many water management decisions (e.g. scheduling and determining water requirements for irrigation) or in capturing land surface-climate interactions in climate modelling (Wang and Dickinson, 2012). Therefore, research conducted even under particular conditions is a valuable contribution to the knowledgebase. Hogan et al. (2020, this issue) used an eddy covariance device to measure the evapotranspiration of a growing maize field in the HOAL research catchment in Austria. Using the concentration and isotopic ratio of water vapour within the canopy, the performance of two partitioning methods, the stable isotope technique and a Lagrangian near field theory (LNF), was compared in partitioning the evapotranspiration into evaporation and transpiration. The two methods gave overall similar results, and the measured values were in line with those from similar experiments with maize. Given the complicated nature of the phenomenon, recommendations for follow-up research are not straightforward, because the robustness and the much larger amount of useable data of the stable isotope method, as well its lower variance, are offset by the need for additional measurements and analyses.

The confrontation of hydrological catchment models with new types of data and process representation for distinct purposes, including testing the appropriateness of models for particular questions are also preferred topics at the HydroCarpath conferences. Formation of runoff on the hillslope and catchment scale during intense precipitation is one of the intensively discussed and researched topics in this respect (e.g. Scherrer et al., 2007; Silasari et al., 2017). The response of catchment runoff to precipitation is highly non-linear due to heterogeneity in inputs and catchment characteristics, threshold behaviour depending on catchment wetness and storage states, varying relative contributions of different landscape units, etc. Besides infiltration excess (Hortonian) and surface flow, subsurface stormflow is generally recognized as a dominant factor in flood generation (e.g., Bachmair and Weiler, 2011). Soils play an important role in runoff formation. Preferential flow in the soil/subsoil/hillslope system through subsurface networks that have developed from a range of botanical, faunal and geophysical processes, also contribute to the transport of fine particles, water and solutes and to soil degradation (Band et al., 2014). Preferential flow in the soils (Beven and Germann, 2013), instability-driven flow (Tesař et al., 2001) or the fill and spill mechanism (Tromp-van Meerveld and McDonnell, 2006) are commonly used to explain the rapid formation of subsurface flow that eventually contributes to catchment stormflow. Soil stoniness can also contribute to rapid flow response as it reduces the soil retention capacity. This phenomenon is still not well studied, and it is often neglected in runoff formation theories and is not included mathematical models (Hlaváčiková et al., 2018). Mujtaba et al. (2020, this issue) used measured catchment runoff of the Jalovecký Creek experimental catchment (West Tatra Mountains, Slovakia) generated by moderate and high-intensity rainfall as a basis for comparison with modelled responses from the HYDRUS 2D model, which accounts for stoniness (Šimůnek et al., 2018). Comparisons of simulated lateral subsurface flow hydrographs with catchment runoff hydrographs have indicated that the shapes of both were similar for about one-half of the examined rainfall events. These findings call for increasing the efforts in obtaining good field and laboratory data characterizing soil stoniness and its variability, since the central idea of this study, the notion that reduced retention of stony soils can have a similar effect on catchment runoff formation as the commonly accepted and more often studied preferential flow, needs to get serious attention in the future.

Experimental data on runoff formation can be useful when a typology of flooding phenomena is sought. Indicators for the intensity of flood generation for different runoff mechanisms can be either direct or indirect. The direct indicators are directly linked to catchment properties, whereas the indirect indicators are linked to flood and flooding properties. The threshold values of these indicators are of a local nature, as they depend on the hydrology of the plot/hillslope/river basin in question. Three specific spatial scales are important for understanding the lateral movement of water on or below the soil surface: the plot, the hillslope, and catchment/river scales (e.g. Smith and Redding, 2012). There cannot be a unique set of indicators for all of these, even under equal environmental/social settings.

Among direct indicators on the catchment scale, which can capture the character of runoff concentration, typically are morphometric parameters (such as stream density, catchment shape, size and distribution of wetlands and sealed surfaces, etc.), anthropogenic disturbances (cross-drain frequency or density of roads, the density of stream crossings, drainage systems, etc.), runoff concentration indices (time of concentration, time to the peak, catchment lag time, etc., see Fang et al. (2005) for a review), landcover (vegetation, land use types and evolution) or geology (Viglione et al., 2018).

As indirect indicators on the catchment/regional scale one could typically use descriptors of flood typology, such as runoff generation process typology (Viglione et al., 2010), the propor-

tion of events of different origins and typical flood time scales (Gaál et al., 2012).

Among these indicators, the event runoff coefficient and the recession coefficient are of special theoretical importance for understanding catchment response and also of practical importance in hydrological design. Both can be regarded as important characteristics of hydrologic response on the event scale. The study of Chen et al. (2020, this issue) aimed at identifying factors which control the variability of event runoff coefficients (and the recession coefficient) in the HOAL research catchment and evaluating the relative importance of the controls in different subcatchments representing different runoff generation mechanisms. Besides that, also the predictive power of three regression-based machine learning techniques was evaluated with respect to their potential for estimating the event runoff coefficient (and the recession coefficient) from their controls. Overall, it was possible to demonstrate that both the performance of estimating the runoff coefficient (and the recession coefficient) and the relative importance of explanatory variables depend on the type of hydrological system, i.e. the runoff generation mechanism. The study, therefore, motivates further research into understanding their controls and their variability, since it has the potential for improving predictions of runoff in ungauged basins.

The estimation of event-based flood events is one of the most important parts of the design process for a large number of engineering projects and studies. A significant problem may arise in small catchments that are poorly gauged or when no recorded data exist. As an indirect indicator of flooding intensity, the CN parameter is important in this respect, which is usually directly used in direct runoff and design discharge estimation. Since its introduction in 1954, the Soil Conservation Service curve number (SCS-CN) method is generally considered a standard tool in practice. It has an empirical origin, lumped character, and even though the SCS-CN method is restricted to certain geographic regions and land use types, it is widely used (Bartlett et al., 2016).

In this method, the relationship between soil and land use characteristics and antecedent rainfall conditions are represented by a Curve Number (CN) parameter, which is tabulated in the original method. With this simple parameter, a rainfall depth is transformed into a runoff depth. Testing of the method under various hydrological conditions, unfortunately, showed several limitations, which were pointed out, e.g., by McCutcheon et al. (2006). Despite rising criticism due to the lack of European data for its verification, see Soulis et al. (2009), in engineering studies (and also in some rainfall-runoff models and, in some cases, even in mitigation policies), the SCN method has remained popular in the Carpathian Basin.

Recently, to address these limitations, the use of empirical CN values calculated from recorded rainfall-runoff events, instead of the tabulated ones, was proposed and tested in the Basin. Banasik et al. (2014) and Rutkowska et al. (2015) introduced a probabilistic approach to the variability of empirical CNs. The main objective of the Kohnová et al. (2020, this issue) is to continue along this line by proposing and evaluating the performance of a regional approach to treat empirical CN values in homogeneous regions statistically and to test the sensitivity of such estimation to different initial abstraction ratios. The popular method of Hosking and Wallis was combined with the ANOVA test to delineate homogenous groups of catchments with similar empirical CN values. The 50% quantile of the regional theoretical regional distribution function of CN estimated from all catchments in the region, was chosen as the regionally representative CN. The regional treatment and introduction of a common regional CN open up the opportunity to pool the information content of the rainfall-runoff process in homogenous catchments and to apply it to similar catchments. Confronting the landuse-based tabulated CN values with the statistically derived counterparts in the region contributes to more reliable estimation of design discharges in small catchments. The paper could, therefore, give rise to an alternative way of estimating CN values in forested catchments and catchments with a lack of data or without observations.

Regionalisation and generalisations of hydrological regimes on various temporal and spatial scales using increased process knowledge was a traditional strength of the hydrology of the Carpathians in the past (e.g. Brilly et al., 2010). The scale and intensity of slow changes in land-use/management due to economic reasons and new political priorities (following changes in 1989, such as the abandonment of land, a new paradigm in the management of forests, increasing protection of ecosystems and introduction of natural water retention measures, changes in agricultural policies, etc.) call for studying the changes of hydrological regimes. Numerous attempts were therefore undertaken to use distributed rainfall-runoff models to assess regime changes resulting from such effects (e.g. Rončák et al., 2016) and to detect signals indicating irregular behaviour of hydrological time series in the Basin (e.g. Pekárová et al., 2011). Less common, and indeed more difficult to conduct, were attempts to explain regularities or potential irregularities in time series by causative factors (e.g. Longman et al., 2019). In this respect, Kundzewicz and Robson (2004) reminded that analyses of time series data should include stages of exploratory data analysis, application of statistical analysis and interpretation of tests results, warning that natural variability could appear like trends and other changes. Merz et al. (2012) suggested that detection only is not sufficient, it should always be accompanied by the more challenging attribution, and both should be positioned within in a hypothesis-testing framework. Holko et al. (2020a, b, this issue) in two companion papers, guided by such principles, analysed the water balance, hydrological response, runoff and snow cover characteristics as well as isotopic data in precipitation and catchment runoff (oxygen 18) in search for changes in the hydrological cycle of a mountain catchment representative of the hydrology of the highest part of the Western Carpathians. Both studies differ from similar studies by the fact that they are conducted in an experimental catchment, where the hydrological cycle is relatively well understood, and many different data series were available for the analysis to identify causal factors. The authors did not restrict themselves to the use of one analytic method. Instead, they focused on the consistency of results from different methods. Even though no clear signals for relating the observed behaviour of the respective time series were found, new insights were gained into the complexities of the components of the hydrological cycle and the behaviour of hydrologic phenomena. At the same time, they stated that despite better data availability and deeper knowledge of the hydrological cycle in the research catchment compared to other, less-studied catchments, the attribution analysis remained uncertain due to the unavailability of data on other possible drivers.

Application of models and ensembles for improved characterisation and prediction of changes in hydrological processes and of climate change impacts on the water cycle is naturally a hot topic for hydrology research in the Basin, too. Diverse approaches on how to assess the impact of changes in climate on the hydrological regime exist. Credible data, methods and tools are needed to evaluate the uncertainty in the projections (Olsson et al., 2016). Regional climate models (RCM) domi-

nate the climate scenarios in regional or local assessments in hydrology either as single- or multi-model studies using again single or ensemble downscaled RCM outputs (e.g. Krysanova and Hattermann, 2017). While a single scenario and model studies were dominating in the past, recent methodical improvements have advanced the quantification of uncertainties in the modelling chain. Past scenario-based climate change impact modelling with rainfall-runoff models in the Carpathian Basin Slovakia rarely accounted for uncertainties due to various climatic models. These assessment methods have limited potential today when various regional climate model outputs with short time steps under several emission scenarios are available. The majority of present studies uses downscaled RCM climate/emission scenarios to drive rainfall-runoff models (Stagl and Hattermann, 2015). Csáki et al. (2020, this issue) conducted a systematic intercomparison of climate change impacts on evapotranspiration and runoff in a catchment supplying water to the largest lake in Central Europe using multiple regional climate change models and a robust climate-runoff model built around a modified Budyko hypothesis. The Budyko framework was extended for areas (e.g. in the lowlands of the Carpathian Basin) where an additional amount of water is available for evapotranspiration above that which the area receives from local precipitation (water bodies or storages with allochthone inflows). The main advantage of the proposed model is its grid-based spatial structure, simple parameterisation and modest requirements for inputs. A complex validation methodology of the climate-runoff model was proposed, which extends the methodology to climate change impact assessments. The trade-off for its robustness is that its present version cannot handle significant changes in the areas receiving allochthone inflows for future climates. Still, it is possible to extend this model in the future.

Future challenges of hydrological research in the Basin

In order to support the needs of integrated water resources management in this transnational Basin, the process-oriented modelling of hydrological processes and parameterization of models need to remain an essential part of future research concerning this set of problems (Wahren et al., 2009). Consequently, there is a continuing necessity to conduct field studies for identifying and quantifying processes of catchment response and assembling field-based evidence for testing the assumptions underpinning model design and for addressing the uncertainties and controversies that continue to frustrate our understanding of catchment behaviour (Bathurst et al., 2018). As an extension of the necessary field experimental research of site-related runoff generation and erosion processes, this also requires the further development of hydrological models that are capable of taking into account the effect of various land uses and agricultural land management practices on the formation of surface and subsurface flows (Montanari et al., 2015). Moreover, this new generation of hydrological models should provide scientifically-based correct answers about runoff generation processes under changed conditions and have the ability to assess the efficiency of currently preferred near-nature management practices of agricultural land aimed at the reduction of floods, erosion and transport processes (Blöschl et al., 2019).

One of the key problems is an appropriate parameterization of the physiographical environment of hillslopes in headwater catchments and process-oriented schemes of extreme runoff and erosion formation. These would comply with the requirements of models and would take into account extremely variable local conditions of runoff generation processes, especially in small catchments and under extreme conditions. A combination of state-of-the-art experimental terrain measurements with a modelling approach is required, as well as the development of methods for the transferability of the results from an experimental site scale to the scale of hillslopes and small headwater catchments. These and other research gaps in understanding flood changes caused by changes in land and forest management, agricultural practices, artificial drainage and terracing have been identified in Rogger et al. (2017). Potential strategies in addressing these gaps were also proposed. Solutions may include complex systems approaches which would link processes across time scales, embedding and upscaling outcomes from experimental research on physical-chemical-biological process interactions on a plot to catchment scales. A focus on connectivity and patterns across spatial scales should be in the centre of interest. This, in turn, calls for interdisciplinary research that will coherently deal with problems across hydrology, soil and agricultural sciences, forest engineering, forest ecology and geomorphology (Rogger et al., 2017). Natural water retention measures, which are a new paradigm in flood hazard mitigation, are a potential integrative agent of these coupled processes. Actions proposed to reduce erosion on hillslopes and store water may decrease the flood risk by overland flow, but will increase infiltration and soil moisture, and thus increase the risk of subsurface stormflow, soil mass movement, the temporary flooding of meadows and agricultural soils, and waterlogging.

Managers and decision-makers have perhaps not fully recognized the associated risks and chances in practice in the Basin (Ninov and Biljaeva, 2017). This, therefore, calls for the introduction of an integrated assessment of methodologies, drivers and impacts. Although scientific advances for developing integrated methodologies are evident, developing robust tools remains a significant challenge. A connected issue is an integration of existing and newly available data and information bases for this purpose with implications for data and monitoring requirements and the selection of new sets of indicators. In order to develop an integrated strategy for addressing the interactions of threats on different spatial and temporal scales, more detailed knowledge of the interactions needs to be gathered for all these threats, including an evaluation of potentially counterproductive impacts of mitigating measures. This knowledge has to be incorporated into water and mass flow generation models to better predict not only water-related processes but also all related ecohydrological aspects (e.g., Band et al., 2014).

Acknowledgements. This study has been supported by project EFOP-3.6.2-16-2017-00018 of the University of Sopron and by the VEGA Scientific Grant Agency Grant No. 1/0632/19. The support is gratefully acknowledged.

REFERENCES

Bachmair, S., Weiler, M., 2011. New dimensions of hillslope hydrology. In: Levia, D.F. (Ed.): Forest Hydrology and Biogeochemistry. Synthesis of Past Research and Future Directions. Ecological Studies, Vol. 2016. Springer, 455–482.

Banasik, K., Rutkowska, A., Kohnová, S., 2014. Retention and curve number variability in a small agricultural catchment: the probabilistic approach. Water, 6, 5, 1118–1133.

Band, L.E., McDonnell, J.J., Duncan, J.M., Barros, A., Bejan, A., Burt, T., Dietrich, W.E., Emanuel, R., Hwang, T., Katul, G., Kim, Y., McGlynn, B., Miles, B., Porporato, A., Scaife, C., Troch, P.A., 2014. Ecohydrological flow networks in the subsurface. Ecohydrology, 7, 4, 1073–1078.

Bartlett, M.S., Parolari, A.J., McDonnell, J.J., Porporato, A., 2016. Beyond the SCS-CN method: A theoretical framework for spatially lumped rainfall-runoff response. Water Resour. Res., 52, 4608–4627.

Bathurst, J., Birkinshaw, S., Johnson, H., Kenny, A., Napier, A., Raven, S., Robinson, J., Stroud, R., 2018. Runoff, flood peaks and proportional response in a combined nested and paired forest plantation/peat grassland catchment. Journal of Hydrology, 564, 916–927.

Beven, K., German, P., 2013. Macropores and water flow in soils revisited. Water Resources Research, 49, 6, 3071–3092.

Bierkens, M.F.P., 2015. Global hydrology 2015: state, trends, and directions. Water Resources Research, 51, 4923–4947.

Blöschl, G., Bierkens, M.F.P., Chambel, A., Cudennec, C., Destouni, G., et al., 2019. Twenty-three unsolved problems in hydrology (UPH) – a community perspective. Hydrological Sciences Journal – Journal des Sciences Hydrologiques, 64, 10, 1141–1158.

Blöschl, G., Blaschke, A.P., Broer, M., Bucher, C., Carr, G., Chen, X., Eder, A., Exner-Kittridge, M., Farnleitner, A., Flores-Orozco, A., Haas, P., Hogan, P., Kazemi Amiri, A., Oismüller, M., Parajka, J., Silasari, R., Stadler, P., Strauss, P., Vreugdenhil, M., Wagner, W., Zessner, M., 2016. The Hydrological Open Air Laboratory (HOAL) in Petzenkirchen: a hypothesis-driven observatory. Hydrol. Earth Syst. Sci., 20, 1, 227–255.

Brilly, M. (Ed.), 2010. Hydrological Processes of the Danube River Basin Perspectives from the Danubian Countries. Springer, 436 p. ISBN 978-90-481-3423-6

Burt, C.M., Mutziger, A.J., Allen, R.G, Howell, T.A., 2005. Evaporation research: review and interpretation. J. Irrig. Drain. Eng., 131, 1, 37–58.

Casper, M.C., Mohajerani, H., Hassler, S., Herdel, T., Blume, T., 2019. Finding behavioral parameterization for a 1-D water balance model by multi-criteria evaluation. J. Hydrol. Hydromech., 67, 3, 2019, 213–224.

Ceola, S., Arheimer, B., Baratti, E., Blöschl, G., Capell, R., Castellarin, A., Freer, J., Han, D., Hrachowitz, M., Hundecha, Y., Hutton, C., Lindström, G., Montanari, A., Nijzink, R., Parajka, J., Toth, E., Viglione, A., and Wagener, T., 2015. Virtual laboratories: new opportunities for collaborative water science. Hydrol. Earth Syst. Sci., 19, 2101–2117.

Chen, X., Parajka, J., Széles, B., Strauss, P., Blöschl., G., 2020. Controls on event runoff coefficients and recession coefficients for different runoff generation mechanisms identified by three regression methods. J. Hydrol. Hydromech., 68, 2, 155–169.

Csáfordi, P., Eredics, A., Gribovszki, Z., Kalicz, P., Koppán, A., Kucsara, M., Moricz, N., Rasztovits, E., Víg, P., 2012. Hidegvíz Valley Experimental Watershed. (Eds.): Gribovszki Z., Kalicz P. Nyugat-magyarországi Egyetem Kiadó, Sopron, 27 p. ISBN 978-963-334-080-6

Csáki, P., Gyimóthy, K., Kalicz, P., Szolgay, J., Zagyvai-Kiss, K.A., Gribovszki, Z., 2020. Multi-model climatic water balance prediction in the Zala River Basin (Hungary) based on a modified Budyko framework. J. Hydrol. Hydromech., 68, 2, 200–210.

Fang, X., Cleveland, T., Garcia, A.C., Thompson, D., Malla, R., 2005. Literature Review on Timing Parameters for Hydrographs. Report 0-4696-1. Department of Civil Engineering College of Engineering at Lamar University, Beaumont, 82 p.

Gaál, L., Szolgay, J., Kohnová, S., Parajka, J., Merz, R., Viglione, A., Blöschl, G., 2012. Flood timescales: Understanding the interplay of climate and catchment processes through comparative hydrology. Water Resources Research, 48, 4, 21.

Gribovszki, Z., 2015. Hungarian National Report on IAHS (2011-2014). Geomatikai Közlemények, 18, 1, 106–113.

HC, 2020. The Hydrocarpath conference. http://hydrocarpath.nyme.hu/index.php/21952/?&L=4

Hlaváčiková, H., Novák, V., Kostka, Z., Danko, M., Hlavčo, J., 2018. The influence of stony soil properties on water dynamics modeled by the HYDRUS model. J. Hydrol. Hydromech., 66, 181–188.

Hogan, P., Parajka, J., Heng, L., Strauss, P., Blöschl., G., 2020. Partitioning evapotranspiration using stable isotopes and Lagrangian dispersion analysis in a small agricultural catchment. J. Hydrol. Hydromech., 68, 2, 134–143. DOI: 10.2478/johh-2020-0009

Holko, L., Sleziak, P., Danko, M., Bičárová, S., Pociask-Karteczka, J., 2020a. Analysis of changes in the hydrological cycle of a pristine mountain catchment. 1. Water balance components and snow cover. J. Hydrol. Hydromech., 68, 2, 180–191. DOI: 10.2478/johh-2020-0010

Holko, L., Danko, M., Sleziak, P., 2020b. Analysis of changes in the hydrological cycle of a pristine mountain catchment. 2. Isotopic data, trend and attribution analyses. Hydrol. Hydromech., 68, 2, 192–199. DOI: 10.2478/johh-2020-0011.

Kohnová, S., Rutkowska, A., Banasik, K., Hlavčová, K., 2020. The L-moment based regional approach to curve numbers for Slovak and Polish Carpathian catchments. J. Hydrol. Hydromech., 68, 2, 170–179. DOI: 10.2478/johh-2020-0004

Krajčí, P., Danko, M., Hlavčo, J., Kostka, Z., Holko, L., 2016. Experimental measurements for improved understanding and simulation of snowmelt events in the Western Tatra Mountains. J. Hydrol. Hydromech., 64, 4, 316–328.

Krysanova, V., Hattermann, F.F., 2017. Intercomparison of climate change impacts in 12 large river basins: an overview of methods and summary of results. Climatic Change, 141, 3, 363–379.

Kundzewicz, Z.W., Robson, A.J., 2004. Change detection in hydrological records—a review of the methodology. Hydrological Sciences Journal, 49, 1, 7–19.

Longman, J., Veres, D., Ersek, V., Haliuc, A., Wennrich, V., 2019. Runoff events and related rainfall variability in the Southern Carpathians during the last 2000 years. Scientific Reports, 9, 1, 5334.

McCutcheon, S.C., Tedela, N.H., Adams, M.B., Swank, W., Campbell, J.L., Hawkins, R.H., Dye, C.R., 2006. Rainfall-runoff relationships for selected eastern U.S. forested mountain watersheds: Testing of the curve number method for flood analysis. Report prepared for the West Virginia Division of Forestry, Charleston, West Virginia.

Merz, B., Vorogushyn, S., Uhlemann, S., Delgado, J., Hundecha, Y., 2012. HESS Opinions "More efforts and scientific rigour are needed to attribute trends in flood time series". Hydrol. Earth Syst. Sci., 16, 1379–1387.

Montanari, A., Bahr, J., Bloeschl, G., Cai, X., Mackay, D.S., Michalak, A.M., Rajaram, H., Sander, G., 2015. Fifty years of Water Resources Research: Legacy and perspectives for the science of hydrology. Water Resour. Res., 51, 6797–6803.

Mujtaba, B., Hlaváčiková, H., Danko, M., de Lima, J.L.M.P., Holko., L., 2020. The role of stony soils in hillslope and catchment runoff formation. J. Hydrol. Hydromech., 68, 2, 144–154. DOI: 10.2478/johh-2020-0012

Ninov, P., Bojilova, E. (Eds.), 2017. XXVII Conference of Danubian Countries on the hydrological forecasting and hydrological bases of water management. Book of proceedings.

Golden Sands, Bulgaria, 624 p. ISBN 978-954-90537-2-2

Olsson, J., Arheimer, B., Borris, M., Donnelly, C., Foster, K., Nikulin, G., Persson, M., Perttu, A-M., Uvo, C.B., Viklander, M., Yang, W., 2016. Hydrological climate change impact assessment at small and large scales: key messages from recent progress in Sweden. Climate, 4, 3, 39, 1–24.

Pekárová, P., Miklánek, P., Halmová, D., Onderka, M., Pekár, J., Kučárová, K., Liová, S., Škoda, P., 2011. Long-term trend and multi-annual variability of water temperature in the pristine Bela River basin (Slovakia). Journal of Hydrology, 400, 3, 333–340.

Prohaska, S., Brilly, M., Kryzanovski, A., 2020. Cooperation of hydrologists from the Danube River Basin. HESS Discussions, 10 p. https://doi.org/10.5194/hess-2020-66

Rogger, M., Agnoletti, M., Alaoui, A., Bathurst, J.C., Bodner, G., Borga, M., Chaplot, V., Gallart, F., Glatzel, G., Hall, J., Holden, J., Holko, L., Horn, R., Kiss, A., Kohnová, S., Leitinger, G., Lennartz, B., Parajka, J., Perdigão, R., Peth, S., Plavcová, L., Quinton, J.N., Robinson, M., Salinas, J.L., Santoro, A., Szolgay, J., Tron, S., van den Akker, J.J.H., Viglione, A., Blöschl, G., 2017. Land use change impacts on floods at the catchment scale: Challenges and opportunities for future research. Water Resour. Res., 53, 5209–5219.

Rončák, P., Hlavčová, K., Látková, T., 2016. Estimation of the effect of changes in forest associations on runoff processes in basins: Case study in the Hron and Topľa River Basins. Slovak Journal of Civil Engineering, 24, 3, 1–7.

Rutkowska, A., Kohnová, S., Banasik, K., Szolgay, J., Karabová, B., 2015. Probabilistic properties of a curve number: a case study for small Polish and Slovak Carpathian Basins. J. Mt. Sci., 12, 3, 533–548.

Scherrer, S., Naef, F., Faeh, A.O., Cordery, I., 2007. Formation of runoff at the hillslope scale during intense precipitation. Hydrol. Earth Syst. Sci., 11, 907–922.

Silasari, R., Parajka, J., Ressl, C., Strauss, P., Blöschl, G., 2017. Potential of time-lapse photography for identifying saturation area dynamics on agricultural hillslopes. Hydrological Processes, 31, 3610–3627. DOI: 10.1002/hyp.11272

Šimůnek, J., Šejna, M., van Genuchten, M.T., 2018. New features of version 3 of the HYDRUS (2D/3D) computer software package, J. Hydrol. Hydromech., 66, 2, 133–142. DOI: 10.1515/johh-2017-0050

Smith, R., Redding, T., 2012. Cumulative effects assessment: runoff generation in snowmelt dominated montane and boreal plain catchments. Watershed Management Bulletin, 15, 24–34.

Soulis, K.X., Valiantzas, J.D., Dercas, N., Londra, P.A., 2009. Investigtion of the direct runoff generation mechanism for the analysis of the SCS-CN method applicability to a partial area experimental watershed. Hydrol. Earth Syst. Sci., 13, 605–615.

Stagl, J.C., Hattermann, F.F., 2015. Impacts of climate change on the hydrological regime of the Danube River and its tributaries using an ensemble of climate scenarios. Water, 7, 6139–6172.

Széles, B., Broer, M., Parajka, J., Hogan, P., Eder, A., Strauss, P., Blöschl, G., 2018. Separation of scales in transpiration effects on low flows: A spatial analysis in the Hydrological Open Air Laboratory. Water Resources Research, 54, 9, 6168–6188.

Tesař, M., Šír, M., Syrovátka, O., Pražák, J., Lichner, Ľ., Kubík, F., 2001. Soil water regime in head water regions - observation, assessment and modelling. J. Hydrol. Hydromech., 49, 6, 355–406.

Tromp-van Meerveld, H.J., McDonnell, J.J., 2006. Threshold relations in subsurface stormflow: 2. The fill and spill hypothesis. Water Resour Res., 42, W02411.

Viglione, A., Chirico, G.B, Komma, J., Woods, R., Borga, M., Blöschl, G., 2010. Quantifying space-time dynamics of flood event types. Journal of Hydrology, 394, 1–2, 213–229.

Viglione, A., Rogger, M., Pirkl, H., Parajka, J., Blöschl, G., 2018. Conceptual model building inspired by field-mapped runoff generation mechanisms. J. Hydrol. Hydromech., 66, 3, 303–315. DOI: 10.2478/johh-2018-0010

Wahren, A., Feger, K.H., Schwärzel, K., Münch, A., 2009. Land-use effects on flood generation – considering soil hydraulic measurements in modelling. Advances in Geosciences, 7, 1–9.

Wang, K., Dickinson, R.E., 2012. A review of global terrestrial evapotranspiration: Observation, modeling, climatology, and climatic variability. Rev. Geophys., 50, RG2005, 54 p.

J. Hydrol. Hydromech., 68, 2020, 2, 134–143
DOI: 10.2478/johh-2020-0009
ISSN 1338-4333

sciendo Journal of Hydrology and Hydromechanics

Partitioning evapotranspiration using stable isotopes and Lagrangian dispersion analysis in a small agricultural catchment

Patrick Hogan[1*], Juraj Parajka[1,2], Lee Heng[3], Peter Strauss[4], Günter Blöschl[1,2]

[1] Centre for Water Resource Systems, TU Wien, Karlsplatz 13, 1040 Vienna, Austria.
[2] Institute of Hydraulic Engineering and Water Resources Management, TU Wien, Karlsplatz 13/222, 1040 Vienna, Austria.
[3] Soil and Water Management and Crop Nutrition Subprogramme, Joint FAO/IAEA Division of Nuclear Techniques in Food and Agriculture, International Atomic Energy Agency (IAEA), 1400 Vienna, Austria.
[4] Institute for Land and Water Management Research, Federal Agency for Water Management, Pollnbergstrasse 1, 3252 Petzenkirchen, Austria.
[*] Corresponding author. Tel.: +43-1-58801-406664. E-mail: hogan@waterresources.at

Abstract: Measuring evaporation and transpiration at the field scale is complicated due to the heterogeneity of the environment, with point measurements requiring upscaling and field measurements such as eddy covariance measuring only the evapotranspiration. During the summer of 2014 an eddy covariance device was used to measure the evapotranspiration of a growing maize field at the HOAL catchment. The stable isotope technique and a Lagrangian near field theory (LNF) were then utilized to partition the evapotranspiration into evaporation and transpiration, using the concentration and isotopic ratio of water vapour within the canopy. The stable isotope estimates of the daily averages of the fraction of evapotranspiration (Ft) ranged from 43.0–88.5%, with an average value of 67.5%, while with the LNF method, Ft was found to range from 52.3–91.5% with an average value of 73.5%. Two different parameterizations for the turbulent statistics were used, with both giving similar R^2 values, 0.65 and 0.63 for the Raupach and Leuning parameterizations, with the Raupach version performing slightly better. The stable isotope method demonstrated itself to be a more robust method, returning larger amounts of useable data, however this is limited by the requirement of much more additional data.

Keywords: Evapotranspiration partitioning; Stable isotopes; Lagrangian dispersion theory.

INTRODUCTION

Evapotranspiration (ET) forms an important part of the water balance across all spatial and temporal scales. For many applications however, further information on the partitioning of evapotranspiration into its constituent components of evaporation and transpiration is required, e.g. for irrigation management (Tong et al., 2009) and climate modelling (Lian et al., 2018).

At different spatial scales ET can be estimated using different methods and techniques such as water balance, remote sensing and energy balance modelling at global and regional scales (Vinukollu et al., 2011), or measured using eddy covariance or scintillometry at field scales. However, these methods provide little or no information on how the ET is partitioned into its components of evaporation (E) and transpiration (T). Other direct measurement techniques at the point scale, such as lysimeters for measuring soil evaporation (Heinlein et al., 2017; Rafi et al., 2019) or sap flow sensors for transpiration (Agam et al., 2012; Zhao et al., 2016) can be used to directly measure the individual components, however they have a very small footprint which requires upscaling to the field scale, which is strongly influenced by the heterogeneity of the surrounding area. For trees in the riparian zone, transpiration can be estimated from groundwater fluctuations (Gribovszki et al., 2008), however this is not applicable for crops with their shallower root systems. Assumptions can be made in order to estimate Ft, such as when E or T could be assumed to be negligible, however these assumptions have been shown to not be applicable to every ecosystem (Stoy et al., 2019). An alternative approach is to partition the measured field scale ET using methods such as Lagrangian dispersion analysis (Raupach, 1989a; Warland and Thurtell, 2000) or stable isotopes (Ma et al., 2018; Wang et al., 2013; Williams et al., 2004; Xiao et al., 2018; Yepez et al., 2003).

The Lagrangian dispersion analysis method an inverse modelling approach, where the source/sink distribution of a scalar is related to a concentration profile of the scalar within a canopy ecosystem through a turbulent dispersion field (Raupach 1989a; Santos et al., 2011; Warland and Thurtell, 2000). Within a plant canopy, the gradient - diffusion relationship cannot be used to calculate the flux of a trace gas due to the role of large turbulent eddies in the vertical transport of the scalar, resulting in the observation of counter-gradient fluxes (Denmead and Bradley, 1985). Instead Raupach (1989a, 1989b) developed a model in a Lagrangian framework where the trajectory of fluid particles released from a source is followed, thereby taking into account the history of the particles. Then the resulting concentration profile can be broken up into two regions, a near field region where the particles disperse linearly in time due to the persistence of the turbulent eddies, and a far field region where the particles disperse with the square root of time diffusively. The method has been used to calculate the flux of CO_2, H_2O and heat within coniferous (Styles et al., 2002) and eucalyptus forest canopies (Haverd et al., 2011). In addition, Haverd et al. (2009) applied the method in a eucalyptus forest along with a Soil-Vegetation-Atmospheric-Transfer model (SVAT) to improve the estimation of turbulent statistics in a forest canopy.

The Keeling Plot (Keeling, 1958) mass balance can be applied within a field ecosystem, to the isotopes of water evaporated from within the canopy. As water evaporated from the soil has a different ratio of light to heavy isotopes compared to water vapour evaporated from plant stomata, this difference in isotopic ratio allows for the estimation of the soil evaporation-

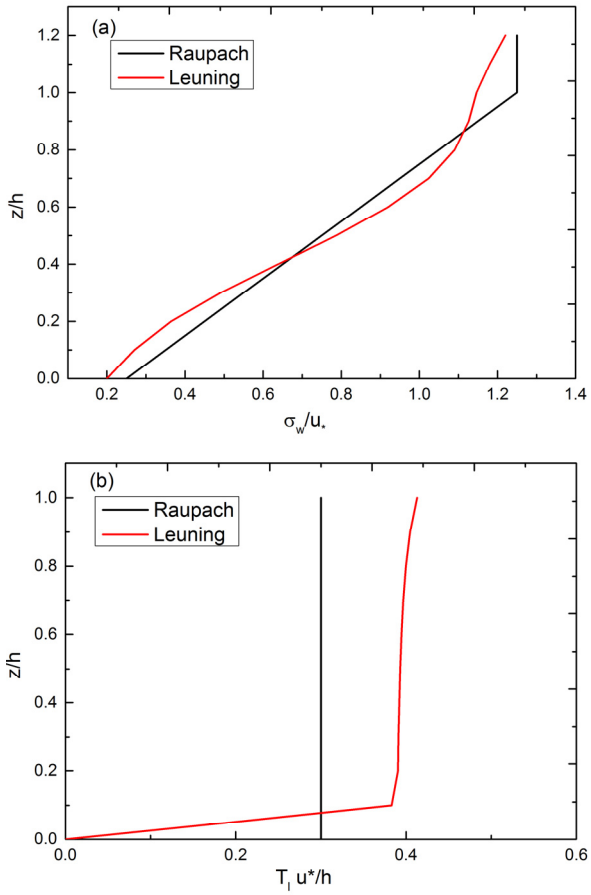

Fig. 1. Normalised profiles of the standard deviation of (a) the vertical velocity, σ_w and (b) the Lagrangian time scale, T_L, according to Raupach (1989a) and Leuning (2000).

transpiration ratio within the ecosystem. This method has been tested in a number of different vegetation and crop types such as an olive orchard (Williams et al., 2004), woodland (Dubbert et al., 2013), beets (Quade et al., 2019) and maize (Wu et al., 2016). Applying the method to determine the temporal variability of root water uptake depth of wheat plants, Zhang et al. (2011) estimated that up to 30% of water consumption during the irrigation season can be evaporation. Using deuterium isotopes in grassland over a short time period, Good et al. (2014) investigated the evolution of the evaporation/transpiration ratio during the growing phase of the grass crop. Wei et al. (2015) measured Ft over a rice field over the course of an entire growing season, with the estimated Ft ranging from 0.2 at the start of the growing season up to a near constant value between 0.8–1.0.

The objective of this study is to estimate the components of evapotranspiration in a vegetative maize field and its response to precipitation events at a high temporal resolution. In this paper we use the stable isotope method and the localised near field theory of Lagrangian dispersion analysis. Both methods use measurements of water vapour concentration within the canopy and a mass balance approach as their basis, while the isotope method requires extra measurements and assumptions, this allows for an additional study of the robustness and effectiveness of the two methods.

THEORY AND METHODS

Lagrangian dispersion analysis

In order to partition the evapotranspiration inside a crop ecosystem between E and T using an inverse method we first divide the source distribution into m vertical layers, where the first layer is just above the surface to account for soil evaporation, and the subsequent layers extend from just above this layer to the top of the canopy for transpiration. The water vapour released from these layers results in a concentration profile, which can be measured at n different heights. The relationship between scalar source density $\varphi(z)$ and concentration $C(z)$ under steady conditions in a horizontally homogenous canopy can be written as

$$C_i - C_r = \sum_{j=1}^{m} D_{ij}\varphi_j \Delta z_j \tag{1}$$

where C_i is the concentration at height z_i, C_r is the concentration at a reference height above the canopy z_r, D_{ij} is the dispersion matrix, with i rows for 1, .., n measurement heights, and j columns for 1, .., m source layers , φ_j is the source strength in layer j, and Δz_j is the thickness of layer j. The inversion of this equation then allows for the estimation of the source strengths, in this case E and T. To calculate the dispersion matrix, the source strength in one layer j is set to be a steady unit source, S_j and set to zero in all other layers. This gives a partial concentration profile C_i, which defines the elements of D_{ij} for dispersion from layer j to the concentration at height z_i

$$D_{ij} = \frac{C_i - C_r}{S_j - \Delta z_j} \tag{2}$$

In a Lagrangian analysis of particle dispersion within a canopy, the trajectory of a particle is followed from its release from a source. The resulting concentration C_i is due to the influence of two different regions on this path, a near field and a far field region.

In the Localised Near Field (LNF) theory of Raupach (1989a, 1989b), the two regions are treated separately, with C_i equal to the sum of both regions

$$C_i = C_n + C_f \tag{3}$$

In the near field, local effects dominate the dispersion of the particles while in the far field, it is assumed that particles diffuse in accordance with gradient-diffusion theory. The near and far field components can be described using the turbulent statistics for the canopy, the vertical profile of the standard deviation of the vertical velocity (σ_w) and the Lagrangian time scale (T_L) according to Raupach (1989a) as

$$C_n(z) = \int_0^{\infty}\int \frac{S(z_s)}{\sigma_w(z_s)}\left\{k_n\left[\frac{z-z_S}{\sigma_w(z_s)T_L(z_s)}\right] + k_n\left[\frac{z+z_S}{\sigma_w(z_s)T_L(z_s)}\right]\right\}dz_S \tag{4}$$

$$C_f(z) = C(z_{ref}) - C_n(z_{ref}) + \int_z^{z_{ref}} \frac{F(z')}{K_f(z')}dz' \tag{5}$$

where z' is the discrete height, z_s is the source height, k_n is a near field 'kernel', $F(z)$ is the flux density, and K_f is the far field diffusivity.

$$k_n(\zeta) = -0.3989\ln\left(1-\exp(-|\zeta|)\right) - 0.1562\exp(-|\zeta|) \tag{6}$$

$$F(z) = -K_f(z)\frac{dc_f}{dz} \tag{7}$$

$$K_f = \sigma_w^2(z) T_L(z) \tag{8}$$

where $\zeta = (z - z_0)/ (\sigma_{w0} T_{L0})$. As T_L cannot be directly measured by fixed sensors as it is a Lagrangian quantity and due to the difficulty of making vertical wind measurements inside a canopy, the profiles of σ_w and T_L needed for the calculation of D_{ij} are normally calculated using turbulent statistical parameterisations. Based on the results of Santos et al. (2011) the parameterisations suggested by Raupach (1989a) and Leuning (2000) were used in this study. Raupach (1989a) proposed that σ_w and T_L profiles could be approximated by the piecewise linear profiles

$$\frac{\sigma_w}{u*} = f(x) = \begin{cases} a_0 + (a_1 - a_0) \times \dfrac{z}{h}, & z < h \\ a_1, & z \geq h \end{cases} \tag{9}$$

$$\frac{T_L u*}{h} = \max\left[c_0, \frac{k(z-d)}{a_1 h} \right] \tag{10}$$

where $a_1 = 1.25$, $a_0 = 0.25$, $c_0 = 0.3$, $d = 2/3h$ is the displacement height, h is the canopy height, $u*$ is the friction velocity and $k = 0.41$ is the von Karman constant.

The parameterisations of Leuning are based on exponential and non- rectangular functions within and above the canopy

$$y = c_1 e^{c_2 z/h} \text{ for } z < 0.8h$$

$$y = \frac{(ax+b) + d_1\sqrt{(ax+b)^2 - 4\theta abx}}{2\theta} \text{ for } z \geq 0.8h \tag{11}$$

where $c_1 = 0.2$ and the other coefficients can be found in Table 1.

Table 1. A list of the variables and parameters used for the determination of normalised profiles of the standard deviation of the vertical velocity, σ_w and the Lagrangian timescale, T_L. (Leuning, 2000).

z/h	x	y	θ	a	b	d
≥0.8	z/h	$\sigma_w/u*$	0.98	0.850	1.25	–1
≥0.25	$z/h - 0.8$	$T_L u*/h$	0.98	0.256	0.40	+1
<0.25	$4z/h$	$T_L u*$/h	0.98	0.850	0.41	–1

These parameterisations were originally derived for near-neutral conditions and corrections functions have been suggested for use in non-neutral conditions (Leuning, 2000). However the performance of these corrections has been mixed, with Santos et al. (2011) reporting an increase in the overestimation of the latent heat flux when the corrections were used.

Stable isotope method

Measurements of isotopes are expressed as the ratio of heavy to light isotopes relative to the international standard and written in (δ) notation in per mil (‰).

The fraction of evapotranspiration that is due to transpiration can be calculated as (Yakir and Sternberg, 2000)

$$F_T(\%) = \frac{\delta_{ET} - \delta_E}{\delta_T - \delta_E} \tag{12}$$

where F_T(%) is (T/ET x 100), δ_{ET} is the isotopic composition of water vapor that has been evapotranspirated, δ_T is the isotopic composition of water vapor that has been transpired, and δ_E is the isotopic composition of soil water that has been evaporated. δ_T and δ_E can be estimated by vegetation and soil sampling whereas δ_{ET} is determined using an ecosystem mass balance equation,

$$\delta_{ebl} = C_a\left((\delta_a - \delta_{ET})\left(\frac{1}{C_{ebl}}\right) + \delta_{ET} \right) \tag{13}$$

where δ_{ebl} is the isotopic composition of water vapor in the system boundary layer, C_a is the water vapor concentration in the atmosphere, δ_a is the isotopic composition of water vapor in the atmosphere and C_{ebl} is ecosystem boundary layer water vapor concentration. Using this linear relationship, measurements of the isotope ratio of the water vapor of the air at different heights within the canopy plotted versus the inverse of the concentration, will yield an estimate of δ_{ET} as the resulting y-axis intercept (Yakir and Sternberg, 2000).

δ_E is usually not measured directly, due to the difficulty of designing non-destructive sampling methods, instead it is indirectly calculated using the Craig-Gordon model and measurements of soil water at the evaporating front within the soil (Craig and Gordon, 1965). The Craig- Gordon model estimates the effects of fractionations on liquid water in the soil as it evaporates (Moreira et al., 1997)

$$R_E = \left(\frac{1}{\alpha_K}\right)\frac{\left(\frac{R_s}{\alpha*}\right) - R_A h}{1 - rh} \tag{14}$$

where R_E is the molar ratio of heavy to light isotopes of: E, the evaporated water vapor, R_s, water in the soil, and R_A, air near the surface, rh is the relative humidity normalised by the saturation pressure at the surface, α_K is the kinetic fraction rate, taken to be 1.0189‰, Flanagan et al., 1991) and $\alpha*$ is the equilibrium fractionation factor as a function of temperature (T) (Majoube, 1971).

$$\alpha* = \frac{1.137 \times 10^6}{T^2} - \frac{0.4156 \times 10^3}{T} - 2.0667 \tag{15}$$

The isotopic signature of transpiration (δ_T) can be determined non-destructively using closed leaf vapor chambers or by measurement of stem water isotopic composition, assuming no isotopic fractionation in the transpiration process (Lin and Sternberg, 1993; Wang and Yakir, 2000).

STUDY AREA

The experiment was performed from the 24th June – 2nd July 2014 at the Hydrological Open Air Laboratory (HOAL) at Petzenkirchen, Austria (48°9' N, 15°9' E) (Blöschl et al., 2016). The catchment has an area of 66 ha, elevation ranges from 268–323 m above sea level, with a mean slope of 8%. Land use comprises of 87% agricultural crops, 5% grassland pasture, 6% forest and 2% paved surfaces. The local climate can be described as humid, with a mean annual precipitation of 823 mm/yr, with larger amounts of precipitation in summer than in winter. The mean annual temperature is 9.5°C. Evapotranspiration in the years from 2013–2017 ranged from 442–518 mm/yr. As the experiment was planned for early summer and a limited time period, a 4.8 ha maize field was selected as the early growing stage and wider spacing between crops would allow for assumptions of turbulent mixing within

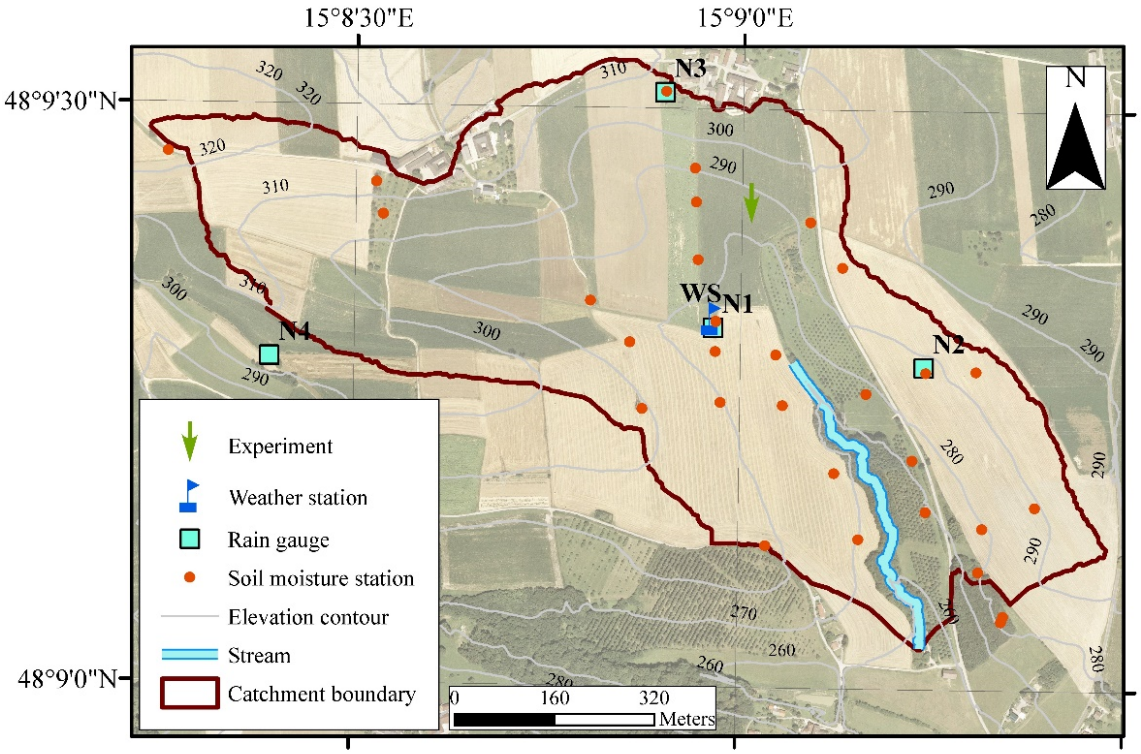

Fig. 2. The experimental catchment showing the location of the measurement devices and the study field (green arrow).

Fig. 3. The experimental area, showing the location of the eddy covariance system (right) and the picaro device (left).

the ecosystem to be fulfilled. The average height of the plants increased from 0.95 m to 1.40 m with the Leaf Area Index (LAI) progressing from 1.2 to 2.4 during this period.

Instrumentation

To measure the profiles of water vapour concentration and isotopic ratio (O_{18}/O_{16}) within the canopy a L2130-i analyser (Picarro) was installed within the maize field. Air was sampled within the canopy and above, using a 6-port intake valve connected to a pump and sampled using the analyser at 1 Hz. To achieve a precision of 0.02‰ an averaging time of at least 100 seconds was required for each individual ports and gave an overall resolution of 20 minutes for δ_{ET} and C across the 6 ports. δ_{ebl} and C_{ebl} were sampled at 4 heights within the canopy (0.1, 0.2, 0.5 and 1.0 m), and 2 additional sample intakes were located above the canopy (1.7 and 2.4 m). The ports at heights 0.5 and 1.0 m were later increased to 0.8 and 1.2 m on the 1st July due to the increase in canopy height. δ_T was estimated from xylem water taken from 4 maize plants, sampled between 11–14 h on each day of the experiment. This assumes that the xylem water is at isotopic steady state is normally is valid between late morning and early afternoon. To estimate δ_E using Equation (14), soil samples were taken daily at 4 locations near the air intake, at depths of 0–2, 2–5 and 5–10 cm to correctly identify the evaporation front according to Rothfuss et al. (2010). All soil and plant samples were sealed in glass vials, frozen and then transported to the laboratory for extraction, according to the guidelines of Mayr et al. (2016).

Evapotranspiration was measured using an open path eddy covariance sensor (IRGASON, Campbell Scientific). The device was installed in the middle of the maize field at a height of 2.20 m before the experiment and moved to a height of 2.80 m during the early morning of the 1st to stay above the minimum height limit described by (Aubinet et al., 2012). The TK3 software was used to calculate the latent heat flux from the raw measurements of the wind speed and water vapour (Mauder and Foken, 2015). As part of the processing procedure a number of corrections must be applied to the raw data: (i) a double rotation of the coordinate system, this was used rather than the planar fit method due to the rapid growth of the maize crop and short time period of the experiment, (ii) the Moore correction for high frequency loss (Moore, 1986), (iii)a sonic air temperature for the sensible heat flux, and (iv) the WPL correction to account for density fluctuations (Webb et al., 1980). The TK3 software includes a quality control analysis and sensible and latent heat flux data of a low quality were removed.

Air temperature and humidity were measured at the eddy covariance station using a HMP155 probe. Precipitation was measured across the catchment using 4 weighing balance gauges (OTT Pluvio). For this experiment the data from the closest rain gauge, located at the nearby weather station was used. The catchment is instrumented with a network of soil moisture stations utilising Time Domain Transmission (TDT) probes. A station was located in the maize field to measure the near surface soil temperature and water content at depths of 0.05 and 0.1 m.

RESULTS

Environmental conditions

Figure 4 shows the environmental conditions over the time period of the experiment. Weather conditions were mixed over the course of the experiment, with most days experiencing periods of sunshine and cloud, except for the 30th where the

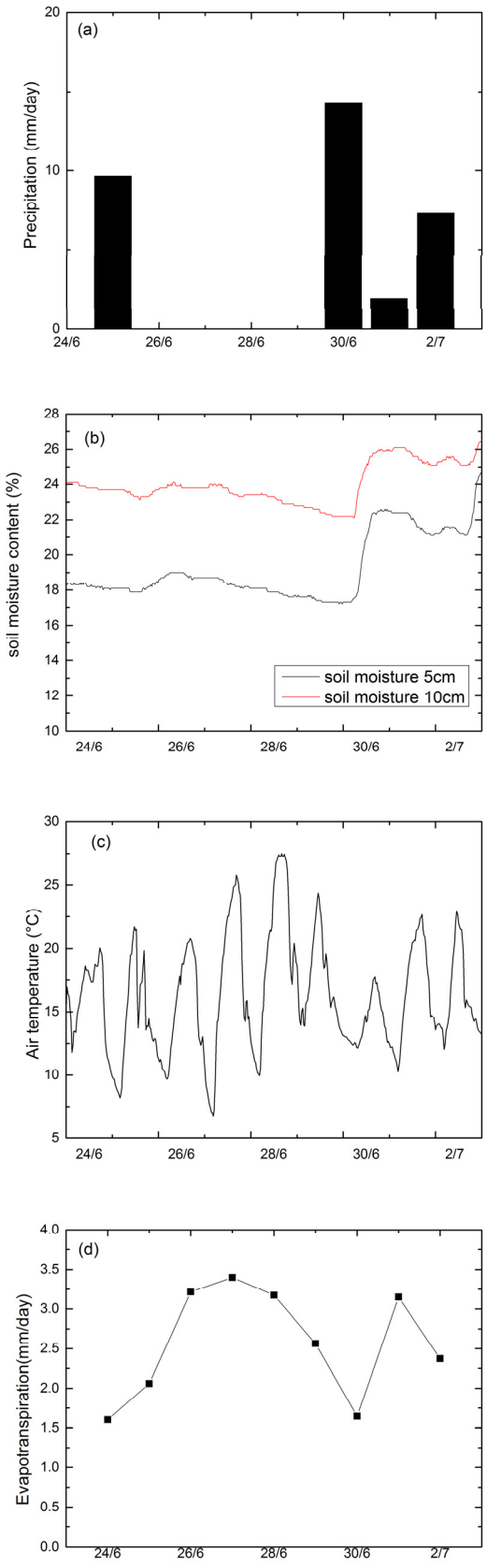

Fig. 4. Half hourly plots of (a) precipitation, (b) soil moisture at 5 and 10 cm, (c) air temperature and (d) daily values of evapotranspiration measured using the eddy covariance system for the period June 24th – July 2nd, 2014.

passage of a frontal system resulted in overcast conditions and persistent rain until late afternoon. In total four precipitation events were recorded, with three of them having a major effect on the near surface soil moisture level. The duration of the event on the 30th meant that it was not possible to use the data from this day, however the shorter nature of the other events meant less loss of data on those days. The average daily mean temperatures ranged from 14.2–20.0°C with maximum daily temperatures between 17.8–27.5°C. Daily evapotranspiration was strongly related to temperature, VPD and net radiation, with a total of 23.2 mm recorded over the experiment, with the highest daily values occurring during the dry period from the 26th – 28th. Figure 5 shows the friction velocity and the virtual stability measured using the eddy covariance system. The friction velocity was in general quite low at this site, following a diurnal pattern during the period of high solar radiation from the 26th – 29th. The atmospheric stability was generally unstable during the daytimes except for the period during the passage of the frontal system, where the stability was very close to neutral.

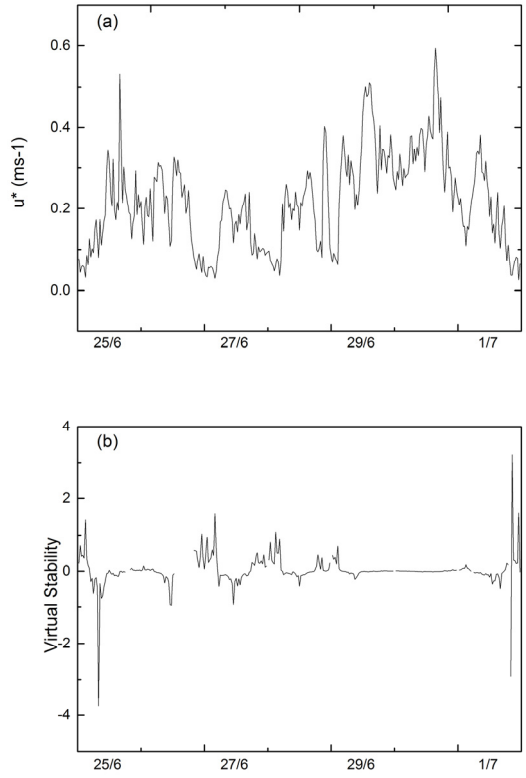

Fig. 5. Half hourly plots of (a) u* and (b) virtual stability over the period June 25th – July 2nd, 2014.

Evapotranspiration partitioning

The steady state assumption for the stable isotope analysis does not hold in the morning, however, it is usually met in the afternoon (Yepez et al., 2005). The analysis in this paper is hence limited to the time from 10:00–17:00, as this corresponds to the time periods with the largest amounts of solar radiation and hence evapotranspiration, there will only be a limited effect on the results. Data from the 30th and during and directly after precipitation events are also excluded, due to the strong neutral stability and change in the atmospheric water vapor resulting from the passage of the frontal system or interception, resulting in values of Ft in excess of 100%. However due to the very strong concentration gradients near the surface when soil evaporation is very close to zero, the inversion matrix can become ill-conditioned resulting in values over 100% for the LNF method. Therefore, in general the values of Ft higher than 110% and lower than –20% were excluded from the results (Wei et al., 2015). For purposes of averaging Ft was capped at 100%.

Using the stable isotope method, the daily averages of Ft_{ISO} ranged from 43.0–88.5%, with anaverage value of 67.5% following a pattern of decreasing after precipitation events and steadily increasing over the following days. Using the LNF method, Ft (Ft_{LNF}) was found to range from 52.3–91.5% with an average value of 73.5%. Figure 6 shows a comparison of the two methods for the entire experimental period. While the two methods show a high level of agreement on average, on the 29th and 1st July the LNF method estimates much higher values of Ft, on the 29th 91.5% versus 81.7% and on the 1st 52.3% versus 44.5%. Ft_{LNF} however shows much greater variance on these days than Ft_{ISO}, with Ft_{LNF} also estimating values of Ft over 100% on the 28th.

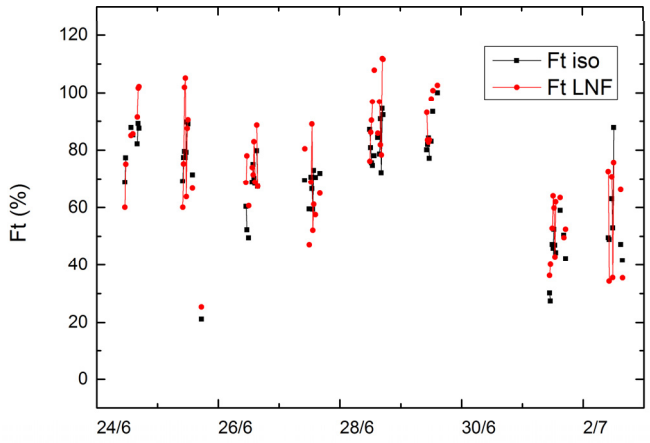

Fig. 6. Twenty-minute values of Ft using the LNF (red circles) and isotope (black squares) methods over the entire experimental period.

Daily ET is strongly dependent on solar radiation and temperature, with the highest values of ET measured from the 26th – afternoon of the 29th. Both Ft_{LNF} and Ft_{ISO} show a similar pattern, with increasing values estimated during this time period. Conversely the soil moisture content in the upper level of the soil at 5 cm was measured decreasing from 19.0% to 17.2%. Following the precipitation event on the 29th – 30th the soil moisture content was recharged up to 22.6%, leading to a marked decrease in Ft_{LNF} from 92.0% to 52.3%. Ft_{ISO} was found to be best correlated with solar radiation (R = 0.68) and showing less correlation with vapor pressure deficit (R = 0.59).

Method comparison

Figure 7 shows a comparison of the two methods on the 26th of June during the daytime period. The uncertainty on the Ft_{iso} estimates was calculated using the single isotope, two source mixing model of Phillips and Gregg (2001). In the late morning period, Ft_{LNF} consistently makes higher estimates of Ft, with a difference of up to 25.8% at 11:00, although closer agreement is noted during the afternoon period, following a gap in the results of Ft_{LNF} from 12:00–13:30 due to overestimation of Ft. During this period Ft_{ISO} continued to give realistic estimates of Ft.

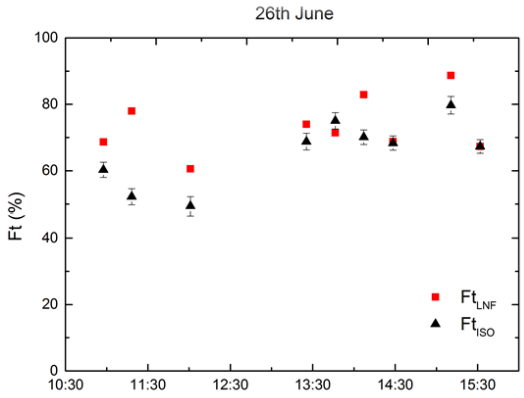

Fig. 7. Comparison of the two methods on the 26th of June during the daytime period.

Throughout the early afternoon Ft_{ISO} and Ft_{LNF} steadily increase with ET, with Ft_{LNF} increasing at a much faster rate to 80–90% by 15:00 while Ft_{ISO} exhibits a slower rate of increase, reaching a maximum of 80%.

Ft was also estimated using the Leuning set of parameterizations for u^* and T_L. In this case Ft_{LNF} varied from 50.1–91.4% with an average of 75.0%. Figure 8 shows a scatterplot of 20 minute values of Ft using the isotope and (a) LNF Raupach and (b) LNF Leuning methods. Both methods give similar R^2 values, 0.65 and 0.63 respectively with the Raupach parameterisations performing slightly better.

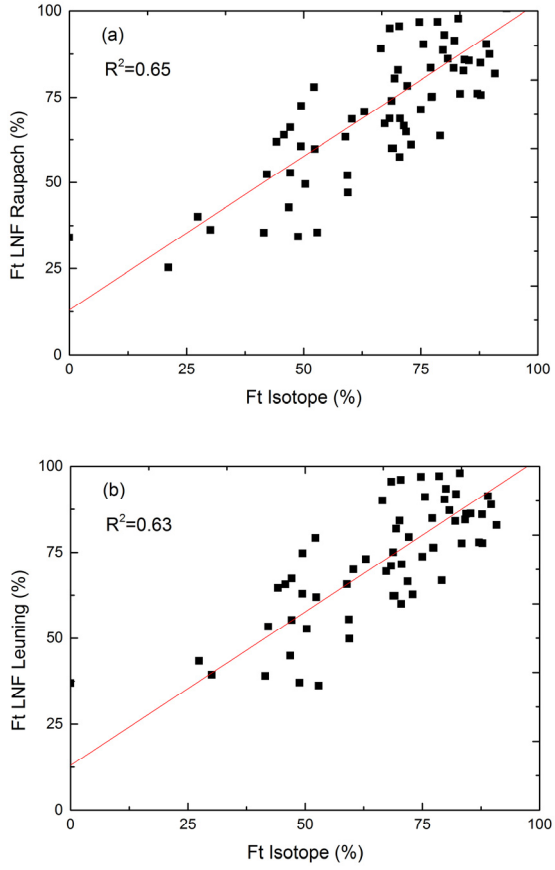

Fig. 8. Scatterplots of 20 minute values of Ft using the isotope and (a) LNF Raupach and (b) LNF Leuning methods for the entire experimental period.

DISCUSSION

In this study we utilize the LNF and ISO methods to partition evapotranspiration. Both methods use water vapor concentration measurements from inside the plant canopy, however, the stable isotope method requires much more additional data as well as equipment and labour for measuring and analysing the isotope samples.

The average Ft estimated by the LNF method was 74.0% and using the stable isotopes 67.5%. The correlation between the two methods was 0.65. These compare well with measurements using lysimeters which gave a range of 71–75% (Kang et al., 2003; Liu et al., 2002) for maize, 69–87% for olive trees (Williams et al., 2004), and 20–100% over the course of the entire season for rice (Wei et al., 2015). Using chamber based measurements to directly measure the isotopic values, Wu et al. (2016) estimated Ft for the entire vegetative growing section to be ~55%, and ~70% using the Craig- Gordon based model approach, with the difference attributed to deviation in measuring δE using the chamber method. Using isotope tracers Ma et al. (2018) found that for a winter wheat field the value of Ft over the entire crop season did not vary significantly with the type of irrigation treatment, however, the value of Ft for each stage of the growing season did. While an average value of for Ft 65% inline with similar experiments was found using 5 different irrigation methods, between these methods a difference of up 25% in Ft was noted. In non-irrigated catchments the precipitation amounts and intervals must be analyzed in order to apply the results from year to year. During the course of this experiment, both a short but intense (~10 mm/hr) and a less intense but longer duration (~1 mm/hr) precipitation event were recorded, allowing for the changes in Ft to be seen. The response of the soil moisture at 5 cm to the intense event was much less than for the longer event, with a large amount of runoff recorded. This results in a much smaller decrease in Ft on the following day, 73.4% versus 52.3%.

Over the course of the experiment the LNF method shows a pattern of slightly larger estimates of Ft, particularly on the 29th and 1st of July. On the 1st this exceptionally large difference is possibly due to the higher levels of soil evaporation after the large precipitation event on the previous day, resulting in reduced water vapor concentration gradients near the surface, which will have a greater effect on the LNF method as it uses less additional data. On the 29th Ft_{LNF} estimated Ft to be over 100%, however this can be explained due to measurement errors as Ft approached 100%, with Wei et al. (2015) reporting similar values while using the stable isotope method. The only slight change in the performance of the LNF method depending on the parameterisation for the turbulent statistics, would suggest either parameterisation can be used. Comparing LNF modelled and eddy covariance measured latent heat flux estimates, Santos ett al. (2011) also noted only slight changes to the results.

Over the course of the experiment the isotope method proved to be less affected by the environmental conditions, excepting the steady state condition that limits the method to the daytime periods. During these periods the LNF method gives 45.2% less data than the isotope method, with a lot less useable data on days where there is less coupling between the canopy and the atmosphere (25th and 29th) due to the changing conditions and precipitation. This reduction in results is offset however by the lower requirements of additional data, with the isotope method needing isotope measurements of the air, plants and soil. An advantage of using the LNF method which gives a high temporal resolution is that the response of the fraction of transpiration to rain events can be seen in Figures 6 and 8 and

used for adjusting transpiration estimates measured using the eddy covariance method. Isotope methods that use only weekly sampling of the soil water (Santos et al., 2012) will not be able to capture changes in δ_E, however even the daily sampling of the soil and plant isotopes in this experiment is limited due to sudden short precipitation events and the isotopic steady state assumption. While the air sampling can be performed at a high resolution using the Picarro device, the sampling of the plants and soil had to be done manually in this experiment, resulting in a much higher workload and limiting the overall length of the measurement campaign. Measurement devices such as leaf and soil flux chambers which allow for automatic sampling of soil and plant isotope values have been developed in recent years (Wu et al., 2016), however they are still limited by the heterogeneity of field conditions, requiring a number of different devices of considerable expense.

With an estimate for Ft during the growing season, where ET and Ft change in response to not only the environmental conditions but due to the changing physical properties of the plant, compared to the more stable initial and mid-season stages of plant development (FAO-56). As it is difficult and expensive to make full season measurements at a high temporal resolution, an alternative approach is to use our estimate for Ft and an evapotranspiration model. Using a modified version of the FAO-56 method, where the crop coefficient is separated into a crop basal coefficient and an evaporation coefficient, Ding et al. (2013) was able to partition the ET by modifying the crop basal coefficient according to crop leaf cover. The model was then validated using soil heat flux and lysimeter measurements. During the vegetative season however the heterogenous canopy cover and rapid growth of the maize plants can lead to errors when upscaling the individual measurements to the field scale, to avoid this the LNF method which is based on vapor measurements allowing for an averaging through the canopy could be used.

CONCLUSIONS

In this experiment the fraction of evapotranspiration that was due to transpiration was estimated for a maize field using two methods, the isotope measurement based stable isotope method, and the Localised Near Field theory of Raupach based on an inverse Lagrangian modelling approach. Both methods are based on measurements of the water vapour concentration within a plant canopy, however they vary greatly in method. The two methods overall gave similar results, with the fraction of transpiration ranging from 43.0–88.5%, with an average of 67.5% for the isotope method, while the fraction of evaporation was found to range from 52.3–91.9% with an average value of 74.8% for the Localised Near Field method. These values were found to be in line with results from similar experiments for this stage of maize development. However, the stable isotope method was found to return a much larger amount of useable data, as well as having a lower variance. This is offset by the need for more additional measurements and analysis, as well the uncertainty due to the need for the Isotopic Steady State assumption. Future experiments should be conducted using chamber methods when possible to account for this. The parameterizations used for the turbulent wind statistics for the Localised Near Field method were found to vary only slightly. Care must also be taken when applying the results over larger time periods or year to year, to account for different precipitation regimes if the field is not irrigated, with different precipitation events giving different soil moisture and hence soil evaporation responses.

Acknowledgements. The authors wish to thank the Austrian Science Foundation for funding this work as part of the Vienna Doctoral Programme on Water Resource Systems (DK Plus W1219-N22). We would also like to thank the staff of the Institute for Land and Water Management Research (IKT) at Petzenkirchen for their technical assistance.

REFERENCES

Agam, N., Evett, S.R., Tolk, J.A., Kustas, W.P., Colaizzi, P.D., Alfieri, J.G., McKee, L.G., Copeland, K.S., Howell, T.A., Chávez, J.L., 2012. Evaporative loss from irrigated interrows in a highly advective semi-arid agricultural area. Adv. Water Resour., 50, 20–30.

Aubinet, M., Vesala, T., Papale, D., 2012. Eddy Covariance. A Practical Guide to Measurements and Data Analysis. Springer, Dorndrecht, 325 p.

Blöschl, G., Blaschke, A.P., Broer, M., Bucher, C., Carr, G., Chen, X., Eder, A., Exner-Kittridge, M., Farnleitner, A., Flores-Orozco, A., Haas, P., Hogan, P., Kazemi Amiri, A., Oismüller, M., Parajka, J., Silasari, R., Stadler, P., Strauss, P., Vreugdenhil, M., Wagner, W., Zessner, M., 2016. The Hydrological Open Air Laboratory (HOAL) in Petzenkirchen: a hypothesis-driven observatory. Hydrology and Earth System Sciences, 20, 227–255. https://doi.org/10.5194/hess-20-227-2016

Craig, H., Gordon, L., 1965. Deuterium and oxygen-18 variations in the ocean and marine atmosphere. In: Tongiorgi, E. (Ed.): Proceedings of the conference on stable isotopes in oceanographic studies and paleotemperatures. Laboratory of Geology and Nuclear Science, Pisa, pp. 9–130.

Denmead, O.T., Bradley, E.F., 1985. Flux-gradient relationships in a forest canopy. In: Hutchison, B.A., Hicks, B.B. (Eds.): The Forest–Atmosphere Interaction. D. Reidel Publishing Co., Dordrecht, pp. 421–442.

Ding, R., Kang, S., Zhang, Y., Hao, X., Tong, L., Du, T., 2013. Partitioning evapotranspiration into soil evaporation and transpiration using a modified dual crop coefficient model in irrigated maize field with ground-mulching. Agricultural Water Management, 127, 85–96.

Dubbert, M., Cuntz, M., Piayda, A., Maguas, C., Werner, C., 2013. Partitioning evapotranspiration: Testing the Craig and Gordon model with field measurements of oxygen isotope ratios of evaporative fluxes. Journal of Hydrology, 496, 142–153.

Flanagan, L.B., Comstock, J.P., Ehleringer, J.R., 1991. Comparison of modeled and observed environmental influences on the stable oxygen and hydrogen isotope composition of leaf water in *Phaseolus vulgaris* L. Plant Physiology, 96, 2, 588–596.

Good, S. P., Soderberg, K., Guan, K., King, E. G., Scanlon, T. M., Caylor, K. K., 2014. δ^2H isotopic flux partitioning of evapotranspiration over a grass field following a water pulse and subsequent dry down. Water Resources Research, 50, 2, 1410–1432.

Gribovszki, Z., Kalicz, P., Szilagyi, J., Kucsara, M., 2008. Riparian zone evapotranspiration estimation from diurnal groundwater-level fluctuations. J. Hydrol., 349, 6–17.

Haverd, V., Leuning, R., Griffith, D., van Gorsel, E., Cuntz, M., 2009. The turbulent Lagrangian time scale in forest canopies constrained by fluxes, concentrations and source distributions. Bound.-Lay. Meteorol., 130, 209–228.

Haverd, V., Cuntz, M., Griffith, D., Keitel, C., Tadros, C., Twining, J., 2011. Measured deuterium in water vapour concentration does not improve the constraint on the partition-

ing of evapotranspiration in a tall forest canopy, as estimated using a soil vegetation atmosphere transfer model. Agric. Forest Meteorol., 151, 645–654.

Heinlein, F., Biernath, C., Klein, C., Thieme, C., Priesack, E., 2017. Evaluation of simulated transpiration from maize plants on lysimeters. Vadose Zone J., 16, 1, 1–16.

Kang, S., Gu, B., Du, T., Zhang, J., 2003. Crop coefficient and ratio of transpiration to evapotranspiration of winter wheat and maize in a semi-humid region. Agricultural Water Management, 59, 3, 239–254.

Keeling, C.D., 1958. The concentration and isotopic abundances of atmospheric carbon dioxide in rural areas. Geochim Cosmochim. Acta, 13, 322–334.

Lian, X., Piao, S., Huntingford, C., Li, Y., Zeng, Z., Wang, X., Ciais, P., McVicar, T.R., Peng, S., Ottlé, C., Yang, H., Yang, Y., Zhang, Y., Wang, T., 2018. Partitioning global land evapotranspiration using CMIP5 models constrained by observations. Nature Climate Change, 8, 640–646.

Lin, L., Sternberg, L., 1993. Hydrogen Isotopic Fractionation by Plant Roots during Water Uptake in Coastal Wetland Plants, Stable Isotopes and Plant Carbon-water Relations, Academic Press, 497–510.

Liu, C., Zhang, X., Zhang, Y., 2002. Determination of daily evaporation and evapotranspiration of winter wheat and maize by large-scale weighing lysimeter and micro-lysimeter. Agricultural and Forest Meteorology, 111, 2, 109–120.

Leuning, R., 2000. Estimation of scalar source/sink distributions in plant canopies using Lagrangian dispersion analysis: corrections for atmospheric stability and comparison with a multilayer canopy model. Bound. Layer Meteorol., 96, 293–314.

Ma, Y., Kumar, P., Song, X., 2018. Seasonal variability in evapotranspiration partitioning and its relationship with crop development and water use efficiency of winter wheat. Hydrology and Earth System Sciences Discussions. https://doi.org/10.5194/hess-2018-234

Majoube, M., 1971. Fractionnement en oxygene-18 et en deuterium entre leau et sa vapaeur. J. Chim. Phys., 68, 1423–1436.

Mauder, M., Foken, T., 2015. Eddy-Covariance Software TK3. url: http://dx.doi.org/10.5281/zenodo.20349.

Mayr, L., Aigner, M., Heng, L., 2016. Supporting Sampling and Sample Preparation Tools for Isotope and Nuclear Analysis, Section 3.

Moore, C.J., 1986. Frequency response corrections for eddy correlation systems. Boundary-Layer Meteorology, 37, 1–2, 17–35.

Moreira, M., Martinelli, L., Victoria, R., Barbosa, E., Bonates, L., Nepstads, D., 1997. Contribution of transpiration to forest ambient vapor based on isotopic measurements. Global Change Biol., 3, 439–450.

Phillips, D.L., Gregg, J.W., 2001. Uncertainty in source partitioning using stable isotopes. Oecologia, 127, 171–179.

Quade, M., Klosterhalfen, A., Graf, A., Brüggerman, N., Hermes, N., Vereecken, H., Rothfuss, Y., 2019. In-situ monitoring of soil water isotopic composition for partitioning of evapotranspiration during one growing season of sugar beet (*Beta vulgaris*). Agricultural and Forest Meteorology, 266–267, 53–64.

Rafi, Z., Merlin, O., Le Dantec, V., Khabba, S., Mordelet, P., Er-Raki, S., Amazirh, A., Olivera-Guerra, L., Ait Hssaine, B., Simonneaux, V., Ezzahar, J., Ferrer, F., 2019. Partitioning evapotranspiration of a drip-irrigated wheat crop: Inter-comparing eddy covariance-, sap flow-, lysimeter- and FAO-based methods. Agricultural and Forest Meteorology, 265, 310–326.

Raupach, M.R., 1989a. Applying Lagrangian fluid mechanics to infer scalar source distributions from concentration profiles in plant canopies. Agricultural and Forest Meteorology, 47, 2–4, 85–108.

Raupach M.R., 1989b. A practical Lagrangian method for relating scalar concentrations to source distributions in vegetation canopies. Q.J.R. Meteorol. Soc., 115:609–632.

Rothfuss, Y., Biron, P., Braud, I., Canale, L., Durand, J.-L. Gaudet, J.-P., Richard, P., Vauclin, M., Bariac, T., 2010. Partitioning evapotranspiration fluxes into soil evaporation and plant transpiration using water stable isotopes under controlled conditions. Hydrological Processes, 24, 22, 3177–3194.

Santos, E., Wagner-Riddle, C., Warland, J.S., Brown, S., 2011. Applying a Lagrangian dispersion analysis to infer carbon dioxide and latent heat fluxes in a corn canopy. Agricultural and Forest Meteorology, 151, 620–632.

Santos, E., Wagner-Riddle, C., Lee, X., Warland, J., Brown, S., Staebler, R., Bartlet, P., Kim, K., 2012. Use of the isotope flux ratio approach to investigate the $C^{18}O^{16}O$ and $^{13}CO_2$ exchange near the floor of a temperate deciduous forest. Biogeosciences, 9, 2385–2399.

Stoy, P.C., El-Madany, T., Fisher, J.B., Gentine, P., Gerken, T., Good, S.P., Liu, S., Miralles, D.G., Perez-Priego, O., Skaggs, T.H., Wohlfahrt, G., Anderson, R.G., Jung, M., Maes, W.H., Mammarella, I., Mauder, M., Migliavacca, M., Nelson, J.A., Poyatos, R., Reichstein, M., Scott, R.L., Wolf, S., 2019. Reviews and syntheses: Turning the challenges of partitioning ecosystem evaporation and transpiration into opportunities. Biogeosciences, 16, 3747–3775.

Styles, J.M., Raupach, M.R., Farquhar, G.D., Kolle, O., Lawton, K.A., Brand, W.A., Werner, R.A., Jordan, A., Schulze, E.D., Shibistova, O., Lloyd, J., 2002. Soil and canopy CO_2, (CO_2)-C-13, H_2O and sensible heat flux partitions in a forest canopy inferred from concentration measurements. Tellus B Chem. Phys. Meterol., 54, 655–676.

Tong, X., Li, J., Yu, Q., Qin, Z., 2009. Ecosystem water use efficiency in an irrigated cropland in the North China Plain. Journal of Hydrology, 374, 3–4, 329–337.

Vinukollu, R.K., Wood, E.F., Ferguson, C.R., Fisher, J.B., 2011. Global estimates of evapotranspiration for climate studies using multi-sensor remote sensing data: evaluation of three process-based approaches. Remote Sens. Environ., 115, 3, 801–823.

Wang, X.F., Yakir, D., 2000. Using stable isotopes of water in evapotranspiration studies. Hydrol. Process., 14, 1407–1421.

Wang, L., Niu, S., Good, S. P., Soderberg, K., McCabe, M.F., Sherry, R.A., Luo, Y., Zhou, X., Xia, J., Caylor, K.K., 2013. The effect of warming on grassland evapotranspiration partitioning using laser-based isotope monitoring techniques. Geochimica et Cosmochimica Acta, 111, 28–38.

Warland, J.S., Thurtell, G.W., 2000. A Lagrangian solution to the relationship between a distributed source and concentration profile. Boundary-Layer Meteorol., 96, 453–471.

Webb, E., Pearman, G., Leuning, R., 1980. Correction of flux measurements for density effects due to heat and water vapor transfer. Q.J.R. Meteor. Soc., 106, 85–100.

Wei, Z., Yoshimura, K., Okazaki, A., Kim, W., Liu, Z., Yokoi, M., 2015. Partitioning of evapotranspiration using high-frequency water vapor isotopic measurement over a rice paddy field: Partitioning of evapotranspiration. Water Resources Research, 51, 5, 3716–3729.

Williams, D., Cable, W., Hultine, K., Hoedjes, J., Yepez, E., Simonneaux, V., Er-Raki, S., Boulet, G., de Bruin, H., Chehbouni, A., Hartogensis, O., Timouk, F., 2004. Evapo-

transpiration components determined by stable isotope, sap flow and eddy covariance techniques. Agricultural and Forest Meteorology, 125, 3–4, 241–258.

Wu, Y., Du, T., Ding, R., Tong, L., Li, S., Wang, L., 2016. Multiple methods to partition evapotranspiration in a maize field. Journal of Hydrometeorology, 18, 1, 139–149.

Xiao, W., Wei, Z., Wen, X., 2018. Evapotranspiration partitioning at the ecosystem scale using the stable isotope method – A review. Agricultural and Forest Meteorology, 263, 346–361.

Yakir, D., Sternberg, L., 2000. The use of stable isotopes to study ecosystem gas exchange. Oecologia, 123, 3, 297–311.

Yepez, E.A., Williams, D.G., Scott, R.L., Lin, G., 2003. Partitioning overstory and understory evapotranspiration in a semiarid savanna woodland from the isotopic composition of water vapor. Agricultural and Forest Meteorology, 119, 1–2, 53–68.

Yepez, E.A., Huxman, T.E., Ignace, D.D., English, N.B., Weltzin, J.F., Castellanos, A.E., Williams, D.G., 2005. Dynamics of transpiration and evaporation following a moisture pulse in semiarid grassland: A chamber-based isotope method for partitioning flux components. Agricultural and Forest Meteorology, 132, 3–4, 359-376.

Zhang, Y., Shen, Y., Sun, H., Gates, J., 2011. Evapotranspiration and its partitioning in an irrigated winter wheat field: A combined isotopic and micrometeorologic approach. Journal of Hydrology, 408, 3, 203–211.

Zhao, L., He, Z., Zhao, W., Yang, Q., 2016. Extensive investigation of the sap flow of maize plants in an oasis farmland in the middle reach of the Heihe River, Northwest China. Journal of Plant Research, 129, 841–851.

Received 8 July 2019
Accepted 7 February 2020

J. Hydrol. Hydromech., 68, 2020, 2, 144–154
DOI: 10.2478/johh-2020-0012
ISSN 1338-4333

sciendo Journal of Hydrology and Hydromechanics

The role of stony soils in hillslope and catchment runoff formation

Babar Mujtaba[1*], Hana Hlaváčiková[2], Michal Danko[3], João L.M.P. de Lima[1], Ladislav Holko[3]

[1] MARE - Marine and Environmental Sciences Centre, Department of Civil Engineering, Faculty of Science and Technology, Pólo II-Universidade de Coimbra, Rua Luís Reis Santos, 3030-788 Coimbra, Portugal.
[2] Slovak Hydrometeorological Institute, Jeséniova 17, 833 15 Bratislava, Slovak Republic.
[3] Institute of Hydrology of the Slovak Academy of Sciences, Dúbravská cesta 9, 841 04 Bratislava, Slovak Republic.
[*] Corresponding author. Tel.: +351912322544. E-mail: uc2015158720@student.uc.pt

Abstract: The role of stony soils in runoff response of mountain catchments is rarely studied. We have compared simulated response of stony soils with measured catchment runoff for events caused by rains of small and high intensities in the mountain catchment of the Jalovecký Creek, Slovakia. The soil water response was simulated for three sites with stoniness 10–65% using the Hydrus-2D single porosity model. Soil hydraulic parameters employed in the modelling, i. e. the saturated hydraulic conductivity and parameters of the soil water retention curves, were obtained by two approaches, namely by the Representative Elementary Volume approach (REVa) and by the inverse modelling with Hydrus-1D model (IMa). The soil water outflow hydrographs simulated by Hydrus-2D were compared to catchment runoff hydrographs by analysing their skewness and peak times. Measured catchment runoff hydrographs were similar to simulated soil water outflow hydrographs for about a half of rainfall events. Interestingly, most of them were caused by rainfalls with small intensity (below 2.5 mm/10 min). The REV approach to derive soil hydraulic parameters for soil water outflow modelling provided more realistic shapes of soil water outflow hydrographs and peak times than the IMa approach.

Keywords: Lateral subsurface flow; Mountain catchment; Soil water flow modelling.

Abbreviations: REV – representative elementary volume; REVa – the REV approach; IMa – the inverse modelling approach; SWRC – soil water retention curve.

INTRODUCTION

Soils play an important role in catchment runoff formation. The response of catchment runoff to precipitation is highly nonlinear due to heterogeneity in inputs and catchment characteristics, threshold behaviour depending on catchment wetness and storage state, varying relative contributions of different landscape units, etc. An excellent state of the art review of the processes and controlling factors affecting runoff formation at hillslopes was recently given by Bachmair and Weiler (2011). Preferential flow in the soils (Beven and Germann, 1982), the instability-driven flow (Tesař et al., 2001) or fill and spill mechanism (Tromp-van Meerveld and McDonnell, 2006) are commonly used to explain rapid formation of the subsurface flow that eventually contributes to catchment stormflow. Soil stoniness can have similar effect (Hlaváčiková et al., 2015, 2016) as the retention capacity of stony soils is reduced. This phenomenon is still not well studied, and it is neglected in runoff formation theories.

Many authors (e.g., Botter and Rinaldo, 2003; Li and Sivapalan, 2011) observed that hillslope processes, mainly the lateral subsurface flow tend to make catchment runoff hydrograph positively skewed. Hillslope lateral subsurface flow is dependent on soil properties such as infiltration capacity, heterogeneity of hydraulic conductivity, soil water retention, thickness of unsaturated zone and preferential pathways.

Stony soils are commonly found in hilly and forested regions of the world. Stoniness, defined as the relative volume of rock fragments, is an important soil property. It can strongly influence water infiltration, movement, retention characteristics and runoff formation (e.g., Al-Qinna et al., 2014; Chen et al., 2012; Hlaváčiková et al., 2015). Correct estimation of the soil hydraulic properties (i.e., hydraulic conductivity and van Genuchten soil water retention functions) is essential to evaluate the water flow (hydrological response) in stony soils. Water flow modelling in a stony soil profile is difficult due to the heterogeneity of rock fragments distribution and quantity. It requires determination of the retention characteristics of fine soil fraction, saturated hydraulic conductivity and stoniness in soil layers. For this, a large representative elementary volume (REV) of soil sample is needed to characterize the bulk characteristics of the stony soil profile (e.g., Hlaváčiková et al., 2015, 2018). Buchter et al. (1994) recommended that the dry mass of a stony soil sample should be at least 100 times the mass of the largest particle. However, there is no rule for how large the REV of a stony soil should be for measuring its hydraulic characteristics. After obtaining the stoniness from REV, the soil water retention curves of the fine soil fraction are corrected to adequately represent the hydraulic characteristics of the studied stony soil profile (e.g., Bouwer and Rice, 1984; Coppola et al., 2013; Ma and Shao, 2008).

An alternative approach to REV, the inverse modelling utilizing measured soil moisture data has been used for the estimation of soil hydraulic parameters (e.g., Šimůnek and van Genuchten, 1996; Šimůnek et al., 1998; Wegehenkel et al. 2017). The inverse modelling uses optimization techniques for the estimation of soil hydraulic parameters from transient flow transport data (Šimůnek et al., 2013). The disadvantage of this approach is that derived soil hydraulic parameters can be applied only to the sample volume around the soil moisture sensors that may be very small (200 cm^3) compared to the REV (1 m^3).

In our knowledge, not a single study addressed the impact of soil hydraulic parameters estimated by both inverse modelling and REV on the lateral subsurface flow simulations in stony soils. The objective of our work was to compare the response of the outflow from stony soils in a small mountain catchment to

rainfall events with different intensity to catchment runoff response. To fulfil the objective, the work was divided into two parts. First, soil hydraulic parameters needed for the subsurface water flow modelling for three study sites with moderate to high stoniness (10–65%) were derived by the REV (REVa) and inverse modelling (IMa) approaches. Then, comparison of lateral subsurface flow hydrographs (hereafter also soil water outflow) and catchment runoff was done by analysing the skewness and peak time of the hydrographs.

STUDY SITE

The study is carried out in the mountain catchment of the Jalovecký Creek (the Western Tatra Mountains, Slovakia), shown in Fig. 1. Catchment area is 22.2 km^2, its mean slope is 30° and the altitude ranges from 800 to 2178 m a.s.l. (mean 1500 a.s.l.). The bedrock is dominantly formed by crystalline and metamorphic rocks. Soils are represented by shallow Cambisol, Pozdol, Lithosol, and Leptosol (the soil depth is about 0.7–1 m). Soil stoniness is high and varies from 10–65% or more. Forest (mostly spruce), dwarf pine and alpine meadows, including bare rocks on the steepest slopes, cover 44%, 31%, and 25% of catchment area, respectively. Most of the forest is over 100 years old. Mean annual precipitation is about 1500 mm and mean air temperature is 3°C. Additional catchment characteristics can be found e.g., in Holko and Kostka (2010); the detailed information about the catchment hydrological cycle over the three decades of its monitoring is presented in Holko et al. (2020a, b, this issue).

Simulation of water outflow from the mountain soils was carried out for three sites located at elevations above 1000 m a.s.l. Two of them are in the forest, one is in the open area covered by grass. The main attributes of the sites are:

Site 1: Červenec – open area, 1500 m a.s.l., a flat terrain with slope angle 2.86°, slightly to moderately stony soil classified as a Leptosol with a sandy loam texture is typical for the site. The site is covered by grass and low vegetation.

Site 2: Červenec – forest, 1450 m a.s.l., a moderately steep terrain with slope angle 14°.

Site 3: Pod Lyscom, 1040 m a.s.l., a steep terrain with slope angle 22°.

Moderate to high soil stoniness is typical for sites 2 and 3. The soil type is classified as Cambisol and has a sandy loam texture. A 130-year old Norway spruce forest (*Picea abies*) and a low understorey vegetation of *Vaccinium myrtillus* L. grow at the sites.

DATA

Rainfall, discharge and soil moisture data of the warm seasons (June to September) measured in years 2013–2016 were used in this study. Rainfall and soil moisture data were measured every 10 minutes at all three sites. Hourly discharge data measured at catchment outlet (820 m a.s.l.) were obtained from the 10-min interval pressure transducer water level measurements and the discharge rating curve.

Rainfall data provided the meteorological inputs for the simulation of the soil water outflow. Fifteen rainfall events separated according to rainfall intensity were used (Table 1).

The small intensity rains had maximum intensity below 2.5 mm/10 min. The large intensity rains had maximum intensity above 3.5 mm/10 min. This division was based on the

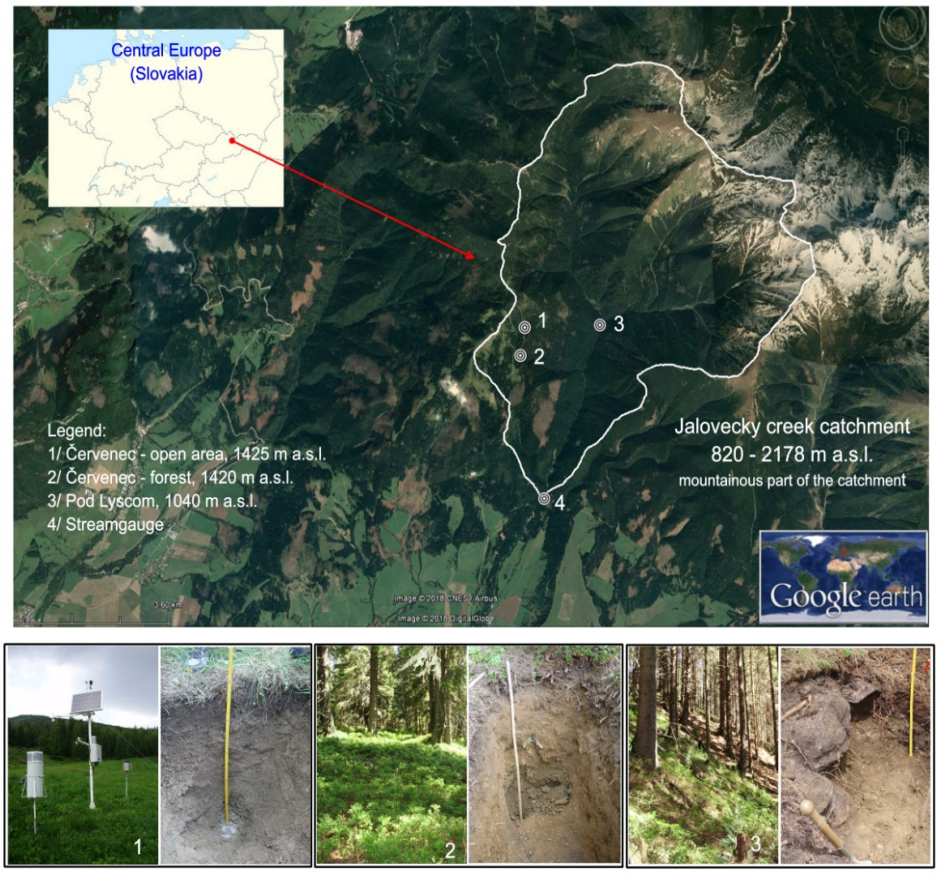

Fig. 1. The Jalovecký Creek catchment, location of the sites for which the soil water outflow was simulated (1, 2 and 3), vegetation and soil profiles at the sites; catchment outlet where catchment runoff was measured is indicated by number 4.

Table 1. Characteristics of the rainfall events and periods used for the lateral subsurface flow simulations at the three study sites; API is total precipitation over the last 10 days, A-I are events with small rainfall intensity, AI-FI are events with large rainfall intensity.

Rainfall event	Study site	Simulation period	Rainfall amount (mm)	10-min maximum (mm)	API (mm)
A	Červenec - open area	22.9.2013–16.10.2013	58.4	1.5	116
	Červenec - forest		72.8	1.4	75
	Pod Lyscom		39.8	1.4	120
B	Červenec - open area	24.6.2014–29.6.2014	19.4	1.6	13
	Červenec - forest		12.8	1.0	8
	Pod Lyscom		14.2	1.4	2
C	Červenec - open area	11.7.2014–14.7.2014	24.4	1.0	103
	Červenec - forest	11.7.2014–18.7.2014	18.4	0.8	66
	Pod Lyscom	11.7.2014–18.7.2014	22.6	1.2	75
D	Červenec - open area	25.9.2014–1.10.2014	38.2	1.5	44
	Červenec - forest		23.6	1.0	25
	Pod Lyscom		27.8	1.0	29
E	Červenec - open area	2.9.2013–9.9.2013	17.3	1.6	31
	Červenec - forest	2.9.2013–11.9.2013	25.4	1.4	14
	Pod Lyscom	2.9.2013–11.9.2013	23.2	1.4	14
F	Červenec - open area	23.8.2014–9.9.2014	39.2	1.7	50
	Červenec - forest		31.2	2.8	24
	Pod Lyscom		18.2	1.0	20
G	Červenec - open area	8.8.2016–14.8.2016	30.4	2.1	14
	Červenec - forest		20.0	1.6	30
	Pod Lyscom		27.2	1.6	40
H	Červenec - open area	5.8.2016–10.8.2016	13.1	1.7	62
	Pod Lyscom	5.8.2016–10.8.2016	12.6	1.6	56
I	Červenec - open area	20.8.2016–4.9.2016	21.2	2.5	25
	Pod Lyscom*	20.8.2016– 5.9.2016	24.6	5.6	22
AI	Červenec - open area	8.8.2013–28.8.2013	28.1	3.8	10
	Červenec - forest	9.8.2013–28.8.2013	15.6	3.8	7
	Pod Lyscom	9.8.2013–28.8.2013	11.6	3.4	6
BI	Červenec - open area	1.7.2014–8.7.2014	51.3	5.7	90
	Červenec - forest		39.6	3.6	55
	Pod Lyscom		36	3.4	62
CI	Červenec - open area	20.7.2014–28.7.2014	40.4	6.3	33
	Červenec - forest	20.7.2014–31.7.2014	38.8	6.0	22
	Pod Lyscom	20.7.2014–31.7.2014	28.0	2.2	27
DI	Červenec - open area	10.8.2014–13.8.2014	50.9	12.0	19
	Červenec - forest		31.4	11.2	17
	Pod Lyscom		35.0	9.4	16
EI	Červenec - open area	3.8.2015–14.8.2015	89.4	12.0	58
	Červenec - forest		71.6	21.2	46
	Pod Lyscom		82.6	19.3	35
FI	Červenec - open area	13.8.2016–21.8.2016	25.3	6.6	43
	Červenec - forest		17.4	4.8	30
	Pod Lyscom		22.2	6.0	40

Pod Lyscom * – event I at the site is classified as large intensity rainfall

unpublished results of the analysis of soil moisture response to rainfall on the study sites. Catchment runoff hydrographs during the rainfall events were used for the comparison of soil and catchment responses. The soil moisture measurements helped to obtain the hydraulic parameters of the soils (i.e. the saturated hydraulic conductivity and parameters of the soil water retention curves) used in the lateral subsurface flow simulation (by inverse modelling). Physical characteristics of the soils were measured in the soil pits of 1 m^2 cross section dug to depths 0.7–0.95 m at each site (Hlaváčiková et al., 2015).

METHODOLOGY

Lateral subsurface flow simulation

Lateral subsurface flow hydrographs were simulated by the well-known finite element model HYDRUS 2D (Šimůnek et al., 2008, 2013) as the outflow from the soil through gradient boundary. The 20 m long hillslope segment with 1 m soil profile depth (Fig. 2) and different slope angles corresponding to the slope angles at the three study sites (2.86°, 14°, and 22° for sites 1, 2, and 3, respectively) were schematized for the simulations. Soil layers in the model corresponded to the layers found in the soil pits. The following boundary conditions were used in the simulations (Fig. 2):

- the upper boundary (surface) was set as atmospheric boundary condition.
- the lower boundary (bottom) and upper vertical boundary (left hand side) were set as no flux conditions. No flux condition at the lower boundary was given because the hydraulic conductivity of the bedrock was much smaller than that of the above soil and water table was not present in the soil profile.
- the lower vertical boundary (right hand side) was set as gradient boundary condition.

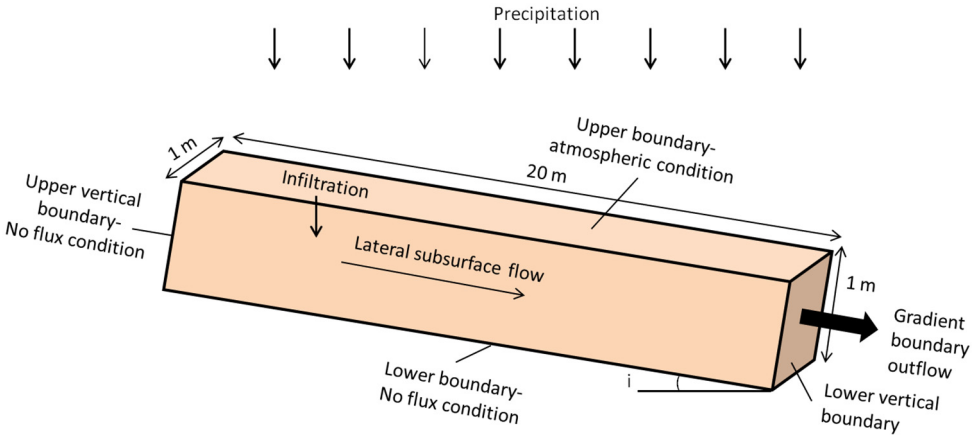

Fig. 2. Schematic sketch of the hillslope section used in simulation of the soil water outflow (lateral subsurface outflow). Boundary conditions are also presented. Gradient boundary outflow is the lateral subsurface outflow. *i* denotes the slope gradient which is 2.86° for site 1 (Červenec – open area), 14° for site 2 (Červenec – forest) and 22° for site 3 (Pod Lyscom), respectively.

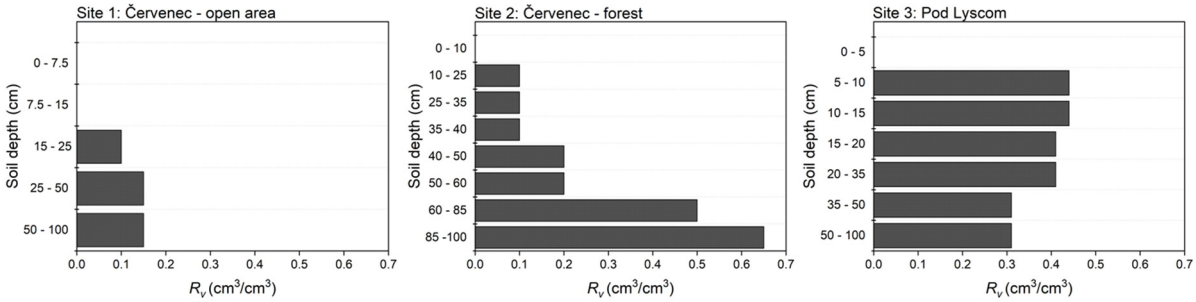

Fig. 3. Stoniness R_v (cm^3 cm^{-3}) in different soil layers on site 1, 2 and 3 measured in the representative elementary volume (REV) of about 1 m^3; modified from Hlaváčiková et al. (2015).

The computation time varied from 40 to 60 minutes for each simulated rainfall event. In total, 86 simulations of the soil water outflow were conducted.

The soil hydraulic parameters required by HYDRUS 2D (i.e. the saturated hydraulic conductivity K_s and parameters of the soil water retention curve θ_s, θ_r, α, n) were obtained by two approaches – the representative elementary volume (REV) and inverse modelling (IM) as described below. The two approaches were used to obtain the hydraulic parameters for the soil depth 0–50 cm. Hydraulic parameters the soil depth 50–100 cm were obtained only from the REV approach.

The REV approach was based on field measurements in soil pits of 1 m^2 cross section dug to depths 0.7–0.95 m at each site (Hlaváčiková et al., 2015). Volumes of stones and boulders were measured directly in the field. Soil stoniness estimated for the soil pits of the REV dimensions is shown in Fig. 3. Additionaly, the disturbed soil samples with volume of 2–3 litres were collected for each characteristic soil layer for the laboratory evaluation of the fine soil fraction and the volume of the gravel part of the stoniness.

Undisturbed and disturbed samples of fine soil with volume 100 cm^3 were collected for each characteristic soil layer at each site to determine the saturated hydraulic conductivity and water retention measurements. The saturated hydraulic conductivity of the fine soil was estimated in the laboratory by the variable hydraulic head method. A small number of field measurements of the saturated hydraulic conductivity was carried out with the single ring infiltrometer as well (Hlaváčiková et al. (2015, 2018)). Drying branches of the soil water retention curves (SWRC) of the fine soil were measured by the pressure plate extractor (Dane and Hopmans, 2002) for pressure heads between –50 and –3000 cm. Drying branches of the soil water retention curves of top soil layer (organic horizon) were measured by the sand tank for pressure heads between –2 and –100 cm, smaller pressure heads were measured by the pressure plate extractor. Measured soil water retention curves were fitted by the analytical model of van Genuchten (1980) and their parameters θ_s (the saturated water content) and θ_r (the residual water content) were corrected for the stoniness using the Bouwer and Rice (1984) equation. The stoniness-corrected soil water retentions curves and measured saturated hydraulic conductivity (an average of the laboratory and field measurements) obtained for different soil layers at all three study sites provided the soil hydophysical parameters needed in the lateral subsurface flow modelling. Stoniness used in the REV approach for the soil water retention correction was determined from the soil pits stoniness measurements shown in Fig. 3.

The IM approach for determination of soil hydraulic parameters was based on the single porosity HYDRUS 1D modelling calibrated against measured soil moisture using the optimization technique available in the Hydrus 1D package. Model parameters were set according to fine soil water retention and the stoniness measurements. Time series of measured soil water contents at three depths (5, 10, 20 cm) at site 1 and two depths (10, 40 cm) at sites 2 and 3 were used in the inverse modelling. Simulated soil profile of all three sites had depth of 50 cm. Soil hydrophysical parameters were determined by the IMa only for the soil depths 0–50 cm because the soil moisture data were not measured at greater depths due to large soil stoniness.

The initial soil conditions for water flow modelling were set for each rainfall event separately according to antecedent soil wetness represented by pressure heads. For this purpose, the soil water potential was estimated from the known soil water retention curves and by taking in account the antecedent precipitation (API). The API was calculated as the sum of 10-day rainfall before the rainfall event. Initial conditions set in the form of pressure heads were chosen because the pressure head can better describe the status of water at the beginning of the simulation. The inverse modelling was done as in Wegehenkel et al. (2017). First, the parameters n and θ_s were calibrated, then K_s and θ_r were obtained, and finally parameter α was calibrated.

Table 2. Soil hydraulic parameters estimated by the REV approach at various soil depths on the three study sites; θ_s is the saturated water content, θ_r is residual water content, α and n are the van Genuchten´s parameters, K_s is the saturated hydraulic conductivity and R_v is the relative volume of rock fragments.

Soil depth	θ_r (cm^3 cm^{-3})	θ_s (cm^3 cm^{-3})	α (cm^{-1})	n (–)	K_s (cm min^{-1})	R_v (cm^3 cm^{-3})
Site 1: Červenec - open area						
0–7.5 cm	0.1	0.63	0.10	1.27	2.42	0.00
7.5–15 cm	0.05	0.51	0.43	1.13	1.00	0.00
15–25 cm	0.05	0.45	0.43	1.13	0.25	0.10
25–50 cm	0.04	0.43	0.41	1.11	0.25	0.15
50–100 cm	0.04	0.41	0.40	1.10	0.25	0.15
Site 2: Červenec - forest						
0–10 cm	0.05	0.64	0.48	1.22	18.33	0.00
10–25 cm	0.05	0.58	0.05	1.24	3.50	0.10
25–35 cm	0.05	0.57	0.07	1.25	1.00	0.10
35–40 cm	0.05	0.57	0.07	1.25	0.67	0.10
40–50 cm	0.04	0.50	0.07	1.25	0.67	0.20
50–60 cm	0.04	0.50	0.07	1.25	0.67	0.20
60–85 cm	0.03	0.31	0.07	1.25	0.33	0.50
85–100 cm	0.02	0.22	0.07	1.25	0.33	0.65
Site 3: Pod Lyscom						
0–5 cm	0.05	0.63	0.56	1.21	46.67	0.00
5–10 cm	0.03	0.36	0.42	1.24	10.00	0.44
10–15 cm	0.03	0.41	0.13	1.27	5.67	0.44
15–20 cm	0.03	0.49	0.12	1.22	2.67	0.41
20–35 cm	0.03	0.49	0.12	1.22	2.42	0.41
35–50 cm	0.03	0.52	0.06	1.25	0.83	0.31
50–100 cm	0.03	0.52	0.06	1.25	0.33	0.31

Table 3. The Mean values of soil hydraulic parameters estimated by the IM approach; the mean values were calculated from the results of simulations for all 15 rainfall events; θ_s is the saturated water content, θ_r is the residual water content, α and n are the van Genuchten´s parameters, K_s is the saturated hydraulic conductivity and R_v is the relative volume of rock fragments.

Soil depth	θ_r (cm^3 cm^{-3})	θ_s (cm^3 cm^{-3})	α (cm^{-1})	n (–)	K_s (cm min^{-1})	R_v (cm^3 cm^{-3})
Site 1: Červenec - open area						
0–7.5 cm	0.10	0.59	0.11	1.25	1.61	–
7.5–15 cm	0.11	0.54	0.41	1.12	0.90	–
15–25 cm	0.02	0.42	0.46	1.14	0.42	0.10
25–50 cm	0.05	0.47	0.42	1.10	1.00	0.15
*50–100 cm	0.04	0.41	0.4	1.1	0.25	0.15
Site 2: Červenec - forest						
0–10 cm	0.12	0.61	0.42	1.26	11.37	–
10–25 cm	0.07	0.54	0.05	1.24	1.99	0.10
25–35 cm	0.14	0.57	0.06	1.25	2.15	0.10
35–40 cm	0.14	0.67	0.06	1.24	2.59	0.10
40–50 cm	0.08	0.61	0.07	1.22	1.97	0.20
*50–60 cm	0.04	0.50	0.07	1.25	0.67	0.20
*60–85 cm	0.03	0.31	0.07	1.25	0.33	0.50
*85–100 cm	0.02	0.22	0.07	1.25	0.33	0.65
Site 3: Pod Lyscom						
0–5 cm	0.12	0.68	0.31	1.23	22.22	–
5–10 cm	0.11	0.68	0.41	1.23	11.41	–
10–15 cm	0.05	0.61	0.12	1.26	5.33	0.20
15–20 cm	0.12	0.54	0.10	1.22	3.76	0.20
20–35 cm	0.09	0.83	0.10	1.21	4.01	0.20
35–50 cm	0.09	0.70	0.06	1.20	2.21	0.20
*50–100 cm	0.03	0.52	0.06	1.25	0.33	0.31

*Parameters for the soil depth of 50–100 cm were the same for the REV and the IM approaches and were derived by the REV approach.

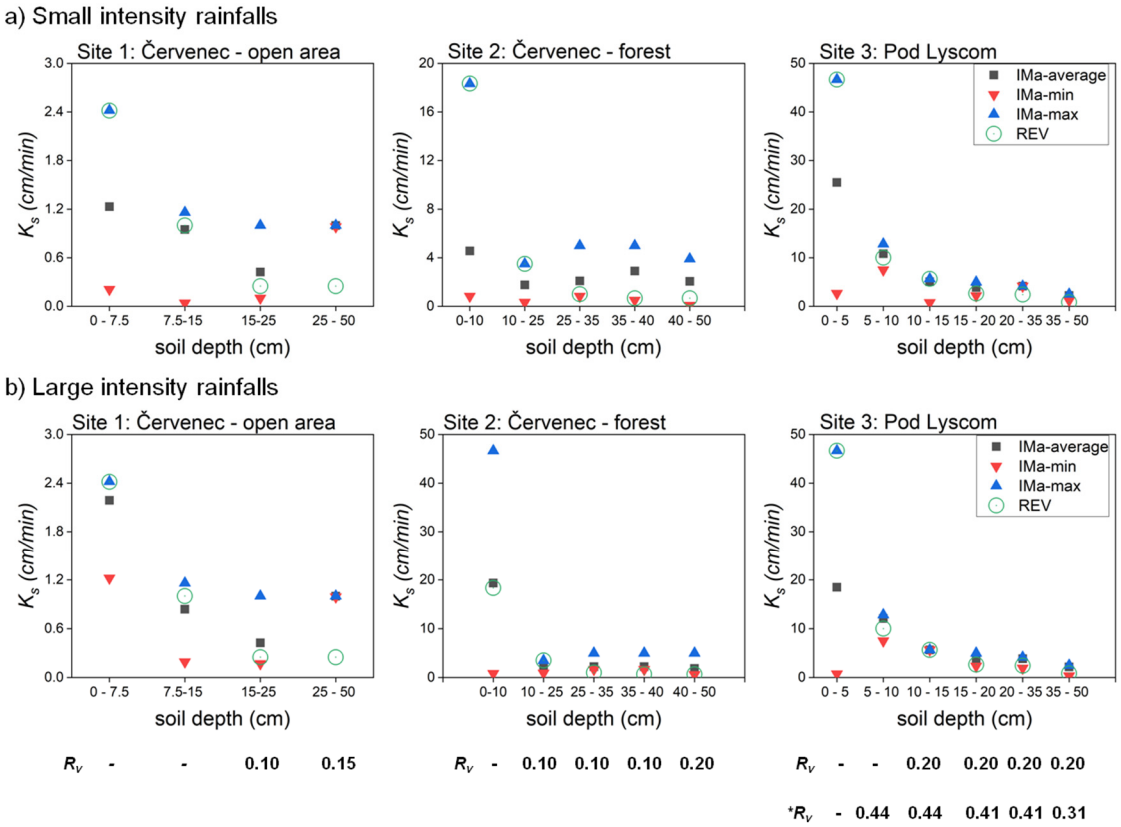

Fig. 4. Saturated hydraulic conductivity K_s estimated by the REV and IM approaches at various soil depths with different stoniness R_v; minimum and maximum K_s values estimated by the IMa are also presented; the asterisk denotes different stoniness at site 3 for REVa.

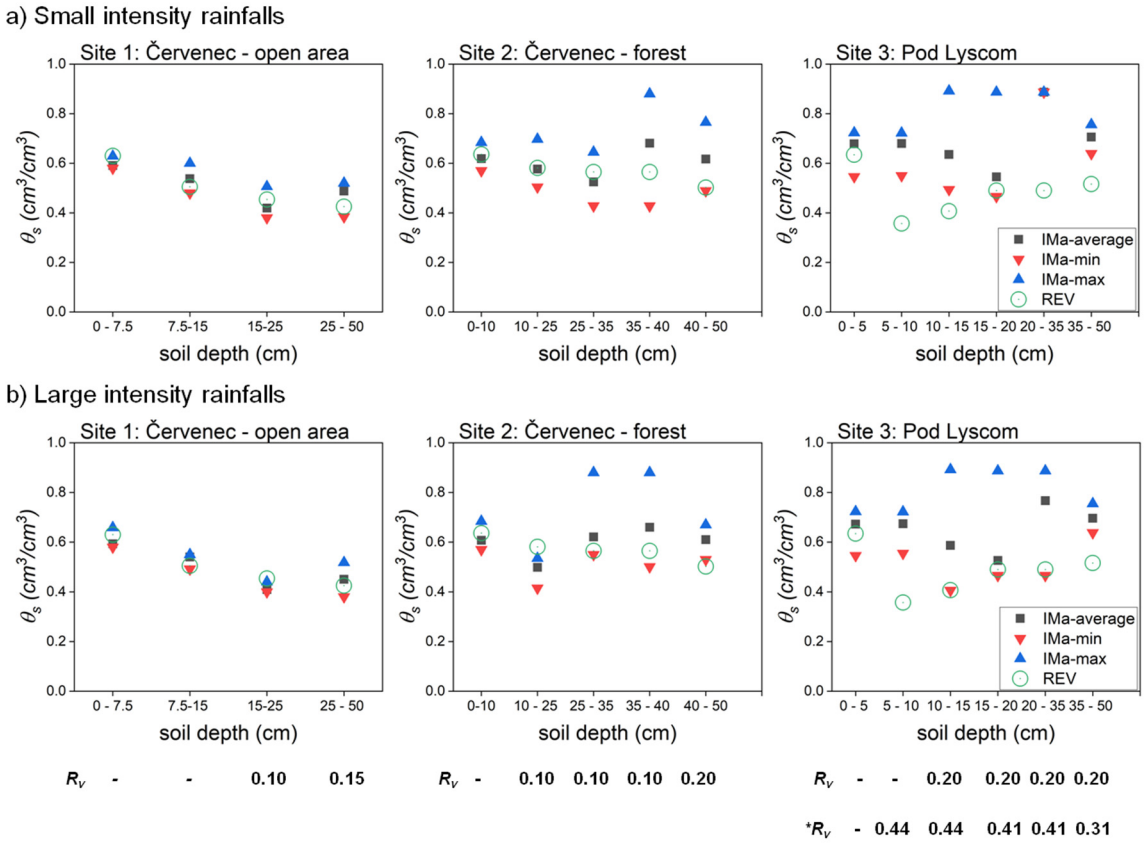

Fig. 5. Saturated moisture content θ_s estimated by the REV and IM approaches at various soil depths with different stoniness R_v of site 1, 2 and 3; minimum and maximum θ_s values estimated by the IMa are also presented; the asterisk denotes different stoniness at site 3 for REV.

Hydrographs comparison

The subsurface lateral flow hydrographs simulated by HYDRUS 2D (with soil hydrophysical parameters from both REVa and IMa) were compared to measured catchment runoff hydrographs. The comparison was based on hydrograph geometry (skewness) and peak times. Skewness as an important characteristic of hydrograph geometry was quantified by the volume before peak (VBP) values (Collischonn et al., 2017). The VBP is the ratio of the flow volume before the peak to total flow volume during an event. Its value ranges between 0 and 1. If VBP is equal to 0.5, the hydrograph is symmetrical. VBP smaller than 0.5 characterizes the positively skewed hydrographs while the negatively skewed hydrograph has the VBP greater than 0.5. Flow volume before the peak was calculated from the discharge data between the rainfall beginning and the hydrograph peak. Total flow volume was calculated from the initiation time of the rainfall until the time when discharge dropped to the value measured before the rainfall. The peak time difference between catchment runoff and lateral subsurface flow hydrographs for every rainfall event at each site was analysed as well. The VBP and peak time difference were used to quantify the geometric similarities of subsurface and catchment runoff hydrographs.

RESULTS

Influence of stoniness on soil hydraulic parameters estimated by the REV and inverse modelling approaches

Soil hydraulic parameters estimated by REVa and IMa which were thereafter used in the soil water outflow simulation are given in Tables 2 and 3. Two out of five parameters, namely the saturated hydraulic conductivity (K_s) and the volumetric saturated soil moisture content (θ_s) were found to be the most sensitive in inverse modelling. Figs. 4 and 5 show the K_s and θ_s values estimated by REVa and IMa at all three sites for different soil depths.

The top soil layers (organic horizons) at all three sites (0–15 cm at Site 1, 0–10 cm at Site 2 and 0–5 cm at Site 3) contained no stones. The highest K_s values were obtained for these layers by both REVa and IMa. The K_s values obtained by both IMa and REVa decreased in the presence of rock fragments at each site for both small and large intensity rainfalls. The largest K_s value difference obtained by inverse modelling for small and large intensity rainfalls was found in the soil depth of 0–7.5 cm at site 1 and 0–10 cm at site 2. Two and four times greater K_s values were obtained for large intensity rainfall at both sites and showed faster water dynamics during large intensity rainfalls. Apart from that, the K_s values obtained by IMa for large rainfalls were 0.7–1.3 times than those for small rainfalls for the remaining corresponding soil layers at all sites.

Soil retention capacity decreased with the increase of stoniness for the REVa at all three sites (Fig. 5). Compared to the top soil, 32%, 15% and 40% reduction in θ_s was observed, on average, at sites 1, 2 and 3, respectively. For the IMa, the retention capacity on site 1 was the highest in the top soil (zero stoniness) for small and large rainfalls. For both small and large rainfalls, the θ_s value was the highest at lower soil layers on site 2 (35–40 cm depth, $R_v = 0.1$) and site 3 (20–35 cm depth, $R_v = 0.2$). The greatest differences in the retention capacity of soils profiles between the REV and IM approaches were found on site 3. These differences correspond to different stoniness related to the particular approach.

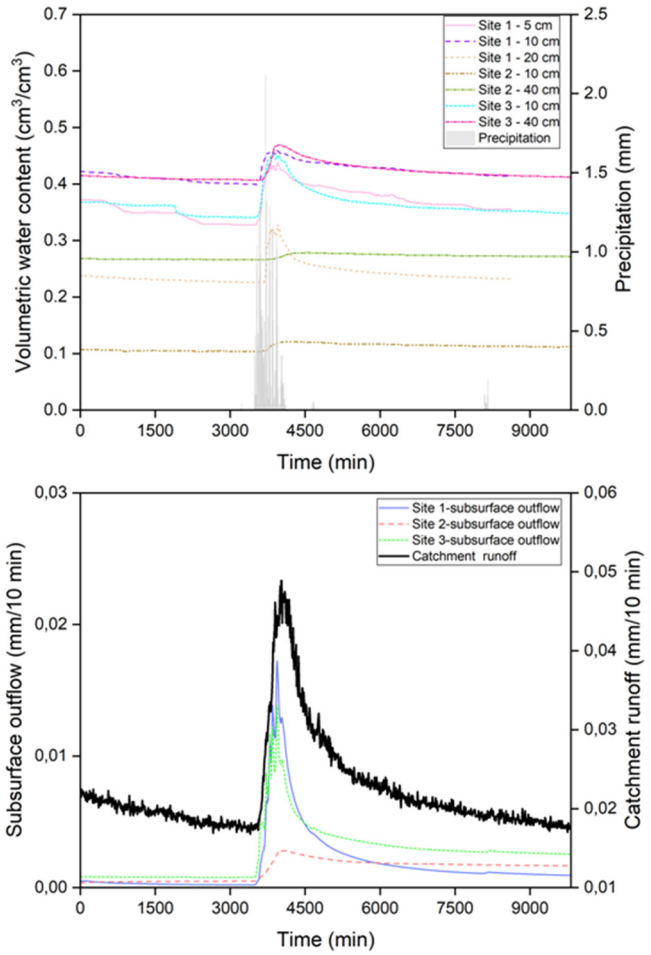

Fig. 6. Comparison of simulated lateral subsurface flow based on the REVa (the bottom panel) and catchment runoff for the small intensity rainfall event G; the soil moisture and rainfall measurements are presented in the top panel.

Comparison of the lateral subsurface flow and catchment runoff hydrographs

Soil moisture of the top soil layer at all three sites significantly increased at the initiation of rainfall and started to decrease slowly when the rain finished (Fig. 6). Patterns of the lateral subsurface flow and catchment runoff hydrographs were similar. An example of the lateral subsurface flow and catchment runoff responses for the small and high intensity rainfalls is shown in Fig. 7. The most pronounced lateral subsurface flow response was simulated for site 1 which is located in the open area. The response at forested sites 2 and 3 was also dynamic, but only for the soil hydraulic parameters estimated by the REV approach. Hydraulic parameters obtained from IMa typically resulted in smaller dynamics of the simulated lateral subsurface flow response on sites 2 and 3.

The VBP (volume before peak) values are given in Table 4. The VBP values for catchment runoff hydrographs varied from 0.11 to 0.4, suggesting positively skewed hydrographs. Among the lateral subsurface flow hydrographs estimated by both REVa and IMa, there were in total 10 hydrographs that were negatively skewed (VBP > 0.5). Table 4 shows that similar skewness of lateral subsurface flow hydrographs and catchment runoff hydrographs was obtained for approximately one half of rainfall events (8 out of 15). The similarity was most often

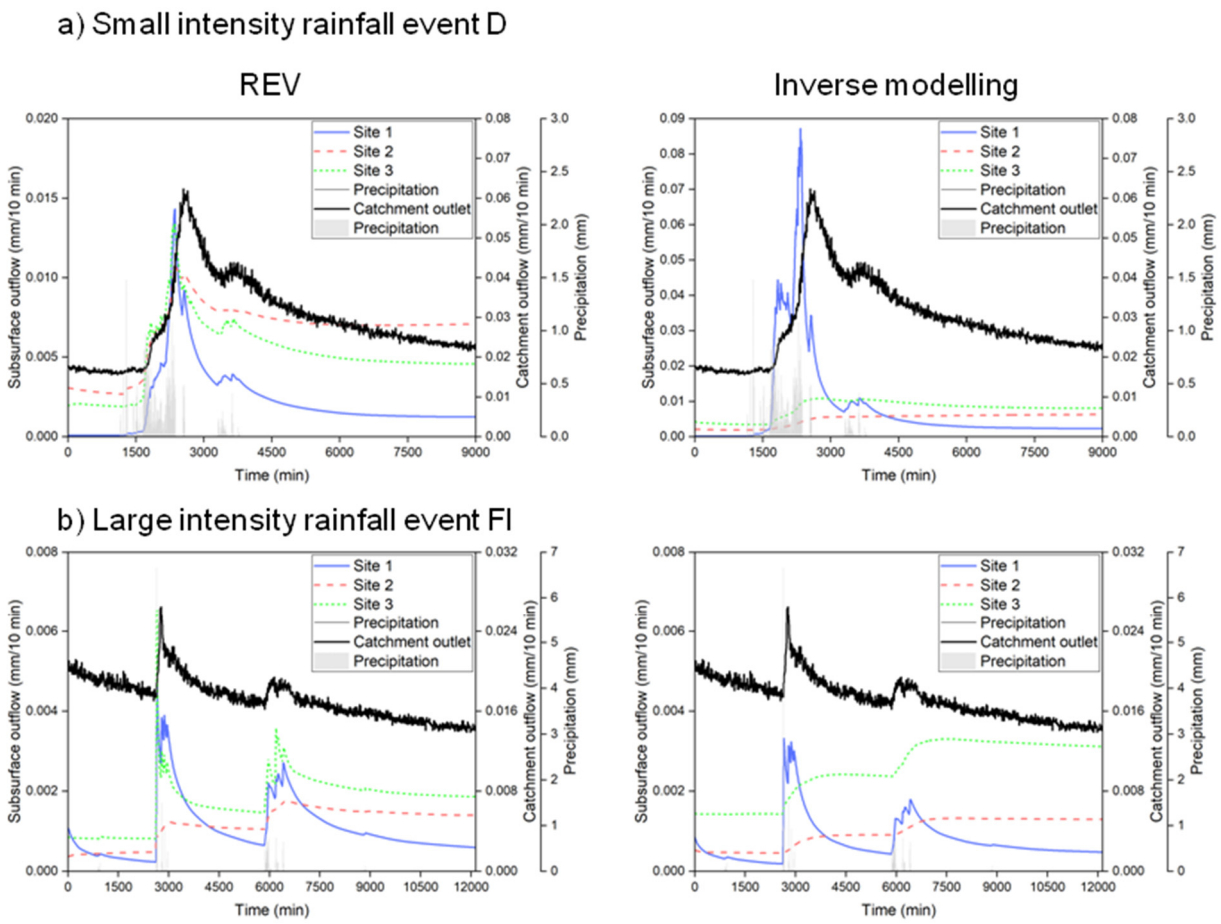

Fig. 7. Catchment runoff and simulated lateral subsurface flow hydrographs estimated by the REVa and the IMa for a small and large intensity rainfalls.

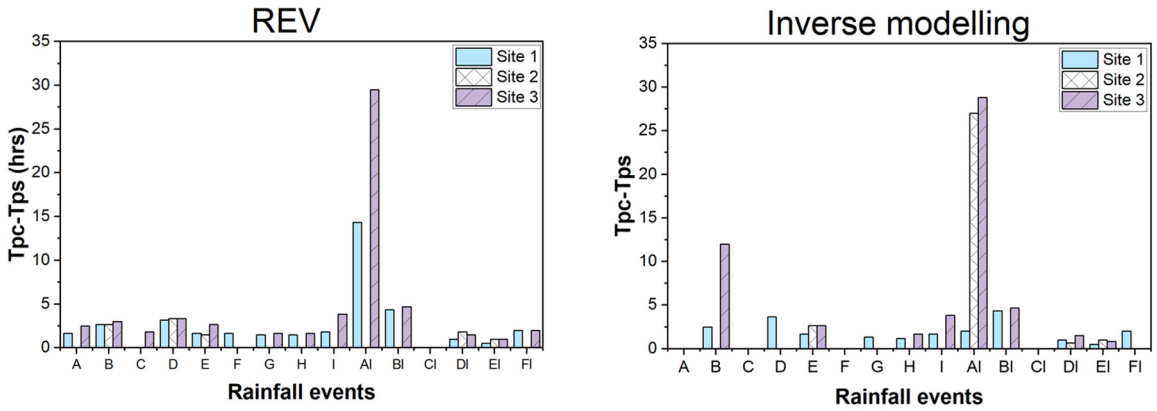

Fig. 8. Peak time difference (in hours) between the lateral subsurface flow (Tps) and catchment runoff (Tpc) hydrographs.

obtained for the small intensity rains and site 3 (and parameters obtained from the IMa) which has the shortest distance to the Jalovecký Creek. The connectivity of that particular site with stream network probably does not develop, but the entire hillslope may be connected to the narrow riparian area existing in that part of the catchment.

The negatively skewed hydrographs were excluded from the peak times comparison. Fig. 8 shows that more realistic results were obtained for simulations with soil hydraulic parameters estimated by the REVa and the time delay between peaks in the lateral subsurface flow and catchment runoff were mostly about 2–3 hours. Three events with the highest rainfall intensities and comparatively higher wetness before the rain (DI, EI, FI) had shorter time delays (about 1–2 hours).

DISCUSSION

Previous studies in the Jalovecký Creek catchment which is representative for the hydrological cycle of the highest part of the Carpathian Mountains, documented the dominant role of the pre-event water, fast runoff response to rainfall and pointed at the importance of the stony soils in catchment runoff generation (e.g., Hlaváčiková et al., 2015, 2018, 2019; Holko and Lepistő, 1997; Holko et al. 2011, 2018; Kostka, 2009).This work indicated that simulation of the lateral subsurface flow in different parts of the catchment and comparison of simulated lateral subsurface flow hydrographs with catchment runoff hydrograph could improve the understanding of the contribution of different parts of the catchment to runoff formation. Comparison of

Table 4. Volume before peak (VBP) values for catchment runoff hydrographs and simulated lateral subsurface flow hydrographs; the bold numbers show the negatively skewed hydrographs (VBP > 0.5), the yellow-marked numbers indicate the lateral subsurface flow hydrographs with skewness most similar to that of catchment runoff hydrograph; A-I are events with small intensity rainfalls, AI-FI are the large intensity rainfalls.

Rainfall event	VBP values for lateral subsurface hydrographs						Catchment's outlet runoff hydrographs VBP values
	Inverse modelling approach			REV approach			
	Site 1	Site 2	Site 3	Site 1	Site 2	Site 3	
A	**1.00**	0.35	0.15	0.02	0.34	0.05	0.11
B	0.13	0.26	0.14	0.10	0.23	0.26	0.40
C	0.39	**1.00**	0.15	0.38	0.15	0.10	0.15
D	0.38	**0.99**	0.18	0.18	0.16	0.18	0.21
E	0.08	0.06	0.08	0.06	0.05	0.08	0.16
F	**0.99**	**0.98**	**0.94**	0.04	0.16	0.18	0.11
G	0.22	0.31	0.34	0.21	0.19	0.21	0.38
H	0.17	–	0.23	0.17	–	0.19	0.37
I	0.05	–	0.04	0.08	–	0.04	0.41
Al	0.05	0.03	0.05	0.01	**0.85**	0.04	0.12
Bl	0.12	**0.98**	0.25	0.11	**1.00**	0.14	0.24
Cl	0.18	**0.99**	0.07	0.12	0.06	0.08	0.11
Dl	0.05	0.18	0.18	0.05	0.11	0.12	0.26
El	0.04	0.02	0.02	0.09	0.01	0.06	0.16
Fl	0.10	0.5	0.49	0.09	0.11	0.11	0.25

Site 1 = Červenec - open area; Site 2 = Červenec - forest; Site 3 = Pod Lyscom.

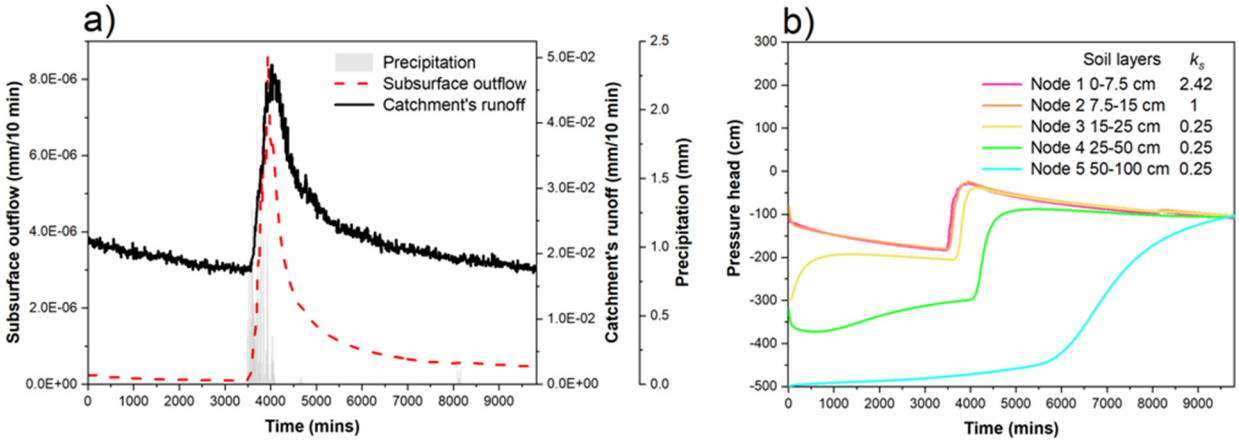

Fig. 9. a) Rainfall, catchment runoff and lateral subsurface flow hydrographs with positive skewness caused by the rainfall event G on site 1; b) temporal evolution of pressure head at the gradient boundary observation nodes at different soil depths estimated by the REVa for the same event and site; K_s is the saturated hydraulic conductivity in cm/min.

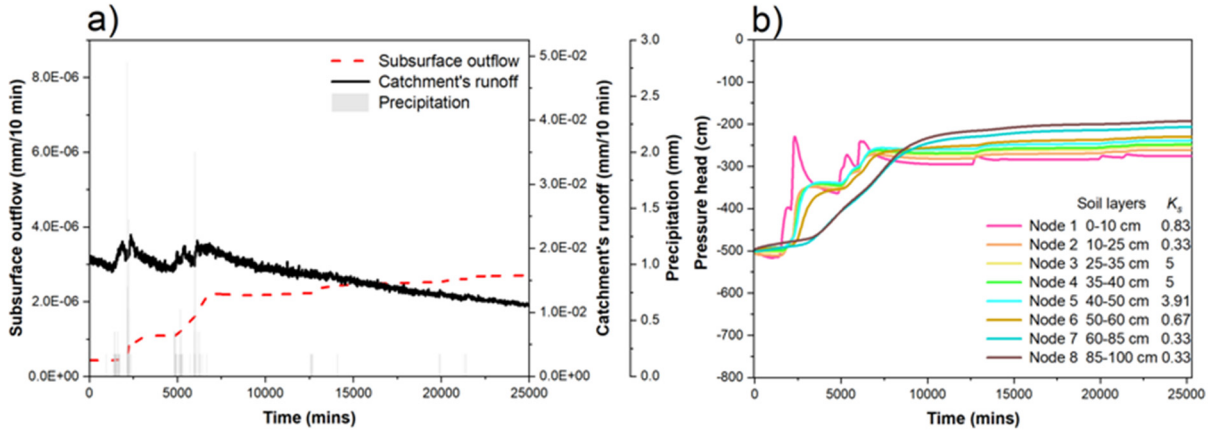

Fig.10. a) Rainfall, catchment runoff hydrograph and soil water outflow hydrograph with negative skewness caused by the rainfall event F on site 2; b) temporal evolution of pressure head with time at the gradient boundary observation nodes at different soil depths estimated by inverse modelling for the same event and site; K_s is saturated hydraulic conductivity in cm/min.

hydrographs shapes based on skewness and peak times was useful to identify the similarity. Additional criteria of hydrograph similarity can be tested when more rainfall events data is available. One of the ultimate aims of such a comparison would be the identification of typical hydrograph shapes related to certain field conditions. An example of the usefulness of such a work was recently given by Brunner et al. (2018) who used flood hydrograph shapes classification to delineate regions of similar flood behavior in Switzerland.

Simulated soil water outflow depends on many factors, e.g. the initial wetness, soil hydraulic properties, rainfall intensity, hillslope inclination, etc. All these factors determine the shape of the lateral subsurface flow hydrographs. Our simulations showed that K_s value of the soil layers played the key role in influencing the hydrograph geometry at different initial soil conditions and rainfall intensities. An example is presented in Figs 9 and 10.

Fig. 9a shows the positively skewed catchment runoff (measured) and lateral subsurface flow (Hydrus 2D simulated) hydrographs that have similar shapes. Temporal evolution of the simulated pressure head at various soil depths is shown in Fig. 9b. The top soil on site 1 had high K_s values and its pressure head hydrograph followed the rainfall pulse pattern. The upper soil layers (0–15 cm) were the dominant contributors to simulated soil water outflow and the obtained hydrograph was positively skewed.

Fig. 10a shows the negatively skewed lateral subsurface flow hydrograph. The lower soil layers on the study site (25–100 cm) had eight times greater K_s value than the top soil layers (0–15 cm) (Fig. 10b). Consequently, the rainfall fed by the top soil layers to lower soil layers resulted in greater outflow from the lower soil layers compared to the top soil layers. The lowest soil profile zone (depth 50–100 cm) was continuously fed by the upper soil layers that significantly increased its water storage. Since, there was no flux condition at the lower soil segment boundary in our numerical simulation (see Fig. 2), the lateral outflow occurred only from the 50–100 cm soil depth layer. The outflow was increasing continuously until the end of the simulation. That resulted in the negative skewness of the simulated soil water outflow hydrograph.

Presence of the rock fragments decreases retention capacity of soil by reducing the soil volume. In case of REVa, it was observed that soil layers with the highest stoniness had the lowest retention capacity at each site. However, it was not like that for the IMa (see Fig. 5).

The IMa optimizes soil hydraulic parameters by simulating moisture content according to observed moisture content. These observed soil moisture data are measured by sensors installed at various soil depths. Soil moisture sensors measure the water content at specific region, without taking in account the entire soil profile, i.e., their sampling area is small. The rock fragments affect the hydraulic characteristics of moderately to highly stony soils by reducing the available soil volume for water flow that increases water dynamics (e.g., Hlaváčiková et al., 2015, 2018). The IMa takes the rock fragments into account, but only in a small area of the sampling volume. On the contrary, the REVa represents the bulk characteristics of the soil profile and changes the soil water retention curves in the soil layers according to variation of stoniness in these layers. The REVa also takes into account field and laboratory measurements of hydraulic conductivity of stony soils that make it more suitable than the IMa.

We assumed constant parameters for each layer over the entire 20 m long section of the hillslope. Future studies are needed to evaluate the performance of REVa for the soil layers which do not have constant soil hydraulic parameters.

CONCLUSIONS

Outflow from stony the soils can contribute to rapid increase of catchment discharge due to small retention of such soils. Comparison of simulated lateral subsurface flow hydrographs with catchment runoff hydrographs indicated that the shapes of both were similar for about one half of the examined rainfall events.

Soil hydraulic parameters obtained from the Representative Elementary Volume approach provided more realistic simulated soil outflow hydrographs than the parameters obtained from the Inverse Modelling approach. The IMa more often resulted in the negatively skewed hydrographs and peaks that occurred after the catchment runoff peaks.

Modelling of water flow in stony soils is rare and we are not aware of studies analyzing subsurface flow and catchment runoff relationships that would consider the stony soils. Future studies could examine the REVa capabilities under different initial soil conditions, soil characteristics, stoniness, rainfall intensities and slope angles.

Limiting factor in a more thorough exploration of the central idea that reduced retention of stony soils can have similar effect on catchment runoff formation as the commonly accepted and more often studied preferential flow, is related to availability of data. While networks of rain gauges supplemented by soil moisture measurements at several depths covering different landscape units of the catchment (e.g., hillslopes, riparian areas) can be established more easily, more effort is needed to obtain good field and laboratory data characterizing soil stoniness and its variability.

Acknowledgements. This research was conducted under research project ASHMOB - Wildfire ASH MOBilization by wind and water erosion (02/SAICT/2017), within the PT2020 Partnership Agreement and Compete 2020 co-funded by FEDER. Also, Erasmus mobility program provided the funding. Collection of field data for numerical simulations and preparation of this paper were supported by the Slovak Research and Development Agency (APVV project No. 15- 0497) and by grant agency of the Slovak Academy of Sciences (VEGA project No. 2/0065/19).

REFERENCES

Al-Qinna, M., Scott, H.D., Brye, K.R., Brahana, J.V., Sauer, T.J., Sharpley, A., 2014. Coarse fragments affect soil properties in a mantled-karst landscape of the Ozark Highlands. Soil Sci., 179, 42–50.

Bachmair, S., Weiler, M., 2011. New dimensions of hillslope hydrology. In: Levia, D.F. (Ed.): Forest Hydrology and Biogeochemistry. Synthesis of Past Research and Future Directions. Ecological Studies, Vol. 2016. Springer, pp. 455–482.

Beven, K., Germann, P., 1982. Macropores and water flow in soils. Water Resour Res., 18, 5, 1311–1325.

Botter, G., Rinaldo, A., 2003. Scale effect on geomorphologic and kinematic dispersion. Water Resour. Res., 39, 1286.

Bouwer, H., Rice, R.C., 1984. Hydraulic properties of stony vadose zones. Ground Water, 22, 696–705.

Brunner, M.I, Viviroli, D., Furrer, R., Seibert, J., Favre, A.C., 2018. Identification of flood reactivity regions via the functional clustering of hydrographs. Water Resources Research, 54, 3, 1852–1867.

Buchter, B., Hinz, C., Flühler, H., 1994. Sample size for determination of coarse fragment content in a stony soil. Geoderma, 63, 265–275.

Chen, H., Liu, J., Zhang, W., Wang, K., 2012. Soil hydraulic properties on the steep karst hillslopes in northwest Guangxi, China. Environ. Earth Sci., 66, 371–379.

Collischonn, W., Fleischmann, A., Paiva, R.C.D., Mejia, A., 2017. Hydraulic causes for basin hydrograph skewness. Water Resour. Res., 53, 10603–10618.

Coppola, A., Dragonetti, G., Comegna, A., Lamaddalena, N., Caushi, B., Haikal, M.A., Basile, A., 2013. Measuring and

modeling water content in stony soils. Soil Till. Res., 128, 9–22.

Dane, J.H., Hopmans, J.W., 2002. Pressure plate extractor. In: Dane, J.H., Topp, G.C., (Eds.): Methods of Soil Analysis, Part 4, Physical Methods. SSSA Book Series 5, SSSA, Madison, WI, pp. 688–690.

Hlaváčiková, H., Novák, V., Holko, L., 2015. On the role of rock fragments and initial soil water content in the potential subsurface runoff formation. J. Hydrol. Hydromech., 63, 71–81.

Hlaváčiková, H., Novák, V., Šimůnek, J., 2016. The effects of rock fragment shapes and positions on modeled hydraulic conductivities of stony soils. Geoderma, 281, 39–48.

Hlaváčiková, H., Novák, V., Kostka, Z., Danko, M., Hlavčo, J., 2018. The influence of stony soil properties on water dynamics modeled by the HYDRUS model. J. Hydrol. Hydromech., 66, 181–188.

Hlaváčiková, H., Holko, L., Danko, M., Novák, V., 2019. Estimation of macropore flow characteristics in stony soils of a small mountain catchment. J. Hydrol., 574, 1176–1187.

Holko, L., Lepistő, A., 1997. Modelling the hydrological behaviour of a mountainous catchment using TOPMODEL. J. Hydrol., 196, 361–377.

Holko, L., Kostka, Z., 2010. Hydrological processes in mountains – knowledge gained in the Jalovecky Creek catchment, Slovakia. IAHS Publication, 336. IAHS Press, Wallingford, pp. 84–89.

Holko, L., Kostka, Z., Šanda, M., 2011. Assessment of frequency and areal extent of overland flow generation in a forested mountain catchment. Soil Water Res., 6*,* 43–53.

Holko, L., Bičárová, S., Hlavčo, J., Danko, M., Kostka, Z., 2018. Isotopic hydrograph separation in two small mountain catchments during multiple events. Cuadernos de Investigación Geográfica, 44, 2, 453–473.

Holko, L., Sleziak, P., Danko, M., Bičárová, S., Pociask-Karteczka, J., 2020a. Analysis of changes in hydrological cycle of a pristine mountain catchment. 1. Hydrometric data. Journal of Hydrology and Hydromechanics, 68, 2, 180–191.

Holko, L., Danko, M., Sleziak, P., 2020b. Analysis of changes in hydrological cycle of a pristine mountain catchment. 2. Isotopic data, trend and attribution analyses. Journal of Hydrology and Hydromechanics, 68, 2, 192–199.

Kostka, Z., 2009. Runoff response to rainfall event in the mountain catchment. Acta Hydrologica Slovaca, 10, 1, 130−139. (In Slovak with English abstract.)

Li, H., Sivapalan, M., 2011. Effect of spatial heterogeneity of runoff generation mechanisms on the scaling behavior of event runoff responses in a natural river basin. Water Resour. Res., 47, Article No. W00H08.

Ma, D.H., Shao, M.A., 2008. Simulating infiltration into stony soils with a dual-porosity model. Eur. J. Soil Sci., 59, 950–959.

Šimůnek, J., van Genuchten, M.T, 1996. Estimating unsaturated soil hydraulic properties from tension disc infiltrometer data by numerical inversion. Water Resour. Res., 32, 2683–2696.

Šimůnek, J., Wendroth, O., van Genuchten, M.T, 1998. A parameter estimation analysis of the evaporation method for determining soil hydraulic properties. Soil Sci. Soc. Am. J., 62, 894–905.

Šimůnek, J., van Genuchten, M.T., Šejna, M., 2008. Development and applications of the HYDRUS and STANMOD software packages and related codes. Vadose Zone J., 7, 587–600.

Šimůnek, J., Šejna, M., Saito, H., Sakai, M., van Genuchten, M.T., 2013. The HYDRUS-1D Software Package for Simulating the One-Dimensional Movement of Water, Heat, and Multiple Solutes in Variably-Saturated Media, Version 4.17. Department of Environmental Sciences, University of California Riverside, Riverside, CA, USA, 308 p.

Tesař, M., Šír, M., Syrovátka, O., Pražák, J., Lichner, Ľ., Kubík, F., 2001. Soil water regime in head water regions - observation, assessment and modelling. J. Hydrol. Hydromech., 49, 6, 355–406.

Tromp-van Meerveld, H.J., McDonnell, J.J., 2006. Threshold relations in subsurface stormflow: 2. The fill and spill hypothesis. Water Resour Res., 42, W02411. DOI: 10.1029/2004WR003800.

van Genuchten, M.T., 1980. A closed-form equation for predicting the hydraulic conductivity of unsaturated soils. Soil Sci. Soc. Am. J., 44, 987–996.

Wegehenkel, M., Wagner, A., Amoriello, T., Fleck, S., Messenburg, H., 2017. Impact of stoniness correction of soil hydraulic parameters on water balance simulations of forest plots. J. Plant Nutr. Soil Sci., 180, 71–86.

Received 10 December 2019
Accepted 1 March 2020

J. Hydrol. Hydromech., 68, 2020, 2, 155–169
DOI: 10.2478/johh-2020-0008
ISSN 1338-4333

sciendo Journal of Hydrology and Hydromechanics

Controls on event runoff coefficients and recession coefficients for different runoff generation mechanisms identified by three regression methods

Xiaofei Chen[1*], Juraj Parajka[1, 2], Borbála Széles[1], Peter Strauss[3], Günter Blöschl[1, 2]

[1] TU Wien, Centre for Water Resource Systems, Karlsplatz 13, A-1040, Vienna, Austria. www.waterresources.at
[2] TU Wien, Institute of Hydraulic Engineering and Water Resources Management, Karlsplatz 13, A-1040 Vienna, Austria.
[3] Federal Agency for Water Management, Institute for Land and Water Management Research, A-3252 Petzenkirchen, Austria.
[*] Corresponding author. E-mail: chen@waterresources.at

Abstract: The event runoff coefficient (*Rc*) and the recession coefficient (*tc*) are of theoretical importance for understanding catchment response and of practical importance in hydrological design. We analyse 57 event periods in the period 2013 to 2015 in the 66 ha Austrian Hydrological Open Air Laboratory (HOAL), where the seven subcatchments are stratified by runoff generation types into wetlands, tile drainage and natural drainage. Three machine learning algorithms (Random forest (RF), Gradient Boost Decision Tree (GBDT) and Support vector machine (SVM)) are used to estimate *Rc* and *tc* from 22 event based explanatory variables representing precipitation, soil moisture, groundwater level and season. The model performance of the SVM algorithm in estimating *Rc* and *tc* is generally higher than that of the other two methods, measured by the coefficient of determination R^2, and the performance for *Rc* is higher than that for *tc*. The relative importance of the explanatory variables for the predictions, assessed by a heatmap, suggests that *Rc* of the tile drainage systems is more strongly controlled by the weather conditions than by the catchment state, while the opposite is true for natural drainage systems. Overall, model performance strongly depends on the runoff generation type.

Keywords: Machine learning; Event runoff analyses; Event runoff coefficient; Recession coefficient; Runoff generation.

INTRODUCTION

The event runoff coefficient and the recession coefficient are important characteristics of hydrologic response at the event scale. Understanding their controls and their variability is essential for predicting runoff in ungauged basins and for extrapolating hydrologic response to extreme events (Blöschl et al., 2013; Sivapalan, 2003; Tarasova et al., 2018ab; Viglione et al., 2009).

The event runoff coefficient *Rc* is defined as the portion of rainfall that becomes direct runoff during an event (Merz et al., 2006). The spatial-temporal variability of *Rc* has been widely studied (e.g. Hayes and Young, 2006; Longobardi et al., 2003; Merz et al., 2006; Merz and Blöschl, 2009; Wainwright and Parsons, 2002). Previous studies show that the magnitude of *Rc* varies between the regions. While regional assessments of meso-scale catchments in Austria or Germany (Merz et al., 2006, Tarasova et al., 2018ab) indicate the median of Rc between 0.18 and 0.43, Rc in small agricultural catchments tends to be lower and varies between 0.03 and 0.10 (Blume et al., 2007; Tachecí et al., 2013) to more than 0.2 over cropland hillslopes in central Iowa (Chen et al., 2019). The controls on *Rc* generally depend on the runoff mechanisms. Precipitation intensity tends to be most important when the infiltration excess mechanism dominates, precipitation depth when the saturation excess mechanism dominates, and soil moisture is important for all mechanisms (Tian et al., 2012). Rodríguez-Blanco et al. (2012) and Palleiro et al. (2014) found that the event runoff coefficient in forested catchments in northwestern Spain depended both on the soil moisture at the start of the event and on rainfall depth, whereas rainfall intensity was less important. They explained this finding by the dominant role of subsurface stormflow in event runoff generation. Based on a comparative study in the eastern Italian Alps, Norbiato et al. (2009) suggested that the effect of antecedent soil moisture on the event runoff coefficient might be largest in catchments with intermediate storage capacities. Besides climate and hydrological conditions, Norbiato et al. (2009) also verified that the 'permeability index' deduced from geology is another considerable control on event runoff coefficient in regions with mean annual precipitation less than 1200 mm. Gottschalk and Weingartner (1998) showed that moderate slopes and low geological permeability in the Swiss midlands basins generally lead to events with low event runoff coefficients.

The recession coefficient, *tc*, is the parameter in a linear function of $\frac{-dQ}{dt} = \frac{1}{tc}Q$ where $\frac{-dQ}{dt}$ is the time derivative of runoff Q (Brutsaert and Nieber, 1977; Tallaksen, 1995). Similarly to the event runoff coefficient, the recession parameter has been widely studied (Biswal and Kumar, 2014; Krakauer and Temimi, 2011; Merz et al., 2006; Patnaik et al., 2015). Krakauer and Temimi (2011) identified soil infiltration capacity and forest cover as important controls on the recession coefficient in small catchments in the United States. Tague and Grant (2004) and Gaál et al. (2012) highlighted the important role of geology for the recession coefficient.

One of the challenges in identifying the controls and predicting *Rc* and *tc* is the typically non-linear nature of the relationships between these two parameters and their controls (Merz and Blöschl, 2009; Krakauer and Temimi, 2011). It is therefore of advantage to use non-linear rather than linear analyses and predictive methods. Machine learning techniques based on regressions are able to capture the non-linearity in the relationship between predictor and predictand (Cánovas-García et al., 2017; Erdal and Karakurt, 2013; Naghibi et al., 2017; Şen and Altunkaynak, 2006). Three widely used methods are random forests (RF), Gradient Boost Decision Trees (GBDT) and Support vector machines (SVM).

RF (Ho, 1995) are a learning method for classification and regression that consists of a number of decision trees at training time and identifies the class that has the greatest number of votes (classification) or the mean prediction (regression) of the individual trees. Random forests have been applied in numerous surface and subsurface hydrological studies (Baudron et al., 2013; Naghibi et al., 2017; Zimmermann et al., 2014).

GBDT make use of the gradient boosting framework to combine decision trees based on the RF algorithm. GBDT are usually composed of hundreds of decision trees with shallow depth. In this algorithm, every decision tree adjusts and modifies the predicted value, finally resulting in the prediction. The trees are trained sequentially, which improves the prediction accuracy but involves a longer training time (Friedman, 2001, 2002). Naghibi et al. (2016) compared boosted regression trees (BRT), classification and regression trees (CART), and RF in producing groundwater spring potential maps according to thirteen hydrological-geological-physiographical factors (Naghibi et al., 2016). Sachdeva et al. (2018) constructed wildfire susceptibility maps by combining evolutionary optimized gradient boosted decision trees, and showed that they outperformed other machine learning models.

SVM are supervised learning models with associated learning algorithms. Given a set of training examples, the training algorithm builds a model that assigns new examples to one of two categories (Basak et al., 2007; Ben-Hur and Weston, 2010; Vapnik et al., 1997). SVM have a number of advantages: they effectively solve the classification and regression problem for high dimensions; they solve various nonlinear classification and regression problems by means of different kernel functions; they are able to generalize well. However, computational costs are very high when the dimension of the mapping kernel function is large, and they are sensitive to missing data. They have been applied to surface flow, evaporation, droughts, soil moisture and groundwater prediction (Asefa et al., 2006; Deka, 2014; Hwang et al., 2012; Maity et al., 2010).

The aim of this paper is (a) to identify factors which control variability of event runoff coefficient (*Rc*) and the recession coefficient (*tc*) in small agricultural catchment; (b) to evaluate the relative importance of the control in different subcatchments representing different runoff generation mechanisms and (c) to compare three regression based machine learning techniques, random forests (RF), Gradient Boost Decision Trees (GBDT) and Support vector machines (SVM), in terms of their ability to estimate the event runoff coefficient and the recession coefficient from their controls.

STUDY CATCHMENT AND DATA

The study is performed in the Hydrological Open Air Laboratory (HOAL). This is a small experimental catchment situated in Lower Austria (Blöschl et al., 2016; Exner-Kittridge, et al., 2016; Széles et al., 2018) (Figure 1). The land use is mainly agricultural (82%) and part of the catchment is tile drained. Runoff is recorded at a number of flumes within the catchment at a time step of 1 minute. In this study, eight flumes are used (Table 1). MW is the catchment outlet of the HOAL and has a catchment area of 65.8 ha. All the other flumes are nested in this catchment (Figure 1). The runoff generation mechanisms of the catchments drained by the flumes differ. Sys4 represents a piped stream and is considered as "natural subsurface drainage" here. Frau1 and Frau2 are tile drained. A1 and A2 drain wetland areas. Sys2, Sys3 and Sys4 are classified as natural drainage here, although (Széles et al., 2018) classified them as tile drains. The reason for the different classification is that the drainage areas of these systems are not fully covered by underground tile pipes and most of the flow is drained from subsurface without tile pipes. All discharge data are processed to remove outliers caused by instrument malfunction and maintenance and aggregated to an hourly time step. Catchment boundaries are identified by analysing a digital elevation model (DEM) and account for the position of tile pipes (Széles et al., 2018). These are used for estimating specific runoff as the ratio of runoff and catchment area and for estimating catchment precipitation (Table 1).

Table 1. Runoff generation mechanism and estimated drainage area of the gauged catchments in the HOAL. Figure 1 shows locations of the gauges. From (Széles et al., 2018).

Gauge	Runoff generation mechanism	Estimated drainage area (ha)	Tile pipe covered area percentage (%)
A1	Wetland	2.1	6.5
A2	Wetland	1.1	11.0
Frau1	Tile drain	3.1	96.6
Frau2	Tile drain	4.8	60.8
Sys2	Natural drainage	2.4	8.7
Sys3	Natural drainage	4.3	10.7
Sys4	Natural drainage	37.4	4.3
MW	Outlet	65.8	12.9

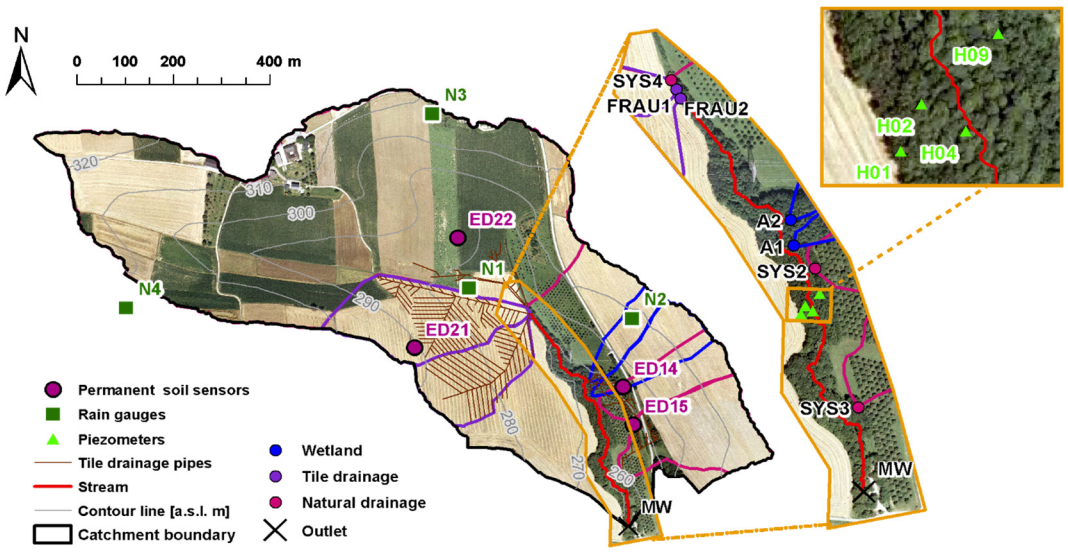

Fig. 1. HOAL catchment and its subcatchments. Locations of stream gauges, soil moisture sensors and piezometers used in the analyses.

Additionally, data from four rain gauges (N1-N4), four soil moisture sensors (ED14, ED15, ED21 and ED22) at 5, 10 and 20 cm depth and four groundwater piezometers (H01, H02, H04 and H09) are used (see (Blöschl et al., 2016) for details). Soil moisture data are averaged over depth for extracting soil moisture related variables. Precipitation measurements are averaged by using Thiessen polygon method, and the catchment averages range from 0 to 21.5 mm/h (average: 0.09 mm/h). The higher and smaller precipitation intensities are observed in summer and in winter periods, respectively (Figure 2a). The mean annual precipitation in the study period is decreasing from 937 mm in 2013 to 573 mm in 2015. Comparison of the frequency of daily maximum precipitation from the period 1946 to 2018 indicates that selected study period represents well the frequency of precipitation intensities larger than 30mm/d or 50mm/d. Observed air temperature ranges from –15.2 to 36.3°C during the period from 2013 to 2015 and seasonal dynamics of potential evapotranspiration corresponds to the seasonal dynamics of air

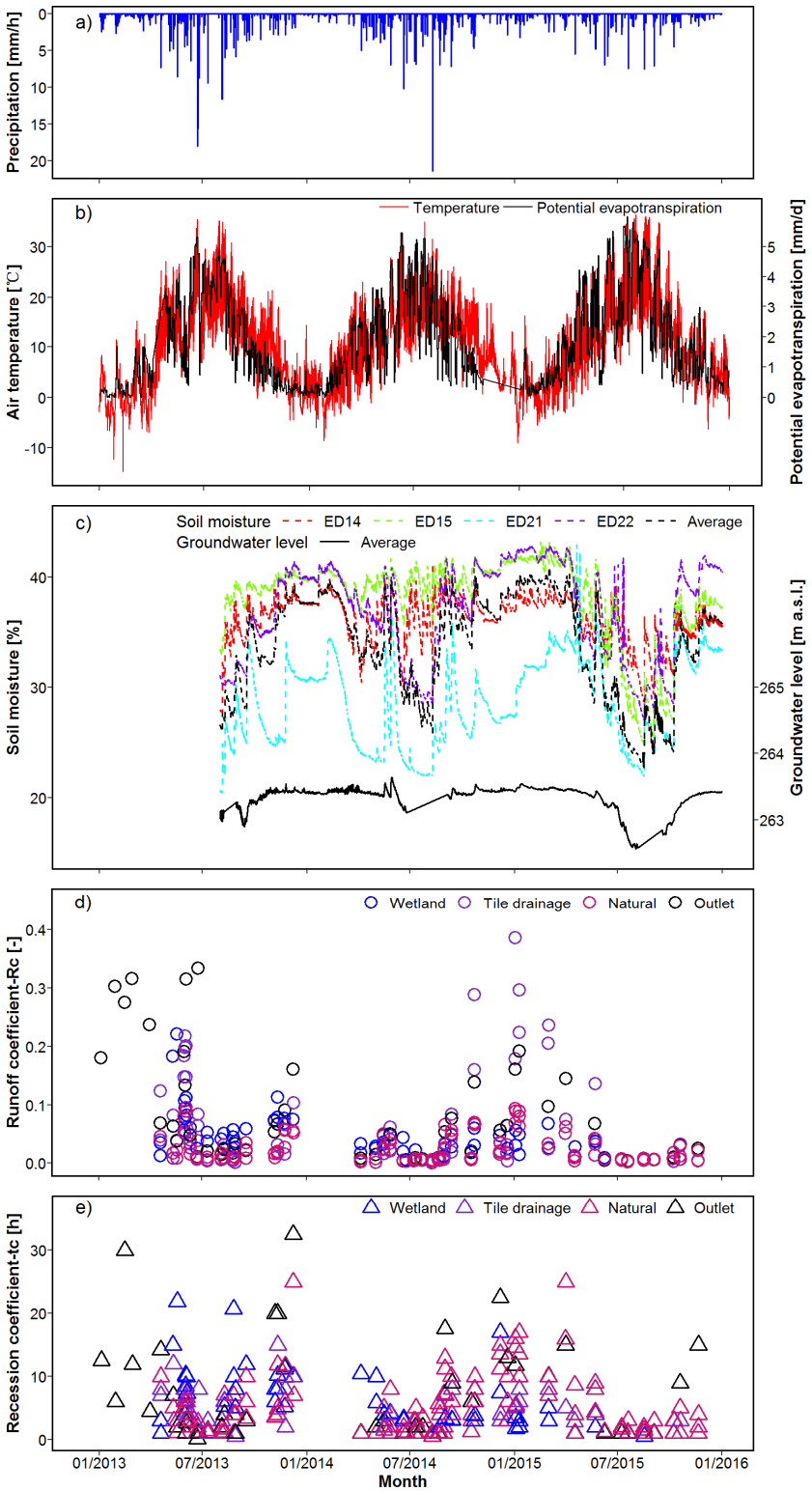

Fig. 2. Temporal variability of precipitation (panel a), air temperature and potential evapotranspiration (panel b), soil moisture and groundwater level (panel c), event runoff coefficient (panel d) and recession coefficient (panel e) in HOAL in the period 2013 to 2015.

temperature (Figure 2b). The effect of increased air temperature and potential evaporation in summer is reflected by decreasing soil moisture and groundwater levels (Figure 2c). The seasonal dynamics of event runoff coefficient (*Rc*) and recession coefficient (*tc*) (Figure 2d, e) indicates smaller values of *Rc* and *tc* in summer and and their gradual increase towards winter season.

METHODS

Estimation of event runoff coefficients and recession coefficients

The event runoff coefficients and recession coefficients are estimated for each of the eight stream gauges separately using the method of (Merz et al., 2006). The analysis is based on an hourly time step and consists of four steps:

(1) Catchment rainfall estimation: For each of the eight stream gauges, catchment average rainfall is estimated at an hourly time step by spatially interpolating the measurements of four rain gauges using the Thiessen polygon method.

(2) Baseflow separation: Baseflow is estimated for each stream gauge using the Chapman and Maxwell (1996) filter. More details about the filter are given in Merz et al. (2006).

(3) Identification of runoff events: An event peak is identified, if the direct flow is more than double of the baseflow at a certain time step and larger runoff is not observed 5 hours before and after the peak. Around these peaks, the beginning and end times are estimated. An example of an identified event in May of 2014 is shown in Figure 3a. This event is driven by a late spring precipitation event with a peak of 7.0 mm/h, which is larger than 80% of identified events. The event runoff coefficient in a tile drain system Frau2 is about 0.06 higher than at the main catchment outlet MW. Figure 3b shows the dynamics of the ratio of cumulative direct runoff to cumulative precipitation as a function of time during an event for different gauges. The ratio gradually increases and approaches a stable value at the end of the event, which is the *Rc* of that event. There is a large difference between Frau1 and Frau2 due to differences in the controls. A total of 57 event periods are identified at MW outlet (Table 4). At the tributaries slightly fewer are identified, as they do not always respond to rainfall. The number of identified events in individual subcatchments and main outlet are 30 (A1), 38 (A2), 21 (Frau1), 30 (Frau2), 32 (Sys2), 39 (Sys3), 51 (Sys4) and 57 (MW outlet), respectively. This results in a total of 298 event hydrographs from 2013 to 2015 to be further analysed.

(4) Fitting a linear reservoir model: In order to reduce the effect of the selection of the end time of the runoff events, a linear reservoir model is fitted to the direct flow by minimizing the root mean square difference between observed and simulated runoff for each event and stream gauge separately. The event runoff coefficient *Rc* (–) and the recession coefficient *tc* (hrs) are the optimised model parameters.

Ensemble learning techniques for regression

For the purpose of the study, three learning techniques are used to build regression models. Ensemble learning techniques have been proved in the past to describe and learn various non-linear relationships (Dietterich, 1997). The main advantage of ensemble learning approaches is that they learn in a hierarchical fashion by repeatedly splitting input dataset into separate branches that maximize the information gain of each split. The challenge with their application is, however, that for the selection of an optimal approach, evaluation of performance of different algorithms is recommended (Shen, 2018). Thus the aim of our study is to test three different approaches (i.e random forest, gradient boost decision trees and support vector machines) individually in four different settings represented by four runoff generation systems (wetland, tile drainage, natural and outlet) which are termed as Classified regression model in our study, and in an aggregated system that combines all runoff generation systems termed here as Unclassified regression model.

Random Forests (RF)

Random forests consist of a number of tree predictors. As the number of trees increases, the mean squared error of out of bag data (*OOBError*) in prediction decreases until it reaches a constant, low level (Ho, 1995). There are two main steps:

(a) Random sampling from the entire database to train a decision tree. The input subsets are different from each other to avoid over-fitting. Out of bag data (OOB) is the remaining subset, which is not used in building a tree. At each node of the trees, the feature that produces the best split in sub-sampling from all features is used for splitting.

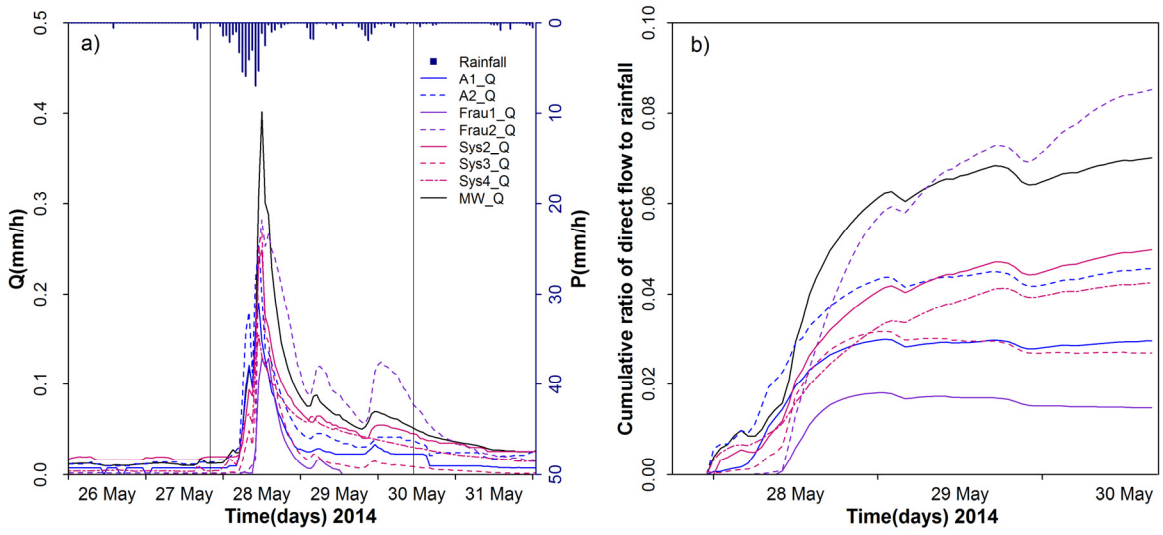

Fig. 3. Example event in May 2014. Line colours according to runoff generation mechanisms (wetland runoff is blue; tile drainage is purple; natural discharge is dark pink and outlet flow is black). (a) Hydrographs. Vertical lines indicate start and end of the event. (b) Ratio of cumulative direct flow to cumulative precipitation during the event.

(b) Splitting at each node: Each decision tree is completely split until all samples belong to one class or the leaf node can not be further divided. The feature importance outputs of the RF model with good predictions are used to evaluate the influence of the variables on *Rc* and *tc*.

Gradient Boost Decision Trees (GBDT)

A Gradient Boost Decision Tree GBDT regression model is established by integrating multiple decision trees (DTs) in an iterative process (Friedman, 2001, 2002). In every iteration (adding a new tree to the model), model losses are reduced. A Gaussian distribution is chosen as a loss function L for minimizing the squared error,

$$L\left(y, f\left(x\right)\right) = \frac{1}{\sum_i \omega_i} \Sigma \omega_i \left(y_i - f\left(x_i\right)\right)^2 \quad (1)$$

where ω_i is the weight of sample i, y_i are the objectives and $f(x_i)$ are the predictions.

Support Vector Machines (SVM)

For a support vector machine (SVM) regression to represent non-linear problems, a proper kernel function needs to be chosen by projecting the data to a high-dimensional space where one can use a linear decision boundary to separate classes (Osuna, 1998). A radial basis function, K, is used here which can be expressed for an infinite dimensional space (Horn, 1985) as (2)

$$K\left(u, v\right) = \mathrm{e}^{-\gamma\left|u-v\right|^2} \quad (2)$$

where u and v are two vectors, $\left|u-v\right|^2$ is the squared Euclidean distance of these two vectors, and γ influences the number of support vectors. Larger γ results in fewer support vectors.

The ε regression option is adopted here for better controlling model error. Errors beyond the specified ε are penalized in proportion to C, which is the regularization parameter. The ε insensitive loss function L_ε proposed by Chapelle and Vapnik (2000) is used according to (3)

$$L_\varepsilon = \begin{cases} 0 & \text{if } \left|y - f\left(x\right)\right| < \varepsilon \\ \left|y - f\left(x\right)\right| - \varepsilon & \text{otherwise} \end{cases} \quad (3)$$

For brevity, only the variable importance of the SVM model, $I_{i,SVM}$ which can reflect the level of variable influences to model objectives (*Rc* and *tc* in this study), are presented in the study. In order to quantify such importance of variables, we take advantage of the Average Absolute Deviation (AAD) from the median in the theory of 1-D sensitivity analysis (Cortez and Embrechts, 2013). $I_{i,SVM}$ is estimated according to the following function

$$\sum_{j=1}^{L} \left|y_j - \tilde{y}\right| / L \quad (4)$$

where $\tilde{y}$ is the baseline of the objectives (median) and y_j is the prediction related to the j^{th} level of input (totally L = 7 levels).

The detailed procedures of building the SVM regression models are introduced by Cortes and Vapnik (1995).

Calibration and validation performance of the non-linear regression models

In order to compare the performance of the three machine learning methods, two types of validations are performed. The first type is the analysis of temporal performance which is evaluated by the coefficients of determination (R^2)

$$R^2 = 1 - \frac{\sum_i \left(y_i - f\left(x_i\right)\right)^2}{\sum_i \left(y_i - \bar{y}\right)^2} \quad (5)$$

where $f(x_i)$ is the prediction of *Rc* or *tc* for event i, y_i is the observed value, and $\bar{y}$ is the mean of the observed values over all events of a particular runoff generation type. R^2 is regarded as 0 when it is negative.

The second type is the validation in space by using leave-one-out cross-validation. Here, the regressions fitted separately to one of the subcatchments representing wetland (A2 station), tile drainage (Frau2 station) and natural drainage (Sys3 and Sys4 stations) are validated in the other stations representing the same runoff generation type, i.e. A1 (wetland), Frau1 (tile drainage), Sys2 (natural drainage). The performance is evaluated by R^2, similarly to (5).

RESULTS

Evaluation of the observed runoff coefficients and recession time constant and their potential controls

In order to analyse the potential controls on *Rc* and *tc*, 22 hydrological variables are considered for each stream gauge (Table 2). Event precipitation (VolP), precipitation peak during the event (PeakP) and precipitation duration during the event (DurP) are estimated from the catchment precipitation time series with hourly temporal resolution. Antecedent soil moisture (PreSM), average soil moisture during the event (AverSM), soil moisture at the end of the event (EndSM), soil moisture at the time of peak rainfall (PeakPSM) and soil moisture peak during the event (PeakSM) are estimated from the soil moisture data. Depending on the stream gauge, different soil moisture sensors are used (ED15 for Sys2 and Sys3; ED22 for Sys4; ED21 for Frau1 and Frau2; ED14 for A1 and A2; and the average of all sensors for MW). Soil moisture peak delay to precipitation (DelaySM) is estimated as the time difference between the precipitation peak and the soil moisture peak. Pre-event groundwater level (PreWL), average groundwater level during the event (AverWL), groundwater level at the end of the event (EndWL), groundwater level at the time of peak precipitation (PeakPWL) and peak groundwater level (PeakWL) are estimated from the average groundwater level of all four piezometers, as no separate piezometer data are available for the individual catchments. Groundwater level peak delay to precipitation (DelayWL) is estimated as the time difference between the precipitation peak and the groundwater peak. Potential evapotranspiration (EP) on the day of the event is estimated by the *Penman-Monteith* equation. Additionally, the month of the event occurred (Month), the Normalized Difference Vegetation Index (NDVI) and the runoff generation type (Type: 1-wetland; 2-tile drainage; 3-outlet; 4-natural drainage) are considered as variables. NDVI represents the mean catchment or subcatchment value and it is estimated by linear interpolation between 57 Landsat 7 and 8 scenes available in the period 2013-2015. Finally, drainage area (Area), percentage of piped area (AreaPipes) and forest cover (AreaForest) are also used.

Table 2. Event based hydrological variables examined as potential controls on *Rc* and *tc*. While the variables differ between stream gauges, the combined statistics of all stream gauges are shown here.

Variables	Explanation	Min	25%	50%	75%	Max
VolP	Volume of precipitation during event (mm)	3.5	12.7	17.5	27.5	99.3
PeakP	Precipitation peak during event (mm/hr)	0.2	2.8	3.7	6.7	21.5
DurP	Precipitation duration during event (hrs)	2.0	9.0	17.0	29.8	102.0
PreSM	Antecedent soil moisture (%)	20.5	30.2	35.5	38.6	42.4
PeakSM	Peak of soil moisture during event (%)	24.9	34.2	38.2	40.0	43.2
PeakPSM	Soil moisture at the time of peak precipitation (%)	20.5	30.2	36.9	39.3	43.0
AverSM	Average soil moisture during event (%)	22.6	31.7	37.0	39.2	42.6
EndSM	Soil moisture at the end of event (%)	23.6	33.6	37.9	39.4	42.6
DelaySM	Soil moisture peak delay to precipitation (hrs) (positive value indicates earlier flow peak than soil moisture)	–13.0	2.0	7.0	11.0	63.0
PreWL	Pre-event groundwater level (m)	262.6	263.3	263.4	263.5	264.7
PeakWL	Peak groundwater level (m)	262.7	263.3	263.5	263.5	264.9
PeakPWL	Groundwater level at the time of peak precipitation (m)	262.7	263.3	263.4	263.5	264.7
AverWL	Average groundwater level during event (m)	262.7	263.3	263.5	263.5	264.7
EndWL	Groundwater level at the end of event (m)	262.7	263.3	263.5	263.5	264.8
DelayWL	Groundwater level peak delay to precipitation (hrs) (positive value indicates earlier flow peak than groundwater table)	–12.0	13.0	18.0	27.0	103.0
EP	Potential evapotranspiration during the day of event (mm/d)	0.0	0.9	1.7	2.7	5.1
Month	Month when event occurred (month)	1	5	7	9	12
NDVI	Normalized Difference Vegetation Index	0.1	0.2	0.3	0.3	0.5
AreaPipes	Piped area relative to drainage area (%)	4.3	6.5	10.7	12.9	96.6
AreaForest	Forest covered area percentage to drainage area (%)	0.0	4.6	9.6	14.2	18.8
Area	Drainage area of subcatchment (ha)	1.1	2.4	4.3	37.4	65.8
Type	Runoff generation type (1-wetland; 2-tile drainage; 3-outlet; 4-natural drainage)	1	2	3	4	4

Table 3. Statistics of the event runoff coefficients *Rc* and recession coefficients *tc*, including minimum, quartiles and maximum, for the eight stream gauges based on 40 events which can be observed at least at 5 stations.

		Rc (–)					*tc* (hrs)				
Gauge	Runoff generation mechanism	Min	25%	50%	75%	Max	Min	25%	50%	75%	Max
A1	Wetland	0.010	0.026	0.033	0.049	0.082	1.00	3.00	4.00	8.00	16.98
A2	Wetland	0.006	0.028	0.048	0.068	0.222	0.50	2.00	3.89	7.57	21.90
Frau1	Tile drain	0.001	0.016	0.033	0.181	0.297	0.50	3.00	4.00	6.00	10.00
Frau2	Tile drain	0.0003	0.026	0.054	0.139	0.386	1.00	3.00	5.50	8.00	15.00
Sys2	Natural drainage	0.006	0.010	0.034	0.058	0.089	1.00	4.00	5.00	7.00	17.00
Sys3	Natural drainage	0.001	0.005	0.018	0.026	0.094	0.50	1.63	4.20	7.60	14.67
Sys4	Natural drainage	0.004	0.008	0.012	0.037	0.096	1.00	1.04	3.36	8.00	25.00
MW	Outlet	0.004	0.014	0.048	0.071	0.316	0.10	1.00	3.00	10.00	32.56
All gauges		0.0003	0.012	0.032	0.063	0.386	0.10	2.00	4.00	8.00	32.56

Table 4. Number of event hydrographs and number of event periods (in brackets) used for the calibration and validation for the *Rc* and *tc* regressions. The models are fitted for the four runoff generation types (wetland, tile drainage, natural and outlet) termed as Classified regression model, and all together (Unclassified regression model).

	Number of events for Classified regression model				Number of events for Unclassified regression model
	Wetland (A1, A2)	Tile drainage (Frau1, Frau2)	Natural (Sys2, Sys3, Sys4)	Outlet (MW)	All
Calibration	54	40	97	45	252 (40 event periods)
Validation	14	11	25	12	46 (17 event periods)
Total	68	51	122	57	298 (57 event periods)

22 hydrological variables and *Rc* and *tc* are normalised to the range between 0 and 1 for all runoff generation systems together.

The statistics and cumulative distributions of the resulting coefficients are respectively showed in Table3 and Figure 4. *Rc* varies from 0.0003 to 0.4. The tile drainage catchment Frau 2 has the highest median (0.054), the natural subsurface drainage Sys4 the lowest (0.012). The tile drainage catchment Frau 2 has the highest median of *tc* (5.5 hrs), the outlet MW the lowest (3.0 hrs) but the 75% quantile is larger than that of the subcatchments (10 hrs). The correlation coefficient of *Rc* and t*c* over all 298 hydrographs is about 0.38. High *Rc* is usually associated with high antecedent flows which may result in slower runoff recession (Patnaik et al., 2015) because of large groundwater contributions (Exner-Kittridge et al., 2016).

Parameter sensitivities of the three non-linear regression models

The parameter sensitivities of the regression models are explored based on 252 event hydrographs, when events are observed at a minimum of 5 stations (Figure 5, 6 and 7). Additionally 46 event hydrographs are used for validation (Table 4).

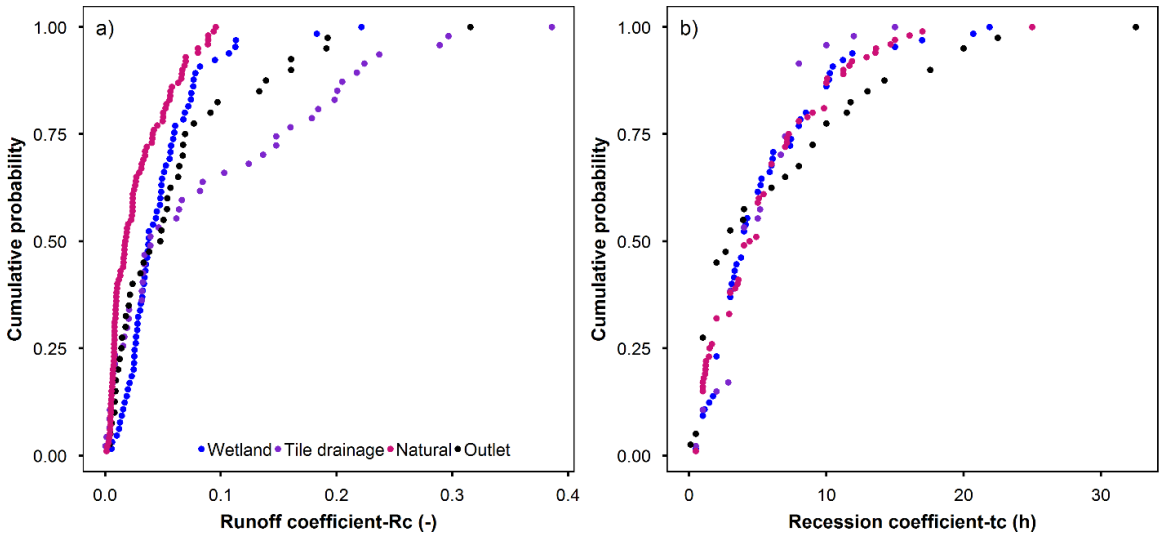

Fig. 4. Cumulative distribution of (a) event runoff coefficients and (b) recession coefficients for the four types of runoff generation mechanisms.

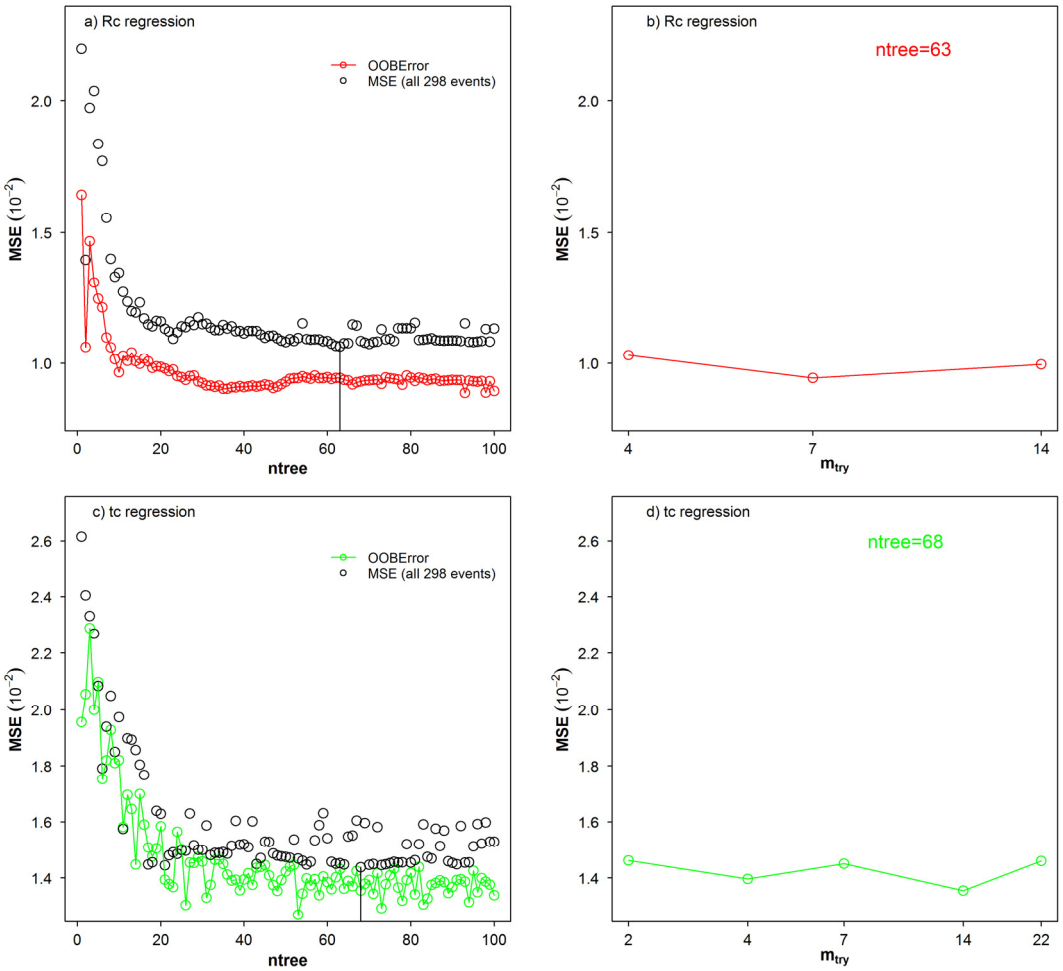

Fig. 5. Sensitivity of the model error, MSE, to *ntree* and m_{try} in the RF models for *Rc* and *tc* regressions based on unclassified events (Table 4). The vertical black line indicates the *ntree* chosen, 63 for the *Rc* regression and 68 for the *tc* regression.

RF model (ntree and m_{try})

The number of trees in the model, *ntree*, has a controlling function in the model performance (Figure 5 a and c). As *ntree* increases, *OOBError*, i.e. the mean squared error (*MSE*) based on out of bag data (*OOB* data), decreases up to a threshold. *OOBError* is calculated according to (7)

$$OOBError = \frac{\sum_i^M (y'_i - y_i)^2}{M} \quad (7)$$

where M is the number of out of bag data, y_i is ith observation value of *OOB* and $y_i^{'}$ is the model prediction of *OOB* based on trees that are not trained by the i^{th} sample.

OOBError stabilises at around 0.009 and 0.013 for *Rc* and *tc*, respectively. The model performance would be improved by diversifying regression trees, however, it is difficult to build a new diverse tree if the ensemble size is large. Therefore, *OOBError* tends to approach a constant level (Breiman, 2001).

If the number of variables m_{try} randomly sampled as candidates at each split is close to the total number of variables, regression trees are more likely to be similar, which will reduce the predictive ability. In our case of only 22 variables, the results do not change much by m_{try} (Figure 5 b and d), as suggested by Liaw and Wiener (2002).

Finally, for the unclassified models, *ntree* is set to 63 and 68 for the *Rc* and *tc* regressions, respectively, by minimizing MSE of all 298 events, while m_{try} is automatically optimized. The parameters of the classified models are calibrated in the same way. The final values of *ntree* and m_{try} are listed in Table 5.

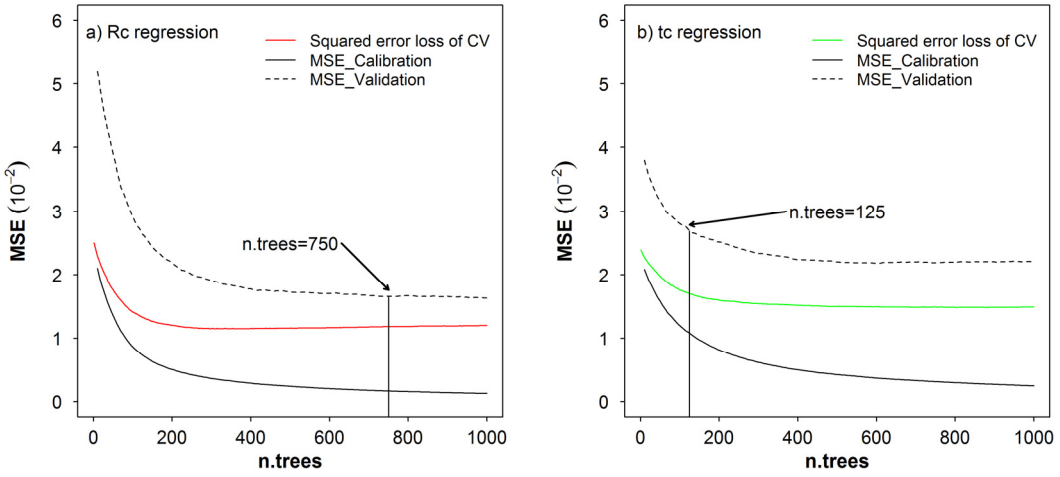

Fig. 6. Sensitivity of the model error, MSE, to *n.trees* in the GBDT regression models for *Rc* and *tc* regressions based on unclassified events (Table 4). Vertical black line indicates *n.trees* chosen: 750 for the *Rc* regression and 125 for the *tc* regression.

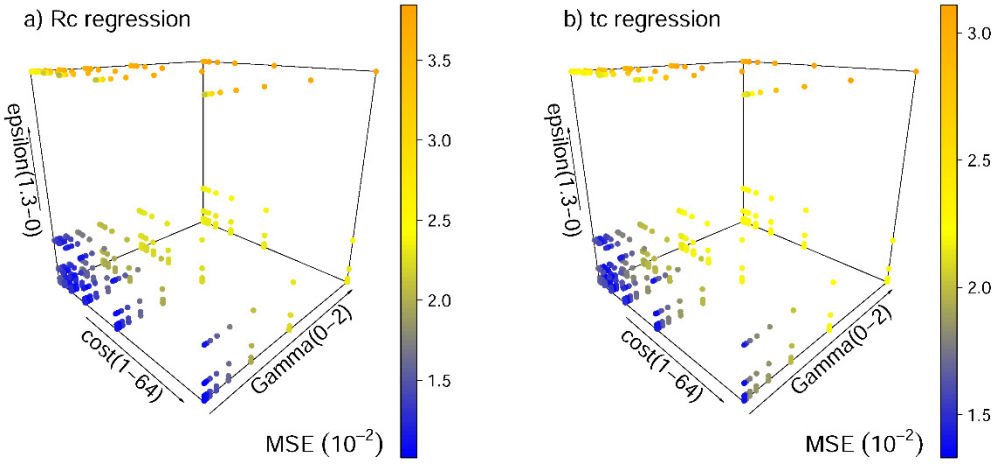

Fig. 7. Sensitivity of the model error, MSE, to different combinations of γ, ε and C for the SVM models based on unclassified events (Table 4). MSE is the squared error loss of 10 fold cross validation.

Table 5. Parameters of *ntree* and m_{try} of the RF models stratified by runoff generation type. The models are fitted for the four runoff generation types (wetland, tile drainage, natural and outlet) termed as Classified regression model, and all together (Unclassified regression model).

Parameters of Random Forest model	*Rc*					*tc*				
	Classified regression model				Unclassified regression model	Classified regression model				Unclassified regression model
	Wetland (A1, A2)	Tile drainage (Frau1, Frau2)	Natural (Sys2, Sys3, Sys4)	Outlet (MW)	All	Wetland (A1, A2)	Tile drainage (Frau1, Frau2)	Natural (Sys2, Sys3, Sys4)	Outlet (MW)	All
Ntree	94	52	28	83	63	86	100	60	58	68
m_{try}	7	22	4	3	7	4	4	2	4	14

GBDT model (n.trees)

There are four main parameters needed for the GBDT model, *shrinkage, n.minobsinnode, interaction.depth* and *n.trees*. Reducing *shrinkage*, the learning rate, improves the performance while increasing the computational cost, so *shrinkage* is set to a low value of 0.001 (Friedman, 2001, 2002). *n.minobsinnode* is the minimum number of observations in a tree's terminal node, and *interaction.depth* represents the number of splits performed on a tree. Model performance is not sensitive to these parameters, so they were set to 10 and 6, respectively, by minimizing the cross validation errors. *n.trees* is the number of iterations, i.e., the number of trees in the GBDT model. Its sensitivity is analysed in Figure 6. The squared error loss of CV is calculated by averaging MSE of $k = 5$ across folders

$$\text{Squared error loss of CV} = \frac{1}{k}\sum_{i=1}^{k}\frac{\sum_{j=1}^{n}\left(y'_{i,j} - y_{i,j}\right)^2}{n} \quad (8)$$

where n is the number of samples in the i th folder (a total of $k = 5$ folders), $y'_{i,j}$ and $y_{i,j}$ are respectively the model prediction and the objective value of sample j in folder i.

The squared error loss of CV in the *Rc* regression is slightly lower than that in the *tc* regression (Figure 6). Increasing *n.trees* provides a greater improvement of performance when *n.trees* is small. The optimum *n.trees* values for the *Rc* and *tc* regressions based on all unclassified events are manually set to *n.trees* = 750 and 125 respectively by minimizing the squared error loss of CV in calibration and by controlling the MSE reduction (e.g. 0.015) between calibration and validation to avoid overfitting. The values of *n.trees* are listed in Table 6.

SVM model (γ, ε and C)

When calibrating the Radial Basis Function (RBF) kernel of the SVM models, three parameters are needed, γ, ε and C. γ is the kernel coefficient of the RBF and reducing γ will increase the performance and reduce the bias, as the number of support vectors increases. ε is a parameter in the insensitive-loss function (Eq. 4). Reducing ε increases the number of support vectors. C is the cost of violating the constraints of the regularization term in the Lagrange formulation. Large C aims at a smaller margin with better prediction but may lead to overfitting.

The squared error loss of 10 fold cross validation (Equation 8 in which k is set to10) and the MSE reduction between calibration and validation is used for optimizing the parameters, thus preventing overfitting. A "grid-search" on γ, ε and C is performed using the R tune.svm function. Various triples of values are tried and the one with the best cross-validation accuracy is selected. The test sequences of the parameters are $\gamma = 2^{(-7:2)}$, $\varepsilon = (0.003, 0.01, 0.03, 0.1, 0.3, 1.3)$ and $C = 2^{(0:6)}$ (Hsu et al., 2003). 3D sensitivity plots of the three parameters are shown in Figure 7. Table 7 gives the optimised parameter value for the classified regression models. There are many good combinations of three parameters resulting in the lowest squared error loss of 10 fold cross validation (Figure 7). The final parameter combinations are chosen by both minimizing the squared error loss of CV in the calibration and controlling the MSE reduction.

Table 6. Parameter of *n.trees* of the GBDT models stratified by runoff generation type. The models are fitted for the four runoff generation types (wetland, tile drainage, natural and outlet) termed as Classified regression model, and all together (Unclassified regression model).

Parameters of GBDT model	*Rc*					*tc*				
	Classified regression model				Unclassified regression model	Classified regression model				Unclassified regression model
	Wetland (A1, A2)	Tile drainage (Frau1, Frau2)	Natural (Sys2, Sys3, Sys4)	Outlet (MW)	All	Wetland (A1, A2)	Tile drainage (Frau1, Frau2)	Natural (Sys2, Sys3, Sys4)	Outlet (MW)	All
n.trees	20	665	180	100	750	20	45	35	80	125
interaction.depth=6 *n.minobsinnode* = 10 *shrinkage* = 0.001 *seed*=537										

Table 7. Parameters of the SVM models stratified by runoff generation type. The models are fitted for the four runoff generation types (wetland, tile drainage, natural and outlet) termed as Classified regression model, and all together (Unclassified regression model).

Parameters of SVM model	*Rc*					*tc*				
	Classified regression model				Unclassified regression model	Classified regression model				Unclassified regression model
	Wetland (A1, A2)	Tile drainage (Frau1, Frau2)	Natural (Sys2, Sys3, Sys4)	Outlet (MW)	All	Wetland (A1, A2)	Tile drainage (Frau1, Frau2)	Natural (Sys2, Sys3, Sys4)	Outlet (MW)	All
γ	2^{-7}	2^{-5}	2^{-7}	2^{-6}	2^{-7}	2^{-6}	2^{-6}	2^{-7}	2^{-5}	2^{-5}
ε	1.3	0.1	0.1	0.03	0.01	1.3	0.1	0.3	0.1	0.03
C	2	2	2^5	2^6	2^6	1	1	1	1	2^3

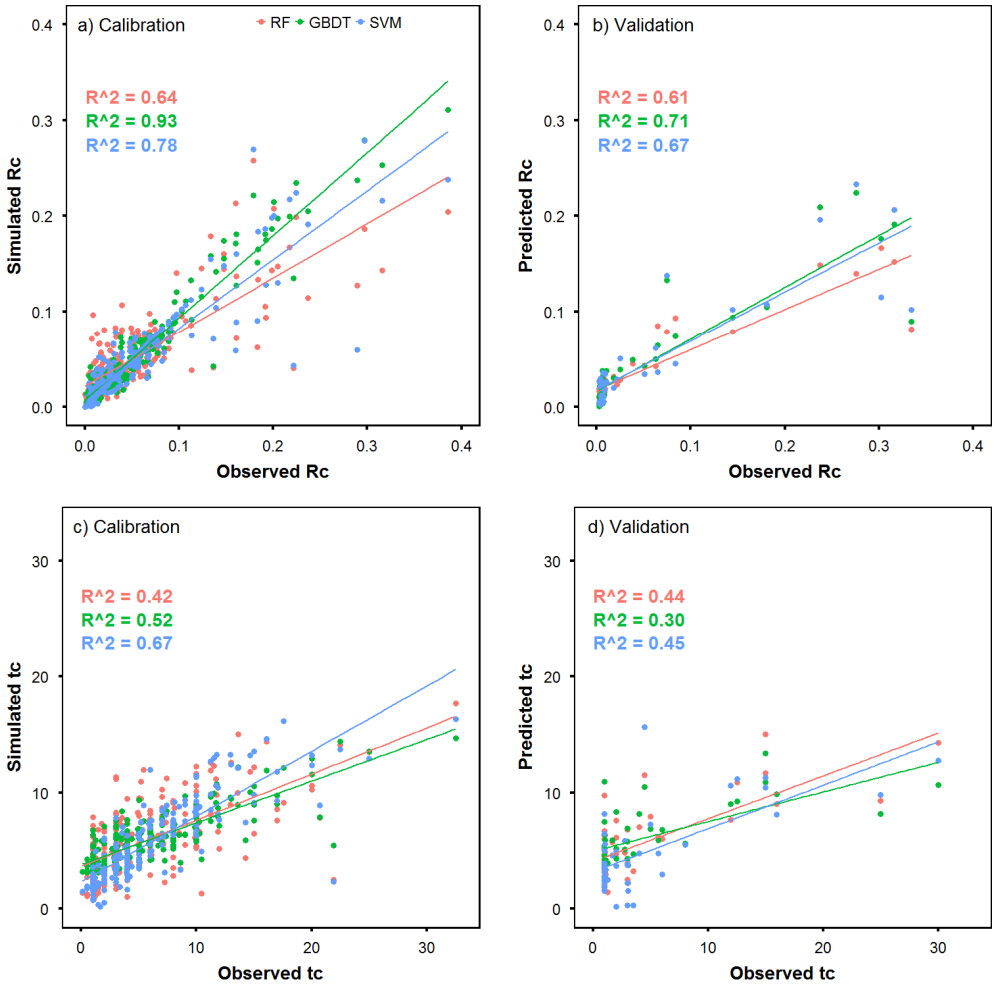

Fig. 8. Estimates of the RF, GBDT and SVM regression models plotted against the observations of *Rc* and *tc*. Estimation is based on unclassified events (252 are used for calibration and 46 for validation). Colours indicate the regression models. Lines represent linear relation between estimation and observation. Panels a) and c): calibration. Panels b) and d): validation.

Temporal calibration and validation performance of the non-linear regression models

Figure 8 shows the estimates of *Rc* and *tc* for the RF, GBDT and SVM models based on unclassified events as in the last column in Table 4. The performances of the *Rc* regressions based on the GBDT and SVM algorithms are better than that of the RF model with R^2 of 0.71 and 0.67 in validation, respectively. The performances of the *tc* regressions based on the RF and SVM algorithms are better than that of the GBDT model with R^2 of 0.44 and 0.45 in validation, respectively.

Figure 9 compares the calibration and validation performance of the regressions (as in Table 4). The performance of the SVM model is generally higher than that of the others, which may be due to the higher dimensional space of the SVM regression (Asefa et al., 2006). The performance of the *tc* regression models is generally low for all methods. This may be due to the lack of subcatchment groundwater data that might improve the performance, particularly for wetlands and natural drainage runoff generation systems which are in HOAL closely related to groundwater level dynamics. On the other hand, the *Rc* and *tc* regressions of the natural drainage subcatchment and the unclassified events have a somewhat higher performance than the other systems, probably because of the larger number of events that are available. The models highlighted by boxes in the left of the figure have higher values of R^2 than 0.6, both in calibration and validation.

Spatial calibration and validation performance of the non-linear regression models

Table 8 lists the number of events used for calibration and validation in a spatial leave one out mode. The classified regressions of *Rc* and *tc* including wetland, tile drainage and natural subsurface flow, are spatially validated. For the wetland regressions, 38 events from station A2 are used for calibration and 30 events from station A1 for validation; for the tile drainage regressions, 30 events from Frau2 are used for calibration and 21 events from Frau1 for validation; for natural subsurface flow, 90 events in Sys3 and Sys4 are used for calibration and 32 events in Sys2 for validation. Additionally, a total of 252 hydrographs during 40 events that are observed in at least 5 stations, are used for building 8 Leave_one_out models in which the events of one of the subcatchments are used for validation and the rest for calibration. The SVM regression models generally have a better performance (measured by R^2) than the other models, which is similar to the temporal validation (Figure 10).

Linear correlations of *Rc* and *tc* with the explanatory variables

Pearson's correlation coefficient *r* of *Rc* and *tc* with the explanatory variables of Table 2 is evaluated for the entire set of 298 events, i.e. for all stream gauges together (Table 9). *Rc* is positively correlated with DurP, VolP, AreaPipes and ground-

Table 8. Number of events used for spatial calibration and validation of the *Rc*/*tc* regressions by runoff generation type. The models are fitted for the four runoff generation types (wetland, tile drainage, natural and outlet) termed as Classified regression model, and all together (Unclassified regression model).

Number of events	Rc/*tc* regression										
	Classified regression model			Unclassified regression model							
	Wet-land	Tile drainage	Natural	Leave_A1 out	Leave_A2 out	Leave_Frau1_ out	Leave_Frau2_ out	Leave_Sys2_ out	Leave_Sys3_ out	Leave_Sys 4_out	Leave_MW out
Calibration	38 (A2)	30 (Frau2)	90 (Sys3, Sys4)	223	216	233	224	223	220	213	212
Validation	30 (A1)	21 (Frau1)	32 (Sys2)	29 (A1)	36 (A2)	19 (Frau1)	28 (Frau2)	29 (Sys2)	32 (Sys3)	39 (Sys4)	40 (MW)
Total	68	51	122	252	252	252	252	252	252	252	252

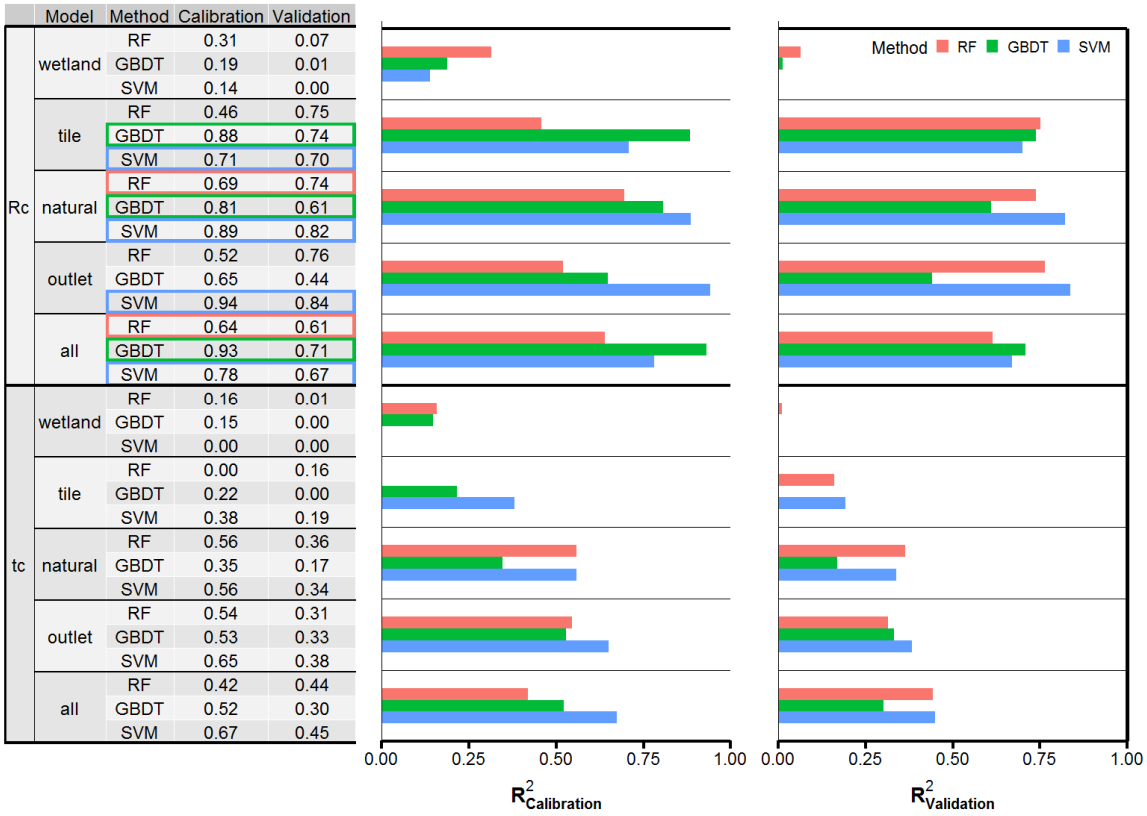

Fig. 9. Comparison of R^2 (coefficients of determination) of temporal calibration and validation between different regression methods (colours) used to estimate *Rc* and *tc* stratified by runoff generation type. Models with $R^2 > 0.6$ both in calibration and validation are highlighted by boxes at the left.

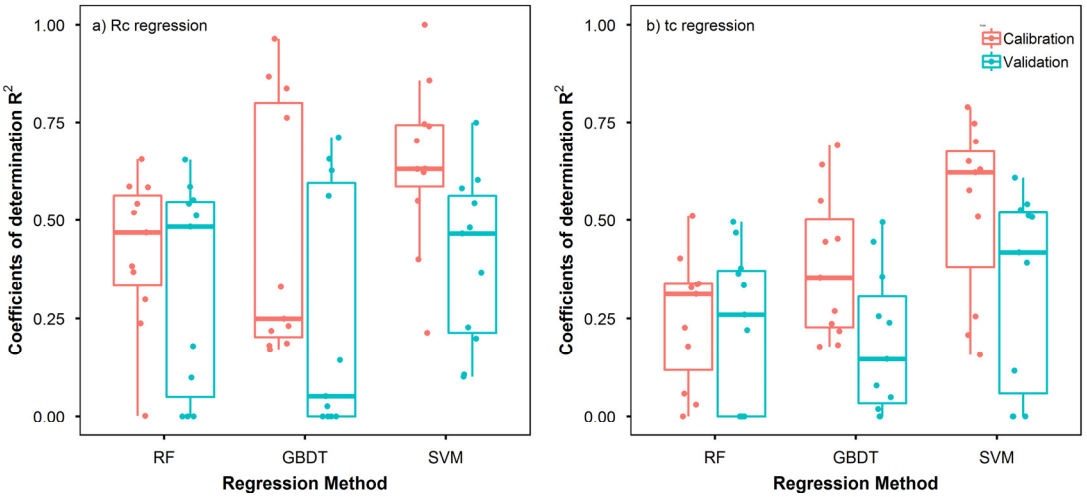

Fig. 10. Performance, R^2 (coefficients of determination), of the *Rc*/*tc* regression methods (RF, GBDT and SVM) with spatial calibration and validation as in Table 8.

Table 9. Correlation coefficient of *Rc* and *tc* with the explanatory variables according to Table 2.

R	VolP	PeakP	DurP	PreSM	PeakSM	PeakPSM	AverSM	EndSM	DelaySM	PreWL	PeakWL
Rc	0.15	–0.29	0.50	–0.04	–0.02	–0.01	–0.01	–0.03	0.02	0.43	0.48
Tc	–0.04	–0.40	0.38	0.30	0.29	0.32	0.31	0.28	–0.01	0.19	0.14
R	PeakPWL	AverWL	EndWL	DelayWL	EP	Month	NDVI	AreaPipes	AreaForest	Area	Type
Rc	0.47	0.47	0.50	0.30	–0.26	–0.32	–0.21	0.28	–0.17	0.08	–0.19
Tc	0.16	0.15	0.14	0.33	–0.33	0.05	–0.22	–0.04	0.05	0.06	–0.002

water related variables (PreWL, PeakWL, PeakPWL, AverWL, EndWL and DelayWL). The highest *r* are obtained for EndWL and DurP ($r = 0.5$), suggesting that groundwater and precipitation are the two factors that are most strongly connected to *Rc*. It is also interesting that the rainfall duration (DurP) affects *r* more strongly than event precipitation volume (VolP). It seems that higher groundwater levels lead to more direct flow generated during an event. The groundwater level data reflect the catchment storage conditions, particularly those close to the stream, as most piezometers are close to the stream. The peak rainfall intensity (PeakP) is negatively correlated with *Rc* (but DurP positively), suggesting that saturation excess runoff tends to be more important than infiltration excess runoff.

A clearly positive effect on *tc* can be found of the variables DurP, DelayWL and the soil moisture related variables (PreSM, PeakSM, PeakPSM, AverSM and EndSM). The largest absolute *r* occurs for the precipitation variables (PeakP and DurP). Longer DurP and lower PeakP generally result in slower recessions. Higher rainfall intensities lead to higher peak flows and thinner shapes of the hydrographs with faster recessions. The influence of soil moisture and groundwater on *tc* is somewhat lower than that of precipitation. In summer, higher precipitation intensity together with low soil moisture and groundwater levels generally come out with quick streamflow recessions with low *tc*, while in winter lower precipitation intensity and wetter conditions usually with higher *tc*.

Importance of explanatory variables for *Rc* and *tc* in the non-linear regression models

The importance of the explanatory variables for estimating *Rc* and *tc* from the non-linear regression models was evaluated on the basis of $I_{i,SVM}$ (section „Ensemble learning techniques for regression“). The heatmap (Figure 11) shows the relative importance of the explanatory variables, where each column represents one model and the colour indicates the importance of the explanatory variables. The temporal non-linear regression models are used for this analysis because of the larger database (Table 4).

For evaluating the effects of multicolinearity to variable importance of regression model, the variance inflation factor (VIF) has been calculated for each variable. VIF of most variables are smaller than 5 apart from soil moisture (PreSM, EndSM, AverSM, PeakSM and PeakPSM) and groundwater

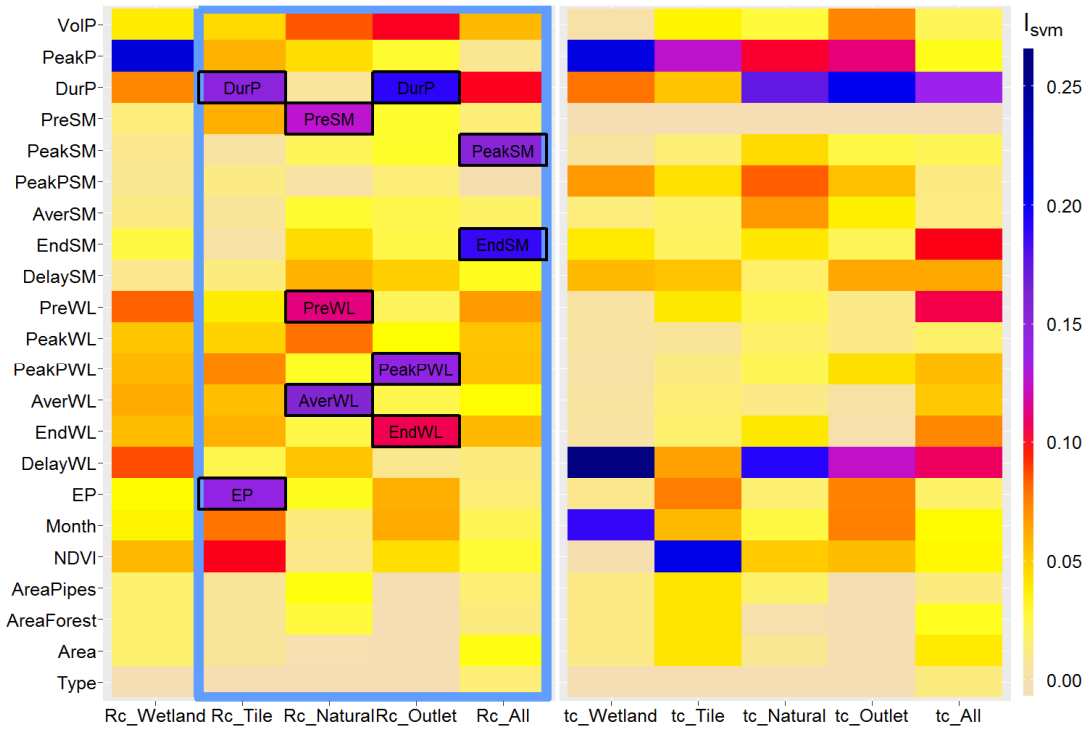

Fig. 11. Heatmap of the variable importance $I_{i,SVM}$ for the classified and unclassified models using the SVM regression method. The Y-axis represents 22 variables, the X-axis the models based on different subcatchment types. Left: *Rc*. Right: *tc*. Models with $R^2 > 0.6$ both in calibration and validation (Fig. 9) are highlighted by a blue box, and the variables with the best $I_{i,SVM}$ performance are highlighted by black rectangles. Database as in Table 4.

related variables (PreWL, EndWL, AverWL, PeakWL and PeakPWL). Therefore the difference from five soil moisture/groundwater variables is difficult to be explained from $I_{i,SVM}$. Figure 11 suggests that both antecedent soil moisture (PreSM) and groundwater related variables (PreWL and AverWL) have a relative high importance for the *Rc* regression of natural subsurface flow. This is in line with Tarasova (2018ab) who found that catchment storage plays a considerable role in the prediction of event runoff response. In the wetland drainage area soil moisture is always high, in the tile drainage area soil moisture varies moderately, and in the natural drainage area the seasonal variability of soil moisture is largest, which is reflected in a larger effect on *Rc*. Precipitation duration (DurP) always shows a large influence on *Rc* in the tile drainage system and at the catchment outlet. Potential evaporation (EP) is another important variable for the *Rc* regression in the tile drainage systems. This suggests that *Rc* in the tile drainage systems is more affected by the weather conditions than the subsurface dynamics. Groundwater related variables are more important in the natural system and for the entire catchment. For the unclassified data set, two soil moisture related variables (PeakSM and EndSM) generally play an important role, which means that soil moisture is a good indicator of catchment storage affecting drainage condition during the events.

The performance of the *tc* regressions is not as good as that of the *Rc* regressions ($R^2 < 0.5$ in validation mode). The precipitation variables (DurP and PeakP) and groundwater peak delay to precipitation (DelayWL) are more important than other variables. Exner-Kittridge et al. (2016) has suggested that most of the HOAL baseflow stems from groundwater, so the time when groundwater starts to contribute to the recession compared to the precipitation peak (DelayWL) may have a controlling function on the discharge recession rate.

DISCUSSION AND CONCLUSIONS

This study addresses two main research questions. The first is the relative performance of three machine learning methods in estimating event runoff coefficients, *Rc*, and recession coefficients, *tc*. We use 22 event based explanatory variables in these methods representing precipitation, soil moisture, groundwater level and season. The regressions are performed for four, classified subcatchment groups (wetland, tile drainage, natural, outlet runoff) and for unclassified regressions using all event hydrographs from all subcatchments. Model performances, measured by the coefficient of determination R^2, shows that the SVM algorithm generally gives more accurate *Rc* and *tc* predictions than the other two methods (RF and GBDT). This is due to the fact that the SVM algorithm can transform the 22 dimensional variables to a higher dimensional space and it generally performs better for small sample sizes. The *Rc* regressions using SVM for tile drainage, natural, outlet and unclassified events show good performances with R^2 greater than 0.6, but the regression for the wetlands perform less well. The latter is presumably related to the lack of infiltration information in the wetland areas. The best *tc* estimates are obtained by the SVM model for unclassified events with $R^2 = 0.45$ in calibration mode. Overall, the *tc* regressions perform less well than those of *Rc* which is likely related to the more complex nature of subsurface and surface routing as compared to runoff generation. New geophysical observations about the structure and connectivity of different groundwater storages and understanding of the connections between shallow and deep aquifers will allow to improve model performance in the future.

The second research question relates to the most relevant variables for the *Rc* and *tc* regression based on the models described above by different categories of runoff systems. The relative importance of the variables of the SVM model is assessed by a heatmap. It suggests that precipitation duration plays an important role in predicting *Rc* for the tile drainage and outlet systems. This is in line with Merz et al. (2006) who concluded that the spatial patterns of median event runoff coefficients are highly correlated with the spatial patterns of mean annual precipitation in this climatic region. Antecedent soil moisture only affects *Rc* for the natural system, but not for the tile drainage and wetland systems. Potential evapotranspiration (EP) is an important factor in the tile drainage systems. It can therefore be concluded that event based *Rc* of the tile drainage systems is more controlled by weather conditions than by the catchment state, while the opposite is true of the natural drainage systems. This behaviour of the natural drainage systems of the HOAL is similar to the results of Tarasova et al. (2018a; 2018b), who found that the response of lowland catchments with substantial storage is driven by pre-event saturation instead of rainfall properties.

Overall, the paper shows that both the performance of estimating *Rc* and *tc* and the relative importance of explanatory variables depends strongly on the types of the hydrological systems, i.e. the runoff generation mechanism. The paper proposes three machine learning techniques as tools for predicting event based *Rc* and *tc* on the basis of weather and land surface characteristics.

Acknowledgements. We thank Matthias and Markus Oismüller for organizing the measurements and managing the data in the Hydrological Open Air Laboratory of Petzenkirchen. Data of soil moisture, groundwater level and weather have been processed by Mariette Vreugdenhil, Lovrenc Pavlin and Patrick Hogan. We acknowledge financial support from the Natural Science Foundation, China, and the Austrian Science Funds (FWF) as part of the Vienna Doctoral Programme on Water Resource Systems (DK W1219-N28).

REFERENCES

Asefa, T., Kemblowski, M., McKee, M., Khalil, A., 2006. Multi-time scale stream flow predictions: the support vector machines approach. Journal of Hydrology, 318, 1–4, 7–16.

Basak, D., Pal, S., Patranabis, D.C., 2007. Support vector regression. Neural Information Processing-Letters and Reviews, 11, 10, 203–224.

Baudron, P., Alonso-Sarría, F., García-Aróstegui, J.L., Canovas-Garcia, F., Martinez-Vicente, D., Moreno-Brotons, J., 2013. Identifying the origin of groundwater samples in a multi-layer aquifer system with Random Forest classification. Journal of Hydrology, 499, 303–315.

Ben-Hur, A., Weston, J., 2010. A user's guide to support vector machines. In: Carugo, O., Eisenhaber, F. (Eds.): Data Mining Techniques for the Life Sciences. Methods in Molecular Biology (Methods and Protocols), Vol 609. Humana Press, 2010, pp. 223–239.

Biswal, B., Kumar, D.N., 2014. What mainly controls recession flows in river basins? Advances in water resources, 65, 25–33.

Blöschl, G., Blaschke, A.P., Broer, M., Bucher, C., Carr, G., Chen, X., Eder, A., Exner-Kittridge, M., Farnleitner, A., Flores-Orozco, A., Haas, P., Hogan, P., Kazemi Amiri, A., Oismüller, M., Parajka, J., Silasari, R., Stadler, P., Strauss, P., Vreugdenhil, M., Wagner, W., Zessner, M., 2016. The

Hydrological Open Air laboratory (HOAL) in Petzenkirchen: a hypothesis-driven observatory. Hydrology and Earth System Sciences, 20, 1, 227.

Blöschl, G., Sivapalan, M., Wagener, T., Viglione, A., Savenije, H., 2013. Runoff Prediction in Ungauged Basins: Synthesis across Processes, Places and Scales. Cambridge University Press, Cambridge.

Blume, T., Zehe, E., Bronstert, A., 2007. Rainfall–runoff response, event-based runoff coefficients and hydrograph separation. Hydrological Sciences Journal, 52, 5, 843–862.

Breiman, L., 2001. Random forests. Machine Learning, 45, 1, 5–32.

Brutsaert, W., Nieber, J.L., 1977. Regionalized drought flow hydrographs from a mature glaciated plateau. Water Resources Research, 13, 3, 637–643.

Cánovas-García, F., Alonso-Sarría, F., Gomariz-Castillo, F., Onate-Valdivieso, F., 2017. Modification of the random forest algorithm to avoid statistical dependence problems when classifying remote sensing imagery. Computers & Geosciences, 103, 1–11.

Chapelle, O., Vapnik, V., 2000. Model selection for support vector machines. In: NIPS'99 Proceedings of the 12th International Conference on Neural Information Processing Systems, Denver, CO, November 29 - December 4, 1999, pp. 230–236.

Chapman, T.G., Maxwell, A.I., 1996. Baseflow separation-comparison of numerical methods with tracer experiments. In: Hydrology and Water Resources 23rd Symposium, Hobart, 1996. National Conference Publication – Institution of Engineers Australia NCP, 2(5), pp. 539–546.

Chen, B., Krajewski, W.F., Helmers, M.J., Zhang, Z., 2019. Spatial variability and temporal persistence of event runoff coefficients for cropland hillslopes. Water Resources Research, 55, 2, 1583–1597.

Cortes, C., Vapnik, V., 1995. Support-vector networks. Machine Learning, 20, 3, 273–297.

Cortez, P., Embrechts, M.J., 2013. Using sensitivity analysis and visualization techniques to open black box data mining models. Information Sciences, 225, 1–17.

Deka, P.C., 2014. Support vector machine applications in the field of hydrology: a review. Applied Soft Computing, 19, 372–386.

Dietterich, T.G., 1997. Machine-learning research. AI Magazine, 18, 4, 97–97.

Erdal, H.I., Karakurt, O., 2013. Advancing monthly streamflow prediction accuracy of CART models using ensemble learning paradigms. Journal of Hydrology, 477, 119–128.

Exner-Kittridge, M., Strauss, P., Blöschl, G., Eder, A., Saracevic, E., Zessner, M., 2016. The seasonal dynamics of the stream sources and input flow paths of water and nitrogen of an Austrian headwater agricultural catchment. Science of the Total Environment, 542, 935–945.

Friedman, J.H., 2001. Greedy function approximation: a gradient boosting machine. Annals of Statistics, 45, 1, 1189–1232.

Friedman, J.H., 2002. Stochastic gradient boosting. Computational Statistics & Data Analysis, 38, 4, 367–378.

Gaál, L., Szolgay, J., Kohnová, S., Parajka, J., Merz, R., Viglione, A., Blöschl, G., 2012. Flood timescales: Understanding the interplay of climate and catchment processes through comparative hydrology. Water Resources Research, 48, W04511.

Gottschalk, L., Weingartner, R., 1998. Distribution of peak flow derived from a distribution of rainfall volume and runoff coefficient, and a unit hydrograph. Journal of Hydrology, 208, 3–4, 148–162.

Hayes, D.C., Young, R.L., 2006. Comparison of peak discharge and runoff characteristic estimates from the rational method to field observations for small basins in Central Virginia. U.S. Department of the Interior, U.S. Geological Survey, Scientific Investigation Reports, 2005-5254.

Ho, T.K., 1995. Random decision forests. In: ICDAR '95 Proceedings of the Third International Conference on Document Analysis and Recognition, 1, IEEE Computer Society Washington, DC, USA, 14–15 August 1995, pp. 278–282.

Horn, R.A., Johnson, C.R., 1985. Matrix Analysis. Cambridge University Press, Cambridge.

Hsu, C.W., Chang, C.C., Lin, C.J., 2003. A practical guide to support vector classification. Technical Report. Department of Computer Science, National Taiwan University, Taipei.

Hwang, S.H., Ham, D.H., Kim, J.H., 2012. Forecasting performance of LS-SVM for nonlinear hydrological time series. KSCE Journal of Civil Engineering, 16, 5, 870–882.

Krakauer, N.Y., Temimi, M., 2011. Stream recession curves and storage variability in small watersheds. Hydrology and Earth System Sciences, 15, 7, 2377–2389.

Liaw, A., Wiener, M., 2002. Classification and regression by random Forest. R News, 2, 3, 18–22.

Longobardi, A., Villani, P., Grayson, R.B., Western, A., 2003. On the relationship between runoff coefficient and catchment initial conditions. In: Proceedings of MODSIM, pp. 867–872.

Maity, R., Bhagwat, P.P., Bhatnagar, A., 2010. Potential of support vector regression for prediction of monthly streamflow using endogenous property. Hydrological Processes, 24, 7, 917–923.

Merz, R., Blöschl, G., 2009. A regional analysis of event runoff coefficients with respect to climate and catchment characteristics in Austria. Water Resources Research, 45, 1, W01405.

Merz, R., Blöschl, G., Parajka, J., 2006. Spatio-temporal variability of event runoff coefficients. Journal of Hydrology, 331, 3–4, 591–604.

Naghibi, S.A., Ahmadi, K., Daneshi, A., 2017. Application of support vector machine, random forest, and genetic algorithm optimized random forest models in groundwater potential mapping. Water Resources Management, 31, 9, 2761–2775.

Naghibi, S.A., Pourghasemi, H.R., Dixon, B., 2016. GIS-based groundwater potential mapping using boosted regression tree, classification and regression tree, and random forest machine learning models in Iran. Environmental Monitoring and Assessment, 188, 1, 44.

Norbiato, D., Borga, M., Merz, R., Blöschl, G., Carton, A., 2009. Controls on event runoff coefficients in the eastern Italian Alps. Journal of Hydrology, 375, 3–4, 312–325.

Osuna, E.E., 1998. Support vector machines: Training and applications. Diss. Massachusetts Institute of Technology.

Palleiro, L., Rodríguez-Blanco, M.L., Taboada-Castro, M.M., Taboada-Castro, M.T., 2014. Hydrological response of a humid agroforestry catchment at different time scales. Hydrological Processes, 28, 4, 1677–1688.

Patnaik, S., Biswal, B., Kumar, D.N., Sivakumar, B., 2015. Effect of catchment characteristics on the relationship between past discharge and the power law recession coefficient. Journal of Hydrology, 528, 321–328.

Rodríguez-Blanco, M.L., Taboada-Castro, M.M., Taboada-Castro, M.T., 2012. Rainfall–runoff response and event-based runoff coefficients in a humid area (northwest Spain). Hydrological Sciences Journal, 57, 3, 445–459.

Sachdeva, S., Bhatia, T., Verma, A.K., 2018. GIS-based evolutionary optimized Gradient Boosted Decision Trees for for-

est fire susceptibility mapping. Natural Hazards: Journal of the International Society for the Prevention and Mitigation of Natural Hazards, Springer. International Society for the Prevention and Mitigation of Natural Hazards, 92, 3, 1399–1418.

Şen, Z., Altunkaynak, A., 2006. A comparative fuzzy logic approach to runoff coefficient and runoff estimation. Hydrological Processes, 20, 9, 1993–2009.

Shen, C., 2018. A transdisciplinary review of deep learning research and its relevance for water resources scientists. Water Resources Research, 54, 8558–8593. https://doi.org/10.1029/2018WR022643

Sivapalan, M., 2003. Prediction in ungauged basins: a grand challenge for theoretical hydrology. Hydrological Processes, 17, 15, 3163–3170.

Széles, B., Broer, M., Parajka, J., Hogan, P., Eder, A., Strauss, P., Blöschl, G., 2018. Separation of scales in transpiration effects on low flows: A spatial analysis in the Hydrological Open Air Laboratory. Water Resources Research, 54, https://doi.org/10.1029/2017WR022037.

Tachecí, P., Žlabek, P., Kvitek, T., Peterkova, J., 2013. Analysis of rainfall-runoff events in four subcatchments of the Kopaninský potok (Czech Republic). Bodenkultur, 64, 3–4, 105–111.

Tague, C., Grant, G.E., 2004. A geological framework for interpreting the low-flow regimes of Cascade streams, Willamette River Basin, Oregon. Water Resources Research, 40, 4, W04303.

Tallaksen, L.M., 1995. A review of baseflow recession analysis. Journal of Hydrology, 165, 1–4, 349–370.

Tarasova, L., Basso, S., Poncelet, C., Merz, R., 2018a. Exploring controls on rainfall-runoff events: 2. Regional patterns and spatial controls of event characteristics in Germany. Water Resources Research, 54, https://doi.org/10.1029/2018WR022588

Tarasova, L., Basso, S., Zink, M., Merz, R. 2018b. Exploring controls on rainfall-runoff events: 1. Time-series-based event separation and temporal dynamics of event runoff response in Germany. Water Resources Research, 54, https://doi.org/10.1029/2018WR022587

Tian, F., Li, H., Sivapalan, M., 2012. Model diagnostic analysis of seasonal switching of runoff generation mechanisms in the Blue River basin, Oklahoma. Journal of Hydrology, 418, 136–149.

Vapnik, V., Golowich, S., Smola, A., 1997. Support vector method for function approximation, regression estimation, and signal processing. In: NIPS'96 Proceedings of the 9th International Conference on Neural Information Processing Systems, Denver, Colorado, 3–5 December 1996, pp. 281–287.

Viglione, A., Merz, R., Blöschl, G., 2009. On the role of the runoff coefficient in the mapping of rainfall to flood return periods. Hydrology and Earth System Sciences, 13, 5, 577–593.

Wainwright, J., Parsons, A.J., 2002. The effect of temporal variations in rainfall on scale dependency in runoff coefficients. Water Resources Research, 38, 12, 1271.

Zimmermann, B., Zimmermann, A., Turner, B.L., Francke, T., Elsenbeer, H., 2014. Connectivity of overland flow by drainage network expansion in a rain forest catchment. Water Resources Research, 50, 2, 1457–1473.

Received 9 May 2019
Accepted 30 January 2020

J. Hydrol. Hydromech., 68, 2020, 2, 170–179
DOI: 10.2478/johh-2020-0004
ISSN 1338-4333

sciendo Journal of Hydrology and Hydromechanics

The L-moment based regional approach to curve numbers for Slovak and Polish Carpathian catchments

Silvia Kohnová[1*], Agnieszka Rutkowska[2], Kazimierz Banasik[3], Kamila Hlavčová[1]

[1] Slovak University of Technology, Faculty of Civil Engineering, Department of Land and Water Resources Management, Radlinskeho 11, 81368 Bratislava, Slovak Republic.
[2] Department of Applied Mathematics, University of Agriculture, Balicka 253C, Cracow, Poland.
[3] Department of Water Engineering and Environment Restoration Faculty of Civil and Environmental Engineering, Warsaw University of Life Sciences-SGGW, Nowoursynowska 166, Warsaw, Poland.
[*] Corresponding author. E-mail: silvia.kohnova@stuba.sk

Abstract: The main objective of the paper was to propose and evaluate the performance of a regional approach to estimate *CN* values and to test the impact of different initial abstraction ratios. The curve number (*CN*) was analyzed for five Slovak and five Polish catchments situated in the Carpathian Mountains. The L-moment based method of Hosking and Wallis and the ANOVA test were combined to delineate the area in two homogenous regions of catchments with similar *CN* values. The optimization condition enabled the choice of the initial abstraction ratio, which provided the smallest discrepancy between the tabulated and estimated *CN*s and the antecedent runoff conditions. The homogeneity in the *CN* within the regions of four Slovak and four Polish catchments was revealed. Finally, the regional *CN* was proposed to be at the 50% quantile of the regional theoretical distribution function estimated from all the *CN*s in the region.

The approach is applied in a group of Slovak and Polish catchments with physiographic conditions representative for the Carpathian region. The main benefit of introducing a common regional *CN* is the opportunity to apply this procedure in catchments of similar soil-physiographic characteristics and to verify the existing tabulated *CN*. The paper could give rise to an alternative way of estimating the *CN* values in forested catchments and catchments with a lack of data or without observations.

Keywords: Catchment curve number; Homogeneity; Regional frequency analysis.

INTRODUCTION

The SCS-CN method is a rainfall-runoff model developed for the United States by the USDA Soil Conservation Service (SCS) (now the Natural Resources Conservation Service (NRCS)) in 1956. In this method the relationship between a watershed´s characteristics and antecedent rainfall is represented by the Curve Number parameter. With this simple parameter, the depth of a rainfall is transformed to the depth of direct runoff. The tables and figures for estimating the *CN* parameter for soil cover groups of the USA are given, e.g., in the publications of NRCS (USDA, 2004). Despite the fact that the *CN* method was developed based on the empirical data of the USA, the method is used in many countries all over the world. The *CN* method is said to be the most often used model for rainfall-runoff (Ajmal et al., 2015), and the main reasons for its use are i) the efficiency of the calculation; ii) the land cover and land use, soil class, and management practices data are easily obtainable; and iii) it generates suitable runoff estimates for agricultural and urban catchments (Yuan et al., 2014). Furthermore, this model provides three important values: (1) it calculates the return period of direct runoff from the same return period of the rainfall depth; (2) it explains the rainfall-runoff for individual events; and (3) it infers the infiltration processes and soil moisture-*CN* relations.

Originally, the *CN* was assumed to be a function of the physiographic-soil properties that are constant in each catchment or in a part of it. This tabulated value is determined using the Hydrologic Soil Groups (USDA, 2004). Soils are placed into groups A, B, C and D, with A being the least runoff-prone and D the most runoff-prone in this system. In practice, however, the parameter changes as a result of variable air conditions, the soil, and storm or catchments morphology. Therefore, some improvements in the method have been introduced according to the seasonal and spatial variability (Geetha et al., 2007; Soulis and Valiantzas, 2012) and sediment yield (Mishra et al., 2006). A great deal of work on the *CN* was conducted by Hawkins (e.g., 1973, 1979) and Hawkins et al. (1985). Hawkins proposed the antecedent moisture conditions (AMC), later converted to antecedent runoff conditions (ARC), introduced an asymptotic approach (Hawkins, 1993), and developed the *CN* infiltration rate equation. Currently, the antecedent runoff conditions (ARC I, ARC III) are recommended (Hawkins et al., 2009) in cases of wet or dry conditions in a catchment, through the formulas of Hawkins or the method of Hjelmfelt (1983). At present, the model is a part of several water management systems, i.e., GLEAMS (Leonard, 1987), SWAT (Arnold et al., 1995), and AnnAGNPS (Bingner and Theurer, 2005). Various modifications of the SCS-CN method are also used (e.g., Sahu et al., 2010; Wałęga et al., 2017).

The original initial abstraction ratio λ equal to 0.20 in the SCS-CN method has also been questioned by many authors. New methods and availability of data with longer observation periods have led to a review of the original value because the mean value of λ is approximate and can have a negative effect on the accuracy of the computed runoff. Mockus (1972) concluded that the coefficient λ varied in the interval $\lambda_{min} = 0.013$, $\lambda_{max} = 2.1$. Cazier and Hawkins (1984) analyzed the data of 109 small catchments and determined that the most common value for the parameter λ was 0, Baltas et al. (2007) analyzed the

relationship $\lambda = \frac{I_a}{S}$ in a catchment in Greece; the average coefficient λ was 0.014, and the design value was determined to be 0.037. Hawkins and Khojeini (2000) analyzed data for 97 small catchments, and the coefficient λ ranged from 0 to 0.0966. Jiang (2001) used two methods to evaluate the coefficient λ which corresponded to empirical data from 307 river basins and proposed λ = 0.05. Lower values, e.g., 0.15, 0.10 or 0.05, are recommended by the American Society of Civil Engineers (Hawkins et al., 2009). Also, studies of Slovak forested catchments revealed that estimated coefficients of λ were below 0.2 (Karabová and Marková, 2013). Among the other authors who observed uncertainties and re-evaluated the λ values and proposed their modification, we can mention, e.g., Elhakeem and Papanicolaou (2009), Shi et al. (2009), Woodward et al. (2003); Yuan et al. (2014) and Durán-Barroso et al. (2017).

Statistical studies have also been undertaken because of the variability of the *CN*. Bondelid et al. (1982) investigated the sensitivity of the SCS-CN model, Banasik and Ignar (1983) and Banasik and Woodward (2010) performed a comprehensive analysis of the empirical *CN*; Hjelmfelt (1983, 1991) introduced a probabilistic approach based on the assumption that *CN* is a random variable and proposed error bands as ARC. McCuen (2002) considered the confidence intervals of the 100-*CN*. The other authors who considered the variability of the CN are Tedela et al. (2008), Hitchcock et al. (2013), Banasik et al. (2014, 1997) and Rutkowska et al. (2015).

The proper calibration of the CN and λ is crucial for a correct assessment of direct runoff volumes for the design of flood control devices such as dams, reservoirs, floodwalls, levees, and channels. Statistical methods can often be helpful in the calibration process of rainfall-runoff data, but they often face the problem of small samples. Therefore, to reduce the uncertainty of the quantile estimates, regional methods are an alternative when several small samples are put together in a large homogeneous sample.

The main objective of the paper was to propose and evaluate the performance of a regional approach to estimate *CN* values and to test the impact of different initial abstraction ratios on 0.20, 0.15, and 0.10. The approach is applied in a group of Slovak and Polish catchments with physiographic conditions representative for the Carpathian region, so the results can be compared to existing tabulated *CN* values and applied to similar ungauged catchments in the region.

METHODS

The SCS-CN method delineates the relationships among the Curve Number [–], the maximum soil potential retention *S* [mm], the rainfall depth *P* [mm], the direct runoff depth *H* [mm], and the initial abstraction ratio λ, namely

$$H = \frac{(P-\lambda S)^2}{P+(1-\lambda)S} \quad \text{for} \quad P > \lambda S \quad \text{and} \quad H = 0 \quad \text{otherwise;} \quad (1)$$

$$CN = \frac{25400}{S+254}. \quad (2)$$

Empirical CNs

The sample *CN* values were computed using Eq. (1) and (2) from rainfall depth *P* and direct runoff *H* values, registered during independent rainfall-runoff events. Three abstraction ratios λ were considered, namely $\lambda = 0.20, \lambda = 0.15, \lambda = 0.10$. The empirical values of *S* were calculated first using solutions of Eq. (1) for various λ values:

$$S = \begin{cases} 5\left(P + 2H - \sqrt{4H^2 + 5PH}\right) & \text{if } \lambda = 0.20 \\ \frac{10}{9}\left(6P + 17H - \sqrt{289H^2 + 240PH}\right) & \text{if } \lambda = 0.15 \\ 5\left(2P + 9H - \sqrt{81H^2 + 40PH}\right) & \text{if } \lambda = 0.10 \end{cases} \quad (3)$$

The empirical *CN*s were calculated next from Eq. (2). Finally, three samples of *CN*s were obtained for every catchment.

The Hosking and Wallis method

The basic equation of the Hosking and Wallis (1997) (HW) method calculates the relationship between $CN_i(F)$, the at-site quantile of order *F*, where $0 < F < 1$, the mean value μ_i, and the regional, dimensionless quantile $q(F)$,

$$CN_i(F) = \mu_i q(F) \quad \text{for } i = 1,\ldots,N, \quad (4)$$

where *i* is the catchment number, and *N* is the number of elements in a homogeneous region (pooling group). Homogeneity in the distribution function of all catchments in a region is represented by the quantile *q* (growth factor), common for all the catchments. Eq. (4) was proposed by Dalrymple (1960) and is known as the "index flood equation".

The regions were delineated using Eq. (3). The homogeneity in the growth factor was tested using the L-moments based method of Hosking and Wallis and the similarity in μ using a variance analysis (a one-way ANOVA). The choice of the optimal λ was conducted according to the mean absolute relative error.

In this paper, the initial delineation of the group of catchments was based on the comparison of the values of *CN*. Afterwards, the Hosking and Wallis method was used to verify the regions.

Comparison of the values of CN

The ANOVA test (Scheffé 1959) allows the comparison between mean values. The analysis was carried out for every λ. The two assumptions of the test, namely normality and equality of variances, were tested first using the Shapiro-Wilk test (Shapiro and Wilk, 1965) and the Levene's test (Levene et al., 1960), respectively. The Levene's test is known to be powerful (Gastwirth et al., 2009) and robust for small violations from normality. If the null hypothesis was rejected then the Scheffe's post-hoc test (Scheffé, 1959) was used to identify the pairs of catchments with different mean values and to establish groups of catchments with similar CN. If the strong assumptions of the ANOVA are not perfectly fulfilled, the non-parametric Kruskal-Wallis test (Kruskal and Wallis, 1952) can be used to verify the groups. The two methods were used in this paper.

L-moments

In the present paper a regionalization based on L-moments was used for estimating the CN. The research made use of the methodology of Hosking and Wallis (1997), which has been

successfully applied for regional flood frequency analysis (RFFA). Its effectiveness in flood frequency analysis has resulted in its broad applicability around the world (e.g., Adamowski, 2000; Burn and Goel, 2000; Kohnová et al., 2006; Yang et al., 2010; Kochanek et al., 2012; Rutkowska et al., 2010; to name but a few). In this method, a homogeneous region (pooling group) is interpreted as a group of catchments for which the quantile functions of design flood discharges are identical, apart from site-specific scaling factor, the index flood. Using the L-moments method, the regional frequency distribution is estimated and the theoretical at-site quantiles are derived. The method of L-moments yields more accurate and efficient parameter estimates than the maximum likelihood method when the sample sizes are small to moderate (Ulrych et al., 2000; Wang, 1996). In the literature, the Hosking and Wallis methodology was applied by Mishra et al. (2009) to delineate the territory of Nepal into homogenous regions. Jeon et al. (2014) found regionalized CN parameter to apply in L-THIA model using methods like soil group area weighted average, spatial nearest neighbour, inverse distance weighted average, global calibration and others.

The L-moment of order r is a linear combination of the expected values of the order statistics $X_{r:n}$, $1 \le r \le n$ (Hosking and Wallis, 1997; Węglarczyk, 2010),

$$L_r = r^{-1} \sum_{k=0}^{r-1} (-1)^k \binom{r-1}{k} E(X_{r-k:r}). \tag{5}$$

Usually, the dimensionless coefficient of L-variation LCV, k and the L-moment ratios τ_r are used for $r \ge 3$, namely

$$LCV = \frac{L_2}{L_1}, \qquad \tau_r = \frac{L_r}{L_2}. \tag{6}$$

Specifically, τ_3, τ_4 are the L-skewness and L-kurtosis, respectively.

The estimators of the L-moments are the sample L-moments, l_r. In an analogous way, they are linear combinations of the sample order statistics $x_{1:n} \le x_{2:n} \le \ldots \le x_{n:n}$,

$$l_1 = b_0, \qquad l_2 = 2b_0 - b_1, \qquad l_3 = 6b_2 - 6b_1 + b_0, \qquad l_4 = 20b_3 - 30b_2 + 12b_1 - b_0, \tag{7}$$

where

$$b_r = \frac{1}{n} \sum_{j=r+1}^{n} \frac{(j-1)(j-2)\ldots(j-r)}{(n-1)(n-2)\ldots(n-r)} x_{j:n}. \tag{8}$$

The sample LCV, L-skewness and L-kurtosis are given by $t = \frac{l_2}{l_1}$, $t_3 = \frac{l_3}{l_2}$, $t_4 = \frac{l_4}{l_2}$, respectively. Note that l_1 is the sample mean value. The sample L-moments are asymptotically unbiased and robust to outliers.

Homogeneity in the distribution function

The tests (Hosking and Wallis, 1997) are based on simulations of equivalent pooling groups. The HW heterogeneity measures are

$$H_j = \frac{V_j - \mu_{V_j}}{\sigma_{V_j}}, \; j = 1,2,3, \tag{9}$$

where V_j are the weighted standard deviations of t (for $j=1$), t_3 (for $j=2$) and t_4 (for $j=3$) of the rescaled data $CN / \overline{CN}$, where μ_{V_j}, σ_{V_j} are the means and standard deviations of $V-$ the statistics derived from the simulated data. The numbers $j = 1,2,3$ represent the tests for heterogeneity in the LCV, L-skewness and L-kurtosis, respectively.

If $H_j < 1$, then the pooling group is considered to be homogeneous; if $1 \le H_j < 2$, then possibly heterogeneous; and if $H_j \ge 2$, then heterogeneous. In flood frequency analysis, the statistic H_1 plays a crucial role (Hosking and Wallis, 1997).

It should be stressed that in practice, no ideal except an approximate agreement of q is required. The spatial proximity is not needed for a group of catchments to be homogeneous. The groups should be as numerous as possible to obtain more benefits from regionalization. In flood frequency analysis the minimum number of station-year data (the sum of all the data in a region) is recommended to be 5T (Castellarin et al., 2001; Merz and Blöschl, 2005) or 3T (Gaál et al., 2013), where T is the target return period of the quantile Q that is to be estimated; $T(Q) = \frac{1}{P(X \ge Q)}$ where X is the flood discharge. Using the criterion 3T in the current paper, the minimum number of *CN*s in a homogeneous group should be 30 for the estimation of the 90%th quantile. Out of the symmetry, the same number was required for the estimation of the 10%th quantile.

Choice of the regional distribution function

If a group of catchments was homogeneous, the regional distribution function (RD) was selected among the Generalized Logistic (GLO), Generalized Extreme Value (GEV), lognormal (LN3), Generalized Pareto (GP), and Pearson III (P3) distributions. The parameters of each distribution were estimated using the L-moments method. The final decision was based on the statistics (Hosking and Wallis, 1997):

$$z^{dist} = \frac{\tau_4^{dist} - t_4 + B_4}{\sigma_4}, \tag{10}$$

where τ_4^{dist}, t_4 are the theoretical and sample L-kurtosis, and B_4, σ_4 are the simulated bias and standard deviation of the regional L-kurtosis. The value z^{dist} closest to 0 pointed at the best fit, assuming that $\left| z^{dist} \right| < 1.64$.

Antecedent runoff conditions of Hawkins and of Hjelmfelt

In the Hawkins method, the tabulated *CN*, denoted here as $CN(II)$, is transformed to $CN(I)$ and to $CN(III)$ using the formulas (ASCE, 2009):

$$CN(I) = \frac{CN(II)}{2.281 - 0.01381 \cdot CN(II)}, \tag{11}$$

$$CN(III)=\frac{CN(II)}{0.427+0.00573\cdot CN(II)}. \quad (12)$$

In the Hjelmfelt method, the moderate value of the CN is the 50%th quantile. It is denoted by $CN(II)_{Hje}$ in the current paper. The 10%th and 90%th quantiles are the ARC I and ARC III, denoted $CN(I)_{Hje}, CN(III)_{Hje}$. These three quantiles were estimated for each catchment from a region using Eq (4), where μ_i and $q(F)$ were the empirical mean values of the CN and the theoretical dimensionless quantiles in the $i-$th catchment, respectively, and where $F=0.1, 0.5$ or 0.9.

Choice of the optimal λ

The $CN(I)$, $CN(II)$ and $CN(III)$ values were compared to the $CN(I)_{Hje}, CN(II)_{Hje}$ and $CN(III)_{Hje}$ for every λ For every catchment in a group, the mean absolute relative error was derived for every λ ,

$$MARE(\lambda)=\frac{1}{3}\left(\begin{array}{l}\dfrac{\left|CN(I)-CN(I)_{Hje}\right|}{CN(I)}+\\ \dfrac{\left|CN(II)-CN(II)_{Hje}\right|}{CN(II)}+\\ \dfrac{\left|CN(III)-CN(III)_{Hje}\right|}{CN(III)}\end{array}\right), \quad (13)$$

and the regional MARE was

$$MARE_R(\lambda)=\frac{1}{N}\sum_{i=1}^{N}MARE_i(\lambda) \quad (14)$$

where N was the number of catchments in the region. The final choice of λ was based on the minimum value of $MARE_R$ over all λ values, $\min_{\lambda\in\Lambda} MARE_R(\lambda)$, to guarantee the minimum discrepancy between the tabulated and estimated CN values.

The regional CN and antecedent runoff conditions of Hjelmfelt

If the mean values μ_i were not significantly different and the region was homogenous, the regional distribution was fitted to all empirical CNs in a region using the method of L-moments. The regional *CN* was proposed as the theoretical 50%th quantile estimated from all the empirical *CN*s in the region. The ARC I and III were the 10%th and the 90%th quantiles,

$$CN_R(I)=CN_{10\%},\ CN_R(II)=CN_{50\%},\ CN_R(III)=CN_{90\%} \quad (15)$$

All the calculations were carried out in the R software environment (Hosking, 2019; R Core Team, 2018; Viglione, 2018). All tests were conducted at the significance level 0.05.

Study region and data

Ten small catchments in Slovakia and Poland were selected for the analysis. Figure 1 presents the location of the study areas in Slovakia and Poland. The Slovak catchments of Stupavský, Račiansky, Gidra, Vištucký, and Petrinovec creeks (denoted by A in Fig. 1) are located in the Inner Western Carpathians in Slovakia. The Stupavský creek rises on the eastern slope of the Little Carpathians. Although the stream is dry most days, it derives storm water from forests and vineyards. The length of the stream to the gauging station equals 16.7 km. The Račiansky creek rises in the southern part of the Little Carpathians on a western slope and flows through woods. The length of the creek to the gauging station is 7.1 km. The Gidra creek flows through forests and various recreational areas. The stream flows through vineyards, where it is aligned and has a straight route. The flow length is approximately 5.4 km. The Vištucký (Vištuk) creek, with a length of 5.9 km, has an oak forest, which covers most of the catchment. The Petrinovec creek is

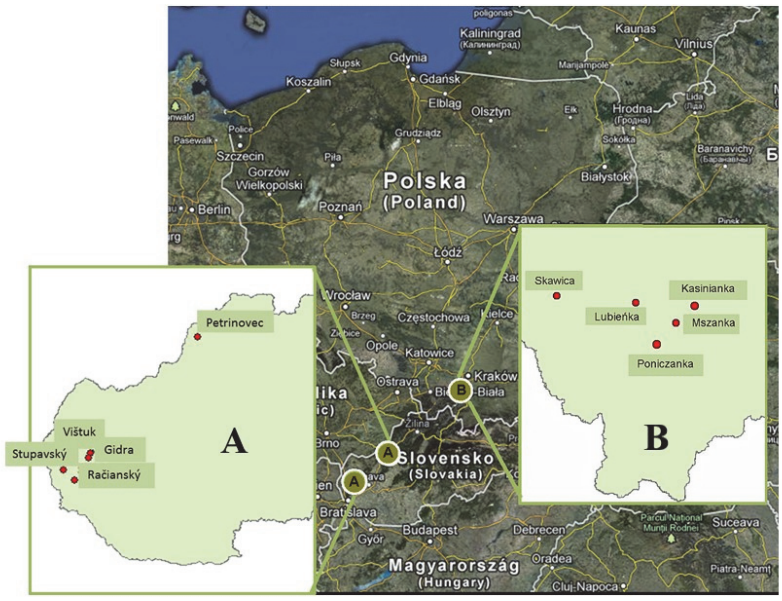

Fig. 1. Location of the study area. Slovak (A) and Polish (B) catchments.

located apart from the four catchments at Stredné Považie in the district of Púchov and rises in the Javorníky Mountains.

Its length is approximately 5.9 km to the gauging station, and it is the steepest catchment among all the catchments analysed. The mean elevation of the Slovak catchments ranges from 126 m a.s.l. at Račiansky to 1472 m a.s.l. at Petrinovec. All the catchments, apart from the Račiansky, have a typically forested character. Only small parts are croplands, urbanized areas, woodland shrubs, and tall grass. The soil type is B (silt loam or loam) in all the Slovak catchments. Therefore, their capability to produce direct runoff is not high. Most of the Slovak catchments have a typically forested character because the forest ratio can reach 0.90 there.

The Polish catchments of Poniczanka, Mszanka, Kasinianka, Lubieńka and Skawica (denoted B in Fig. 1) are located in the Central Carpathian Mountains (Fig. 1). The mean elevation of these catchments ranges from 570 m a.s.l. at Kasinianka to 900 m a.s.l. at Skawica. Skawica is the steepest catchment among the Polish ones. The catchments are mainly covered by forests, croplands, grasslands and pastures. Spruce, birch, fir, pine and oak trees dominate in the forests. Twenty percent of the arable lands are root crops (potatoes, beetroots, onions); 55% are corn (oats, wheat and rye), and 25% are legumes (clover, alfalfa, peas, beans). The thickness of the soil is low, and the two main soil types are C (over 90%, skeletal and loamy soils) and D (less than 10%, alluvial soils).

The capability to produce direct runoff is higher in the Polish catchments than in the Slovak catchments, which is reflected in the lower retention parameters and higher CNs. The average annual rainfall depth varies from 880 mm at Mszanka to 1200 mm at the Skawica catchments.

More detailed information about the creeks, catchments and sample lengths is given in Table 1. The tabulated values of the *CN*, which were determined from the soil and topography properties, are placed in the second column. They range from 62–72 for the Slovak catchments; similarly, the four Polish catchments of Poniczanka, Mszanka, Kasinianka and Lubieńka possess tabulated *CN*s of about 79. This observation was the main impulse for investigating as to whether each region was homogenous in *CN*.

Table 1. Summary of the selected catchment characteristics.

Creek	CN weighted tabulated values	Catchment area [km^2]	Forest ratio [–]	Number of events
Stupavský	65	33.0	0.89	28
Račiansky	72	21.0	0.35	23
Gidra	62	33.0	0.90	14
Vištucký	67	9.8	0.89	18
Petrinovec	65	6.0	0.86	28
Poniczanka	79.5	33.1	0.42	12
Mszanka	79.9	51.0	0.38	12
Kasinianka	79.7	32.0	0.44	13
Lubieńka	80.2	48.7	0.35	16
Skawica	75.3	48.6	0.78	11

The Slovak data from the selected catchments are provided by the Slovak Hydrometeorological Institute and the Department of Land and Water Resources Management, Slovak University of Technology, Bratislava, Slovakia. The Polish data were collected by the Department of Hydraulic Structures, University of Agriculture, Cracow, Poland.

To obtain the rainfall-runoff data (*P*, *H*), the discharge data for a 60 min time step were initially collected from all the stations analyzed. The 1-day heavy rainfall totals from the summer season, which were of a convectional rainfall origin, were recorded at the climatological gauging stations. Only the rain-gauge stations representative of the Vištucký and Gidra catchments have a one-hour resolution of rainfall. The lengths of the rainfall-runoff data observations range from 11 (Skawica station) to 28 (Petrinovec station) events, and the observation period ranges between the years 1988–2013. Secondly, clearly defined, single, extreme rainfall-runoff events were selected. The rainfall-runoff events had to be independent of other events and visibly distinguishable in the runoff data records. Additionally, the hyetographs that caused the runoff were approximately uniform. Subsequently, the hydrograph was analyzed for each event, and the direct runoff was separated by drawing a line from the point of the hydrograph rise to the beginning point of a fitted part of the recession curve matched to the recession segment, see Fig. 2 for an example.

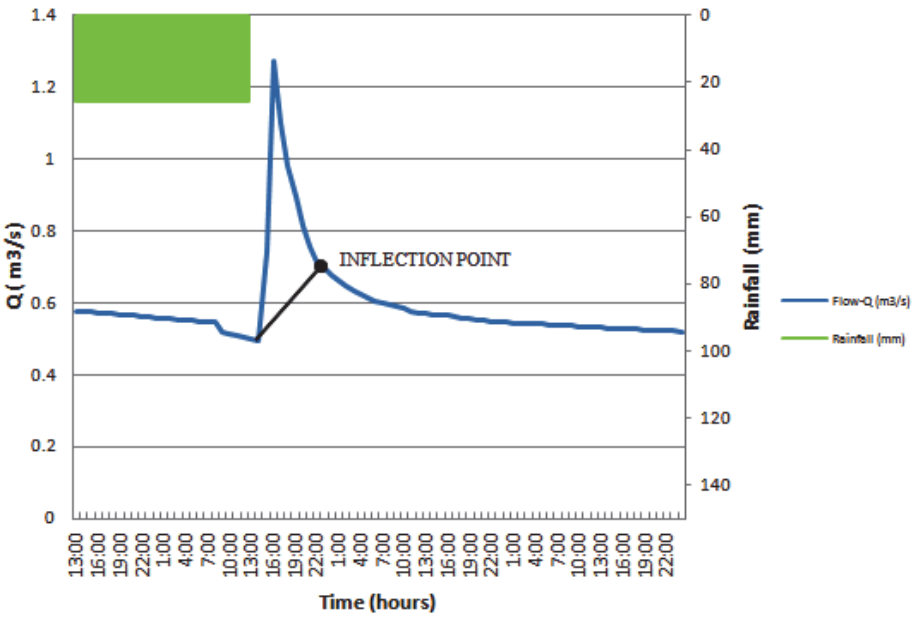

Fig. 2. An example of a hydrograph separation and a hyetograph for the Gidra River catchment.

RESULTS

The Hosking and Wallis regionalization method enables the verification of tabulated CN values based on rainfall-runoff data measurements. Specifically, it makes use of merging small samples into a large sample where the distribution fitting may lead to more reliable CN values than for each small sample separately.

The sample L-moments, l_1, t, t_3 and t_4 are collected in Table 2.

The mean values l_1 decrease with the decreasing λ, because the lower values of λ result in a lower CN, which can be concluded from Eq. (4). The characteristic t slightly grows with decreasing λ. The sample skewness t_3 is negative, apart from the Vištucký, and increases with decreasing λ. Hence, for a low λ, the empirical distribution function tends to be more symmetrical. This tendency can be also observed in the sample kurtosis t_4, which decreases with decreasing λ and is close to the kurtosis of the normal distribution, i.e. 0.12 for certain catchments.

The Slovak catchments have lower mean values and slightly higher variations in comparison to the Polish catchments. The Slovak catchments have a lower range of t_3 and t_4 than the Polish catchments. Among the Polish catchments, B2 has the highest skewness in its absolute value and the highest kurtosis for all λ.

The normality assumption for the ANOVA test was fulfilled in all catchments and for all λ, apart from the Gidra catchment for $\lambda = 0.2$ with p-value $= 0.01$ and for $\lambda = 0.1$ with p-value $= 0.04$. However, because of robustness of ANOVA to small deviations from normality, all the catchments were designated for further analysis. The Levene's test resulted in high p-values, from 0.39 to 0.76 for both groups of catchments and all λ, apart from the Slovak group for $\lambda = 0.2$ with p-value = 0.02.

The ANOVA and Scheffe's tests revealed that in the group of the Slovak catchments, the Petrinovec differed from the others in the mean value of the CN of every λ. No differences in the mean values were identified in the group of Polish catchments for $\lambda = 0.20$. However, for $\lambda = 0.15$ and $\lambda = 0.10$, the Poniczanka catchment had higher mean value than the others. The results were confirmed by the Kruskal-Wallis test and by its post-hoc versions which has been applied due to some violations from normality. This means that there are no significant differences in CN between catchments within every group. The following groups were established:

SL_λ = {Stupavský, Račiansky, Gidra, Vištucký} for $\lambda = 0.20, 0.15, 0.10$,

$PL_{0.20}$ = {Poniczanka, Mszanka, Kasinianka, Lubieńka, Skawica}

PL_λ = {Mszanka, Kasinianka, Lubieńka, Skawica} for $\lambda = 0.15$ and $\lambda = 0.10$.

The results of the HW tests are presented in Table 3. All H_1 values were less than 1 within the groups SL_λ and PL_λ, which proved the homogeneity in L-CV within every group. Similarly, SL_λ and $PL_{0.20}$ were homogeneous in L-skewness and L-kurtosis; however, H_2 and H_3 were greater than 1 for $PL_{0.15}$ and $PL_{0.10}$, which suggested heterogeneity in these two parameters. The Generalized Logistic (GLO) was designated to the regional distribution function, apart from $SL_{0.10}$ where the Pearson 3 distribution (P3) gave a better fit.

Table 2. Sample L-characteristics of CN the Slovak and Polish catchments for various initial abstraction ratios λ.

	Stupavský	Račiansky	Gidra	Vištucký	Petrinovec	Poniczanka	Mszanka	Kasinianka	Lubieńka	Skawica
	$\lambda = 0.20$									
l_1	65.74	65.64	67.02	66.90	73.30	88.34	82.55	79.68	80.67	80.79
t	0.05	0.05	0.05	0.05	0.07	0.04	0.05	0.06	0.05	0.03
t_3	–0.10	–0.15	–0.72	–0.25	–0.19	–0.23	–0.63	–0.06	–0.13	–0.28
t_4	0.14	0.16	0.66	0.14	0.19	0.29	0.44	0.00	0.09	0.27
	$\lambda = 0.15$									
l_1	64.04	60.44	66.54	63.29	71.48	87.78	80.67	76.50	77.64	78.60
t	0.06	0.06	0.07	0.06	0.09	0.04	0.05	0.07	0.06	0.04
t_3	–0.10	–0.12	–0.41	–0.08	–0.10	–0.19	–0.67	–0.04	–0.10	–0.29
t_4	0.06	0.14	0.65	0.19	0.22	0.21	0.50	0.02	0.08	0.25
	$\lambda = 0.10$									
l_1	58.30	53.12	64.82	57.00	68.98	85.64	76.64	71.92	73.28	76.08
t	0.09	0.07	0.08	0.08	0.10	0.05	0.05	0.08	0.08	0.06
t_3	–0.03	–0.06	–0.25	0.02	–0.11	–0.16	–0.64	–0.02	–0.07	–0.07
t_4	0.10	0.10	0.18	0.21	0.20	0.17	0.52	0.04	0.07	0.39

Table 3. Measures of the heterogeneity test in the groups of Slovak (SL) and Polish (PL) catchments for various initial abstraction ratios λ, the measure z^{dist}, and the regional distribution (RD).

	$SL_{0.2}$	$SL_{0.15}$	$SL_{0.1}$	$PL_{0.2}$	$PL_{0.15}$	$PL_{0.1}$
H_1	–1.36	–1.52	–1.41	–0.82	–0.42	–0.34
H_2	0.21	–0.78	–0.35	0.11	1.52	1.49
H_3	0.00	0.10	–0.70	0.25	1.31	1.97
z^{dist} / RD	–0.18 / GLO	0.08 / GLO	–0.29 / P3	0.15 / GLO	0.20 / GLO	–1.13 / GLO

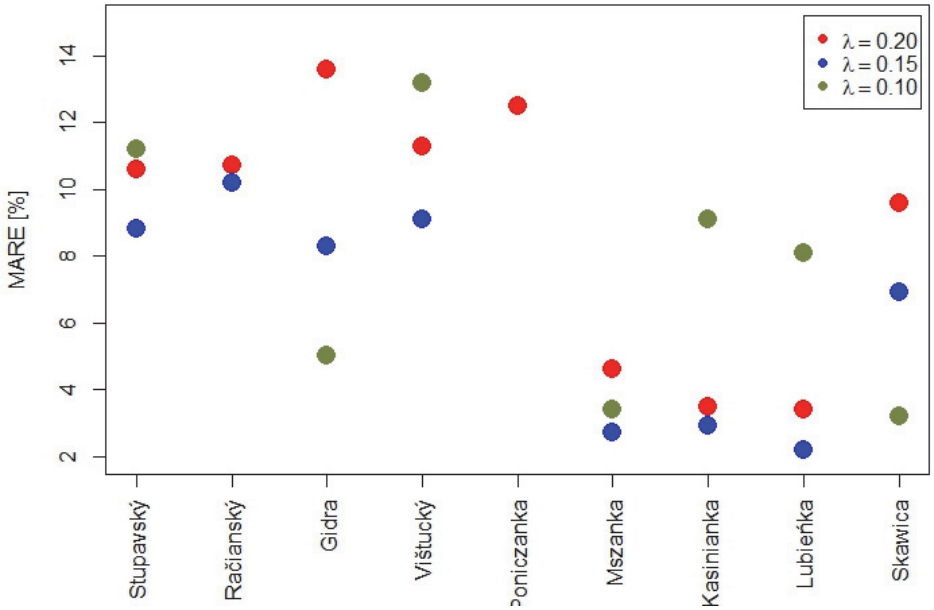

Fig. 3. The error $MARE(\lambda)$ (Eq. (13)) (in %).

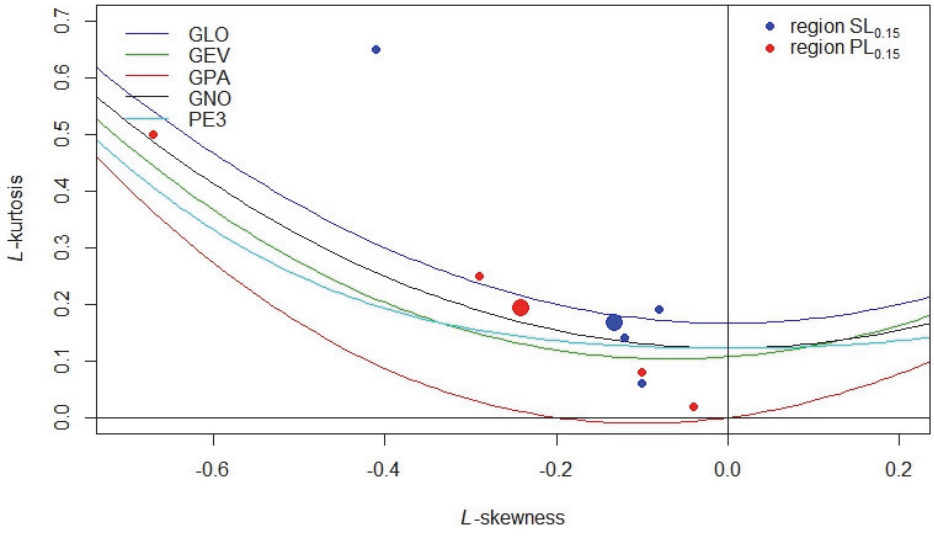

Fig. 4. The L-moment ratio diagram for the Slovak and Polish regions with abstraction ratios λ = 0.15 *(*$SL_{0.15}$ and $PL_{0.15}$). The small bullet points depict the catchment characteristics and the thick bullet points depict the regional characteristics.

For the choice of the optimal abstraction ratios λ, the $MARE(\lambda)$ error (Eq. (13)) was derived for every catchment from groups SL_λ and PL_λ. The results are presented in Fig 3.

The lowest regional $MARE_R(\lambda)$ (Eq. (14)) equal to 9.1% was achieved for λ = 0.15 in the group $SL_{0.15}$ and equal to 3.6% in the group $PL_{0.15}$.

Finally, the following homogenous regions were delineated: $SL_{0.15}$ = {Stupavský, Račiansky, Gidra, Vištucký} and $PL_{0.15}$ = {Mszanka, Kasinianka, Lubieńka, Skawica}.

The L-moment ratio diagram for the regions $SL_{0.15}$ and $PL_{0.15}$ was plotted in Fig. 4. The catchment's and regional L-skewness and L-kurtosis are depicted there. The closeness of the GLO line to the regional points confirms the final choice of the regional distribution.

For those groups the regional *CN* s were obtained from Eq. (15), namely

$$CN_{SL_{0.15}}(I) = 54.50 \qquad CN_{SL_{0.15}}(II) = 64.28$$
$$CN_{SL_{0.15}}(III) = 72.20$$
$$CN_{PL_{0.15}}(I) = 68.15 \qquad CN_{PL_{0.15}}(II) = 79.43$$
$$CN_{PL_{0.15}}(III) = 87.01$$

Observe that $CN_{SL_{0.15}}(II)$ slightly differed from the tabulated values with a mean value of about 66 in the Slovak catchments and of about 75.3 in the Skawica catchment. These findings permit the conclusion that, for practical purposes, the tabulated *CN*s should be corrected in those catchments, because they seem to be too high in the Račiansky and Vištucký and too low in the Skawica catchments.

Apart from the main subject of the study, the heterogeneity in q was tested in all ten catchments. Surprisingly, all the H_js were less than one, which proved similarity in the distribution of the rescaled *CN* for all the Carpathian catchments investigated.

DISCUSSION AND CONCLUSION

The paper focuses on an estimation of the regional *CN* values for a group of ten small Slovak and Polish catchments. The Slovak catchments are located in the Inner Western Carpathians in Slovakia; the areas of the catchments are in a range of 6 – 33 km^2. Most of the Slovak catchments have a typically forested character, achieving a forest ratio of 0.90. The tabulated values of the *CN*, which were determined from soil and topography properties range from 62 to 72. The Polish catchments with areas in a range from 33.1 to 51 km^2, are located in the Central Carpathian Mountains. The four Polish catchments of Poniczanka, Mszanka, Kasinianka, and Lubieńka possess tabulated *CN*s of about 79, the Skawica catchment has a lower *CN* about 75.

For estimating empirical *CN*s, the individual rainfall-runoff events were collected for all the catchments from the summer season of 1988-2013; the number of events analyzed ranged from 11 to 28. The discharge data were collected in a 60 min time step, and the direct runoff was separated from all the selected hydrographs by a graphic separation method. Rainfall data were collected in a 1-day time step; only the rain-gauge stations representative of the Vištucký and Gidra catchments have a one-hour resolution of rainfall.

The L-moment based method of Hosking and Wallis and the ANOVA test were combined to delineate the area in two homogenous regions of catchments with similar *CN* values. The combination of these methods revealed homogeneity in *CN* within the regions of the four Slovak and four Polish catchments. They possessed similar mean *CN* values and were similarly distributed.

For the choice of the optimal λ, the $MARE(\lambda)$ error was derived for every catchment from groups SL_λ and PL_λ. The lowest $MARE_R(\lambda)$ was achieved for λ = 0.15,which is equal to 9.1 % for the group $SL_{0.15}$ and 3.6% for the group $PL_{0.15}$.

The optimization condition allowed for the choice of λ = 0.15 in every region. This is in accordance with other studies in forested catchments in Slovakia, e.g., Karabová and Marková (2013), revealed the estimated coefficients λ below 0.2.

The regional *CN* was proposed as the 50%th quantile of the theoretical distribution function estimated from all the *CN*s in the region. These estimations of the *CN*, which are more representative of catchment heterogeneities, slightly differed from the tabulated *CN*s. The ARC of Hjelmfelt were estimated as the 10%th and 90%th quantiles. In the future, further catchments can also be added to the study to broaden the groups with similar *CN*s.

In relation to the problem of forming regions, it is worth remembering that the HW tests were designed to flood frequency where the distributions of annual maxima flows are skewed while the ANOVA test assumes normality to enable the comparison between mean values. The procedure presented in this paper can therefore be applied when the violations from normality are not large and the variances are not far different. The use of the Kruskall-Wallis test enabled the verification and potential re-delineation of groups if the assumptions of ANOVA were not fulfilled. On the other side, in general, the strong ANOVA assumptions may not always be fulfilled in groups of catchments with similar *CN* values. The expert knowledge about the study area is sometimes needed to verify the regions. Summarizing, the procedure presented in this paper is useful when the distributions of CNs are not very far from symmetrical and the differences between variances are not large. Another method of regionalization should be used instead.

Due to its basic empirical character, the SCS-CN method has several limitations and drawbacks, and it is restricted to certain geographic regions and land use types. It works well for small agricultural catchments but has significant shortcomings for other types of catchments, specifically forested catchments (Barlett et al., 2016, 2017). The *CN* values determined from look-up tables as a dimensionless catchment index are usually considered as a fixed parameter. However, they are random variables that change with regional rainfall-runoff processes, hydrological soil groups, land-use conditions, antecedent rainfall and soil moisture, and vary across different sources of spatio-temporal variability. Besides, the tabulated *CN* values are appropriate for slopes of around 5% because these reference values were identified from small agricultural catchments where slope does not play a significant role (Verma et al., 2017).

To move beyond some of these limitations and extend the applicability of the SCS-CN method for forested catchments in the Carpathian Mountains, the *CN* values for individual catchments treated were determined from observed rainfall-runoff events. A statistical framework that provides a quantitative basis for regional estimates of the *CN* values together with the optimization of the initial abstraction of λ was developed. Accordingly, the paper brings a novel approach to the estimation of *CN* value based on regional *CN* that may better represent geographic regions and site types that the traditional SCS-CN method and can give rise to verify this approach in other regions of the world. The additional benefit of introducing a common regional *CN* is the opportunity to apply in catchments with a lack of data or without observations, and with similar soil-physiographic characteristics. Accuracy of estimated empirical CNs strongly depends on a number of analyzed rainfall-runoff events. Therefore, regional methods for estimating empirical CN are helpful where several small samples are put together in a large homogeneous sample and where the distribution fitting may lead to more reliable *CN* values than for each small sample separately.

The methodology still has issues requiring further improvement, which can also be achieved by estimating λ as a regional parameter.

Acknowledgements. This work was supported by the Slovak Research and Development Agency under Contract No. APVV-15-0497, VEGA Grant No. 1/0891/17, and by the Ministry of Science and Higher Education, Republic of Poland, Grant No. DS 3376/KZM/2018.

REFERENCES

Adamowski, K., 2000. Regional analysis of annual maximum and partial duration flood data by nonparametric and L-moment methods. J. Hydrol., 229, 219–231.

Ajmal, M., Wassem, M., Ahn, J.-H., Kim, T.-W., 2015. Improved runoff estimation using event-based rainfall-runoff models. Water Resour. Manag., 29, 6, 1995–2010. http://dx.doi.org/10.1007/s11269-015-0924-z.

Arnold, J.G., Williams, J.R., Srinivasan, R., King, K.W., 1995. SWAT: Soil Water Assessment Tool. Texas Agricultural Experiment Station: Blackland Research Center, Texas A&M University, Temple, TX, USA.

Baltas, E.A., Dervos, N.A., Mimikou, M.A., 2007. Research on the initial abstraction – storage ratio and its effect on hydrograph simulation at a watershed in Greece. Hydrol. Earth Syst. Sci. Discuss., 4, 2169–2204. DOI: 10.5194/hessd-4-2169-2007.

Banasik, K., Ignar, S., 1983. Estimation of effective rainfall using the SCS method on the base of measured rainfall and runoff. Rev. Geophys., XXVII (3–4), 401–408. (In Polish.)

Banasik, K., Madeyski, M., Więzik, B., Woodward, D.E. 1997. Applicability of curve number technique for runoff estimation from small Carpathian catchments. In: Proceedings of the International Conference on Developments of Hydrology of Mountainous Areas. Slovak Committee of Hydrology, Stara Lesna, Sept. 14–16, 1994, pp. 240–242. IHP-Projects, H-5-5/H-5-6, Unesco, Paris. https://unesdoc.unesco.org/ark:/48223/pf0000109610.

Banasik, K., Woodward, D., 2010. Empirical determination of runoff curve number for a small agricultural watershed in Poland. In: Proc. 2nd Joint Federal Interagency Conference, Las Vegas: NV, USA, June 27–July 1, 2010, pp. 1–11. http://acwi.gov/sos/pubs/2ndJFIC/Contents/10E_Banasik_28_02_10.

Banasik, K., Woodward, D.E., Hawkins, R., 2014. Curve numbers for two agro-forested watersheds. In: Proceedings of the World Environmental and Water Resources Congress "Water Without Borders", ASCE, Portland: Oregon, USA, June 1–5, 2014, pp. 2235–2246. Abstract available at: https://ascelibrary.org/doi/10.1061/9780784413548.223.

Banasik, K., Rutkowska, A., Kohnová, S., 2014. Retention and curve number variability in a small agricultural catchment: the probabilistic approach. Water, 6, 5, 1118–1133.

Bartlett, M.S., Parolari, A.J., McDonnell, J.J., Porporato, A., 2016. Beyond the SCS-CN method: A theoretical framework for spatially lumped rainfall-runoff response. Water Resour. Res., 52, 4608–4627. DOI: 10.1002/2015WR018439.

Bartlett, M.S., Parolari, A.J., McDonnell, J.J., Porporato, A., 2017. Reply to comment by Fred L. Ogden et al. on "Beyond the SCS-CN method: A theoretical framework for spatially lumped rainfall-runoff response." Water Resour. Res., 53, 6351–6354. DOI: 10.1002/2017WR020456.

Bingner, R.L., Theurer, F.D., 2005. AnnAGNPS Technical Processes: Documentation Version 3.2. USDA-ARS, National Sedimentation Laboratory, Oxford, Miss., USA.

Bondelid, T., McCuen, R., Jackson, T., 1982. Sensitivity of SCS Models to curve number variation. J. Am. Water Resour. As., 18, 1, 111–116.

Burn, D.H., Goel, N.K., 2000. The formation of groups for regional flood frequency analysis. Hydrolog. Sci. J., 45, 97–112. DOI: 10.1080/02626660009492308.

Castellarin, A., Burn, D.H., Brath, A., 2001. Assessing the effectiveness of hydrological similarity measures for flood frequency analysis. J. Hydrol., 241, 270–285.

Cazier, D.J., Hawkins, R.H., 1984. Regional application of the curve number method. In: Proceedings of Specialty Conference, Irrigation and Drainage Division, American Society of Civil Engineers, Flagstaff, AZ, abstract, p. 710.

Dalrymple, T., 1960. Flood Frequency Analyses, Manual of Hydrology. Water Supply Paper 1543-A, U.S. Geological Survey, Reston, USA.

Durán-Barroso, P., González, J., Valdés, J.B., 2017. Sources of uncertainty in the NRCS CN model: recognition and solutions. Hydrol. Process., 31, 22, 3898–3906. http://dx.doi.org/10.1002/hyp.11305

Elhakeem, M., Papanicolaou, A.N., 2009. Estimation of the runoff curve number via direct rainfall simulator measurements in the state of Iowa, USA. Water Resour. Manag., 23, 12, 2455–2473. http://dx.doi.org/10.1007/s11269-008-9390-1.

Gaál, L., Kohnová, S., Szolgay, J., 2013. Regional flood frequency analysis in Slovakia: Which pooling approach suits better? In: Klijn, Schweckendiek (Eds): Comprehensive Flood Risk Management: Research for policy and practice. pp. 27–30.

Gaswirth, J.L., Gel, Y.R., Miao, W., 2009. The impact of Levene's test of equality of variances on statistical theory and practice. Stat. Sci., 24, 3, 343–360. DOI: 10.1214/09-STS301.

Geetha, K., Mishra, S., Eldho, T., Rastogi, A., Pandey, R., 2007. Modifications to SCS-CN method for long-term hydrologic simulation. J. Irrig. Drain. Eng., 133, 5, 475–486.

Hawkins, R., 1973. Improved prediction of storm runoff in mountain watersheds. J. Irrig. Drain. Div., 99, 4, 519–523.

Hawkins, R., 1979. Runoff Curve Numbers from Partial Area Watersheds. J. Irrig. Drain. Div., 105, 4, 375–389.

Hawkins, R., 1993. Asymptotic determination of curve numbers from data. J. Irrig. Drain. Div., 119, 334–345.

Hawkins, R.H., Khojeini, A.V., 2000. Initial abstraction and loss in the curve number method. Proc. of Arizona Hydrological Society, Tucson, Arizona.

Hawkins, R.H., Hjelmfelt, Jr. A.T., Zevenbergen, A.W., 1985. Runoff probability, storm depth, and Curve Numbers. J. Irrig. Drain. Div., 111, 4, 330–340.

Hawkins, R.H., Ward, T.J., Woodward, D.E., van Mullem, J.A. (Eds.), 2009. Curve Number Hydrology: State of the Practice. American Society of Civil Engineers, Reston, VA, USA.

Hitchcock, D.R., Jayakaran, A.D., Loflin, D.R., Williams, T.M., Amatya, D.M., 2013. Curve number derivation for watersheds draining two headwater streams in Lower Coastal Plain of South Carolina, USA. J. Am. Water. Resor. As., 49, 1284–1295.

Hjelmfelt, A., 1991. Investigation of curve number procedure. J. Hydraul. Eng., 117, 6, 725–737.

Hjelmfelt Jr., A.T., Kramer, L.A., Burwell, R.E., 1983. Curve numbers as random variables. In: Proceedings of the Specialty Conference on Advances in Irrigation and Drainage: Surviving External Pressures. Jackson, Wy, USA, pp. 365–370.

Hosking, J.R.M., Wallis, J.R., 1990. L-moments: analysis and estimation of distributions using linear combinations of order statistics. J. R. Stat. Soc. B., 52, 1, 105–124.

Hosking, J.R.M., Wallis, J.R., 1997. Regional Frequency Analysis. An Approach Based on L-Moments. Cambridge University Press, Cambridge, UK, 244 p.

Hosking, J.R.M., 2019. Regional frequency analysis using L-moments. R package, version 3.2. URL: https://cran.r-project.org/web/packages/lmomRFA/lmomRFA.pdf

Jiang, R., 2001. Investigation of runoff curve number initial abstraction ratio. MS thesis. Watershed Management, University of Arizona, Tucson, AZ, 120 p.

Jeon, J.-H., Lim, K. J., Engel, B.A., 2014. Regional calibration of CSC-CN L-THIA model: application for ungauged basins. Water, 6, 1339–1359. DOI: 10.3390/w6051339.

Karabová, B., Marková, R., 2013. Testing of regionalization of SCS-CN parameters in the Upper Hron River region, Slovakia. Adolf Patera Seminar 2013, Prague, Czech Republic.

Kochanek, K., Strupczewski, W.G., Bogdanowicz, E., 2012. On seasonal approach to flood frequency modelling. Part II: flood frequency analysis of Polish rivers. Hydrol. Process., 26, 71–73. DOI: 10.1002/hyp.8178.

Kohnová, S., Szolgay, J., Solin, L., Hlavčova, K., 2006. Regional Methods for Prediction in Ungauged Basins. Case Studies. KEY Publishing s.r.o. in cooperation with the Slovak Committee for Hydrology, Bratislava.

Kruskal, W.H., Wallis, W.A., 1952. Use of ranks in one-criterion variance analysis. J. Am. Stat. Assoc., 47, 260, 583–621.

Leonard, R.A., Knisel, W.G., Still, D.A., 1987. GLEAMS: Groundwater loading effects of agricultural management systems. Trans. ASAE, 30, 5, 1403–1418.

Levene, H., 1960. Robust tests for equality of variances. In: Olkin, I., Hotteling, H. et al. (Eds.): Contributions to Probability and Statistics: Essays in Honor of Harold Hotelling. Stanford University Press, pp. 278–292.

Merz, R., Blöschl, G., 2005. Flood frequency regionalization - spatial proximity vs. catchment attributes. J. Hydrol., 302, 1–4, 283–306.

McCuen, R., 2002. Approach to confidence interval estimation for curve numbers. J. Hydraul. Eng., 7, 1, 43–48.

Mishra, S.K., Tyagi, J.V., Singh, V.P., Singh, R., 2006. SCS-CN-based modeling of sediment yield. J. Hydrol., 324, 301–322.

Mishra, B.K., Takara, K., Tachikawa, Y., 2009. Integrating the NRCS runoff curve number in delineation of hydrologic homogeneous regions. J. Hydrol. Eng., 14, 10, 1091–1097.

Mockus, V., 1972. Chapter 21: Design hydrographs. In: McKeever, V., Owen, W., Rallison, R. (Eds.): National Engineering Handbook, Section 4, Hydrology. U.S. Department of Agriculture, Soil Conservation Service, Washington, DC.

R Core Team, 2018. R: A language and environment for statistical computing. R Foundation for Statistical Computing, Vienna, Austria. URL http://www.R-project.org/.

Rutkowska, A., Kohnová, S., Banasik, K., Szolgay, J., Karabová, B., 2015. Probabilistic properties of a curve number: a case study for small Polish and Slovak Carpathian Basins. J. Mt. Sci., 12, 3, 533–548. https://doi.org/10.1007/s11629-014-3123-0

Rutkowska, A., Żelazny, M., Kohnová, S., Łyp, M., Banasik, K., 2010. Regional L-moment-based flood frequency analysis in the Upper Vistula River basin, Poland. Pure Appl. Geophys., 174, 2, 701–721. DOI: 10.1007/s00024-016-1298-8

Sahu, R.K., Mishra, S.K., Eldho, T.I., 2010. An improved AMC-coupled runoff curve number model. Hydrol. Process., 24, 20, 2834–2839.

Scheffé, H., 1959. The Analysis of Variance. Wiley, New York. 477 p.

Shi, Z.H., Chen, L.-D., Fang, N.-F., Qin, D.-F., CAI, C.-F., 2009. Research on the SCS-CN initial abstraction ratio using rainfall-runoff event analysis in the Three Gorges Area, China. Catena, 77, 1, 1–7. http://dx.doi.org/10.1016/j.catena.2008.11.006.

Shapiro, S.S, Wilk, M.B., 1965. An Analysis of Variance Test for Normality, Biometrica, 52, 3–4, 591–611.

Soulis, K.X., Valiantzas, J.D., 2012. SCS-CN parameter determination using rainfall-runoff data in heterogeneous watersheds - the two-CN system approach. Hydrol. Earth Syst. Sci. Discuss., 16, 1001–1015. DOI: 10.5194/hessd-8-8963-2011.

Tedela, N.M., McCutcheon, S.C., Rasmussen, T.C., Tollner, E.W., 2008. Evaluation and Improvements of the Curve Number Method of Hydrological Analysis on Selected Forested Watersheds of Georgia. The University of Georgia, report submitted to Georgia Water Resources Institute. USA. Available at: http://water.usgs.gov/wrri/07grants/progress/2007GA143B.pdf (accessed on 6th February 2014).

Ulrych, T.J., Velis, D.R., Woodbury, A.D., Sacchi, M.D., 2000. L-moments and C-moments. Stoch. Env. Res. Risk A., 14, 50–68.

USDA, 2004. Estimation of direct runoff from storm rainfall. In: National Engineering Handbook, Chapter 10, part 630. Dept of Agriculture NRCS, Washington, DC, pp. 1–22.

Verma, S., Verma, R.K., Mishra, S.K., Singh, A., Jayaraj, G.K., 2017. A revisit of NRCS-CN inspired models coupled with RS and GIS for runoff estimation. Hydrological Sciences Journal, 62, 12, 1891–1930. DOI: 10.1080/02626667.2017.1334166

Viglione, A., 2018. nsRFA: Non-supervised Regional Frequency Analysis. R package version 0.7-14. https://cran.r-project.org/web/packages/nsRFA/nsRFA.pdf

Wang, Q.J., 1996. Direct sample estimators of L moments. Water Resour. Res., 32, 3617–3619.

Wałęga, A., Cupak, A., Amatya, D.M., Drożdżal, E., 2017. Comparison of direct outflow calculated by modified SCS-CN methods for mountainous and highland catchments in upper Vistula Basin, Poland and lowland catchment in South Carolina, U.S.A. Acta Scientiarum Polonorum Formatio Circumiectus, 16, 1, 187–207.

Węglarczyk, S., 2010. Statystyka w inżynierii środowiska (Statistics in Environmental Engineering). Politechnika Krakowska, Cracow, Poland, 376 p.

Woodward, D.E., Hawkins, R.H., Jiang, R., Hjelmfelt Jr., A.T., Van Mullem, J.A., Quang, D.Q., 2003. Runoff curve number method: examination of the initial abstraction ratio. In: Bizier, P., DeBarry, P. (Eds.): Proceedings of the World Water & Environmental Resources Congress 2003 and Related Symposia, EWRI, ASCE, 23–26 June, 2003, Philadelphia, Pennsylvania, USA, p. 10. DOI: 101061/40685(2003)308.

Yang, T., Xu, C.-Y., Shao, Q.-X., Chen, X., 2010. Regional flood frequency and spatial patterns analysis in the Pearl River Delta region using L-moments approach. Stochastic Environmental Research and Risk Assessment, 24, 165–182. DOI: 10.1007/s00477-009-0308-0.

Yuan, Y., Nie, W., McCutcheon, S.C., Taguas, E.V., 2014. Initial abstraction and curve number for semiarid watersheds in Southeastern Arizona. Hydrol. Process., 28, 3, 774–783. http://dx.doi.org/10.1002/hyp.9592

Received 30 July 2019
Accepted 12 January 2020

J. Hydrol. Hydromech., 68, 2020, 2, 180–191
DOI: 10.2478/johh-2020-0010
ISSN 1338-4333

sciendo Journal of Hydrology and Hydromechanics

Analysis of changes in hydrological cycle of a pristine mountain catchment. 1. Water balance components and snow cover

Ladislav Holko[1], Patrik Sleziak[1], Michal Danko[1], Svetlana Bičárová[2], Joanna Pociask-Karteczka[3]

[1] Institute of Hydrology of the Slovak Academy of Sciences, Dúbravská cesta 9, 841 04 Bratislava, Slovakia.
[2] Institute of Earth Sciences of the Slovak Academy of Sciences, Dúbravská cesta 9, 840 05 Bratislava, Slovakia.
[3] Institute of Geography and Spatial Management, Jagielonian University Krakow, ul. Gronostajowa 7, PL 30-387 Krakow, Poland.
* Corresponding author. E-mail: holko@uh.savba.sk

Abstract: We analyse water balance, hydrological response, runoff and snow cover characteristics in the Jalovecký Creek catchment (area 22 km^2, mean elevation 1500 m a.s.l.), Slovakia, in hydrological years 1989–2018 to search for changes in hydrological cycle of a mountain catchment representing hydrology of the highest part of the Western Carpathians. Daily air temperature data from two meteorological stations located in the studied mountain range (the Tatra Mountains) at higher elevations show that the study period is 0.1°C to 2.4°C warmer than the climatic standard period 1951–1980. Precipitation and snow depth data from the same stations do not allow to conclude if the study period is wetter/drier or has a decreasing snow cover. Clear trends or abrupt changes in the analysed multivariate hydrometric data time series are not obvious and the oscillations found in catchment runoff are not coherent to those found in catchment precipitation and air temperature. Several time series (flashiness index, number of flow reversals, annual and seasonal discharge maxima, runoff coefficients) indicate that hydrological cycle is more dynamic in the last years of the study period and more precipitation runs off since 2014. The snow cover characteristics and climatic conditions during the snow accumulation and melting period do not indicate pronounced changes (except the number of days with snowfall at the Kasprowy Wierch station since 2011). However, some data series (e.g. flow characteristics in March and June, annual versus summer runoff coefficients since 2014) suggest the changes in the cold period of the year.

Keywords: Mountain catchment; Hydrological cycle; Time series.

INTRODUCTION

Detection of changes in the long time series of hydrological data using various approaches is a traditional part of hydrological research (e.g. Buishand, 1984; Chiverton et al., 2015; Conte et al., 2019; Górnik, 2020; Hurst, 1951; Klemeš, 1974; Koutsoyiannis, 2003; Kundzewicz and Robson, 2004; Lettenmaier and Burges, 1978; Merz et al., 2012; Pettitt, 1979; Sharma et al., 2016; Xiong et al., 2015; Zégre et al., 2010; etc.). Despite caution that mathematics can tell us little about the physical signals in the nonstationary world, because "our mathematical models … by which we try to describe geophysical records are only as good as is our understanding of the processes that generated them" (Klemeš, 2000), variability and change in hydrological time series will remain important research themes also in the near future (Blöschl et al., 2019). Increasing interest in such analyses in the last two decades is related to the effort to identify the impacts of climate or global changes on the hydrological cycle.

All big river systems are born in mountain environments which are fragile and sensitive to climate or landuse changes (e.g. Kohler and Maselli, 2009; Mastrotheodoros et al., 2020). Good long-term hydrological data from the mountains are difficult to obtain due to a number of factors including the inaccessibility, harsh climatic conditions, great spatial and temporal variability of the water balance components. This study examines 30-years long time series of hydrological data from a pristine research catchment of the Jalovecký Creek in the Western Tatra Mountains. Catchment monitoring provided the long data series that are not common in many small mountain catchments, e.g. spatially distributed snow cover measurements or isotopic composition of precipitation and runoff. The main objective of this study is to investigate temporal changes in the water balance components (precipitation, runoff) and snow cover in hydrological years 1989–2018. The companion paper (Holko et al., 2020, this issue), presents the analysis of changes in isotopic composition of precipitation and runoff, examination of trends and abrupt changes in the data series and the attribution analysis.

CATCHMENT AND DATA

The Jalovecký Creek catchment (Fig. 1) has the area 22.2 km^2 and mean altitude 1500 m a.s.l. (820–2178 m a.s.l.). Crystalline rocks (schist, paragneiss, migmatite) and granodiorite build 48% and 21% of the catchment, respectively. Approximately 7% of the catchment along its western boundary is built by the nappes of Mesozoic rocks (mainly limestone and dolomite). About 24% of the catchment is covered by Quaternary sediments (morraines, slope debries, etc.). Catchment morphology is characterised by steep slopes (mean 30°) and mostly narrow valleys with missing or just small alluvium. Wider segments of the main valleys that are located in the upper parts of the catchment, were modelled by Pleistocene glaciers.

The main soil types in the catchment are cambisols, podzols and lithosols. Rendzinas occur on the Mesozoic rocks. All soils have high stoniness that is often 40–50% and more (Hlaváčiková et al., 2019; Kostka and Holko, 1997).

Forest (dominated by Norway spruce), dwarf pine and the zone of alpine meadows and bare rocks cover 44%, 31% and 25% of the catchment, respectively. Most of the forest is over 100 years old. Because the catchment is located in the protected

Fig. 1. The Jalovecký Creek catchment from the south; the light blue line indicates part of the water divide.

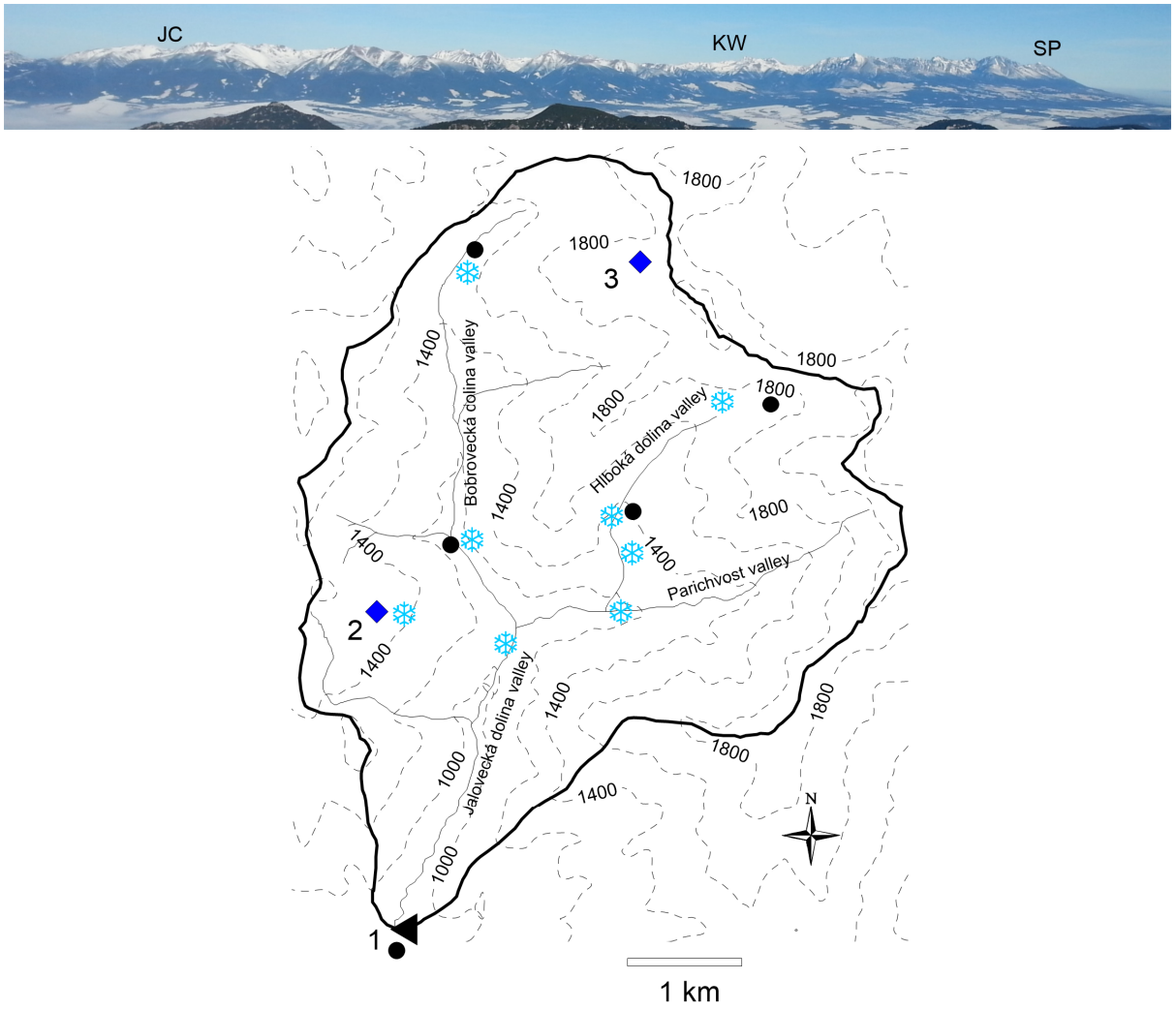

Fig. 2. Basic hydrological monitoring network in the Jalovecký Creek catchment; 1 – stream gauge (triangle) and meteorological station nearby (black circle), 2– the main meteorological station located at catchment mean elevation, 3 – meteorological station at 1875 m a.s.l. providing the air temperature data since the hydrological year 2003; snow courses (snowflakes) and storage gauges (1989–2008; black circle), water divide (thick black line) and contour lines; the photo on the top gives an idea on the approximate distance of the Jalovecký Creek Catchment (JC) from meteorological stations at Kasprowy Wierch (KW, 20 km) and Skalnaté Pleso (SP, 38 km).

area of the Tatra National Park (TANAP), human activities in the last decades are strongly restricted (absence of paved roads, occasional removal of wood after calamities, hiking on a sparse network of marked trials). However, larger scale forest dieback that started approximately in 2013 after greater windthrows and bark beetle outbreak are rapidly changing the forest structure (Bartík et al., 2019).

The basic monitoring network is shown in Fig. 2. Catchment runoff is measured at 820 m a.s.l. The main meteorological station (precipitation, air temperature and humidity, snow course) is located at catchment mean elevation (1500 m a.s.l.). Additional meteorological stations providing precipitation and air temperature data are located near the catchment outlet at 750 m a.s.l. and in the foreland part of the catchment at 570 m a.s.l.

(not shown in Fig. 2). The air temperature data are available also from the elevation of 1875 m a.s.l. since hydrological year 2003. Precipitation network in the years 1989–2008 (20 hydrological years) included four additional storage gauges at elevations 1100–1775. The tipping bucket gauges have been operating at the same points in summer months (June-September) since 2013 (e.g. Holko et al., 2014). Snow depth and water equivalent are measured at the end of January, February and March at snow courses located at elevations 1100–1700 m a.s.l. More frequent snow measurements (every two weeks during snow accumulation, every week since the snow water equivalent maximum) are conducted near the main meteorological station at 1500 m a.s.l. and in the nearby forest at 1450 m a.s.l. (e.g. Holko and Kostka, 2008; Holko et al., 2009).

Catchment areal precipitation and air temperature for this study were obtained by interpolation of point measurements using the elevation gradient. The air temperature data from elevations 570, 750 and 1500 m a.s.l. were used in the interpolation. Elevation gradients for the precipitation interpolation were based on data measured at 570, 750, 1100, 1400, 1500 (two gauges) and 1775 m a.s.l.

Information about the snow cover is obtained from the snow water equivalent (SWE) measured at varying time interval (from monthly to weekly) at snow courses located at 1100, 1400, 1500 and 1700 m a.s.l. This information is supplemented by simulated daily values of catchment SWE. Because catchment SWE cannot be obtained from direct measurements in larger mountain catchments, it was simulated by the spatially distributed hydrological model MikeSHE. The model was calibrated and validated against SWE data measured at ten snow courses located at the elevations 1100–1900 m a.s.l. (five of them were in the open area, five in the forest) and catchment runoff (Danko et al., 2015). The volume of snowmelt water measured at the elevations 1000–1500 m by six snow lysimeters in winter 2012 was used in the calibration as well. The model was calibrated for the period 2010–2014 and validated for the period 2002–2009.

Hydrological cycle of small mountain catchments (elevation ranges approximately 800–2200 m a.s.l.) in the Tatra Mountains is significantly affected by climatic conditions at higher elevations. Therefore, daily data on precipitation, air temperature and snow depth from the high-elevation meteorological stations at Kasprowy Wierch (Poland, 1991 m a.s.l., mountain ridge position) and Skalnaté Pleso (Slovakia, 1778 m a.s.l., the leeward side of the mountains) from period 1951–2018 are used to characterize climatic conditions in the Tatra Mountains in the study period from the longer time perspective. Although the Kasprowy Wierch and Skalnaté Pleso stations are about 20 and 38 km from the study catchment, respectively (Fig. 2), they are the only representative meteorological stations in the Tatra Mountains with the long-term data that are located at higher altitudes. The observations are carried out there by the permanent professional staff and both stations operate since the 1940‘s.

METHODOLOGY

A time series analysis should consist of exploratory data analysis, application of statistical tests and interpretation of tests results (e.g., Kundzewicz and Robson, 2004). Kundzewicz and Robson (2004) listed some commonly used tests, proposed greater use of the distribution-free testing methods and pointed at the role of exploratory data analysis as an essential part of any statistical analysis. They reminded that climate variability can cause an apparent trend and obscures other changes. Therefore, we start the analysis of data from the Jalovecký Creek catchment by characterizing climatic conditions in the study period (1989–2018) with respect to the longer time period (1951–2018) and estimation of structural changes (cycles) in the data series. Then, we analyse the water balance, hydrological response of the catchment, runoff and snow cover variability.

Climatic conditions in the study period

The long-term means representing the climatic standard are calculated for the air temperature, precipitation and snow cover data from meteorological stations at Kasprowy Wierch and Skalnaté Pleso for the period 1951–1980. This period is a good representation of climate in Slovakia in the 20th century (1901–1980) due to stationarity and absence of trends in air temperature and precipitation (Lapin, 2013).

Anomalies (deviations from the long-term means) of annual precipitation, air temperature, permanent snow cover duration, maximum winter snow depth and the number of days with new snow as a surrogate for the number of days with solid precipitation at both stations are calculated and analysed. Permanent snow cover is defined in agreement with previous climatological studies in the Tatra Mountains as a period (in days) with snow cover depth 1 cm and more that was not interrupted for more than 3 successive days (Briedoň et al., 1974). Number of days with snowfall is calculated from the daily snow depth records as a positive difference of snow depth on the current and previous days.

Daily precipitation data from Kasprowy Wierch and Skalnaté Pleso are also used to analyse the frequency of wet and dry periods with varying durations and days with precipitation that could cause flood hazard. Such an analysis could indicate changes in temporal variability of the main driver of floods and droughts (precipitation). Number of short-(uninterrupted duration of 1–5 days), mid- (6–9 days) and long term- (more than 10 days) wet and dry periods in individual years are calculated. Small, medium and extreme risk of flooding is assumed when daily precipitation is 40–60 mm, 60–90 mm and above 90 mm, respectively. The criteria defining the above wet/dry periods and flood hazards are taken from a similar analysis conducted by Bičárová and Holko (2013).

Structural changes in the time series

Meteorological and hydrological data vary in cycles (e.g., Pekárová and Pekár, 2007). We use the wavelet transform (WT) method to determine oscillations and periodicities in daily time series of catchment precipitation, air temperature and runoff in the Jalovecký Creek catchment. The same analysis is conducted for the time series of point precipitation and air temperature from meteorological stations at Kasprowy Wierch and Skalnaté Pleso to compare the catchment (interpolated) and station (directly measured) climatic data.

The WT method searches for wavelet coefficients which are used to estimate the power spectrum. The wavelet coefficients form a scalogram which characterises distribution of the spectral density of the time series (Fig. 3). The horizontal axis of a scalogram denotes time (i.e., the duration of a signal), while the vertical axis denotes period (i.e., the cyclical components). The values of the wavelet coefficients are identified by the colour – the highest values are shown in red. The white line in the scalogram encompasses an area with statistically significant periodicity (i.e., the cycle with certain period). The global wavelet spectrum (averaged scalogram) on the right side of the scalogram indicates the periodicity. The section of the

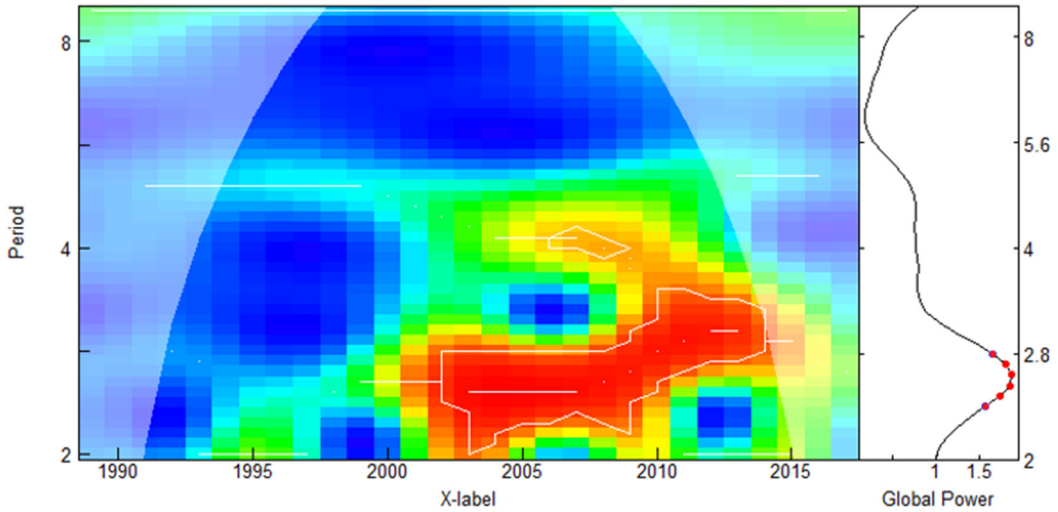

Fig. 3. Scalogram and its components (explained in the text); the red points shown on the right side of the scalogram identify the cycle with a statistically significant period of duration approximately 2.6 years that started approximately in 2003 and ended in 2013 (as indicated by the white line in the coloured raster encompassing the red wavelet coefficients).

scalogram outside the cupola shape represents an area with problematic counting of wavelet coefficients (e.g., because of the edge effects; Sabo, 2012). The WaveletCo package (Tian and Cazelles, 2013) in R software environment is used in the WT method application. More details about the scalogram and the WT method can be found in Daubechies et al. (1992) and Torrence and Compo (1998).

Water balance

Temporal variability of annual catchment precipitation, runoff and runoff coefficients in the Jalovecký Creek catchment is explored first. Then, the same data aggregated for the summer months (June to September) are examined. The idea behind the analysis is to check if the storage/release of water from the catchment given by the relationship between catchment precipitation and runoff changed in the study period.

Hydrological response of the catchment

Runoff response to snowmelt or rainfall is another indicator of changes in catchment hydrological cycle. We use flashiness index calculated from daily discharges and characteristics of runoff events derived from hourly discharges to investigate possible changes in catchment hydrological response.

Flashiness index

Flashiness index of streamflow is quantified by the ratio of absolute day-to-day fluctuations of streamflow relative to total flow in a year (Baker et al., 2004):

$$FI_y = \frac{\sum_{i=1}^{n} |q_i - q_{i-1}|}{\sum_{i=1}^{n} q_i} \quad (1)$$

where FI is the flashiness index, q is the mean daily discharge, i is day, n = 365 (366) and y indicates the year of estimation.

The flashiness index is a dimensionless index which ranges between 0 and 2 (Fongers et al., 2007). Zero represents an absolutely constant flow; increasing *FIy* values indicate increasing flashiness (fluctuations) of streamflow.

Runoff events characteristics

Catchment hourly discharge in the period 1989–2018 was about 0.73 $m^3\ s^{-1}$. About 80% of measured discharges were smaller than 1.0 $m^3\ s^{-1}$ and discharges exceeding 2.2 $m^3\ s^{-1}$ represent only about 6% of measured values. These values help to determine the criteria for selection of runoff events which is a subjective procedure. The hourly discharge data are used to analyse the total number of runoff events with peakflow exceeding 1 $m^3\ s^{-1}$ in the entire hydrological year and in the summer period (June to September). Annual and seasonal maximum discharges and the date of their occurrence in winter (December–February), spring (March–May), summer (June–September) and autumn (October–November) periods of individual years are evaluated as well.

Runoff response to rainfall does not reflect only current meteorological and catchment conditions such as rainfall amount, intensity and spatial distribution, catchment wetness state, etc. It can also indicate the change in conditions affecting runoff formation such as increasing areas producing overland flow (deforested or compacted areas), change in catchment storage, vegetation cover, etc. Summer is the period of maximum annual precipitation in the study catchment. Frequent occurrence of summer rains results in complex runoff events. Determination of characteristics of such events is complicated, because the ends and beginnings of the events overlap. Therefore, we select and analyse only simple runoff events in summer periods (June-September). Runoff events that start and end at discharges less than 1 $m^3\ s^{-1}$ and have peak discharge at least two times greater than the discharge at the beginning of the event are taken into account. The following characteristics of the simple runoff events are determined from the hourly discharge data:

- date and discharge at the beginning of an event (T_0 and Q_0)
- date and discharge at the peak (T_{max} and Q_{max})
- date of the quick flow termination (T_{end} and Q_{end})
- daily catchment rainfall on the day when the peakflow occured (hourly rainfall data are not available for the entire study period)

The quick flow is separated by the Eckhardt filter (Eckhardt, 2005) that was previously shown to provide results similar to

isotopic hydrograph separation in the Jalovecký Creek catchment (Holko and Špánková, 2014). The filter has two parameters. The value of filter parameter alpha is set to 0.95, maximum baseflow index is set to 0.90. Intersection of the hydrograph with the quick flow given by the Eckhardt filter determines the quick flow termination.

The above listed runoff events characteristics allow calculation of hydrograph increasing limb duration, rate of discharge increase until the peakflow, duration and intensity of discharge decrease until the quick flow termination, total duration of an event and the rough estimate of the runoff coefficient (having only daily precipitation). Variability of all characteristics in summer periods 1989–2018 is examined with the aim to search for trends or changes.

Runoff variability

Catchment runoff represents a spatially integrated characteristic which is measured with the highest accuracy compared to other components of the water balance equation. Daily discharge is used in this study to examine a number of runoff characteristics. They include monthly flows (i.e., mean monthly discharges) and flow minima and maxima (1-day, 3-day, 7-day, 30-day and 90-day), baseflow, dates of minimum and maximum annual discharges, number of flow reversals (changes from increasing to decreasing discharge and vice versa) and characteristics of extreme low flows, high flow pulses, small floods and large floods (peak, duration, time, frequency). The analysis is conducted using the IHA software (The Nature Conservancy, 2009). Classification of flows into extremely low, low, high and of floods into small and large, is given by statistics of measured discharge data mentioned above and the threshold values shown in Fig. 4. Variability of all characteristics in the study period is examined.

Snow cover

Climatic variability affects snow cover and the changes in snow cover can be manifested in catchment runoff. Examination of measured SWE data in this study is focused on the variability of maximum winter SWE at different elevations (measured) and in the entire catchment (simulated). We also examine the total amount of snow accumulated in the catchment (simulated) in individual winters defined as periods from November 1st until May 31st. The number of days with negative mean daily air temperature in December to April and total precipitation amount on those days at catchment mean elevation (1500 m a.s.l.) are examined as well.

RESULTS

Climatic conditions in the study period with regard to the climatic standard

Air temperature data from the high-elevation meteorological stations at Kasprowy Wierch and Skalnaté Pleso show that study period 1989–2018 is warmer compared to the climatic standard period 1951–1980 (Fig. 5). Air temperature in the study period is in almost all years 0.1°C to 2.4°C higher than in the climatic standard period. In contrast to air temperature, the two stations give a different message about precipitation. While annual precipitation at Kasprowy Wierch (the mountain ridge position) in the study period does not differ from that in the climatic standard period, at Skalnaté Pleso (the lee position) it is in the majority of years greater than during the climatic standard period.

Similarly to precipitation, anomalies of snow cover characteristics (Fig. 6) do not indicate clear changes with regard to the climatic standard period. The patterns at Kasprowy Wierch and Skalnaté Pleso differ. Duration of permanent snow cover at Kasprowy Wierch is much less variable than at Skalnaté Pleso, but clear trends are not visible at any of the two stations. Maximum winter snow depth (SD_{max}) at Skalnaté Pleso is smaller than the mean of climatic standard period already since the 1960'. Such a behavior is not observed at Kasprowy Wierch where positive and negative deviations are more regular during both climatic standard and study periods. Negative deviations are prevailing at both stations in the period 1968–1991.

Patterns of the number of days with new snow during the winter used as a surrogate for the frequency of snowfalls (on the daily scale) at the two stations differ approximately until the mid-1970's (Fig. 7). The Kasprowy Wierch station exhibits a relatively regular variability of positive and negative anomalies while the Skalnaté Pleso station shows positive deviations until

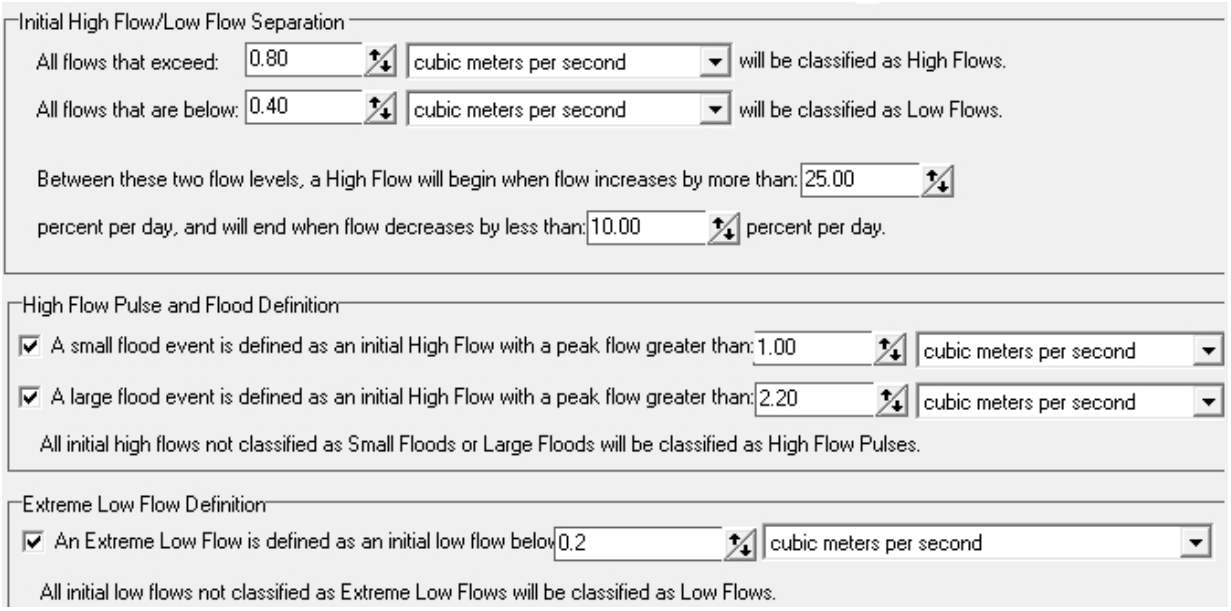

Fig. 4. Criteria for classification of flows and flood events; a window from the IHA software.

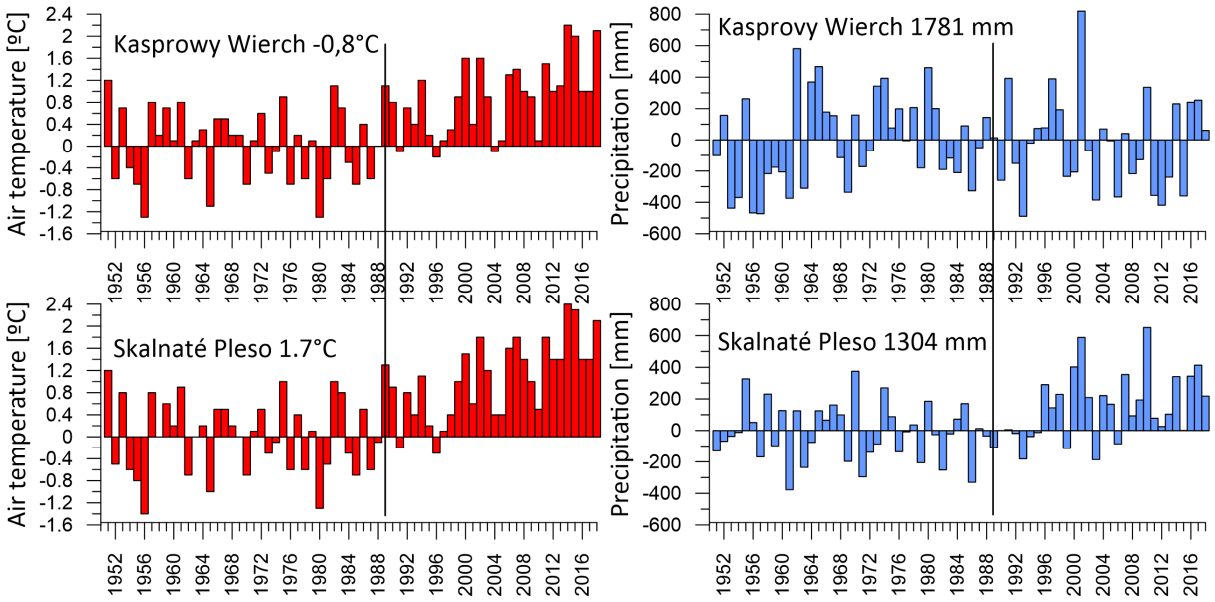

Fig. 5. Anomalies of mean annual air temperature (left) and annual precipitation (right) at the high-mountain meteorological stations Kasprowy Wierch and Skalnaté Pleso in the years 1951–2018; the numbers show the mean values calculated for the climatic standard period (1951–1980); the vertical lines indicate the beginning of the study period (1989–2018).

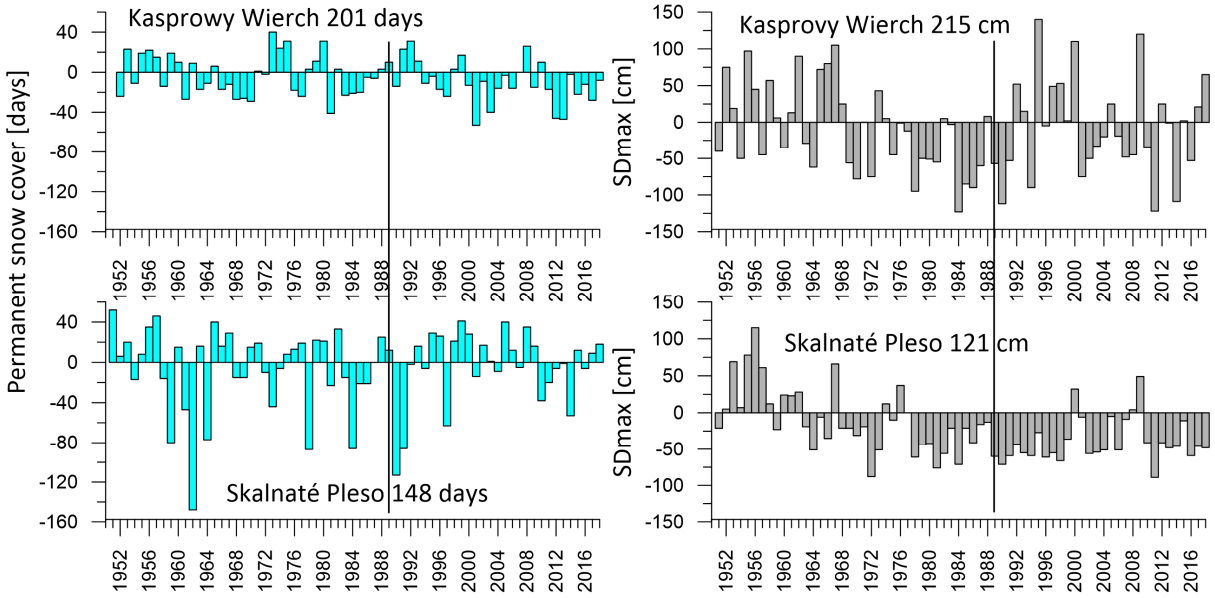

Fig. 6. Anomalies of permanent snow cover duration (left) and maximum winter snow depth (right) at Kasprowy Wierch and Skalnaté Pleso in the years 1951–2018; the numbers show the mean values calculated for the climatic standard period (1951–1980); the vertical lines indicate the beginning of the study period (1989–2018).

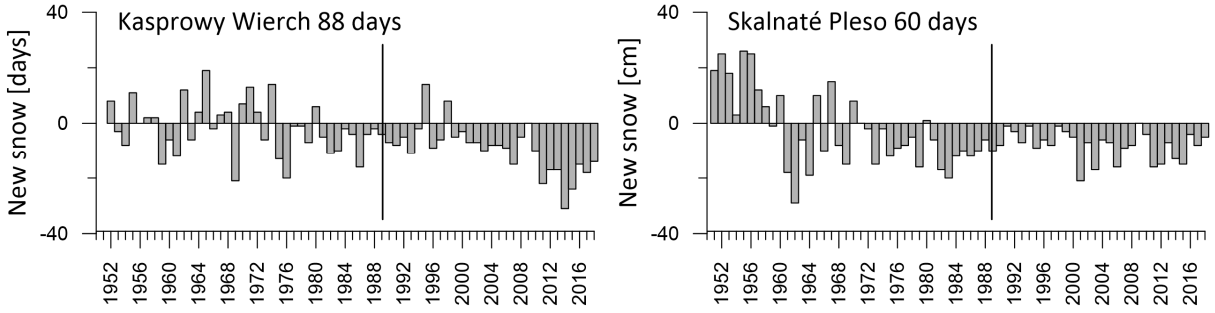

Fig. 7. Anomalies of the number of days with new snow (a surrogate for the number of daily snowfalls during a winter) at Kasprowy Wierch and Skalnaté Pleso in the years 1951–2018; the numbers show the mean values calculated for the climatic standard period (1951–1980); the lines indicate the beginning of the study period (1989–2018).

1962 and mostly negative variations after that. Negative deviations, i.e. fewer days with new snow are recorded at Skalnaté Pleso since the beginning of the 1970's and at Kasprowy Wierch since the mid-1970's. Greater negative deviations are observed at Kasprowy Wierch since 2011.

The snow cover data show that duration of permanent snow cover during the study period was similar to that of the climatic standard. Maximum snow depth at Skalnaté Pleso and number of days with new snow at both stations in the study period were smaller than during the climatic standard period, but it was like that already since the 1970's, i.e. almost two decades earlier. Negative deviations of the number of days with new snow at Kasprowy Wierch became greater since 2011.

Numbers of wet and dry periods (see Methodology) do not indicate trends or abrupt changes in the study period. According to precipitation data from Kasprowy Wierch (and Skalnaté Pleso), there are on average 43 (47) short-term wet periods, 9 (9) mid-term wet periods and 4 (2) long-term wet periods in a year. Average numbers of the short-, mid- and long term- dry periods are 51 (52), 4 (5) and 1 (1) per year, respectively. There are about 2–3 days with precipitation at each station representing small and medium flood risk per year. The number of days with precipitation representing extreme flood risk varies from 0 to 3 per year, but in most years such a precipitation does not occur. Greater number of days with low flood risk precipitation was recorded at Skalnaté Pleso in 2010 (9 days) - the year when a number of floods in the entire Slovakia was observed, in 2014 (7 days) and in 2016 (5 days). In all other years there are no more than four such days at the two stations.

Structural changes in the time series

The scalogram of daily air temperatures in the Jalovecký Creek catchment (Fig. 8a left) indicates a significant cycle with period ranging between 6 and 8 years that occurred approximately between the years 1995–2010. Daily precipitation data do not indicate any significant cycles. Daily runoff (Fig. 8a right) shows a significant cycle with period of 4 years that occurred approximately between 2000 and 2013.

Scalograms for daily precipitation and air temperature at Kasprowy Wierch and Skalnaté Pleso indicate significant cycles only for precipitation at Kasprowy Wierch with period of about 3 years in 1997–2004 (Fig. 8b). Snow depth at both stations shows significant cycles (Fig. 8c) with shorter period at

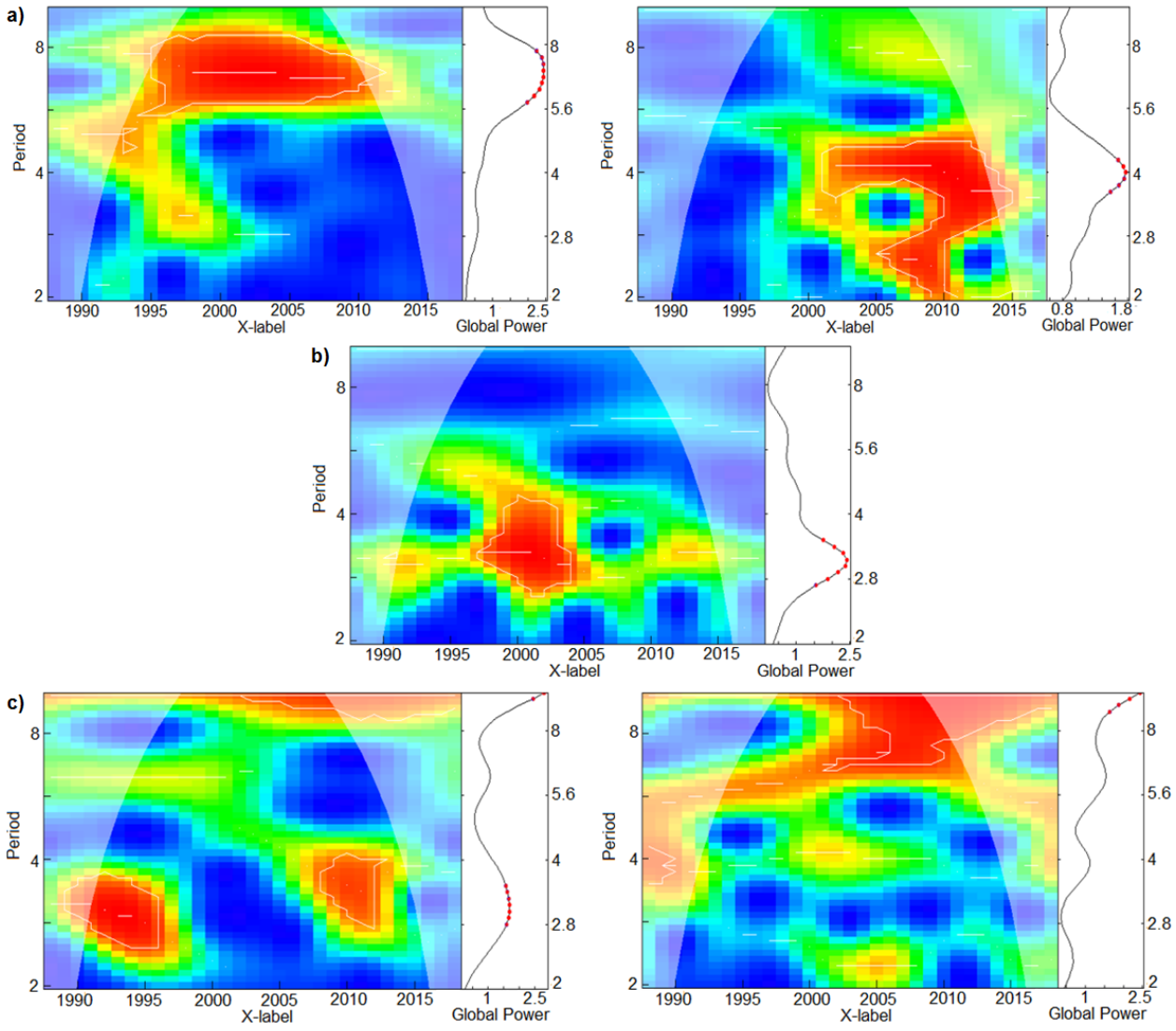

Fig. 8. Scalograms indicating cycles with significant periods revealed from daily data in the hydrological years 1989–2018; a) air temperature (left) and runoff (right) in in the Jalovecký Creek catchment; b) daily precipitation at Kasprowy Wierch c) daily snow depths at Kasprowy Wierch (left) and Skalnaté Pleso (right).

Kasprowy Wierch (about 3–4 years in the years 1990–1997 and 2008–2014) and an insignificant cycle with period of about 8 years in 2004–2010 at Skalnaté Pleso.

Water balance

Annual catchment precipitation and runoff are relatively stable until the mid-1990' (Fig. 9a). Annual runoff coefficients do not vary much until 2001 (Fig. 9b). However, since 2014, they are clearly and permanently higher than before. The annual runoff coefficient was high also in 2010 which was the wettest year on record.

Precipitation and runoff in the summer period (June to September) exhibits a regular variability. Summer runoff coefficients since 2012 (Fig. 9b) are in most years close to the lower range of the values (40% to 50%) calculated for the entire study period. A significant difference between the annual and summer runoff coefficients is visible since 2014.

Scatterplots of precipitation against runoff have smaller vertical scatter in the summer compared to the annual data (Fig. 10). The annual data clearly show higher runoff coefficients in years 2015, 2016, 2017 and 2010. Wetter summers that plot apart from the points representing other years occurred in 2010 and 2001. The driest year on the record is the year 2003.

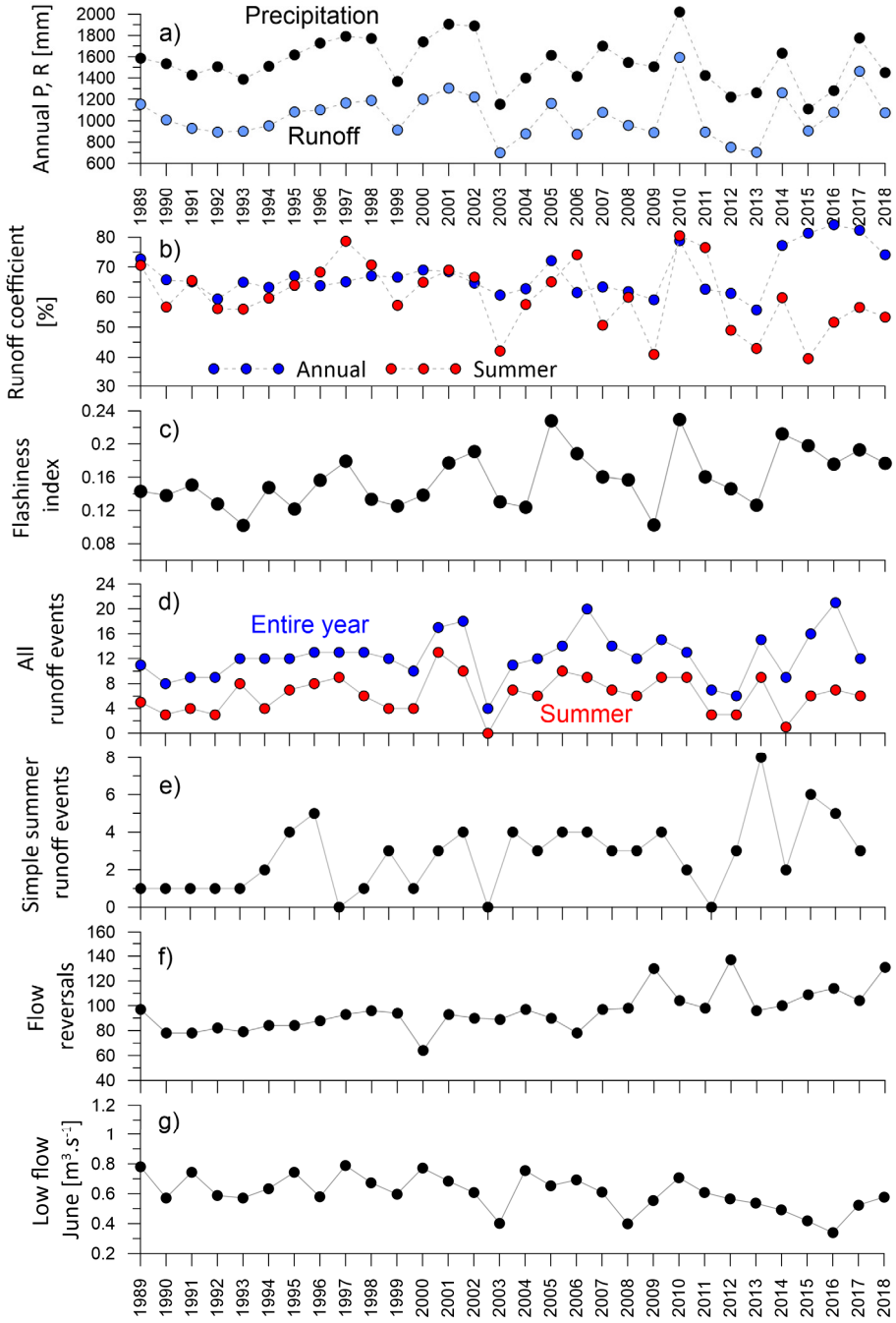

Fig. 9. Temporal variability of selected characteristics in the hydrological years 1989–2018; a) annual precipitation and runoff; b) annual and summer (June to September) runoff coefficients; c) flashiness index; d) number of runoff events (both simple and complex) in the entire hydrological year (November–October) and in the summer period (June–September); e) number of simple summer runoff events; f) number of flow reversals; g) June low flow.

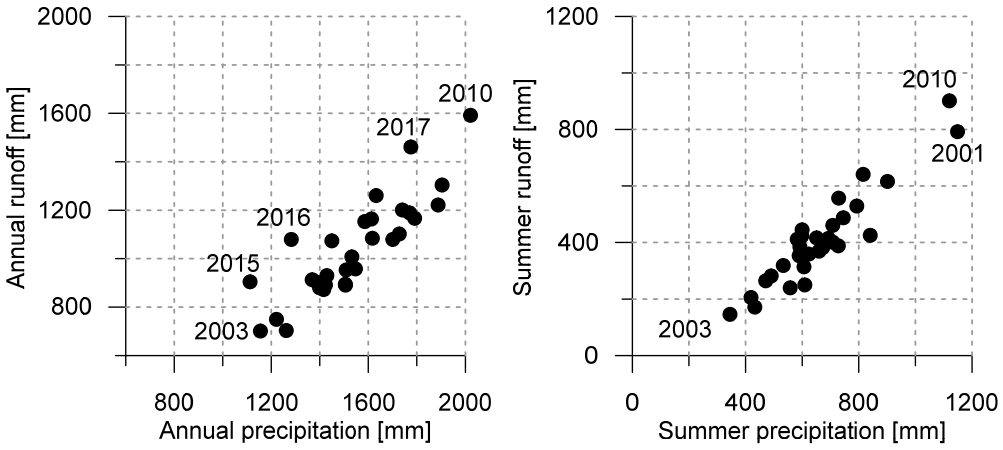

Fig. 10. Scatterplots of annual (November to October) and summer (June to September) precipitation and runoff in the hydrological years 1989–2018; note that scales of the axes differ.

The water balance data show that greater part of precipitation began to run off from the catchment in the last years of the study period. Because such a behaviour was not observed for the data from summer periods (June to September), it indicates a change in the colder part of the year. The same is suggested by the great difference between summer and annual runoff coefficients since 2014.

Hydrological response of the catchment

The flashiness index (Fig. 9c) is smaller at the beginning of the study period. Later, greater variability becomes visible between 2005 and 2013. The values since 2014 are comparatively greater and their interannual variability is smaller than before 2014.

The number of runoff events in the entire hydrological year is relatively stable (about 9–13 events per year) until the year of 2000. After 2000, the variability increases (Fig. 9d). About a half of runoff events occurs in summer. The share of summer events in the annual totals does not change over the study period. The lowest number of runoff events in the entire year is recorded in the hydrological year 2003 which was the driest year in the study period. No summer runoff events as defined in Methodology occurred in that year.

Annual and seasonal (spring, summer, autumn, winter) discharge maxima and days of their occurrence do not indicate any trend or change in variability. However, three highest annual discharge maxima (22.5 $m^3 s^{-1}$, 17.9 $m^3 s^{-1}$, and 18.0 $m^3 s^{-1}$) are recorded in 2014, 2017 and 2018, respectively, i.e. in the last five years of the study period. Annual maximum in 2014 was observed in spring (mid-May). It was caused by a combination of snowmelt and rainfall that produced the greatest peak discharge measured in the entire study period (Danko, 2014). Annual maxima in 2017 and 2018 are recorded in spring (end of April) and summer (mid-July), respectively. The analysis of seasonal maxima shows that the highest values often occurred in the last years of the study period as well (in spring 2014 and 2017, summer 2018, autumn 2016).

Majority of simple summer runoff events characteristics does not indicate trends over the study period. However, changing variability or different behaviour in some periods is found for some characteristics. Characteristics of all 82 events show greater number of events at the end of the study period (2014, 2016, 2017). Ony one simple summer runoff event is mostly recorded until 2000 (in 8 out of 12 summers between 1989 and 2000) while the typical number of events since 2001 increases to 3–4 (Fig. 9e). Characteristics of the entire pool of simple summer runoff events do not indicate any trends or changes in the study period. Therefore, we focused on the events with the fastest response, i.e. with the shortest rising limbs of the hydrographs (1–4 hours from the beginning of an event). These events represent about one third of all selected runoff events (28 out of 82). Shorter recessions of the hydrograph (until the quick flow termination) appear after 2006 (Fig. 11). The duration of runoff events becomes shorter since 2006 as well (approximately 7–8 hours instead of 12 hours).

Runoff variability

The most pronounced changes in characteristics derived from daily flows are found for the number of runoff reversals and June mean and low flows. Number of flow reversals (Fig. 9f) remains high since 2015, although the two highest values occurred in 2009 and 2012. June flows (mean discharge in June) are relatively small after 2012. Low flows in June (Fig. 9g) show similar behaviour as the June flows.

The daily flow data indicate smaller discharge increase and faster decrease during runoff events since 2003 as well. Other examined flow characteristics mentioned in Methodology, among them flow maxima and minima, do not indicate clear trends or changes in the behavior in the study period.

Snow cover

Measured data from snow courses located at the altitudes 1100 to 1700 m a.s.l. do not indicate any clear change in SWE in the study period. The data suggest that SWE maxima in the last winters (2013–2018) are smaller than in the previous period when greater SWE maxima occurred in 2000, 2002, 2005, 2009, 2012 (Fig. 12b). However, maximum in winter 2019 (the first winter after the study period) which is not shown here, is greater again.

The simulated amount of snow accumulated in the catchment in individual winters (Fig. 12c) does not show any apparent changes either. The same holds for the climatic conditions in the period which is the most important for snow accumulation and melt in the catchment (December to April; Fig. 12a). The number of days with negative/positive mean daily air temperature or total amount of solid/liquid precipitation (as suggested by the mean daily air temperature) exhibit a great variability, but no trends or abrupt changes.

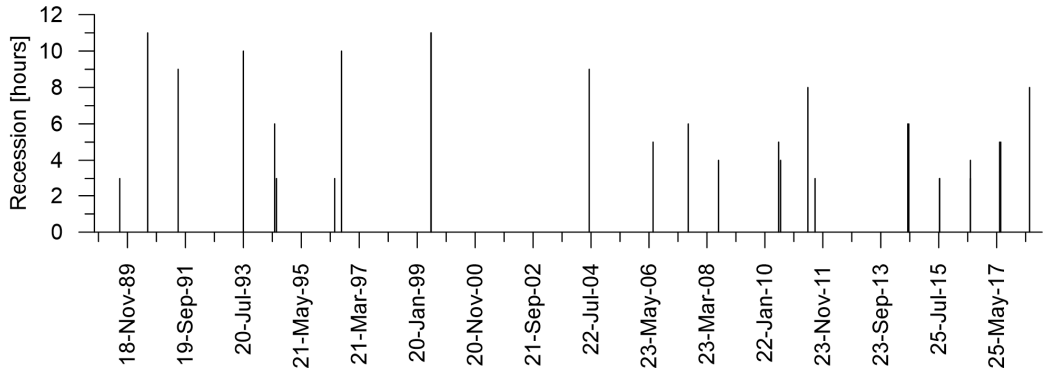

Fig. 11. Duration of runoff recession during simple summer runoff events with short time to peak (up to 4 hours) in the hydrological years 1989–2018.

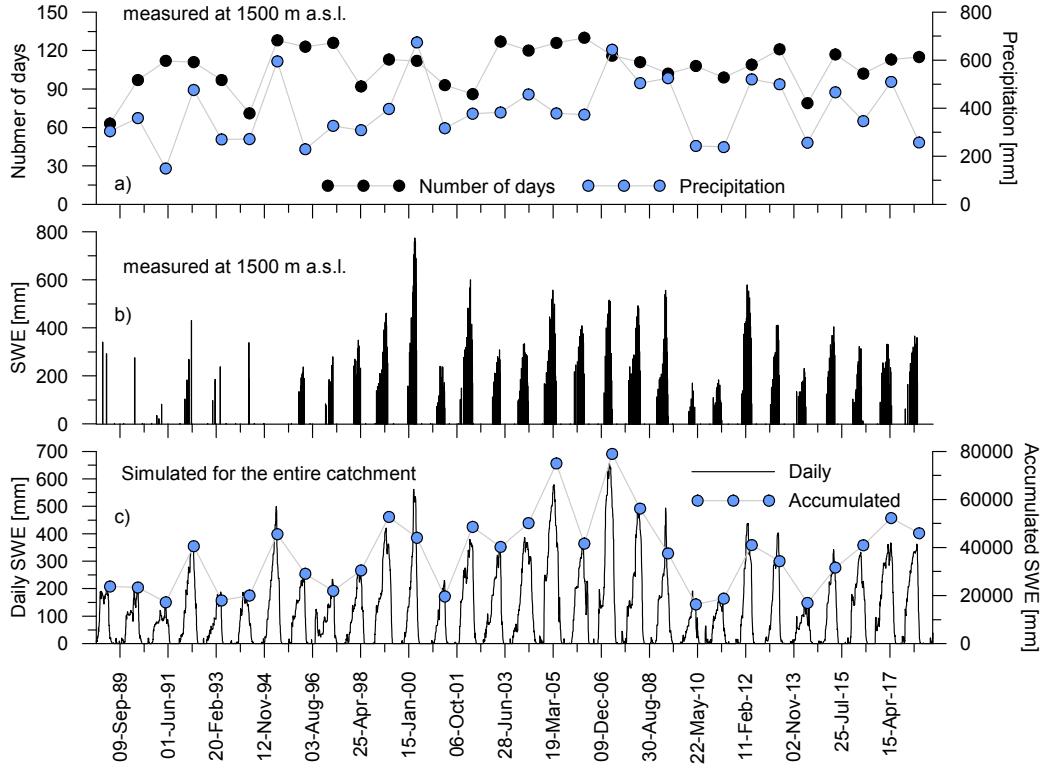

Fig. 12. a) number of days with negative mean daily air temperature in the snow accumulation and melt period (December to April) at catchment mean elevation in winters 1989–2018 and total precipitation on those days; b) SWE measured at the same site during field campaigns (i.e. approximately once in 1–2 weeks); c) MikeSHE simulated catchment daily SWE and snow accumulation over the winter period.

DISCUSSION

Numerous studies reported increasing trends in air temperature in the Tatra Mountains area in the last decades while the conclusions on trends in precipitation and runoff were not so unvivocal (a brief overview is given in Górnik et al., 2017). Precipitation, air temperature and snow cover data from the high-elevated meteorological stations Kasprowy Wierch and Skalnaté Pleso analysed in this study lead to similar result. The study period in which the hydrological cycle in the Jalovecký Creek has been monitored, is warmer than the climatic standard period and the annual air temperatures at the end of the study period are higher than at its beginning. Unlike the air temperature, precipitation patterns at Kasprowy Wierch and Skalnaté Pleso differ. Thus, precipitation data from the two stations do not provide an unambiguous information on whether the study period is wetter or drier than the climatic standard period.

It would be assumed that an increasing air temperature should result in changes of snow cover and runoff characteristics related to snowmelt. However, the changes in snow cover characteristics at Kasprowy Wierch and Skalnaté Pleso during the study period are not confirmed except the decrease in the number of days with new snow at the Kasprowy Wierch station since 2011.

Wavelet analysis is used in geophysical time series processing including climatic and hydrological data since the 1990' (e.g. Pišoft et al., 2004; Qian et al., 2014; Torrence and Compo, 1998). Oscillations found in the Jalovecký Creek catchment runoff do not correspond to the oscillations detected in the air temperature and precipitation as the main local climatic drivers. While the oscillations in the air temperature covered almost the entire study period, in catchment runoff they were found only in its second half. The periodicities in the two data series were different as well (4 years for runoff and 6–8 years for the air temperature). Precipitation did not exhibit any significant oscillations at all.

Oscillations of the areal catchment data (precipitation, air temperature, runoff) differ from those found in the data series measured at meteorological stations Kasprowy Wierch and Skalnaté Pleso. The snow depth data series at Kasprowy Wierch and Skalnaté Pleso show different oscillations as well. Processes affecting the snow cover formation at the two meteorological stations can partially differ due to different position (the mountain ridge versus the leeward, south oriented mountain slope position) and the distance between the stations.

As for the Jalovecký Creek catchment, we expected that oscillations found in catchment runoff would be consistent with those found either in the air temperature or in the precipitation data. Additional work is needed to explain the links among the oscillations found in the data series of the main water balance and climatic components and catchment hydrological cycle. Szolgayova et al. (2014) also found differences among the Danube River discharge, precipitation and air temperature oscillations and periodicities. However, they documented strong correlation between the precipitation and discharge spectra in the low frequency intervals and propagation of the long cycles from precipitation to discharge. Qian et al., 2014 found different significant periods for annual precipitation, air temperature, evapotranspiration and runoff, whereas two periods (7–8 years and 42–43 years) were the same for runoff and meteorological data. Zhang et al. (2015) employed the wavelet coherence to investigate the coherence among inconsistent changes in annual precipitation/potential evapotranspiration and annual streamflow in the Yangtze River basin.

Unlike many time series analyses studies that focused just on one or a few time series, we have attempted to analyse as many data sets describing various aspects of the hydrological cycle in the study catchment as possible. Although the clear changes in snow cover characteristics were not found, some of the time series indicate that hydrological cycle in colder part of the year might be changing (e.g., annual versus summer runoff coefficients, June flows and low flows). Others suggest that hydrological cycle in the catchment was more stable approximately until the end of the 1990'and became more dynamic in the last years of the study period (i.e., higher runoff coefficients, number of flow reversals, flashiness index, number of simple summer runoff events and shorter runoff events recession). However, the trends over the entire study period are not very distinct. Changes in the behaviour of several characteristics are more pronounced in the last five years of the study period.

CONCLUSIONS

The exploratory analysis of numerous data sets does not confirm distinct trends or change points in the pristine mountain catchment of the Jalovecký Creek in hydrological years 1989–2018. The data indicate greater dynamics of the hydrological cycle in the last years of the study period. It is manifested in higher runoff coefficients, number of flow reversals per year or flashiness index, or the fact that most of the greatest annual and seasonal discharge maxima occurred in years 2014–2018. Regular snow cover measurements at different elevations are perhaps the only data series that are not commonly measured in similar small mountain catchments on the long–term basis. An extended snow cover monitoring based on cheap approaches like the soil surface temperature (e.g. Krajčí et al., 2016; Lundquist and Lott, 2008) or time lapse photography (Parajka et al., 2012) could be useful in the long-term monitoring and future evaluations of changes in hydrological cycle in seasonally snow-covered catchments.

Acknowledgements. This study was supported by grants from the Slovak Academy of Sciences VEGA (project No. 2/0065/19) and the Slovak Research and Development Agency (APVV) (project No. 15-0497).

Data collection was supported by project ITMS 26210120009 Infrastructure completion of hydrological research stations, of the Research & Development Operational Programme funded by the ERDF. The work of PS was supported by the Stefan Schwarz grant of the Slovak Academy of Sciences.

REFERENCES

Bartík, M., Holko, L., Jančo, M., Škvarenina, K., Danko, M., Kostka, Z., 2019. Influence of mountain spruce forest dieback on snow accumulation and melt. J. Hydrol. Hydromech., 67, 2019, 1, 59–69. DOI: 10.2478/johh-2018-0022.

Baker, D.B., Richards, P.R., Loftus, T.T., Kramer, J.W., 2004. A new flashiness index: characteristics and applications to Midwestern Rivers and streams. Journal of the American Water Resources Association, 4, 503–522.

Bičárová, S., Holko, L., 2013. Changes of characteristics of daily precipitation and runoff in the High Tatra Mountains, Slovakia over the last fifty years. Contributions to Geophysics and Geodesy, 43, 2, 157–177.

Blöschl, G. et al., 2019. Twenty-three Unsolved Problems in Hydrology (UPH) – a community perspective, Hydrological Sciences Journal, 64. DOI: 10.1080/02626667.2019.1620507.

Briedoň. V., Chomicz, K., Konček, M., 1974. Snow conditions. In: Konček, M. (Ed.): Klíma Tatier. Slovenská akadémia vied, pp. 537–600. (In Slovak.)

Buishand, T.A., 1984. Tests for detecting a shift in the mean of hydrological time series. J. Hydrol., 73, 51–69. https://doi.org/10.1016/0022-1694(84)90032-5.

Conte, L.Ch., Bayer, D.M., Bayer, F.M., 2019. Bootstrap Pettitt test for detecting change points in hydroclimatological data: case study of Itaipu hydroelectric plant, Brazil. Hydrological Sciences Journal, 64, 1312–1326. DOI: 10.1080/02626667.2019.1632461.

Chiverton, A., Hannaford, J., Holman, I.P., Corstanje, R., Prudhomme, C., Hess, T.M., Bloomfield, J.P., 2015. Using variograms to detect and attribute hydrological change. Hydrol. Earth Syst. Sci., 19, 2395–2408. DOI: 10.5194/hess-19-2395-2015.

Danko, M., 2014. Reconstruction of extreme flood wave, 16th May 2014, Jalovecký Creek catchment. Acta Hydrologica Slovaca, 15, 2, 298–307. (In Slovak.)

Danko, M., Holko, L., Kostka, Z., Tachecí, P., 2015. Simulation of snow water equivalent, snowmelt rate and runoff in mountain catchment during winter period. Acta Hydrologica Slovaca, 16, 1, 42–50. (In Slovak.)

Daubechies, I., Mallat, S., Willsky, A., 1992. Special issue on wavelet transforms and multiresolution signal analysis. IEEE Trans. Information Theory, 38, 2, 528–531.

Eckhardt, K., 2005. How to construct recursive digital filters for baseflow separation. Hydrological Processes, 19, 507–515.

Fongers, D., Manning, K., Rathbun, J., 2007. Application of the Richards-Baker Flashiness Index to Gage Michigan rivers and streams. DEQ Michigan's Nonpoint Source Program, 102 p.

Górnik, M., 2020. Changing trends of river flows in the Upper Vistula basin (East-Central Europe). Acta Geophysica, https://doi.org/10.1007/s11600-020-00400-9

Górnik, M., Holko, L., Pociask-Karteczka, J., Bičárová, S., 2017. Variability of precipitation and runoff in the entire

High Tatra Mountains in the period 1961-2010. Prace Geograficzne, zeszyt 151, 2017, 53–74. DOI: 10.4467/20833113PG.17.022.8034.

Hlaváčiková, H., Holko, L., Danko, M., Novák, V., 2019. Estimation of macropore flow characteristics in stony soils of a small mountain catchment. Journal of Hydrology, 574, 1176–1187.

Holko, L., Hlavčo, J., Kostka, Z., 2014. Spatial distribution of precipitation in a mountain catchment. Acta Hydrologica Slovaca, 15, 1, 102–109. (In Slovak.)

Holko, L., Kostka, Z., 2008. Hydrological characteristics of snow cover in the Western Tatra Mountains in winters 1987-2008. Folia Geographica, series Geographica Physica, 39, 63–77.

Holko, L., Škvarenina, J., Kostka, Z., Frič, M., Staroň, J., 2009. Impact of spruce forest on rainfall interception and seasonal snow cover evolution in the Western Tatra Mountains, Slovakia. Biologia, 64, 3, 594–599. DOI: 10.2478/s11756-009-0087-6.

Holko, L., Španková, D., 2014. Baseflow in the mountain catchment of the Jalovecký Creek in hydrological years 1988-2013. Acta Hydrologica Slovaca, 15, 2, 229–237. (In Slovak.)

Holko, L., Danko, M., Sleziak, P., 2020. Analysis of changes in hydrological cycle of a pristine mountain catchment. 2. Isotopic data, trend and attribution analyses. Journal of Hydrology and Hydromechanics, 68, 2, 192–199.

Hurst, H.E., 1951. Long-term storage capacity of reservoirs. Trans. Amer. Soc. Civil Eng., 116, 770–808.

Klemeš, V., 1974. The Hurst phenomenon: A puzzle? Water Resources Research, 10, 4, 675–688. https://doi.org/10.1029/WR010i004p00675.

Klemeš, V., 2000. Geophysical Time Series and Climatic Change (A Sceptic's View). In: Common sense and other heresies: selected papers on hydrology and water resources engineering. Canadian Water Resources Association, pp. 311–331.

Kohler, T., Maselli, D., 2009. Mountains and Climate Change - From Understanding to Action. Published by Geographica Bernensia with the support of the Swiss Agency for Development and Cooperation (SDC), and an international team of contributors, Bern, 75 p.

Kostka, Z., Holko, L., 1997. Soil moisture and runoff generation in small mountain basin. Institute of Hydrology SAS. Slovak Committee for Hydrology, Bratislava, 84 p.

Koutsoyiannis, D., 2003. Climate change, the Hurst phenomenon, and hydrological statistics. Hydrological Sciences Journal, 48, 1, 3–24. DOI: 10.1623/hysj.48.1.3.43481.

Krajčí, P., Danko, M., Hlavčo, J., Kostka, Z., Holko, L., 2016. Experimental measurements for improved understanding and simulation of snowmelt events in the Western Tatra Mountains. J. Hydrol. Hydromech., 64, 4, 316–328. DOI: 10.1515/johh-2016-0038.

Kundzewicz, Z.W., Robson, A., 2004. Change detection in hydrological records – a review of the methodology. Hydrological Sciences Journal, 49, 1, 7–19.

Lapin, M., 2013. Which temperature standard is the best for practical use? http://www.milanlapin.estranky.sk/clanky/coje-to-klimaticky-normal--/; assessed on April 4, 2019.

Lettenmaier, D.P., Burges, S.J., 1978. Climate change: Detection and its impact on hydrologic design. Water Resources Research, 14, 4, 679–687. https://doi.org/10.1029/WR014i004p00679

Lundquist, J.D., Lott, F., 2008. Using inexpensive temperature sensors to monitor the duration and heterogeneity of snow-covered areas, Water Resour. Res., 44, W00D16. DOI: 10.1029/2008WR007035.

Mastrotheodoros, T., Pappas, C., Molnar, P., Burlando, P., Manoli, G., Parajka, J., Rigon, R., Szeles, B., Bottazzi, M., Hadjidoukas, P., Fatichi, S., 2020. More green and less blue water in the Alps during warmer summers. Nature Climate Change, 10, 155–161.

Merz, B., Vorogushyn, S., Uhlemann, S., Delgado, J., Hundecha, Y., 2012. HESS Opinions "More efforts and scientific rigour are needed to attribute trends in flood time series", Hydrol. Earth Syst. Sci., 16, 1379–1387. DOI: 10.5194/hess-16-1379-2012.

Parajka, J., Haas, P., Kirnbauer, R., Jansa, J., Blöschl, G., 2012. Potential of time-lapse photography of snow for hydrological purposes at the small catchment scale. Hydrol. Process., 26, 3327–3337. DOI: 10.1002/hyp.8389.

Parajka, J., Holko, L., Kostka, Z., Blöschl, G., 2012. MODIS snow cover mapping accuracy in a small mountain catchment – comparison between open and forest sites. Hydrol. Earth Syst. Sci., 16, 2365–2377. DOI:10.5194/hess-16-2365-2012.

Pekárová, P., Pekár, J., 2007. Teleconnections of Inter-Annual Streamflow Fluctuation in Slovakia with Arctic Oscillation, North Atlantic Oscillation, Southern Oscillation, and Quasi-Biennial Oscillation Phenomena. Advances in Atmospheric Sciences, 24, 4, 655–663.

Pettitt, A.N., 1979. A non-parametric approach to the change point problem. Journal of the Royal Statistical Society. Series C (Applied Statistics), 28, 2, 126–135. DOI: 10.2307/2346729.

Pišoft, P., Kalvová, J., Brázdil, R., 2004. Cycles and trends in the Czech temperature series uning wavelet transforms. Int. J. Climatol., 24, 1661–1670.

Qian, K., Wang, X.-S., Lv, J., Wan, L., 2014. The wavelet correlative analysis of climatic impacts on runoff in the source region of Yangtze River, in China. Int. J. Climatol., 34, 2019–2032.

Sabo, M., 2012. How to analyze time series with wavelet transform. Acta Hydrologica Slovaca, 13, 1, 233–241. (In Slovak.)

Sharma, S., Swayne, D.W., Obimbo, C., 2016. Trend analysis and change point techniques: a survey. Energ. Ecol. Environ., 1, 3, 123–130. DOI 10.1007/s40974-016-0011-1.

Szolgayova, E., Parajka, J., Blöschl, G., Bucher, C., 2014. Long term variability of the Danube River flow and its relation to precipitation and air temperature. Journal of Hydrology, 519, 871–880.

The Nature Conservancy, 2009. Indicators of Hydrologic Alteration Version 7.1 User's manual.

Tian, H., Cazelles, B., 2013. WaveletCo: Wavelet Coherence Analysis. http://www2.uaem.mx/r-mirror/web/packages/WaveletCo/WaveletCo.pdf.

Torrence, C., Compo, G.P., 1998. A Practical Guide to Wavelet Analysis. Bulletin of the American Meteorological Society, 79, 1, 61–78.

Xiong, L., Jiang, C., Xu, C.-Y., Yu, K.-X., Guo, S., 2015. A framework of changepoint detection for multivariate hydrological series, Water Resour. Res., 51, 8198–8217. DOI: 10.1002/2015WR017677.

Zégre, N., Skaugset, A. E., Som, N.A., McDonnell, J.J., Ganio, L.M., 2010. In lieu of the paired catchment approach: Hydrologic model change detection at the catchment scale. Water Resour. Res., 46, W11544. DOI: 10.1029/2009WR008601.

Zhang, D., Hong, H., Zhang, Q., Li, X., 2015. Attribution of the changes in annual streamflow in the Yangtze River basin over the past 146 years. Theor. Appl. Climatol., 119, 323–332.

Received 30 September 2019
Accepted 21 February 2020

J. Hydrol. Hydromech., 68, 2020, 2, 192–199
DOI: 10.2478/johh-2020-0011
ISSN 1338-4333

sciendo Journal of Hydrology and Hydromechanics

Analysis of changes in hydrological cycle of a pristine mountain catchment. 2. Isotopic data, trend and attribution analyses

Ladislav Holko*, Michal Danko, Patrik Sleziak

Institute of Hydrology of the Slovak Academy of Sciences, Dúbravská cesta 9, 841 04 Bratislava, Slovakia.
* Corresponding author. E-mail: holko@uh.savba.sk

Abstract: $\delta^{18}O$ in precipitation at station Liptovský Mikuláš (about 8.5 km south from the outlet of the Jalovecký Creek catchment) remains constantly higher since 2014 that might be related to greater evaporation in the region of origin of the air masses bringing precipitation to the studied part of central Europe. Increased $\delta^{18}O$ values are reflected also in the Jalovecký Creek catchment runoff. Seasonality of $\delta^{18}O$ in the Jalovecký Creek became less pronounced since 2014. The most significant trends found in annual hydrological data series from the catchment in the study period 1989–2018 have the correlation coefficients 0.4 to 0.7. These trends are found in the number of flow reversals (change from increasing to decreasing discharge and vice versa), June low flow, number of simple runoff events in summer months (June to September) and the flashiness index. The attribution analysis suggests that drivers responsible for the changes in these data series include the number of periods with precipitation six and more days long, total precipitation amount in February to June, number of days with precipitation in June to September and total precipitation in May on days with daily totals 10 mm and more, respectively. The coefficients of determination show that linear regressions between the drivers and supposedly changed data series explain only about 31% to 36% of the variability. Most of the change points detected in the time series by the Wild Binary Segmentation method occur in the second and third decades of the study period. Both hydrometric and isotopic data indicate that hydrological cycle in the catchment after 2014 became different than before.

Keywords: Oxygen isotope in precipitation and runoff; Time series; Trends and break points.

INTRODUCTION

Stable isotopes of oxygen and hydrogen in water are commonly used as tracers in climatology, hydrology and ecohydrology to determine sources of water, investigate the runoff formation and mean transit times of water in catchments (e.g., Clark and Fritz, 1997; Gat, 1996; Kendall and McDonnell, 1998). The long-term data on isotopic composition of precipitation and runoff can be helpful in identification of climatic variability. Rozanski et al. (1992) concluded that long-term changes in isotopic composition of precipitation over mid- and high-latitudes closely followed the long-term changes of surface air temperature. They also noted that isotopic composition of precipitation in mountain regions seemed to be more sensitive to the long-term air temperature fluctuations than in the low-altitude regions. Kendall and Coplen (2001) showed that isotopic composition of modern precipitation is well reflected in the rivers and that the isotopic composition of the rivers represents the best available dataset on spatial distribution of stable isotopes in precipitation. Rank et al. (2014) reported significant changes in stable isotopic composition of the Danube River in Vienna on a decadal scale and attributed the remarkable increase in $\delta^{18}O$ in the 1980's mainly to temperature rising. Panarello and Dapeña (2009) used 10 years of monthly data on the isotopic composition of the Paraná River to conclude that the isotopic composition of the river is defined by the large-scale meteorological phenomena ENSO and ITCZ.

Concentration of heavy isotopes in water vapour above the oceans depends primarily on the air temperature. Increasing global temperature should therefore be reflected in an increased concentration of heavy isotopes in water vapour above the oceans caused by greater evaporation. The isotopic composition of precipitation on the continents differs from that of water vapour above the oceans. However, conditions at the source regions of vapour are among the main factors controlling the isotopic composition of precipitation over the mid- and high-latitudes (Rozanski et al., 1992). Therefore, we hypothetise that greater concentrations of heavy isotopes in the original vapour should be reflected also in continental precipitation and the long term data on the isotopic composition of precipitation and runoff could be used to detect the change in evaporation from the oceans.

Despite an obvious link between the isotopic composition of precipitation and local air temperature, the correlation is often not very strong. Stumpp et al. (2014) found an increase in oxygen 18 concentrations only at 20 out of 28 stations in Germany while the air temperature increased at almost all stations. They concluded that changes in isotopic composition of precipitation are influenced also by local factors which need to be further investigated. Pirk (2015) and Reckerth et al. (2017) presented the evaluation of the long-term data (12 or 26 years) on isotopic composition of rivers representing nine large catchments in Germany. They confirmed that isotopic composition of rivers can serve as a proxy for precipitation and that it can be an indicator for hydrological processes even in large basins.

Exploratory analysis of hydrometric and isotopic data identifies the data series showing trends or sudden changes that deserve additional examination. Merz et al. (2012) highlighted the need of going beyond the identification of change and focus on the search of the drivers by the attribution analysis. They conclude that in the studies analysing flood trends, the attribution statements are mostly based on qualitative reasoning or even speculations. Blöschl et al. (2019) stressed regional patterns of European floods that are attributed to different drivers - increasing autumn and winter rainfall in the northwestern Europe; decreasing precipitation and increasing evaporation in southern

Europe, and decreasing snow cover and snowmelt, resulting from warmer temperatures, in eastern Europe. Stone et al. (2013) state that the key problems in detection and attribution of climate change impacts comprise limited availability of long-term observations, limited knowledge on processes and mechanisms involved in changing environmental systems, and widely different concepts applied in the scientific literature. This statement is in our opinion not valid only for the climate change impact studies, but also for the studies that "only" attempt to explain the drivers of variability found in the time series of hydrological data.

This study analyses multivariate time series of data from a small mountain catchment of the Jaloveký Creek (including the time series presented in the companion article Holko et al. 2020, this issue) with the aim to detect trends or changes in behaviour over the study period 1989–2018 and attempt to find the drivers of suggested changes. We first present the time series of isotopic data in precipitation and catchment runoff (oxygen 18). Then, the trends and change points in selected data series are determined and the attribution analysis is conducted. The study differs from similar studies in that the analysis involves many different data series and the hydrological cycle of the studied research catchment is relatively well understood.

DATA

Data on isotopes of oxygen and hydrogen in water samples ($\delta^{18}O$, $\delta^{2}H$) are collected in the Jalovecký Creek catchment since the 1990'. Isotopic composition of monthly precipitation (station Liptovský Mikuláš, elevation 570 m a.s.l.) is monitored since November 1990. Samples for the analysis of isotopic composition of the Jalovecký Creek have been collected at catchment outlet (elevation 820 m a.s.l.) with varying time steps (monthly, weekly, daily, sub-daily) between November 1991 and October 1993, in years 1988–2002 and since the year 2004. The variability of these two data sets in hydrological years 1991–2018 is examined here (see the companion article Holko et al. 2020, this volume, for the catchment and network descriptions).

Isotopic analysis of the samples was carried out by mass spectrometers (before 2011) and laser analyzers (since 2011) in Austria, Slovakia, Germany, Switzerland and in the Czech Republic. All precipitation samples were analysed for both oxygen and deuterium. Deuterium data on the stream samples are not available for the entire study period. An overall analytical accuracy of $\delta^{18}O$ and $\delta^{2}H$ (VSMOW) measurements is better than 0.2‰ and 1‰, respectively.

The exploratory analysis of the water balance and snow data series in the companion article (Holko et al., 2020, this volume) indicated several data series that exhibit the greatest (although not very pronounced) trends or abrupt changes which are statistically examined in this study.

METHODOLOGY

Isotopic composition of water ($\delta^{18}O$, $\delta^{2}H$)

The long-term variability in isotopic composition of precipitation and runoff based on monthly data is explored first. Because the ranges of monthly values in individual years are similar, raw monthly data could not indicate the longer-term variability. Therefore, the 12-months moving averages are calculated to remove the influence of seasonality (Rozanski et al., 1992) and the variability in isotopic composition of precipitation ($\delta^{18}O$, $\delta^{2}H$, deuterium excess $d = \delta^{2}H - 8\ \delta^{18}O$) and air temperature in Liptovský Mikuláš is compared. The variability in moving averages of $\delta^{18}O$ in catchment runoff is explored as well, although the data do not cover the entire period 1991–2018.

We further examine the variability in annual values of the isotopic composition of precipitation and runoff. Volume weighted mean annual values of $\delta^{18}O$ in precipitation in Liptovský Mikuláš in hydrological years 1991–2018 are calculated and compared with the values observed at the two nearest stations having the long-term data on isotopic composition of precipitation in Krakow and Vienna (IAEA/WMO, 2019). The annual weighted mean values are calculated according to the following formula (written for the $\delta^{18}O$):

$$\delta^{18}O_{annual} = \frac{\sum_{i=1}^{12} P_i \delta^{18}O_i}{\sum_{i=1}^{n} P_i} \quad (1)$$

where P is monthly precipitation amount [mm] i is month (November to October).

If the number of missing data (months) in a particular year is greater than two, the annual weighted mean is not calculated. Months with precipitation, having the deuterium excess less than 3 are excluded from calculations.

Annual volume weighted values of $\delta^{18}O$ in precipitation and runoff are compared as well. The annual volume weighted values of $\delta^{18}O$ in runoff are available for 18 years.

The stream water samples provide also an information on the isotopic composition of groundwater which is represented by samples collected in winter months, during the annual minimum flow period (usually from January to early March). Since the mean transit time of streamflow in the catchment is about one year (Dóša et al., 2011; Holko and Kostka, 2006), these values represent the combined contribution of rainfall and snowmelt from the previous year (mainly) to catchment storage. Stream water samples with the smallest concentration of heavy isotopes during the spring period indicate the contribution of the snowmelt to catchment runoff. Both characteristics, i.e the $\delta^{18}O$ values representing the groundwater and the greatest snowmelt contribution, are presented, although due to shorter time series they are not used in the estimation of trends or abrupt changes.

Trends and change points in the annual data series

Our exploratory data analysis involves various types of data related to several components of the hydrological cycle, i.e., the water balance, runoff response and global evaporation and contribution of snowmelt to catchment runoff inferred from the oxygen isotope. It identifies the data series that appear to exhibit trends or changes in behaviour, either in magnitude or in variability. Trends and change points detection are calculated for these time series using the Mann-Kendall test and the Wild Binary Segmentation (WBS) method (Fryzlewicz, 2014), respectively. The two approaches are among the most common methods used in the time series analyses (e.g., Sharma et al., 2016; Yue et al., 2012). The Mann-Kendall test is a non-parametric test that analyses data for the increasing or decreasing (monotonic) trends. The test does not gain any information on the type (gradual or abrupt) or timing of the change (Chiverton et al., 2015). The WBS method is a relatively new method that has been shown to identify the change points correctly and that is computationally not very demanding. However, Sharma

et al. (2016) showed that the method (like other methods they tested) failed to detect the change point location for the change in variance only.

Merz et al. (2012) proposed a framework for hypothesis testing in attribution analyses comprising the evidence of consistency, evidence of inconsistency and provision of confidence levels. According to this framework, the evidence of consistency should show that the detected change is consistent with the assumed drivers of change. The evidence of inconsistency should show that changes in other possible drivers are inconsistent with the change in the studied characteristic. Finally, the provision of confidence levels should quantify the strength of the attribution statement in terms of a likelihood statement. We apply this approach in the search of drivers that might be responsible for the changes detected in our data series. Selected data series in which a trend or change are indicated and correlation coefficients of linear regression with time exceed the value of 0.4, are compared to the data series of possible drivers represented by precipitation characteristics. The correlation between the two data series (the data series with an identified change and the driver data series) is evaluated by Pearson correlation coefficient at significance level 0.05.

RESULTS

Isotopic composition of water

Moving averages of monthly air temperature and isotopic composition of precipitation (Fig. 1) in Liptovský Mikuláš do not indicate a trend over hydrological years 1989–2018. Compared to the long-term average, a longer period of isotopically depleted precipitation was observed approximately between December 2002 and December 2006 that corresponds to lower air temperatures. A longer period of isotopically enriched precipitation occured approximately between January 2014 and December 2017. Isotopic enrichment of precipitation in that period is slightly shifted in time compared to the air temperature increase (Fig. 1). Similarity of the isotopic composition of precipitation and local air temperature over the entire period 1991–2018 is obvious, but the correlation is not very good (the correlation coefifcient of linear regression between $\delta^{18}O$ in precipitation and air temperature is 0.523).

Although the data on isotopic composition of runoff do not cover the entire period 1991–2018, it is obvious that the values since 2014 are less variable and higher than in period 2005–2013 (Fig. 1, Fig. 2). These higher values correspond to the period of isotopically enriched precipitation mentioned above.

Seasonality in isotopic composition of catchment runoff since 2014 is less pronounced than before, except the significant spring depletion in 2018 (Fig. 2). It could be related to a change in temporal evolution of snow accumulation and melt during winter seasons.

Higher concentrations of heavy isotopes in precipitation in Liptovský Mikuláš since 2014 are even better visible in the annual volume weighted data (Fig. 3). Similar behaviour seems to be observed also at the nearest neighbouring stations in Krakow and Vienna although the data from hydrological years 2017 and 2018 are not available. Higher concentrations of heavy isotopes in precipitation in the last years of the study period are reflected also in catchment runoff. We note that isotopic composition of precipitation in Liptovký Mikuláš (570 m a.s.l.) shown in Figs. 1 and 3 does not represent the isotopic composition of water feeding the Jalovecký Creek catchment

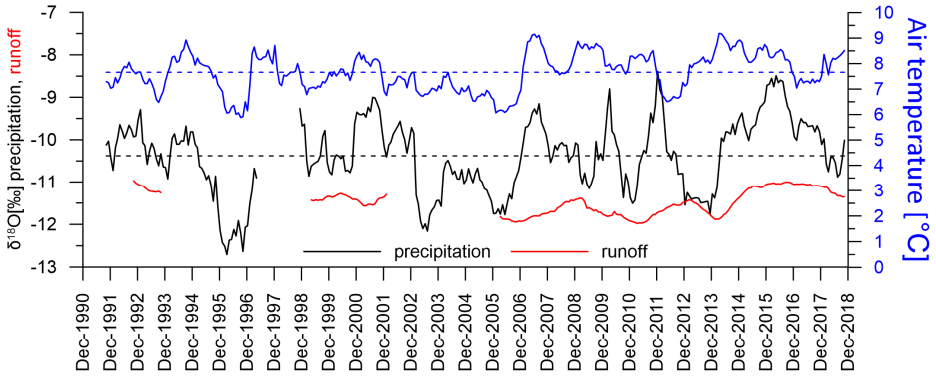

Fig. 1. Moving average of monthly $\delta^{18}O$ in precipitation in Liptovský Mikuláš (the black line), air temperature in Liptovský Mikuláš (the blue line) and $\delta^{18}O$ in the Jalovecký Creek catchment runoff (the red line) in hydrological years 1991–2018; the dotted lines indicate the long-term averages of air temperature (blue) and $\delta^{18}O$ in precipitation (black); note that elevation of station Liptovský Mikuláš is 570 m a.s.l. while the mean elevation of the Jalovecký Creek catchment is 1500 m a.s.l.

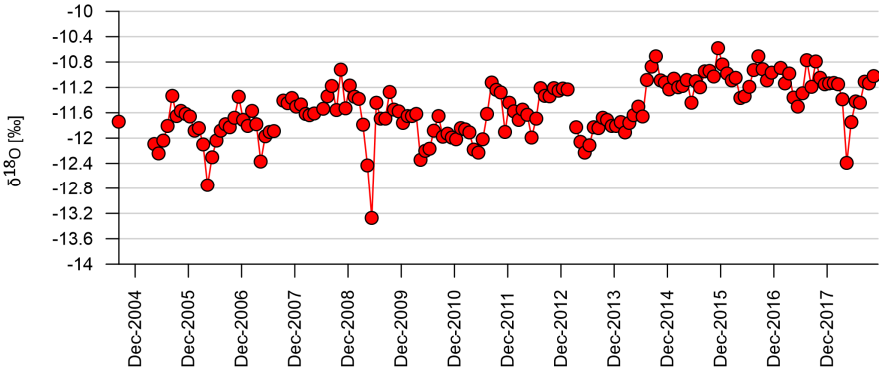

Fig. 2. Monthly weighted $\delta^{18}O$ in the Jalovecký Creek at catchment outlet in period August 2004–October 2018.

that has much higher elevation (820–2178 m a.s.l., mean 1500 m a.s.l.) and thus receives isotopically lighter precipitation.

Isotopic composition of the Jalovecký Creek during winter low flow period that represents catchment groundwater, is shown in Fig. 4. Although the data series does not fully cover the entire study period, the interannual variability of the groundwater $\delta^{18}O$ is approximately 0.5‰ with greater values measured until 2002 followed by smaller values in the years 2005–2014. The greater values since 2015 correspond to the pattern of isotopic composition of precipitation. The interannual variability of $\delta^{18}O$ in the stream water during the time of maximum spring discharge that represents the greatest influence of the snowmelt is almost 2‰. This variability does not correlate well with the simulated catchment snow characteristics (SWE, accumulated SWE). The difference between the isotopic composition of groundwater (as defined above) and the isotopic composition of the stream water during the snowmelt period could be interpreted as a qualitative measure of the snowmelt contribution to catchment runoff. Fig. 4 shows a negligible difference in spring 2014 and indicates a smaller influence of the snowmelt water in years 2015–2017 compared to most of the previous years (as suggested also above by Fig. 2). However, the influence of snowmelt in spring 2018 is greater again.

Trends and change points in the annual data series

Summary information on the results of trend and change point analyses is given in Table 1. The table lists the time series (denoted as Indicators) in which the exploratory analysis indicates the most pronounced trends or changes in behaviour over the study period 1989–2018. For the convenience they are divided into data related to water balance, hydrological response, storage and other. Some of them are plotted in Fig. 5 that shows that the only time series exhibiting a clear monotonic increasing trend is the number of flow reversals per year. Other data series contain abrupt changes in some part of the study period rather than monotonic trends (e.g. the annual runoff coefficients or June low flow). As written above, the Mann-Kendall test (MK in Table 1) does not provide an information on the type of change. Therefore, the years indicated by the WBS method as change points (abrupt changes in the time series) are given in Table 1 and Fig. 5 as well.

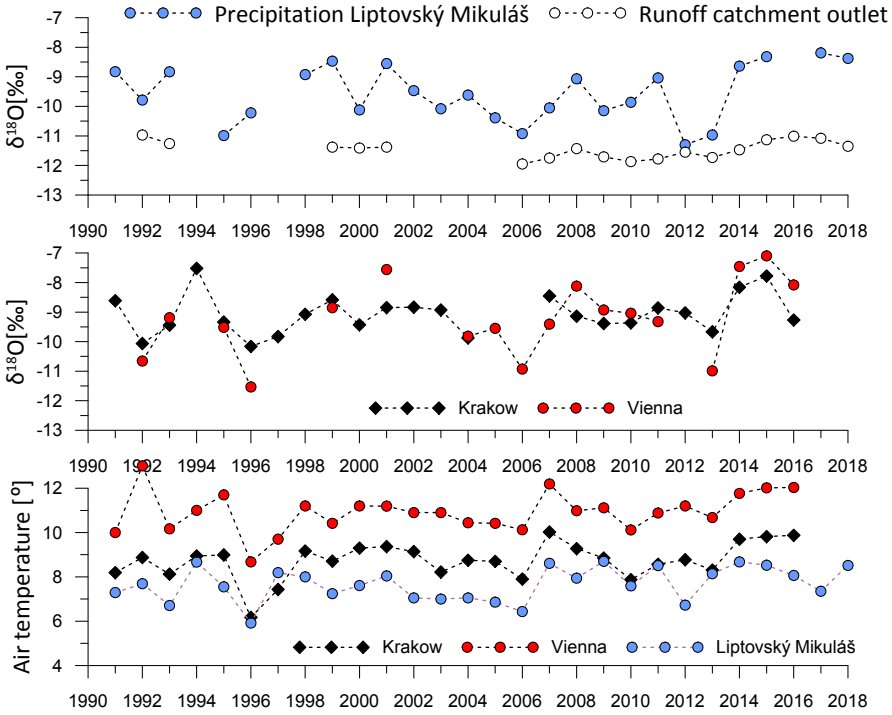

Fig. 3. Annual volume weighted values of $\delta^{18}O$ in precipitation in Liptovský Mikuláš, Krakow and Vienna and in the Jalovecký Creek at the outlet of the catchment (the top and middle panels) and mean annual air temperatures in hydrological years 1991–2018 (the bottom panel).

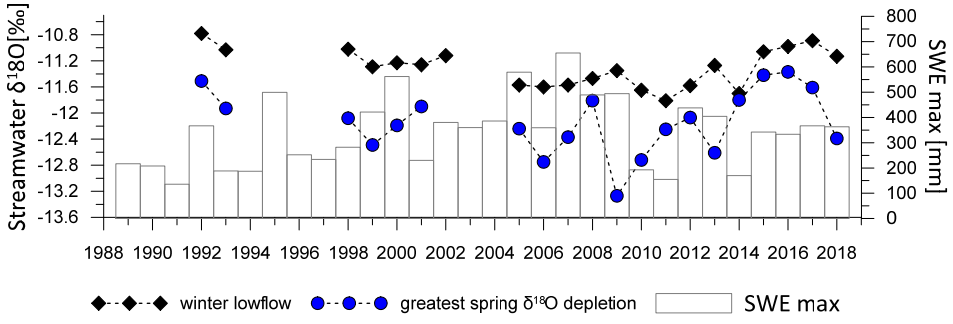

Fig. 4. $\delta^{18}O$ in the Jalovecký Creek during winter low flow conditions and during the greatest $\delta^{18}O$ depletion caused by the snowmelt and simulated maximum SWE in the catchment.

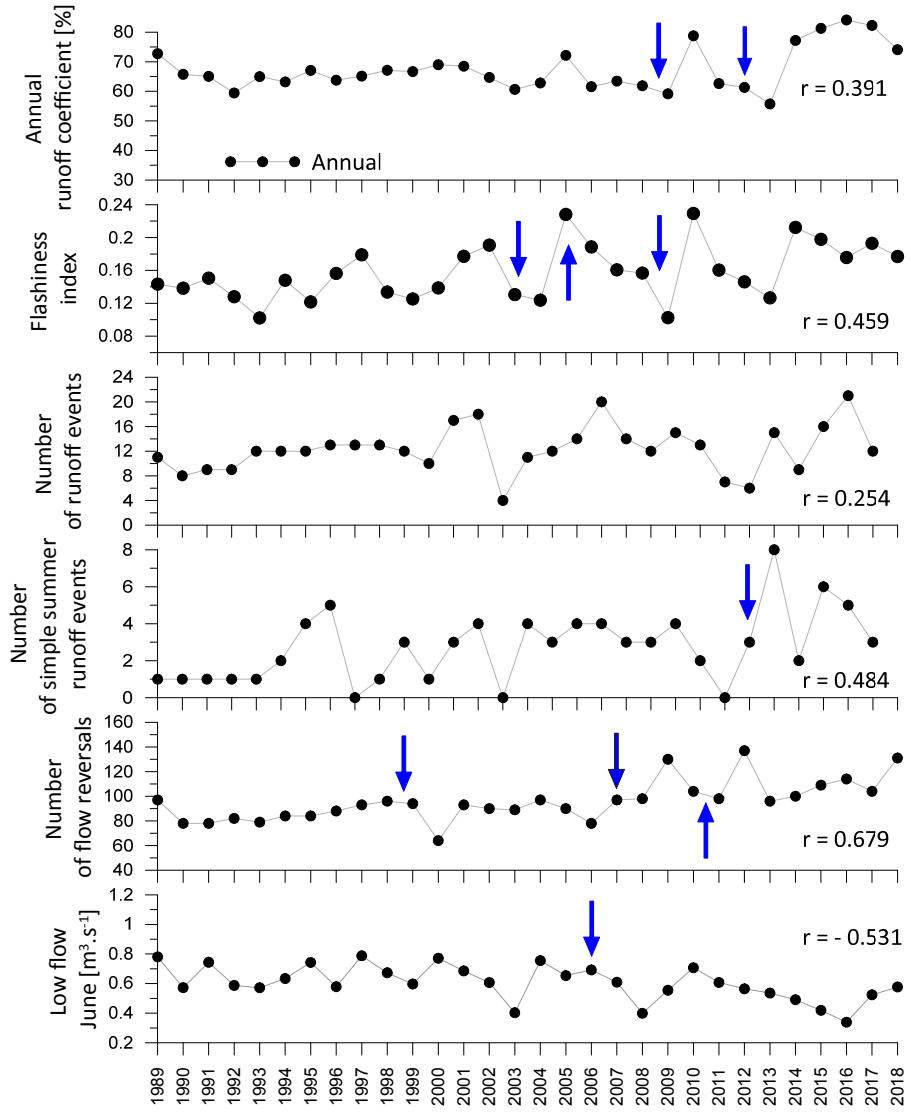

Fig. 5. The time series of annual data in which the exploratory data and statistics (trends and change points determination) indicated pronounced changes; r is the correlation coefficient of the linear trend over the study period (linear regression of annual values of indicators against time); the arrows indicate change points determined by the WBS method; if the arrows point between the years, both years were identified by WBS as the change points.

Table 1 shows that the greatest correlation coefficients (i.e. mathematically the closest relationships of an indicator with time) are obtained for:

- number of flow reversals
- low flow in June
- number of simple summer events and
- flashiness index.

We have attempted to find drivers of changes for these four time series by an attribution analysis described in Methodology (i.e., find the possible driver, examine the consistency, confirm the inconsistency with other potential drivers and examine the statistical significance). All time series seem to be dominantly related to precipitation regime (the relationships with air temperature were poor). Therefore, the attribution focused on finding characteristics of catchment precipitation that correlate best with the above data series. Tested precipitation characteristics include precipitation amounts for different time steps (annual, seasonal, monthly) and thresholds (e.g., total precipitation for days with more than 10 mm per day), number of days with precipitation and number of wet and dry periods of different duration (from 1 to more than 10 successive days with/without precipitation).

Change in the number of flow reversals was attributed to the change in the number of wet periods with six and more successive days with precipitation per year. Linear regression between the two data series (wet periods as an independent variable and number of flow reversals as a dependent variable) has coefficient of determination $R^2 = 0.353$ (Fig. 6) and the correlation is statistically significant at level 0.05. The total number of days with precipitation per year was rejected as a possible driver because the correlation is worse ($R^2 = 0.275$) and it is not statistically significant.

Low flow in June is the only of the four data series in the attribution analysis that might not be affected only by precipitation characteristics, but also by possible changes in the snow accumulation and melt. However, the best correlation and statistically significant Pearson correlation coefficient (i.e., the driver of the change) were found only for the total precipitation amount in February to June (Fig. 6). Coefficient of determination obtained by linear regression of the two data series was 0.343. Analysis of monthly air temperature as another possible driver does not indicate pronounced changes during the snow accumulation and melt periods and the air temperature was thus rejected as the driver of the June low flow change.

Table 1. Time series in which the exploratory analysis indicated the most pronounced changes during the study period; significance of the monotonic trend was tested by the Mann-Kendall test (MK trend) at significance level 0.05 (YES if the trend is significant); identification of change points employed the WBS method; "–" means that a significant trend or change point were not found.

Data type	Indicator (time series examined)	Obtained from, time step	Correlation coefficient (linear regression of an indicator versus time)	MK trend	Change point
Water balance	Runoff coefficient	precipitation and runoff, annual	0.391	–	2008, 2009, 2012
Runoff response	Rise rate	discharge, daily	–0.448	Yes	–
	Number of events per year	discharge, hourly	0.254	Yes	1999, 2001, 2002, 2010, 2014
	Annual maximum	discharge, hourly	0.306	–	1994, 2012, 2013, 2015
	Fall rate	discharge, daily	0.316	Yes	–
	Flashiness index	discharge, daily	0.459	Yes	2003, 2005, 2008, 2009
	No. of simple summer events	discharge, hourly	0.484	Yes	2012
	No. of flow reversals	discharge, daily	0.679	Yes	1998, 1999, 2007, 2010, 2011
Storage	June low flow	discharge, daily	–0.531	Yes	2006
	June flow	discharge, daily	–0.366	Yes	2005
	March low flow	discharge, daily	0.275	–	2001, 2002, 2003, 2005
Other	$\delta^{18}O$ Liptovský Mikuláš	precipitation, annual	–0.166	–	2012

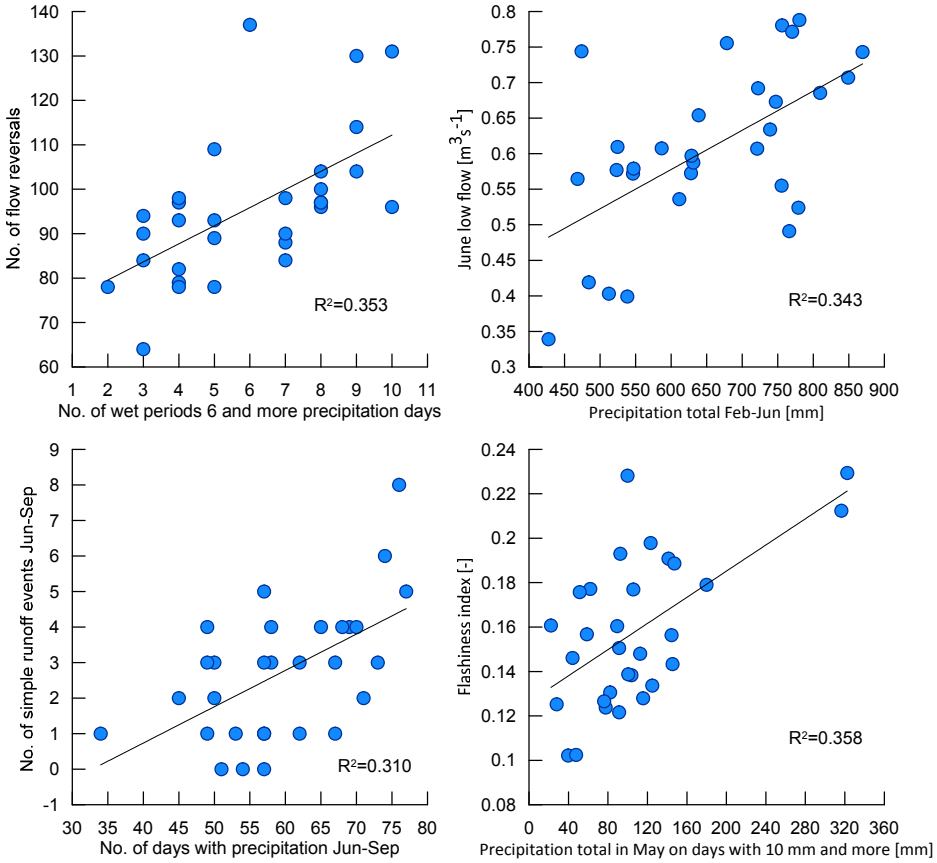

Fig. 6. Correlations between the drivers (plotted on the horizontal axes) and changed time series (vertical axes) found in the attribution analysis for the time series that exhibited the greatest changes over the study period (see also Fig. 5).

The change in the number of simple runoff events in summer seasons (June to September) is best correlated ($R^2 = 0.310$) with the number of days with precipitation in the same period (Fig. 6). Precipitation amount or number of days with precipitation above certain thresholds were rejected as possible drivers due to much worse and statistically insignificant correlations.

Flashiness index reflects the magnitude of changes in discharge of the successive days standardized by the total discharge over the studied period (hydrological year in this study). The analysis of monthly flashiness indices revealed that the greatest trends over the study period (1989–2018) occurred in November, April and May. Therefore, the attribution of changes in annual flashiness index focused on spring months. Sum of precipitation in May on days with precipitation amount 10 mm and more is identified as the driver. The correlation between this driver and the flashiness index is statistically significant and coefficient of determination is 0.358 (Fig. 6). Number of days with precipitation in the entire hydrological year, in individual months or in a combination of several months as well as precipitation amounts were rejected as possible drivers.

DISCUSSION

We are not aware of other studies analysing similar multivariate data series from small mountain catchments. Therefore, instead of comparing our results with the results of other studies, we focus on some thoughts on the uncertainties that might be related to our analyses and additional data series or approaches that might be useful in similar studies.

Higher concentrations of heavy isotopes in precipitation (both oxygen and hydrogen) in the last years of the study period might reflect increased global evaporation. Similarity with data from Krakow and Vienna suggests that the pattern observed in Liptovský Mikuláš is not caused by local drivers. Although Figs. 1 and 3 confirm the links between the local air temperatures and isotopic composition of precipitation, the correlations over the entire period (1991–2018) are not very strong at any of the three stations. This is a known fact that has already been mentioned in other studies (e.g. Rozanski et al., 1993; Stumpp et al., 2014). Yet, our data show that an increase of the air temperature since 2013 corresponds to that of $\delta^{18}O$ in precipitation. Global data sets (e.g., https://data.giss.nasa.gov/gistemp/) indicate an unprecedented increase in air temperature in northern hemisphere or in northern Atlantic (the main source of precipitation for the study area) since 2014 that might result in greater evaporation. Although the analysis comprising global data (both climatic and isotopic) is beyond the scope of this study, it would be an interesting topic of further research.

Quantification of snowmelt contribution to catchment runoff or groundwater recharge from winter and summer precipitation using stable isotopes (e.g., Jasechko et al., 2014; Šanda et al., 2019) are other approaches that could point at changes in hydrological cycle of catchments. However, previous studies in the Jalovecký Creek catchment showed that isotopic composition of the snowmelt water is rather different from that of winter precipitation and has a significant spatial variability (Holko, 1995; Holko et al., 2013). Thus, the results of calculations based on the two-component mixing model (Jasechko et al., 2014; Šanda et al., 2019) would be very uncertain in the study catchment in which the detailed data on isotopic composition of the snowmelt water which is not available for the entire study period. Comparison of the isotopic composition of stream during periods when the runoff is fed from the groundwater storage with periods of maximum annual isotopic depletion (the spring snowmelt and in some years perhaps also the isotopically lighter spring precipitation) therefore only qualitatively indicates smaller contribution of snowmelt water between 2011 and 2017. However, this smaller snowmelt water contribution agrees with the change in snow accumulation and melting suggested by the less pronounced seasonal variability of the isotopic composition of the Jalovecký creek shown in Fig. 2.

Change points identified with the help of statistics (the WBS method) do not clearly show one well defined period for all or majority of studied data series. However, apart from two exceptions, all identified change points occur in the second and third decades of the study period (Table 1).

We would like to stress that the objective of this study is not to look for evidences of climate change. The 30 years long data series are not long enough to examine the effects of climate change (Kundzewicz and Robson, 2004). Furthermore, data from the Kasprowy Wierch and Skalnaté Pleso stations show that the air temperature, precipitation and snow cover did not significantly change during the study period and that the study period is already warmer than previous decades. The objective of this study is to examine if and which changes can be identified in relatively long data series characterizing the hydrological cycle of a small mountain catchment that has been little affected by direct human activities and relatively well studied.

The results show that despite a number of experiments conducted in the catchment which provided some unique data, examination of the changes in catchment hydrological cycle has to rely on the standard data sets of precipitation, air temperature, and runoff. Precipitation does not appear to exhibit changes at the time scales studied and evapotranspiration cannot be measured at catchment scale. Thus, runoff remains the only water balance component that can be analysed more carefully. Chiverton et al. (2015) proposed an approach based on variograms that might be useful in our future analyses.

Regular snow cover measurements at snow courses located at different elevations are perhaps the only data series, available in our catchment that are not commonly measured in similar catchments on the long–term basis. Because such measurements cannot be conducted very frequently and in a very dense network, some important snow cover characteristics such as dates of its beginning and end that could indicate the long-term changes, cannot be evaluated from measured snow course data on a catchment scale. The only reasonable approach to obtain the catchment-scale snow characteristics in mountain catchments of a similar size (too big for the detailed measurements, too small for the remotely sensed data that would cover the entire study period) is mathematical modelling. Because of uncertainties that are always present in modelling, we do not evaluate duration of snow cover in individual winters. Simulated SWE is only used to supplement the information on SWE maxima obtained from measured data and provide an information on total accumulation of snow in the catchment that we believe is less sensitive to modelling uncertainties.

Our effort in focusing on catchment scale rather than on point data (we do not analyse air temperature data from the stations for example) also leads to the uncertainty related to extrapolation of the point precipitation and air temperature data.

Merz et al. (2012) noted that in most flood time series analyses studies, very little effort is devoted to attribution of the trends and change points to the drivers that caused them. The same applies to other studies analysing hydrological and meteorological time series data. While the detection of changes is an important component of the time series analysis, in our opinion the only effort possibly leading to a progress in understanding of hydrological cycle is the search for the drivers of the changes. We have attempted to search for the drivers responsible for the changes in our data series suggested by the exploratory analysis. Because the air temperature and snow accumulation are poorly correlated with the data series in interest, our search for the drivers was limited to precipitation characteristics with not better than daily temporal resolution. It is possible that some changes (e.g., greater runoff coefficients) are also related to the change of the short-time precipitation characteristics (e.g., rainfall intensity), which are not available in the study catchment for the entire study period. Fig. 6 shows that regressions obtained in the attribution analysis are not very strong. Other possible drivers describing for example the wetness or storage states of the catchment are not available. Naturally, it is also possible that there are other drivers we are not aware of or the influence of which is currently not well understood (e.g. changing forest structure). Useful thoughts about the uncertainties in our ability to understand the drivers and predict future behaviour are given by Taleb (2007).

Some relationships obtained by the attribution analysis suggest new directions in the research of hydrological response of our catchment, e.g., of the role of short and long term wet periods or number of days with precipitation rather than precipita-

tion totals or thresholds. Evaluation of additional isotopic data (e.g. weekly samples of catchment runoff) could provide better understanding of the changes that probably occurred after 2014.

CONCLUSIONS

Isotopic data indicate greater concentrations of heavier isotopes in precipitation since 2014 and less pronounced seasonality in the isotopic composition of stream water. The attribution analysis related the most pronounced (although statistically weak) changes to characteristics of precipitation regime and indicated some interesting relationships that may be subject of future research.

The study shows the value of the long-term hydrological and isotopic monitoring in small mountain catchments. At the same time, it documents that despite better data and knowledge of the hydrological cycle in a research catchment compared to other, less-studied catchments, the attribution analysis is still uncertain due to the unavailability of data on possible drivers. While the time series analysis of longer hydrological data sets should remain part of routine data processing (to check for an unusual behaviour), the ability of hydrologists to explain the variability found in the hydrological time series is in our opinion still rather limited due to an inadequate understanding of the hydrological cycle.

Acknowledgements. This study was supported by grants from the Slovak Academy of Sciences VEGA (project No. 2/0065/19) and the Slovak Research and Development Agency (APVV) (project No. 15-0497). Data collection was supported by project ITMS 26210120009 Infrastructure completion of hydrological research stations, of the Research & Development Operational Programme funded by the ERDF. The work of PS was supported by the Stefan Schwarz grant of the Slovak Academy of Sciences.

REFERENCES

Blöschl, G. et al., 2019. Changing climate both increases and decreases European river floods. Nature, 573, 108–111.

Chiverton, A., Hannaford, J., Holman, I.P., Corstanje, R., Prudhomme, C., Hess, T.M., Bloomfield, J.P., 2015. Using variograms to detect and attribute hydrological change. Hydrol. Earth Syst. Sci., 19, 2395–2408. DOI: 10.5194/hess-19-2395-2015.

Clark, I.D., Fritz, P., 1997. Environmental Isotopes in Hydrogeology. CRC Press, New York., 352 p.

Dóša, M., Holko, L., Kostka, Z., 2011. Estimation of the mean transit times using isotopes and hydrograph recessions. Die Bodenkultur, 62, 1–4, 47–52.

Fryzlewicz, P., 2014. Wild binary segmentation for multiple change-point detection. The Annals of Statistics, 42, 6, 2243–2281.

Gat, J., 1996. Oxygen and hydrogen isotopes in the hydrologic cycle. Annu. Rev. Earth Planet. Sci., 24, 225–262.

Holko, L., 1995. Stable environmental isotopes of ^{18}O and ^{2}H in hydrological research of mountainous catchment. J. Hydrol. Hydromech., 43, 4–5, 249–274.

Holko, L., Kostka, Z., 2006. Hydrological research in a high-mountain catchment of the Jalovecký Creek. J. Hydrol. Hydromech., 54, 2, 192–206. (In Slovak.)

Holko, L., Danko, M., Dóša, M., Kostka, Z., Šanda, M., Pfister L., Iffly, J.F., 2013. Spatial and temporal variability of stable water isotopes in snow related hydrological processes. Die Bodenkultur, 64, 3–4, 39–45.

Holko, L., Sleziak, P., Danko, M., Bičárová, S., Pociask-Karteczka, J., 2020. Analysis of changes in hydrological cycle of a pristine mountain catchment: 1. Hydrometric data. Journal of Hydrology and Hydromechanics, 68, 2, 180–191.

IAEA/WMO 2019. Global Network of Isotopes in Precipitation. The GNIP Database. Accessible at: https://nucleus.iaea.org/wiser, assessed in August 2019.

Jasechko, S., Birks, S.J., Gleeson, T., Wada, Y., Fawcett, P.J., Sharp, Z.D., McDonnell, J.J., Welker, J.M., 2014. The pronounced seasonality of global groundwater recharge. Water Resour. Res., 50, 8845–8867, DOI: 10.1002/2014WR015809.

Kendall, C., Coplen, T.B., 2001. Distribution of oxygen-18 and deuterium in river waters across the United States. Hydrol. Process., 15, 1363–1393.

Kendall, C., McDonnell, J.J. (Eds.), 1998. Isotope Tracers in Catchment Hydrology. Elsevier Science, 839 p.

Kundzewicz, Z.W., Robson, A., 2004. Change detection in hydrological records – a review of the methodology. Hydrological Sciences Journal, 49, 1, 7–19.

Merz, B., Vorogushyn, S., Uhlemann, S., Delgado, J., Hundecha, Y., 2012. HESS Opinions "More efforts and scientific rigour are needed to attribute trends in flood time series". Hydrol. Earth Syst. Sci., 16, 1379–1387. DOI: 10.5194/hess-16-1379-2012.

Panarello, H.O., Dapeña, C., 2009. Large scale meteorological phenomena, ENSO and ITCZ, define the Paraná River isotope composition. J. Hydrol., 365, 105–112.

Pirk, A., 2015. Long-term data set analysis of stable isotopic composition in German rivers. MSc Thesis, Albert-Ludwigs-University Freiburg, 92 p.

Rank, D., Wyhlidal, S., Schott, K., Jung, M., Heiss, G., Tudor, M., 2014. A 50 years' isotope record of the danube river water and its relevance for hydrological, climatological and environmental research. Acta Zoologica Bulgarica 66, 109–115.

Reckerth, A., Stichler, W., Schmidt, A., Stumpp. C., 2017. Long-term data set analysis of stable isotopic composition in German rivers. J. Hydrol., 552, 718–731.

Rozanski, K., Araguás-Araguás, L., Gonfiantini, R., 1992. Relation between long-term trends of oxygen-18 isotope composition of precipitation and climate. Science, 258, 981–985.

Rozanski, K., Araguás-Araguás, L., Gonfiantini, R., 1993. Isotopic Patterns in Modern Global Precipitation. In: Climate Change in Continental Isotopic Records. Geophysical Monograph 78, 36 p.

Sharma, S., Swayne, D.W., Obimbo, C., 2016. Trend analysis and change point techniques: a survey. Energ. Ecol. Environ., 1, 3, 123–130. DOI: 10.1007/s40974-016-0011-1.

Stone, D., Auffhammer, M., Carey, M. et al., 2013. The challenge to detect and attribute effects of climate change on human and natural systems. Climatic Change, 121, 381. https://doi.org/10.1007/s10584-013-0873-6.

Stumpp, C., Klaus, J., Stichler, W., 2014. Analysis of long-term stable isotopic composition in German precipitation. J. Hydrol., 517, 351–361.

Šanda, M., Vitvar, T., Jankovec, J., 2019. Seasonal subsurface water contributions to baseflow in the mountainous Uhlířská catchment (Czech Republic). J. Hydrol. Hydromech., 67, 2019, 1, 41–48. DOI: 10.2478/johh-2018-0018.

Taleb, N.N., 2007. The Black Swan: The Impact of the Highly Improbable. Random House, ISBN 978-1400063512.

Yue, S., Kundzewicz, Z.W., Wang, L., 2012. Detection of changes. In: Kundzewicz, Z.W. (Ed.): Changes in Flood Risk in Europe. IAHS Press, Wallingford, UK, pp. 387–408.

Received 30 September 2019
Accepted 21 February 2020

J. Hydrol. Hydromech., 68, 2020, 2, 200–210
DOI: 10.2478/johh-2020-0016
ISSN 1338-4333

sciendo Journal of Hydrology and Hydromechanics

Multi-model climatic water balance prediction in the Zala River Basin (Hungary) based on a modified Budyko framework

Péter Csáki[1*], Kitti Gyimóthy[1], Péter Kalicz[1], Ján Szolgay[2], Katalin Anita Zagyvai-Kiss[1], Zoltán Gribovszki[1]

[1] Institute of Geomatics and Civil Engineering, University of Sopron, Bajcsy-Zsilinszky street 4., Sopron, H-9400, Hungary.
[2] Department of Land and Water Resources Management, Slovak University of Technology, Radlinského 11, 810 05, Bratislava, Slovakia.
[*] Corresponding author. Tel.: +36 99 518-146. E-mail: csaki.peter@uni-sopron.hu

Abstract: Providing information on the impacts of climate change on hydrological processes is becoming ever more critical. Modelling and evaluating the expected changes of the water resources over different spatial and time scales can be useful in several fields, e.g. agriculture, forestry and water management. Previously a Budyko-type spatially distributed long-term climate-runoff model was developed for Hungary. This research includes the validation of the model using historical precipitation and streamflow measurements for three nested sub-catchments of the Zala River Basin (Hungary), an essential runoff contributing region to Lake Balaton (the largest shallow lake in Central Europe). The differences between the calculated (from water balance) and the estimated (by the model) mean annual evapotranspiration varied between 0.4% and 3.6% in the validation periods in the sub-catchments examined. Predictions of the main components of the water balance (evapotranspiration and runoff) for the Zala Basin are also presented in this study using precipitation and temperature results of 12 regional climate model simulations (A1B scenario) as input data. According to the projections, the mean annual temperature will be higher from period to period (2011–2040, 2041–2070, 2071–2100), while the change of the annual precipitation sum is not significant. The mean annual evapotranspiration rate is expected to increase slightly during the 21st century, while for runoff a substantial decrease can be anticipated which may exceed 40% by 2071–2100 relative to the reference period (1981–2010). As a result of this predicted reduction, the runoff from the Zala Basin may not be enough to balance the increased evaporation rate of Lake Balaton, transforming it into a closed lake without outflow.

Keywords: Evapotranspiration; Runoff; Budyko-model; Water balance; Climate change.

INTRODUCTION

One of the most significant effects of climate change in Hungary and the Carpathian Basin region is its impact on the water cycle through the change in precipitation and evapotranspiration patterns at multiple scales (Kohnová et al., 2019; Labudová et al., 2015; Nováky and Bálint, 2013; Pongrácz et al., 2014; Rončák et al., 2019; Szilágyi and Józsa, 2008). The global hydrological cycle has accelerated in recent decades (Cui et al., 2018; Lugato et al., 2013; Troch, 2008), and according to climate projections, this will probably continue (IPCC, 2019). This acceleration may cause more frequent and severe hydrological extremes with possible negative impacts on ecosystems, human health, water system reliability and operating costs (Bates et al., 2008; Kundzewicz and Matczak, 2015).

The frequency of climatic extremes (e.g. the number of consecutive dry days, the number of heavy precipitation days, the number of hot days, the number of hot nights) has increased in the Carpathian Basin region by the end of the 20th century (Pogačar et al., 2019; Pongrácz and Bartholy, 2006; Spinoni et al., 2015). Increasing average air temperature and decreasing summer precipitation are projected for the region (Anders et al., 2014; Kohnová et al., 2019; Nováky and Bálint, 2013). These will probably lead to increased evapotranspiration and decreased runoff. As a result, less water will be available to meet various demands, especially irrigation. A significant reduction of water resources is expected, which may cause a considerable decrease in the inflows of the Lake Balaton, the largest shallow lake in Central Europe.

Information on local or regional climate change impacts on hydrological processes is becoming increasingly significant (Karamouz et al., 2013; Stagl et al., 2014). Modelling and evaluating the expected changes in water resources over different time scales is important for water management, agriculture and forestry in the Carpathian Basin region (Hlásny et al., 2014; Mátyás et al., 2018; Škvarenina et al., 2009).

Several water balance models/frameworks have been developed, which are based on the relationship between an aridity index (e.g. the ratio of annual potential evapotranspiration to precipitation) and the evapotranspiration ratio (e.g. the ratio of actual annual evapotranspiration to precipitation) (e.g. Budyko, 1974; Fu, 1981; Mezentsev, 1955; Ol'dekop, 1911; Pike, 1964; Parajka et al., 2004; Porporato et al., 2004; Schreiber, 1904; Turc, 1954; Wang and Tang, 2014; Zhang et al., 2004). They are often used to estimate the long-term hydrological impacts of climate change (e.g. Arora, 2002; Jiang et al., 2015; Lv et al., 2019; Ning et al., 2018; Renner and Bernhofer, 2012; Shen et al., 2017; Teng et al., 2012; Wang et al., 2016), as catchment scale (lumped) models. Based on these frameworks, the elasticity of climate change impacts has also been tested in numerous studies (Andréassian et al., 2016; Gao et al., 2016; Konapala and Mishra, 2016; Liang et al., 2015; Tian et al., 2018; Wang and Hejazi, 2011; Zhang et al., 2016; Zhou et al., 2015).

The frameworks, as mentioned above, have also been used for hydrological studies in the Carpathian Basin region. Water balance estimations based on the Turc (1954) model were completed in Slovakia by Danihlik et al. (2004) for the upper part of the Hron river basin and Hlavčová et al. (2006) for the whole

country. Nováky (1985, 2002) developed a Budyko-type spatially distributed (grid-based) empirical climate-runoff model for the Zagyva catchment in Hungary. This model has also been applied for the Lake Balaton basin (Nováky, 2008) and the Bácsbokodi-Kígyós catchment (Keve and Nováky, 2010).

There are many areas in the Carpathian Basin where the long-term mean annual actual evapotranspiration exceeds the long-term mean annual precipitation, that is, an additional amount of water is available for evapotranspiration above that which the area receives from local precipitation. These are mainly water bodies or storages with allochthone inflow, such as lowland rivers, lakes, wetlands and groundwater exfiltration areas. The additional incoming water can originate from surface or groundwater inflows (we use the term additional water here). The Budyko framework is not valid for these areas. A limited number of previous studies deal with the extension of the framework for conditions with additional water (Chen et al., 2013; Greve et al., 2016; Zhang et al., 2008). Csáki et al. (2014, 2018) extended the Budyko framework-based Nováky (1985, 2002) model to handle the areas (grid clusters) with additional water in Hungary. However, a detailed assessment of the accuracy, as well as the validation of the spatially distributed model, has not yet been performed.

Thus, an objective of this study was a validation of the spatially distributed climate-runoff model (Csáki et al., 2014, 2018), including areas with additional water. Further, based on the validation, hydrological predictions for the 21st century were performed in order to analyze the possible climate change impacts in the Zala River Basin (Hungary), which is the most important water supply region of Lake Balaton.

We structured the paper in the following manner. After the "Introduction", the "Material and methods" section describes the spatially distributed climate runoff model, its calibration and validation methodology as well as the procedure of the model application for the hydrological predictions. The description of the pilot basin and the data used are included here, too. "Results and discussion" contain the model validation, the prediction of the hydrological balance under climate change and the discussion of the results. The following "Conclusions" complete the study.

MATERIAL AND METHODS

Long-term mean annual climate-runoff model

Previously a Budyko-type gridded climate-runoff model (Nováky, 2008) was developed by Csáki et al. (2014, 2018) for estimating the long-term mean annual actual evapotranspiration and runoff in Hungary. The model employs two parameters, α and β mapped in grids. These parameters aggregate all of the factors affecting evapotranspiration, the most dominant of them being the land cover (Keve and Nováky, 2010).

The α parameter follows the Budyko framework (Budyko, 1974), more precisely, the Schreiber equation (Fraedrich, 2010; Schreiber, 1904) and a pan-evaporation equation for the "class U" evaporation pan according to Nováky (1985, 2002).

The long-term mean annual potential evapotranspiration, as proposed by Schreiber, is estimated as:

$$ET_P = -P\left(\ln\left(\frac{P-ET_A}{P}\right)\right), \quad (1)$$

where ET_P is the long-term mean annual potential evapotranspiration (mm yr^{-1}), P is the long-term mean annual precipitation (mm yr^{-1}), and ET_A is the long-term mean annual actual evapotranspiration (mm yr^{-1}).

Long-term mean annual potential evapotranspiration can also be expressed as a function of the "class U" (with 3 m^2 water surface area, 0.5 m depth) pan evaporation, according to a general relationship valid for Hungary (Nováky, 1985, 2002), as:

$$ET_P = f\left(E_{pan}\right) = \alpha E_{pan} = \alpha\left(36400\frac{T}{P}+104\right), \quad (2)$$

where E_{pan} is the long-term mean annual pan evaporation (mm yr^{-1}), T is the long-term mean annual air temperature (°C), and α is a regional calibration parameter. Note that the long-term mean annual pan evaporation equation $\left(36400\frac{T}{P}+104\right)$ was developed for Hungary by Nováky (2002), using data from several "class U" evaporation pans (Nováky, 1985). We may consider these pan evaporation rates as close to the wet environment evapotranspiration rates (Priestley and Taylor, 1972); therefore, they are more appropriate for climate change modelling than the "class A" pan-based potential evapotranspiration rates, which are very sensitive to the local environmental conditions (e.g. the dryness of the area surrounding the pan).

The parameter α can be calculated from the Equations (1) and (2) as:

$$\alpha = \frac{ET_P}{E_{pan}} = -\frac{P\left(\ln\left(\frac{P-ET_A}{P}\right)\right)}{36400\frac{T}{P}+104}. \quad (3)$$

Under local conditions where additional water is available for actual evapotranspiration to that of the local precipitation, the Budyko model cannot be valid, thus the α parameter in Eq. (3) is not defined. For these areas, another local/regional calibration parameter β, which relates E_{pan} to ET_A (McMahon et al., 2012), can be proposed as:

$$\beta = \frac{ET_A}{E_{pan}} = \frac{ET_A}{36400\frac{T}{P}+104}. \quad (4)$$

For such conditions, we assume in our model that the actual evapotranspiration is not water-limited, therefore it depends only on the land cover type of the given grid(s). The parameter β is similar to the crop coefficient as used by Allen et al. (1998), which is the ratio of crop evapotranspiration (in our model represented by ET_A for an area with additional water) to reference potential evapotranspiration (in our model represented by E_{pan}). The β parameter integrates the specific local conditions of that area with additional water. The actual evapotranspiration (ET_A) of such area (grid) in our model is calculated by multiplying the estimate of the "class U" pan evaporation (E_{pan}) by the value of β.

The spatially distributed values of the parameters α and β in our model are derived using Eq. (3) and Eq. (4), (with map algebra in a GIS) from maps of ET_A, P and T with a spatial resolution of 1 km^2. These parameter maps can be used for evaluating ET_A in a spatially distributed manner, for which only spatial estimates of T and P are required as gridded inputs.

Actual evapotranspiration (ET_A) in grids, where the Budyko hypothesis holds, the model calculations are based on α:

$$ET_A = P\left(1-\exp\left(-\frac{\alpha\left(36400\frac{T}{P}+104\right)}{P}\right)\right), \quad (5)$$

whereas in grids with additional water ET_A is calculated using β as:

$$ET_A = \beta E_{pan} = \beta\left(36400\frac{T}{P}+104\right). \quad (6)$$

The study area and input data

The Zala River provides the most significant inflow of water to Lake Balaton (Virág, 1997), which is the largest shallow lake in Central Europe (Dokulil et al., 2010). The Zala River Basin flows through the western part of Hungary (Fig. 1). The basin covers an area of 1520.7 km^2, the length of the main channel is 104 km. The long-term (1980–2008) mean discharge is 4.6 m^3 s^{-1} at the "Zalaapáti" gauging station.

The altitude ranges from 100 m a.s.l. to 334 m a.s.l. The basin has a moderately cool and moderately humid climate with a mean annual temperature of 10.4°C. The mean monthly temperature varies from about −1.7°C (West) and −0.9°C (East) in January to 19.5°C (West) and 20.5°C (East) in July. The long-term mean annual precipitation is 800 mm in the west and 660 mm in the eastern part of the basin.

The hydrological balance of the basin was studied in three nested sub-catchments, with increasing basin area. The three sub-catchments are labelled by the names of the cities/towns of the respective gauging stations: 1 - "Zalaegerszeg", 2 - "Zalabér" and 3 - "Zalaapáti" (Fig. 1). According to the CORINE Land Cover database (CLC, 2006; Table 1), agriculture is the dominant land use of the Zala Basin (57.5% of the total area). "Forests and semi-natural areas" cover 36.5% of the area, while "Artificial surfaces" (which include urban areas, roads, mines, and similar categories) cover 5.1% of the surface. The categories "Wetlands" and "Water bodies" are rather insignificant, comprising 0.3% and 0.6% of the total area, respectively.

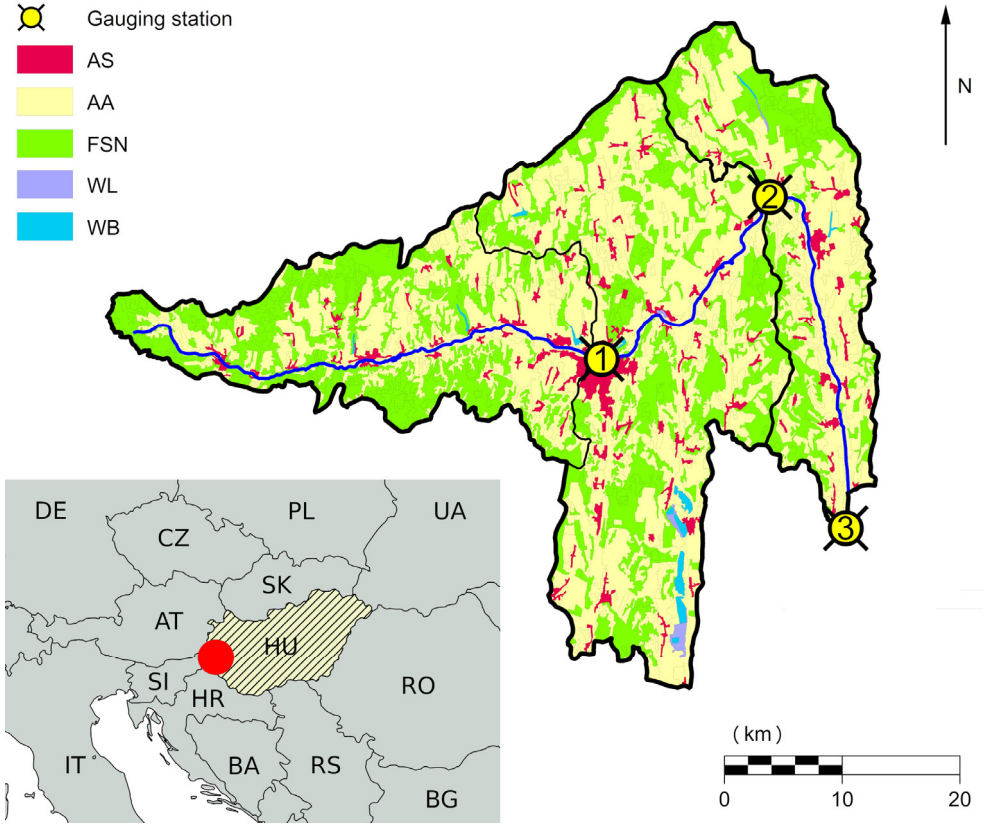

Fig. 1. Location of Hungary (hatched lines) and the Zala River Basin (red) within Europe, the three nested sub-catchments, their land cover and location of the gauging stations. CORINE Land Cover (CLC, 2006) categories are labelled as: AS - Artificial surfaces, AA - Agricultural areas, FSN - Forest and semi-natural areas, WL - Wetlands, WB - Water bodies. The sub-catchments are labelled by the names of the cities/towns of the respective gauging stations: 1 - "Zalaegerszeg"; 2 - "Zalabér"; 3 - "Zalaapáti".

Table 1. The proportions of the respective land cover categories within the three nested sub-catchments: AS - Artificial surfaces, AA - Agricultural areas, FSN - Forest and semi-natural areas, WL - Wetlands, WB - Water bodies.

Corine land cover categories	Sub-catchment					
	1 - "Zalaegerszeg"		2 - "Zalabér"		3 - "Zalaapáti"	
	(km^2)	(%)	(km^2)	(%)	(km^2)	(%)
AS	21.3	4.7	61.9	5.3	78.0	5.1
AA	228.3	49.7	654.7	56.1	874.2	57.5
FSN	207.9	45.3	439.1	37.6	554.9	36.5
WL	–	–	3.8	0.3	4.3	0.3
WB	1.4	0.3	8.6	0.7	9.3	0.6
Catchment area (km^2)	458.9		1168.1		1520.7	

For the Carpathian Basin, a gridded database of climate data was made available in the frame of the "CarpatClim" project (Lakatos et al., 2013; Szalai et al., 2012). The database includes gridded precipitation and air temperature data (P, T) with a spatial resolution of 0.1° (8 km × 12 km) for the period 1961–2010, estimated using the MISH (Meteorological Interpolation based on Surface Homogenized data basis) interpolation method for gridding (Szentimrey and Bihari, 2007) from climatological observations. As part of the EU-national project "Agroclimate" (Gálos et al., 2015) the "CarpatClim" precipitation and temperature data were further downscaled to a finer resolution of 1 km × 1 km, using a GIS software module developed by Czimber and Gálos (2016).

Monthly actual evapotranspiration (ET_{Am}) rates for the period of 2000–2008 have been mapped (in 1 km × 1 km spatial resolution) by Szilágyi and Kovács (2011) with the CREMAP (complementary-relationship-based evapotranspiration mapping) model, which is an established method in Hungary. Using their grid-based monthly maps, we prepared the long-term mean annual actual evapotranspiration (ET_A) map for the same nine-year period, which was used in this study.

Validation methodology of the CREMAP model outputs and the parameters maps of α and β

As for the validation of the CREMAP model data, we simply compared the estimated nine-year mean annual actual evapotranspiration (as estimated by CREMAP) with their water balance-based values (calculated using discharge data).

For the validation of our model (the parameters maps of α and β), 20 years (1980–1999) from the downscaled observed precipitation and temperature gridded data (based on the "CarpatClim" database) and observed streamflow (runoff, R) data were used for the Zala Basin's three nested sub-catchments. The runoff data, which was provided by the West-Transdanubian Water Directorate ("NYUDUVIZIG"), was estimated for each of the nested sub-catchments using rating curves and the measured water levels. For validation, the data was divided into three 10-year, partially overlapping, periods: 1980–1989, 1985–1994, and 1990–1999. For each of the periods and each of the sub-catchments, the long-term mean annual actual evapotranspiration values were calculated from the simplified water balance equation (Eq. (7)) and were also estimated by our model (with the α and β maps created by Eq. (5) and Eq. (6)).

$$ET_A = P - R, \tag{7}$$

where ET_A is the long-term mean annual actual evapotranspiration (mm yr^{-1}), P is the long-term mean annual precipitation (mm yr^{-1}), and R is the long-term mean annual runoff (mm yr^{-1}).

Then, we determined the difference (bias) between the water balance-based and the modelled values of the actual evapotranspiration.

Data for model predictions for future water balance estimations

For estimating the future long-term mean annual actual evapotranspiration, besides the Budyko-type α and β parameter maps (which were estimated using Eq. (3) and Eq. (4) on the data from the instrumental period), projected air temperature and precipitation data for the changing climate were required. They were obtained from outputs of 12 regional climate models (RCMs) using the SRES A1B (moderate) emission scenario (ENSEMBLES project: van der Linden and Mitchell, 2009; IPCC, 2007; Table 2). The original grid size of the RCM data was 25 km × 25 km. They were disaggregated (downscaled) to the resolution of 1 km × 1 km, using a GIS software module developed in C++ by Czimber and Gálos (2016), in the frame of the "Agroclimate" project (Gálos et al., 2015).

Table 2. The used regional climate models (RCMs) from the ENSEMBLES project (van der Linden and Mitchell, 2009), and the respective original General Circulation Models (GCM).

Nr.	RCM	GCM
1.	RCA3	HadCM3Q16
2.	REMO	ECHAM5
3.	CLM	HadCM3Q0
4.	RACMO2	ECHAM5-r3
5.	HIRHAM5	ARPEGE
6.	HIRHAM5	ECHAM5
7.	RCA	BCM
8.	RCA	HadCM3Q3
9.	RCA	ECHAM5-r3
10.	HadRM3Q0	HadCM3Q0
11.	HadRM3Q3	HadCM3Q3
12.	HadRM3Q16	HadCM3Q16

In the predictions of the future climate Eq. (5) and Eq. (6) were used for estimating the spatially distributed (gridded) future long-term mean annual actual evapotranspiration. The predictions of the long-term mean annual runoff on sub-catchment scale were calculated from the long-term water balance equation (Eq. (7)) as the difference between the areal average of the long-term mean annual precipitation and the estimated future actual evapotranspiration over each sub-catchment.

We made such estimates for three time periods (2011–2040, 2041–2070, 2071–2100) and determined the expected changes in the water balance components relative to the reference period (1981–2010) for each sub-catchment.

RESULTS AND DISCUSSION

Evaluation and validation of the CREMAP model data over the period 2000-2008

Table 3 contains the meteorological data (temperature, precipitation), the measured runoff data and the results of the CREMAP actual evapotranspiration validation over the 2000–2008 period for the three sub-catchments of the Zala River Basin (as the nine-year mean annual rates, averaged for the sub-catchment areas). For the CREMAP validation, the nine-year mean annual actual evapotranspiration was calculated for the sub-catchments using the simplified long-term water-balance equation (Eq. (7)).

The western sub-catchment (1 - "Zalaegerszeg") was colder and wetter than the two larger sub-catchments (2 - "Zalabér" and 3 - "Zalaapáti") in the validation period. The nine-year mean annual (water balance-based) actual evapotranspiration of the total area examined (3 - "Zalaapáti") was 555 mm yr^{-1}, 89.7% of the mean annual precipitation. The mean annual measured runoff was 64 mm yr^{-1}, the 10.3% of the mean annual precipitation.

Table 3. Validation of the CREMAP model actual evapotranspiration against the water balance equation in the 2000–2008 period in the three nested sub-catchments. T is the mean annual air temperature ("CarpatClim"), P is the mean annual precipitation ("CarpatClim"), R is the mean annual measured runoff ("NYUDUVIZIG"), ET_{WB} is the mean annual actual evapotranspiration from water balance calculation ($ET_{WB} = P - R$), ET_{CREMAP} is the estimated mean annual actual evapotranspiration (CREMAP model), and ET_{diff} is the difference between the water balance-based and the estimated evapotranspiration ($ET_{diff} = ET_{WB} - ET_{CREMAP}$). ET_{WB}/P and R/P represent the proportions of actual evapotranspiration to precipitation and runoff to precipitation, respectively.

Sub-catchment	T	P	R	ET_{WB}	ET_{CREMAP}	ET_{diff}		ET_{WB}/P	R/P
	(°C)	(mm yr^{-1})	(mm yr^{-1})	(mm yr^{-1})	(mm yr^{-1})	(mm yr^{-1})	(%)	(%)	(%)
1 - "Zalaegerszeg"	10.7	640	63	577	567	10	1.7	90.1	9.9
2 - "Zalabér"	10.8	629	67	562	566	−4	0.6	89.4	10.6
3 - "Zalaapáti"	10.9	619	64	555	569	−14	2.4	89.7	10.3

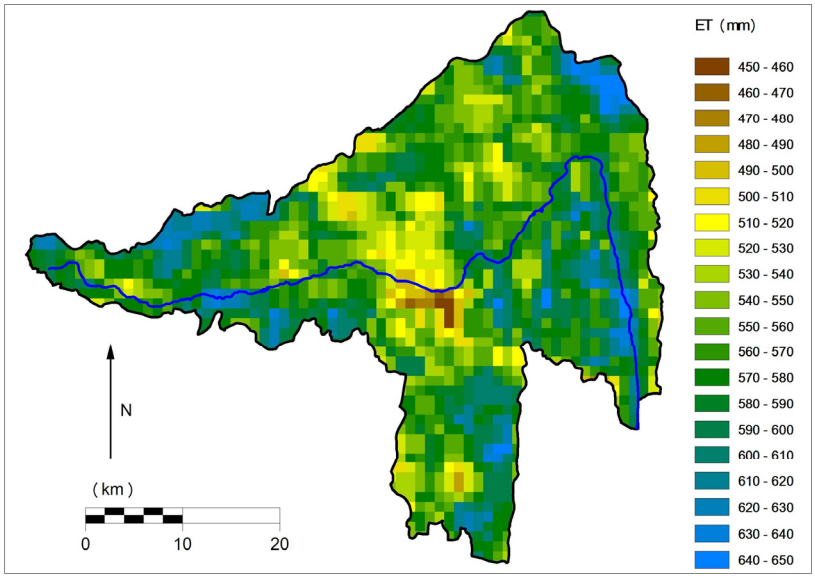

Fig. 2. The nine-year (2000–2008) mean actual annual evapotranspiration over the Zala River Basin based on CREMAP model data (spatial resolution 1 km^2).

The differences between the nine-year mean annual water balance-based and the mean estimated (CREMAP model) actual annual evapotranspiration are: 1.7% (10 mm yr^{-1}) for the 1 - "Zalaegerszeg" sub-catchment, 0.6% (−4 mm yr^{-1}) for the 2 - "Zalabér" sub-catchment, and 2.4% (−14mm yr^{-1}) for the total area examined (3 - "Zalaapáti"). These results verify that the CREMAP spatially distributed gridded evapotranspiration data can be used for water balance modelling in the Zala River Basin and as a basis for the estimation of the two parameters of our model.

The spatial variability of the nine-year (2000–2008) mean actual annual evapotranspiration (ET_{CREMAP}) based on the CREMAP data is depicted in Fig. 2. Brown and yellow grids show lower rates (e.g. the city Zalaegerszeg and its surroundings in the centre of the basin), green and blue grids show higher evapotranspiration rates (mainly in the western, north-eastern and south-eastern parts of the basin).

Evaluation and validation of the proposed climate-runoff model parameters

The α and β parameter maps, as estimated by Eq. (3) and Eq. (4) using the CREMAP model data, for the Zala Basin can be seen in Fig. 3. The α values cover 89% of the basin, and only 11% belongs to β (additional water-affected areas). In the case of α, violet and blue grids show higher, red and orange grids show lower parameter values. In the case of β, the parameter values are growing from light blue to the direction of dark blue. The validation process of the model parameters was done according to the method described in the previous chapter using data from the partially overlapping decades 1980–1989, 1985–1994, 1990–1999. Table 4 contains the results of the validation.

The differences (ET_{diff}, i.e. model bias) between the calculated (from the water balance, ET_{WB}) and the estimated (by the proposed model, ET_{model}) mean annual evapotranspiration are 0.7% (4 mm yr^{-1}), 1.2% (7 mm yr^{-1}) and 3.6% (22 mm yr^{-1}) in the 1 - "Zalaegerszeg" sub-catchment, and 0.5% (3 mm yr^{-1}), 1.0% (6 mm yr^{-1}) and 3.3% (20 mm yr^{-1}) in the 2 - "Zalabér" sub-catchment. In the case of the total basin area (3 - "Zalaapáti") the differences are 0.4% (2 mm yr^{-1}), 0.7% (4 mm yr^{-1}) and 2.7% (16 mm yr^{-1}). In the period 1990–1999 the model bias is a bit higher (but still relatively low) for all three sub-catchments. One possible explanation of it is that this period was relatively wet (compared to the other two periods) and therefore the areas with additional water probably expanded during these years. In consequence, the number of model grids with the β parameter (Eq. (6)) was underestimated using the information of the calibration period (2000–2008). A larger number of grids with β would increase evapotranspiration, and this cannot be followed by the model based on the 2000–2008 period, so for the period 1990–1999 the model slightly underestimates ET.

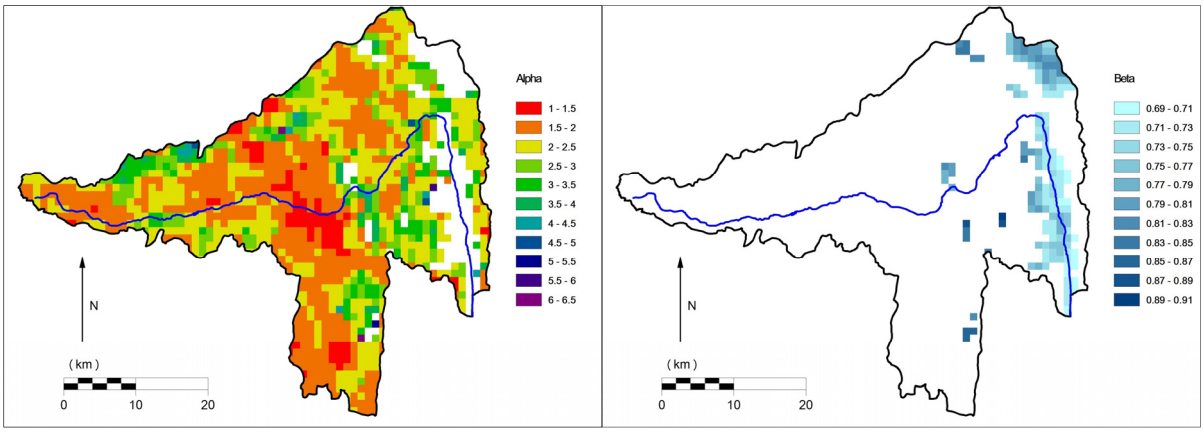

Fig. 3. The spatial variability of the α (left) and β parameters (right) of the proposed climate-runoff model over the Zala River Basin (spatial resolution 1 km^2).

Table 4. Validation results of the proposed climate-runoff model for the sub-catchments of the Zala River Basin in the three validation periods. P is the mean annual precipitation ("CarpatClim"), R is the mean annual measured runoff ("NYUDUVIZIG"), ET_{WB} is the mean annual actual evapotranspiration from water balance calculation ($ET_{WB} = P - R$), ET_{model} is the mean annual estimated actual evapotranspiration and ET_{diff} is the difference between the water balance-based and the estimated evapotranspiration ($ET_{diff} = ET_{WB} - ET_{model}$) in absolute values and in percentages.

Sub-catchment	Period	P	R	ET_{WB}	ET_{model}	ET_{diff}	
		(mm yr^{-1})	(mm yr^{-1})	(mm yr^{-1})	(mm yr^{-1})	(mm yr^{-1})	(%)
1 - "Zalaegerszeg"	1980–1989	698	131	567	571	4	0.7
	1985–1994	684	117	567	574	7	1.2
	1990–1999	716	108	608	586	22	3.6
2 - "Zalabér"	1980–1989	687	112	575	572	3	0.5
	1985–1994	676	107	569	575	6	1.0
	1990–1999	713	104	609	589	20	3.3
3 - "Zalaapáti"	1980–1989	680	114	566	568	2	0.4
	1985–1994	671	103	568	572	4	0.7
	1990–1999	706	106	600	584	16	2.7

Table 5. The average of the long-term changes of mean annual temperature (dT), precipitation (dP), actual evapotranspiration (dET), runoff (dR) predicted by 12 RCMs, and the standard deviations (SD) of dET and dR. Reference period: 1981–2010.

Sub-catchment	Period	Change (relative to 1981–2010)			
		dT	dP	dET (SD)	dR (SD)
		(°C)	(mm yr^{-1})	(mm yr^{-1})	(mm yr^{-1})
1 - "Zalaegerszeg"	2011–2040	0.9	0	7 (16)	−8 (27)
	2041–2070	2.1	8	22 (21)	−14 (23)
	2071–2100	3.2	−12	20 (36)	−31 (29)
2 - "Zalabér"	2011–2041	0.9	1	8 (15)	−7 (27)
	2041–2071	2.0	9	22 (21)	−14 (23)
	2071–2101	3.2	−11	20 (35)	−31 (28)
3 - "Zalaapáti"	2011–2042	0.9	1	10 (14)	−9 (30)
	2041–2072	2.0	10	25 (21)	−16 (26)
	2071–2102	3.2	−9	27 (36)	−36 (35)

Evapotranspiration and runoff predictions for future climates

Modelling the possible climate change impacts in the Zala River Basin and its sub-catchments was performed according to the previously described methodology. We estimated the long-term mean annual actual evapotranspiration (ET_A) and runoff (R) for three time periods (2011–2040, 2041–2070, 2071–2100) with downscaled data from the 12 RCMs (Table 1) and evaluated the expected changes relative to the reference period 1981–2010. The average of the respective long-term means of the changes predicted by the RCMs (relative to the reference period) of mean annual temperature, precipitation, evapotranspiration and runoff are summarized in Table 5.

According to the RCMs' projections, in the case of the long-term mean annual temperature, an increasing trend is expected during the 21st century. It is projected to be more than 3°C higher in the period 2071–2100 relative to the reference period

in all three sub-catchments. However, the change in the long-term mean annual precipitation (*dP*) is not significant; a small increase (8–10 mm yr^{-1}) is projected for 2041–2070, and a slight decrease (9–12 mm yr^{-1}) for 2071–2100, when compared to the time period of 1981–2010. In consequence, an increase can be detected in the long-term mean annual actual evapotranspiration rates for all sub-catchments during the 21st century. A smaller increase (7–10 mm yr^{-1}) is expected for the first, and higher increases (20–27 mm yr^{-1}) for the second and third periods. Due to this, in the case of long-term mean annual runoff, a significant decrease can be detected. The highest decrease is estimated for the third period (31–36 mm yr^{-1}), compared to the reference period. The highest standard deviation values belong to the last period for both cases.

Figs. 4 and 5 illustrate the expected changes of long-term mean annual actual evapotranspiration and runoff in percentages across the ensemble of the 12 RCMs as box and whiskers plots (Venables and Ripley, 1999). The spread – based on the simulation results of the ensemble of 12 RCMs – shows the uncertainty in the predictions, which grows from period to period (in the 21st century). For the middle of the century (2041–2070), on average, a higher evapotranspiration increase is predicted (3.3–4.2%, Fig. 4). In the case of 3 - "Zalaapáti", 1.6%, 4.2%, and 4.4% increases in the averaged long-term mean evapotranspiration can be detected in the first, second, and third time period, respectively, compared to the reference period (1981–2010). The maximum increase can exceed 12.0% by the end of the century. The decrease in the averaged long-term mean runoff may exceed 40.0% by the end of the century, compared to the reference period, for all sub-catchments (Fig. 5). For the examined total basin area ("Zalaapáti"), the averaged long-term mean values may decrease by 21.2%, 33.2% and 53.4%, respectively. The estimated overall increase in the long-term evapotranspiration and the significant decrease in long-term runoff can lead to possible serious consequences, such as the risk of the severe deterioration of the local wetlands (e.g., Little-Balaton wetland area) no excluding a drying out. According to the predictions, the water supply to Lake Balaton may significantly decline.

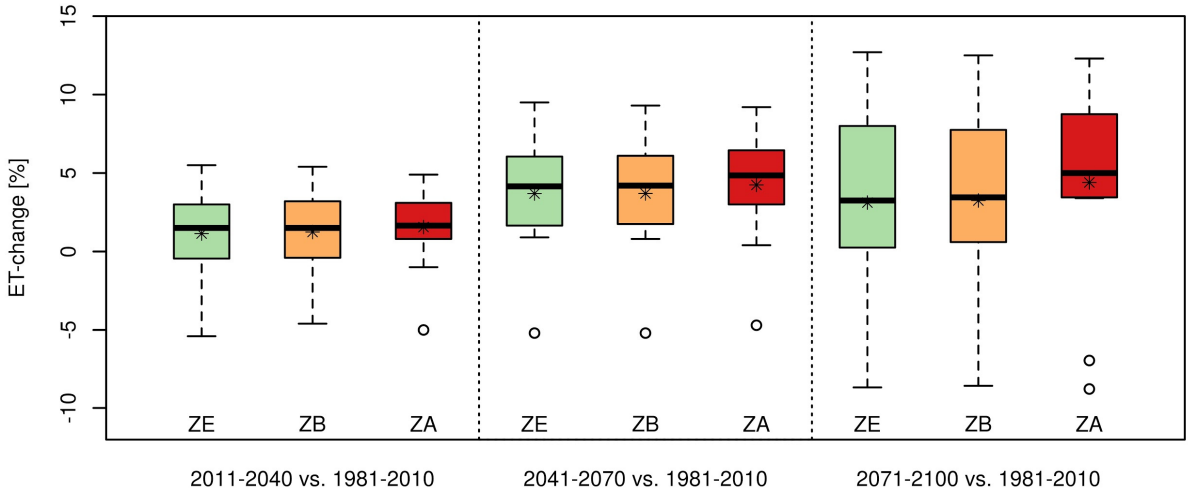

Fig. 4. The predicted changes in long-term mean annual actual evapotranspiration (*ET*) rates across the RCM ensemble. Reference period: 1981–2010. ZE: 1 - "Zalaegerszeg", ZB: 2 - "Zalabér", ZA: 3 - "Zalaapáti".

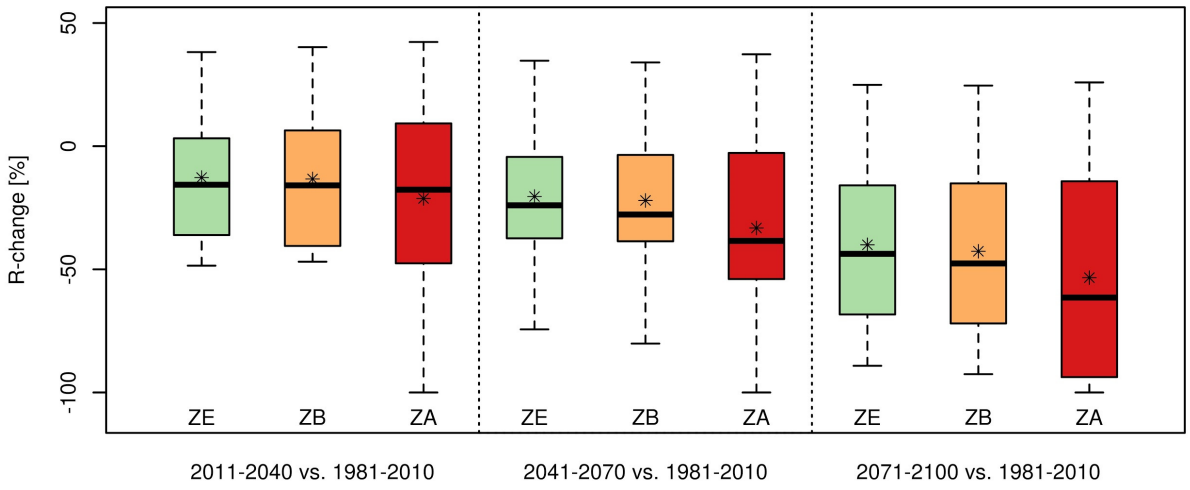

Fig. 5. The predicted changes in long-term mean annual runoff (*R*). Reference period: 1981–2010. ZE: 1 - "Zalaegerszeg", ZB: 2 - "Zalabér", ZA: 3 - "Zalaapáti".

The uncertainties of the presented model predictions stem from the following sources: uncertainty of the CREMAP model evapotranspiration and the interpolated "CarpatClim" meteorological data (used for calculating the presented climate-runoff model parameters), and the spread of the downscaled climate projections (the regional climate models). Further, although an increase in the frequency and duration of the dry periods are expected, the proposed climate-runoff model cannot handle the reduction of the number of β-type grids (areas with additional water) for such scenarios in the future. In its present version, we cannot change the β-type grids to α-type ones, since during the model calibration period (2000−2008) these grids were affected by additional water, where the Budyko hypothesis (used for calculating the α model parameters) was not valid. Thus, our future aim is to solve the β to α transformation of a given grid in the development of the next version of the model.

Comparison with other model predictions for the Carpathian Basin

In order to examine the credibility of the results obtained, we compared them with other predictions made for the region. For Hungary and the Carpathian Basin, relatively few long-term hydrological climate change predictions have been published. Comparing hydrological predictions achieved by different models is not a simple task. The predictions were made for diverse areas, with various time steps (daily, monthly, seasonal, annual, long-term), reference and predicted time periods. In order to underpin the plausibility of our results, a comparison of the tendencies of the different predictions is attempted.

Nováky (2008) examined the possible effects of climate change on the water balance of Lake Balaton, until the middle of the 21st century. The runoff from the basin of the lake was calculated with the Budyko-type spatially distributed empirical climate-runoff model. The conclusions of the analysis are supporting our results: the drying climate is very likely to lead to worsening of the average water balance of the lake. By 2050 the decreasing runoff and inflow may not be enough to balance the increasing rate of evaporation from the lake, which could degrade into a closed lake without outflow (which is feeding the Sió River in present climatic conditions).

Keve and Nováky (2010) also used the Budyko-type spatially distributed empirical climate-runoff model for the Bácsbokodi-Kígyós watershed (South Hungary), under different climate scenarios. According to their results, by the period 2021–2040, the average decrease of the mean annual runoff may be 43%, compared to the reference period (1977–1998). Based on the most pessimistic climate scenario, the decrease can reach 61%.

The expected changes of runoff for the watershed of Zagyva-Tarna (North Hungary) were modelled in Kis et al. (2015) by the DIWA (Distributed Watershed hydrological model, Szabó, 2007), on daily and annual time steps. By the period of 2070–2099, much lower annual runoff rates appeared than in the reference period (1976–2005). However, floods may become more intense and more frequent. Kis et al. (2017) also examined the Upper Tisza Basin by the DIWA model. They concluded that the yearly average of the runoff values is estimated to decrease during the 21st century. On a seasonal scale, decreasing runoff is predicted for spring, summer, and autumn, while a substantial runoff increase in winter.

Herceg et al. (2016) developed a Thornthwaite-type monthly water balance model, which is also based on the CREMAP evapotranspiration rates as reference values. They examined the possible future changes of actual evapotranspiration and soil moisture for two study areas in Northwest Hungary (a forested catchment and an area with mixed land cover). Although the model is not spatially distributed and it uses a monthly time step, the analysis arrived at similar tendencies like our results here. According to their estimates, the long-term monthly average evapotranspiration may increase by 11% for both areas by the end of the 21st century, compared to the 1980–2010 reference period. In addition, sharply decreasing values of the soil moisture minimum (i.e. the minimum soil moisture available for the plants) are predicted: −48% and −32%, for the area with mixed land cover and the forested area, respectively. The soil water resources may decrease drastically in the summer periods because of the increasing evapotranspiration and declining recharge from precipitation.

Danihlik et al. (2004) evaluated the potential impact of climate change on river runoff in the upper part of the Hron River in Slovakia. For long-term predictions an empirical grid-based model (Parajka et al., 2004; based on the Turc (1954) model), while for monthly predictions a conceptual spatially-lumped water balance model was used (Hlavčová et al., 2002). They examined the possible changes for the time horizons 2010, 2030 and 2075 compared to a reference period (1951–1980), using data from four climate change scenarios. A decrease in the long-term mean annual runoff is expected in the upper Hron River basin, according to all scenarios and time horizons (−5% to −16% for the time horizon 2010, −5% to −27% for 2030, and −13% to −45% for 2075). They concluded that the effects of an increase in temperature would be decisive for these changes, even in cases when an increase in precipitation is expected. According to the seasonal analysis, the basin could become vulnerable to drought in the summer and early autumn, and the intensity of the changes could increase towards the time horizon 2075. These findings are in agreement with our results and the results of Hlavčová et al. (2006), who used the same method for estimating changes in the long-term mean annual runoff for the whole Slovakia including its border regions with Hungary, and the seasonal changes for five selected basins in Slovakia. It was concluded that – according to two climate change scenarios – most of the territory of the country would be affected by a decrease in the long-term runoff.

All these hydrological predictions may be regarded as an indirect verification of our results for the region. They showed similar tendencies, which validate our main result, namely that a significant long-term mean annual runoff decrease may be expected for the end of the 21st century in the Carpathian Basin.

CONCLUSIONS

Regional modelling and evaluating the possible impacts of climate change on water resources over different time scales is essential for agriculture, forestry, and water management in Hungary and the Carpathian Basin. For this purpose, a long-term climate-runoff model proposed by Csáki et al. (2014, 2018) was further developed in this paper. We presented a complex validation methodology of the climate-runoff model, which was verified for the Zala River Basin (which is an essential runoff contributing region to Lake Balaton, the largest shallow lake in Central Europe). Furthermore, our aim was also extending the methodology to enable climate change impact assessment. In a case study, we performed hydrological predictions for the 21st century using the proposed model and analyzed the possible climate change impacts in the study area. These results were compared to similar studies in the region in order to underpin the plausibility of our results.

The averaged long-term mean annual evapotranspiration and runoff predictions performed for three periods (2011–2040, 2041–2070, 2071–2100) over the Zala River Basin, using the proposed climate-runoff model and downscaled scenarios from an ensemble of 12 regional climate models. The predictions showed, that by the end of the century due to the increase of the long-term mean annual evapotranspiration rate by 4.4% relative to the reference period (1981–2010) a substantial decrease can be detected in the case of long-term mean annual runoff, which may exceed 40.0% for all sub-catchments. It can be concluded that the decreasing runoff from the catchments may not be enough to balance the increased evaporation rate of Lake Balaton, transforming it into a closed lake without outflow with severe ecological consequences.

The main advantage of the proposed model is its robust nature, requiring few input parameters that in turn, result in the lower potential of errors. It can be applied if temperature and precipitation time series (e.g. from regional climate models) are available. Predictions obtained using the model can assist in long-term planning in different fields (water management, agriculture, forestry, etc.) and help decision-makers in formulating the necessary courses of action.

Acknowledgement. This research has been supported by the EFOP-3.6.2-16-2017-00018 in University of Sopron project. Péter Kalicz's work has also been supported by the János Bolyai Scholarship of the Hungarian Academy of Sciences. The participation of Ján Szolgay was supported by the VEGA Scientific Grant Agency Grant No. 1/0632/19. The supports are gratefully acknowledged.

REFERENCES

Allen, R.G., Pereira, L.S., Raes, D., Smith, M., 1998. Crop evapotranspiration-Guidelines for computing crop water requirements. FAO Irrigation and Drainage Paper, 56, 333.

Anders, I., Stagl, J., Auer, I., Pavlik, D., 2014. Climate change in central and eastern Europe. In: Rannow. S., Neubert, M. (Eds.): Managing Protected Areas in Central and Eastern Europe Under Climate Change. Springer, Dordrecht. pp. 17–30.

Andréassian, V., Coron, L., Lerat, J., Moine, N. Le, 2016. Climate elasticity of streamflow revisited – an elasticity index based on long-term hydrometeorological records. Hydrology and Earth System Sciences, 20, 4503–4524. DOI: 10.5194/hess-20-4503-2016

Arora, V.K., 2002. The use of the aridity index to assess climate change effect on annual runoff. Journal of Hydrology, 265, 164–177. https://doi.org/10.1016/S0022-1694(02)00101-4

Bates, B.C., Kundzewicz, Z.W., Wu, S., Palutikof, J.P. (Eds.), 2008. Climate change and water. Technical Paper of the Intergovernmental Panel on Climate Change, IPCC Secretariat, Geneva, 210 p.

Budyko, M.I., 1974. Climate and Life. Academic, Orlando, Fla.

Chen, X., Alimohammadi, N., Wang, D., 2013. Modeling interannual variability of seasonal evaporation and storage change based on the extended Budyko framework, Water Resources Research, 49, 9, 6067–6078.

CLC, 2006. Corine Land Cover. European Environment Agency, European Topic Centre for Spatial information and Analysis, Copenhagen, Denmark.

Csáki, P., Kalicz, P., Brolly, G.B., Csóka, G., Czimber, K., Gribovszki, Z., 2014. Hydrological impacts of various land cover types in the context of climate change for Zala County. Acta Silvatica et Lignaria Hungarica, 10, 2, 115–129. https://doi.org/10.2478/aslh-2014-0009

Csáki, P., Szinetár, M.M., Herceg, A., Kalicz, P., Gribovszki, Z., 2018. Climate change impacts on the water balance - case studies in Hungarian watersheds. Időjárás, 122, 1, 81–99. https://doi.org/10.28974/idojaras.2018.1.6

Cui, Y., Chen, X., Gao, J., Yan, B., Tang, G., Hong, Y., 2018. Global water cycle and remote sensing big data: overview, challenge, and opportunities. Big Earth Data, 2, 3, 282–297.

Czimber, K., Gálos, B., 2016. A new decision support system to analyse the impacts of climate change on the Hungarian forestry and agricultural sectors. Scandinavian Journal of Forest Research, 31, 7, 664–673.

Danihlik, R., Hlavčová, K., Kohnová, S., Parajka, J., Szolgay, J., 2004. Scenarios of the change in the mean annual and monthly runoff in the Hron Basin. Journal of Hydrology and Hydromechanics, 52, 4, 291–302.

Dokulil, M.T., Teubner, K., Jagsch, A., Nickus, U., Adrian, R., Straile, D., Jankowski, T., Herzig, A., Padisák, J., 2010. The impact of climate change on lakes in Central Europe. In: D. George, G. (Ed.): The impact of climate change on European lakes. Aquatic Ecology Series 4. Springer Science+Business Media B. V. DOI: 10.1007/978-90-481-2945-4_20

Fraedrich, K., 2010. A parsimonious stochastic water reservoir: Schreiber's 1904 equation. Journal of Hydrometeorology, 11, 2, 575–578.

Fu, B.P., 1981. On the calculation of the evaporation from land surface. Scientia Atmospherica Sinica, 5, 1, 23–31.

Gálos, B., Führer, E., Czimber, K., Gulyás, K., Bidló, A., Hänsler, A., Jacob, D., Mátyás, C., 2015. Climatic threats determining future adaptive forest management – a case study of Zala County. Időjárás, 119, 4, 425–441.

Gao, G., Fu, B., Wang, S., Liang, W., Jiang, X., 2016. Determining the hydrological responses to climate variability and land use/cover change in the Loess Plateau with the Budyko framework. Science of the Total Environment, 557, 331–342.

Greve, P., Gudmundsson, L., Orlowsky, B., Seneviratne, S.I., 2016. A two-parameter Budyko function to represent conditions under which evapotranspiration exceeds precipitation. Hydrology and Earth System Sciences, 20, 6, 2195–2205.

Herceg, A., Kalicz, P., Kisfaludi, B., Gribovszki, Z., 2016. A monthly-step water balance model to evaluate the hydrological effects of climate change on a regional scale for irrigation design. Slovak Journal of Civil Engineering, 24, 4, 27–35. https://doi.org/10.1515/sjce-2016-0019

Hlásny, T., Mátyás, C., Seidl, R., Kulla, L., Merganičová, K., Trombik, J., Dobor, L., Barcza, Z., Konôpka, B., 2014. Climate change increases the drought risk in Central European forests: What are the options for adaptation? Central European Forestry Journal, 60, 5–18. https://doi.org/10.2478/forj-2014-0001

Hlavčová, K., Kalaš, M., Szolgay, J., 2002. Impact of climate change on the seasonal distribution of runoff in Slovakia. Slovak Journal of Civil Engineering, 10, 2, 10−17.

Hlavčová, K., Parajka, J. D., Szolgay, J., Kohnová, S., 2006. Grid-based and conceptual approaches to modelling the impact of climate change on runoff. Slovak Journal of Civil Engineering, 14, 1, 19–29.

IPCC, 2007. Climate Change 2007: Synthesis Report. In: Core Writing Team, Pachauri, R.K, Reisinger, A. (Eds.): Contribution of Working Groups I, II and III to the Fourth Assessment Report of the Intergovernmental Panel on Climate Change. IPCC, Geneva, Switzerland, 104 p.

IPCC, 2019. Shukla, P.R., Skea, J., Slade, R., van Diemen, R., Haughey, E., Malley, J., Pathak, M., Portugal Pereira, J.

(Eds.): Technical Summary. In: Shukla, P.R., Skea, J., Calvo Buendia, E., Masson-Delmotte, V., Pörtner, H.-O., Roberts, D.C., Zhai, P., Slade, R., Connors, S., van Diemen, R., Ferrat, M., Haughey, E., Luz, S., Neogi, S., Pathak, M., Petzold, J., Portugal Pereira, J., Vyas, P., Huntley, E., Kissick, K., Belkacemi, M., Malley, J. (Eds.): Climate Change and Land. An IPCC Special Report on climate change, desertification, land degradation, sustainable land management, food security, and greenhouse gas fluxes in terrestrial ecosystems. IPCC. (In press.) Available at: https://www.ipcc.ch/srccl/

Jiang, C., Xiong, L., Wang, D., Liu, P., Guo, S., Xu, C., 2015. Separating the impacts of climate change and human activities on runoff using the Budyko-type equations with time-varying parameters. Journal of Hydrology, 522, 326–338. https://doi.org/10.1016/j.jhydrol.2014.12.060

Karamouz, M., Ahmadi, B., Zahmatkesh, Z., 2013. Developing an agricultural planning model in a watershed considering climate change impacts. Journal of Water Resources Planning and Management, 139, 4, 349–363.

Keve, G., Nováky, B., 2010. Klímaváltozás hatásának vizsgálata a Bácsbokodi-Kígyós csatorna vízgyűjtőjén Budyko modell alkalmazásával. In: XXVIII. National Conference of the Hungarian Hydrological Society, Sopron, 7–9th July, 2010. (In Hungarian.)

Kis, A., Szabó, J.A., Pongrácz, R., Bartholy, J., 2015. A klímaváltozás extrém lefolyási karakterisztikákra gyakorolt hatásainak elemzése a Zagyva vízgyűjtőn. Eötvös Loránd Tudományegyetem, Egyetemi Meteorológiai Füzetek, 26, 41–48. (In Hungarian.)

Kis, A., Pongrácz, R., Bartholy, J., Szabó, J.A., 2017. Application of RCM results to hydrological analysis. Időjárás, 121, 4, 437–452.

Kohnová, S., Rončák, P., Hlavčová, K., Szolgay, J., Rutkowska, A., 2019. Future impacts of land use and climate change on extreme runoff values in selected catchments of Slovakia. Meteorology Hydrology and Water Management. Research and Operational Applications, 7, 1, 47–55.

Konapala, G., Mishra, A.K., 2016. Three-parameter-based streamflow elasticity model: Application to MOPEX basins in the USA at annual and seasonal scales. Hydrology and Earth System Sciences, 20, 6, 2545–2556.

Kundzewicz, Z. W., Matczak, P., 2015. Extreme hydrological events and security. Proceedings of the International Association of Hydrological Sciences, 369, 181–187.

Labudová, L., Faško, P., Ivaňáková, G., 2015. Changes in climate and changing climate regions in Slovakia. Moravian Geographical Reports, 23, 3, 71–82.

Lakatos, M., Szentimrey, T., Bihari, Z., Szalai, S., 2013. Creation of a homogenized climate database for the Carpathian region by applying the MASH procedure and the preliminary analysis of the data. Időjárás, 117, 1, 143–158. WWW.CARPATCLIM-EU.ORG

Liang, W., Bai, D., Jin, Z., You, Y., Li, J., Yang, Y., 2015. A study on the streamflow change and its relationship with climate change and ecological restoration measures in a sediment concentrated region in the Loess Plateau, China. Water resources management, 29, 11, 4045–4060.

Lugato, E., Alberti, G., Gioli, B., Kaplan, J.O., Peressotti, A., Miglietta, F., 2013. Long-term pan evaporation observations as a resource to understand the water cycle trend: Case studies from Australia. International Association of Scientific Hydrology Bulletin, 58, 1287–1296.

Lv, X., Zuo, Z., Ni, Y., Sun, J., Wang, H., 2019. The effects of climate and catchment characteristic change on streamflow in a typical tributary of the Yellow River. Scientific Reports, 9, 14535. DOI: 10.1038/s41598-019-51115-x

Mátyás, C., Berki, I., Bidló, A., Csóka, G., Czimber, K., Führer, E., Gálos, B., Gribovszki, Z., Illés, G., Hirka, A., Somogyi, Z., 2018. Sustainability of forest cover under climate change on the temperate-continental xeric limits. Forests, 9, 8, 489.

McMahon, T.A., Peel, M.C., Lowe, L., Srikanthan, R., McVicar, T.R., 2012. Estimating actual, potential, reference crop and pan evaporation using standard meteorological data: a pragmatic synthesis. Hydrology and Earth System Sciences Discussions, 9, 11829–11910. https://doi.org/10.5194/hessd-9-11829-2012

Mezentsev, V., 1955. Back to the computation of total evaporation. Meteorologia i Gidrologia, 5, 24–26.

Ning, T., Li, Z., Feng, Q., Liu, W., Li, Z., 2018. Comparison of the effectiveness of four Budyko-based methods in attributing long-term changes in actual evapotranspiration. Scientific Reports, 8, 1, 1–10. https://doi.org/10.1038/s41598-018-31036-x

Nováky, B., 1985. A lefolyás éghajlati adottságai a Zagyva-Tarna vízrendszerben. Vízügyi Közlemények, 1, 78–93. (In Hungarian.)

Nováky, B., 2002. Mapping of mean annual actual evaporation on the example of Zagyva catchment area. Időjárás, 106, 3–4, 227–238.

Nováky, B., 2008. Climate change impact on water balance of Lake Balaton. Water Science and Technology, 58, 9, 1865–1869.

Nováky, B., Bálint, G., 2013. Shifts and modification of the hydrological regime under climate change in Hungary. In: Singh, B.R. (Ed.): Climate change - realities, impacts over ice cap, sea level and risks. InTech. https://doi.org/10.5772/54768

Ol'dekop, E.M., 1911. On evaporation from the surface of river basins. Transactions on meteorological observations, 4, 200.

Parajka, J., Szolgay, J., Meszaros, I., Kostka, Z., 2004. Grid-based mapping of the long-term mean annual potential and actual evapotranspiration in upper Hron River basin. Journal of Hydrology and Hydromechanics, 52, 4, 239–254.

Pike, J.G., 1964. The estimation of annual runoff from meteorological data in a tropical climate. Journal of Hydrology, 2, 2, 116–123.

Pogačar, T., Žnidaršič, Z., Črepinšek, Z., Bogataj, L.K., 2019. Aggravated Occupational Heat Stress Recognition and Mitigation in Slovenia. In: Leal Filho, W., Trbic, G., Filipovic, D. (Eds.): Climate Change Adaptation in Eastern Europe. Climate Change Management. Springer, Cham, pp. 267–277.

Pongrácz, R., Bartholy, J., 2006. Tendency analysis of extreme climate indices with special emphasis on agricultural impacts. In: Proc. Int. Conf. Bioklimatológia a voda v krajine, Strečno, 11, 14, 9.

Pongrácz, R., Bartholy, J., Kis, A., 2014. Estimation of future precipitation conditions for Hungary with special focus on dry periods. Időjárás, 118, 4, 305–321.

Porporato, A., Daly, E., Rodriguez-Iturbe, I., 2004. Soil water balance and ecosystem response to climate change. The American Naturalist, 164, 5, 625–632.

Priestley, C.H.B., Taylor, R.J., 1972. On the assessment of surface heat flux and evaporation using large-scale parameters. Monthly Weather Review, 100, 2, 81–92.

Renner, M., Bernhofer, C., 2012. Applying simple water-energy balance frameworks to predict the climate sensitivity of streamflow over the continental United States. Hydrology

and Earth System Sciences, 16, 2531–2546. https://doi.org/10.5194/hess-16-2531-2012

Rončák, P., Hlavčová, K., Kohnová, S., Szolgay, J., 2019. Impacts of future climate change on runoff in selected catchments of Slovakia. In: Leal Filho, W., Trbic, G., Filipovic, D. (Eds.): Climate Change Adaptation in Eastern Europe. Climate Change Management. Springer, Cham. pp. 279–292.

Schreiber, P., 1904. Über die Beziehungen zwischen dem Niederschlag und der Wasserführung der Flüsse in Mitteleuropa. Z. Meteorol., 21, 10, 441–452. (In German.)

Shen, Q., Cong, Z., Lei, H., 2017. Evaluating the impact of climate and underlying surface change on runoff within the Budyko framework: A study across 224 catchments in China. Journal of Hydrology, 554, 251–262. https://doi.org/10.1016/j.jhydrol.2017.09.023

Škvarenina, J., Tomlain, J., Hrvol', J., Škvareninová, J., 2009. Occurrence of dry and wet periods in altitudinal vegetation stages of West Carpathians in Slovakia: Time-Series Analysis 1951–2005. In: Střelcová, K. et al. (Eds.): Bioclimatology and Natural Hazards. Springer, Dordrecht, pp. 97–106.

Spinoni, J., Lakatos, M., Szentimrey, T., Bihari, Z., Szalai, S., Vogt, J., Antofie, T., 2015. Heat and cold waves trends in the Carpathian Region from 1961 to 2010. International Journal of Climatology, 35, 14, 4197–4209. https://doi.org/10.1002/joc.4279

Stagl, J., Mayr, E., Koch, H., Hattermann, F.F., Huang, S., 2014. Effects of climate change on the hydrological cycle in Central and Eastern Europe. In: Rannow. S., Neubert, M. (Eds.): Managing Protected Areas in Central and Eastern Europe under Climate Change. Springer, Dordrecht, pp. 31–43.

Szabó, J.A., 2007. Decision supporting hydrological model for river basin flood control. In: Peckham, R.J., Jordan, G. (Eds.): Digital Terrain Modelling: Development and Applications in a Policy Support Environment. Springer-Verlag, Berlin, 145–182.

Szalai, S., Antofie, T., Barbosa, P., Bihari, Z., Lakatos, M., Spinoni, J., Szentimrey, T., Vogt, J., 2012. The CARPATCLIM project: Creation of a gridded climate atlas of the Carpathian regions for 1961–2010 and its use in the European Drought Observatory of JRC. ECAC2012, Lodz.

Szentimrey, T., Bihari, Z., 2007. Mathematical background of the spatial interpolation methods and the software MISH (Meteorological Interpolation based on Surface Homogenized Data Basis). In: Proceedings from the Conference on Spatial Interpolation in Climatology and Meteorology, Budapest, Hungary, 2004, COST Action 719. COST Office, pp. 17–27.

Szilágyi, J., Józsa, J., 2008. Klímaváltozás és a víz körforgása. Magyar Tudomány, 6., 698. (In Hungarian.)

Szilágyi, J., Kovács, Á., 2011. A calibration-free evapotranspiration mapping technique for spatially-distributed regional-scale hydrologic modeling. Journal of Hydrology and Hydromechanics, 59, 2, 118–130.

Teng, J., Chiew, F.H.S., Vaze, J., Marvanek, S., Kirono, D.G.C., 2012. Estimation of climate change impact on mean annual runoff across continental Australia using Budyko and Fu equations and hydrological models. Journal of Hydrometeorology, 13, 1094–1106. https://doi.org/10.1175/JHM-D-11-097.1

Tian, L., Jin, J., Wu, P., Niu, G., 2018. Assessment of the effects of climate change on evapotranspiration with an improved elasticity method in a nonhumid area. Sustainability, 10, 12, 4589. https://doi.org/10.3390/su10124589

Troch, P.A., 2008. Global warming and the acceleration of the hydrological cycle. In: Bierkens, M.F., Dolman, A.J., Troch, P.A. (Eds.): Climate and the Hydrological Cycle, 8. International Association of Hydrological Sciences.

Turc, L., 1954. Le bilan d'eau des sols: Relations entre les precipitations l'evaporation et l'ecoulement. Annales Agronomiques, No. 4, 491–595.

van der Linden, P., Mitchell, J.F.B. (Eds.), 2009. ENSEMBLES: Climate Change and its Impacts: Summary of research and results from the ENSEMBLES project. Met Office Hadley Centre, FitzRoy Road, Exeter EX1 3PB, UK.

Venables, W.N., Ripley, B.D., 1999. Modern Applied Statistics with S– PLUS. Third Edition. Springer, New York. https://doi.org/10.1007/978-1-4757-3121-7

Virág, Á., 1997. A Balaton múltja és jelene. Egri Nyomda Kft., Eger, Hungary, 904 p. (In Hungarian.)

Wang, C., Wang, S., Fu, B.J., Zhang, L., 2016. Advances in hydrological modelling with the Budyko framework: A review. Progress in Physical Geography, 40, 409–430. https://doi.org/10.1177/0309133315620997

Wang, D., Hejazi, M., 2011. Quantifying the relative contribution of the climate and direct human impacts on mean annual streamflow in the contiguous United States. Water Resources Research, 47, 10.

Wang, D., Tang, Y., 2014. A one-parameter Budyko model for water balance captures emergent behavior in Darwinian hydrologic models. Geophysical Research Letters, 41, 13, 4569–4577. http://dx.doi.org/10.1002/2014GL060509

Zhang, L., Hickel, K., Dawes, W.R., Chiew, F.H.S., Western, A.W., Briggs, P.R., 2004. A rational function approach for estimating mean annual evapotranspiration. Water Resources Research, 40, 2.

Zhang, L., Potter, N., Hickel, K., Zhang, Y., Shao, Q., 2008. Water balance modeling over variable time scales based on the Budyko framework – Model development and testing. Journal of Hydrology, 360, 1–4, 117–131.

Zhang, S., Yang, H., Yang, D., Jayawardena, A.W., 2016. Quantifying the effect of vegetation change on the regional water balance within the Budyko framework. Geophysical Research Letters, 43, 3, 1140–1148.

Zhou, G., Wei, X., Chen, X., Zhou, P., Liu, X., Xiao, Y., Sun, G., Scott, D.F., Zhou, S., Han, L., Su, Y., 2015. Global pattern for the effect of climate and land cover on water yield. Nature communications, 6, 1, 1–9. https://doi.org/10.1038/ncomms6918

Received 26 September 2019
Accepted 28 April 2020